

3837

NATIONAL LIBRARY

BIBLIOTHÈQUE NATIONALE

OTTAWA



OTTAWA

NAME OF AUTHOR... DURDEN DAVID A.

TITLE OF THESIS... Thermal ion-molecule reactions

at pressures up to 10 torr with a pulsed

Mass spectrometer. a) Reactions of methane in krypton  
b) Condensation reactions in ethylene c) Attachment reactions, in oxygen  
UNIVERSITY... ALBERTA and nitrogen

DEGREE... PhD YEAR GRANTED... 1969

Permission is hereby granted to THE NATIONAL LIBRARY OF CANADA to microfilm this thesis and to lend or sell copies of the film.

The author reserves other publication rights, and neither the thesis nor extensive extracts from it may be printed or otherwise reproduced without the author's written permission.

(Signed) David A. Durden

PERMANENT ADDRESS:

c/o A.E. Durden  
947 Foul Bay Rd  
Victoria B.C.

DATED... March 19 1969

NL-91

THE UNIVERSITY OF ALBERTA

Thermal Ion-Molecule Reactions at Pressures up to 10 Torr

With a Pulsed Mass Spectrometer

- (a) Reactions of Methane in Krypton
- (b) Condensation Reactions in Ethylene
- (c) Attachment Reactions in Oxygen and Nitrogen

by



David Alan Durden

A THESIS

SUBMITTED TO THE FACULTY OF GRADUATE STUDIES

IN PARTIAL FULFILMENT OF THE REQUIREMENTS FOR THE DEGREE

OF DOCTOR OF PHILOSOPHY

Department of Chemistry

Edmonton, Alberta

Spring, 1969

UNIVERSITY OF ALBERTA  
FACULTY OF GRADUATE STUDIES

The undersigned certify that they have read, and recommend to the Faculty of Graduate Studies for acceptance, a thesis entitled THERMAL ION-MOLECULE REACTIONS AT PRESSURES UP TO 10 TORR WITH A PULSED MASS SPECTROMETER (a) Reactions of Methane in Krypton, (b) Condensation Reactions in Ethylene, (c) Attachment Reactions in Oxygen and Nitrogen submitted by David Alan Durden in partial fulfilment of the requirements for the degree of Doctor of Philosophy.

*P. Kettle*  
.....  
Supervisor

*G. P. Straw*  
.....

*J. R. Cremonesi*  
.....

*H. Roy House*  
.....

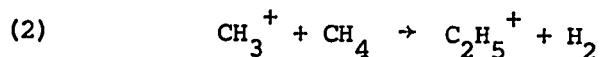
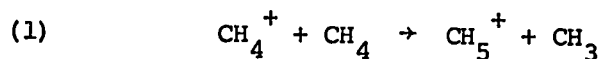
*Fred Fehsenfeld*  
.....  
External Examiner

Date *March 13 1968*  
.....

ABSTRACT

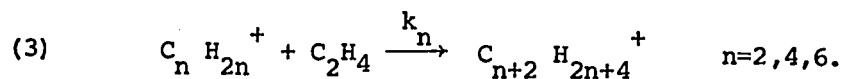
A pulsed mass spectrometer is described which was constructed for the measurement of rate constants of ion-molecule reactions at thermal energies. The mass spectrometer could be operated with ion source pressures up to 10 torr. The reactions studied were condensation and attachment reactions which can only be observed at high pressures.

Reactions of millitorr traces of methane in 3.5 torr of krypton were first studied to check the pulsing technique. The values of the rate constants for reactions (1) and (2) (both  $1.0 \times 10^{-9}$  cc/molecule sec.) were found to be close to previously



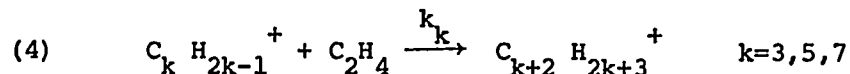
determined values and thus the validity of the pulse technique could be established.

The ionic condensation reactions (3) and (4) were studied in the xenon-sensitized ionization of ethylene to gain information on the radiolysis of ethylene. The values for the rate constants  $k_n$



were found to agree with values which had been estimated from results of a previous technique in which the reaction times were not well known  $k_2 = 2.1 \times 10^{-9}$ ,  $k_4 = 4.35 \times 10^{-12}$  and  $k_6 = 1.14 \times 10^{-12}$  (cc/molecule

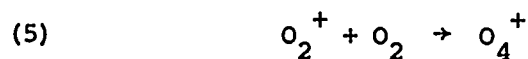
sec.). The values  $k_k$  for reaction (4) were measured as



$k_3 = 0.76 \times 10^{-9}$ ,  $k_5 = 0.46 \times 10^{-12}$  and  $k_7 = 0.27 \times 10^{-12}$  (cc/molecule sec.).

These had not been previously measured. The rapid decrease of rate constant with increasing ionic size was explained in terms of the ion structure. The effect of  $Xe^+$  on the stabilization of the condensation product  $C_4H_8^+$  was observed. Ethylene pressures were varied from  $1 \times 10^{-3}$  to 0.5 torr and xenon pressures from 0.5 to 8 torr.

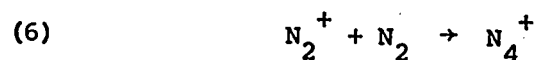
The rate constants and equilibrium constant for the attachment reaction (5), which appears to be of aeronomic interest, were



measured over the pressure range of 1 to 8 torr at temperatures from 298 to 341°K. The reaction was found to have third order kinetics. The rate constant for the forward reaction was measured as  $2.90 \times 10^{-30}$  cc<sup>2</sup>/molecule<sup>2</sup> sec. at 298°K with a negative activation energy of 2.0 kcal/mole. The reverse rate constant was  $2.44 \times 10^{-13}$  cc/molecule sec. at 298°K. The values of the equilibrium constant 0.385 (standard state 1 torr), entropy -22.4 cal/mole deg. and enthalpy -9.98 kcal/mol. agree very well with previous results obtained under equilibrium conditions.

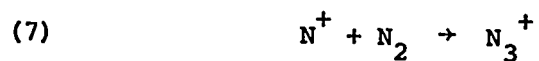
Attachment reactions in nitrogen were studied at pressures from 0.4 to 3.6 torr at temperatures from 297 to 420°K. A forward

rate constant for the attachment (6) was measured as  $8.3 \times 10^{-29}$  cc<sup>2</sup>/molecule<sup>2</sup> sec. at 298°K with a negative activation energy



of 2.3 kcals/mole. These values support previous observations. The equilibrium constant could not be measured.

Under identical conditions as those used above, the attachment reaction (7) displayed second order kinetics. The



rate constant was measured as  $1.5 \times 10^{-12}$  cc/molecule second. No temperature dependence was observed. The rate constants and equilibrium constants for the oxygen and nitrogen reactions were compared by means of theoretical equations.

ACKNOWLEDGMENTS

I wish to express my sincere appreciation to Dr. Paul Kebarle for his advice and encouragement throughout the course of this work.

I wish to acknowledge the cooperation of Dr. Anthony Good in part of this work. The collection of the data for oxygen and nitrogen system (chapter 6) and the interpretation of the results was done jointly by Dr. Good and myself.

I wish to thank the staff of the Chemistry Department Electronic and Machine Shops for their able assistance in construction of the mass spectrometer and Mrs. Gladys Whittal for typing the manuscript.

The financial assistance provided by the University of Alberta is gratefully acknowledged.

TABLE OF CONTENTS

	<u>Page</u>
Abstract . . . . .	i
Acknowledgments . . . . .	iv
List of Figures . . . . .	xi
List of Tables . . . . .	xvi
1. <u>INTRODUCTION</u>	1
1:1 The present study . . . . .	1
1:2 Development of ion-molecule reaction studies . . . . .	1
1:3 Thermal rate constants of ion-molecule reactions at low pressures with pulsed instruments . . . . .	8
1:4 Limitations of low pressure studies . . . . .	9
1:5 Types of reactions observed from low pressure experiments and the need for high pressures . . . . .	10
i Simple charge transfer . . . . .	11
ii Charge transfer induced dissociation . . . . .	12
iii Abstraction or transfer of atoms or atomic ions	12
a. Proton donation . . . . .	13
b. Hydrogen abstraction . . . . .	13
c. Hydride ion abstraction . . . . .	14
d. Atom-ion interchange reactions . . . . .	15
iv Condensation reactions . . . . .	15
v Attachment reactions . . . . .	17



	<u>Page</u>
1:6 Previous experimental work at high pressures, instrumental developments . . . . .	17
1:7 The development of the present instrument . . .	23
2. <u>EXPERIMENTAL</u>	25
2:1 Requirements and design of the present instrument .	25
2:2 The ion source. . . . .	25
2:3 Temperature control and measurement . . . . .	31
2:4 Vacuum chamber . . . . .	31
2:5 Gas inlet system . . . . .	33
2:6 The electron gun . . . . .	35
2:7 Ion acceleration and gating . . . . .	39
2:8 Travel time of the ion from the ion source to the gate electrodes . . . . .	43
2:9 Pulse circuits. . . . .	47
2:10 Quadrupole mass analyser and detection system. The measurement of the transmission of the analyser. .	47
2:11 Discrimination in detection by the electron multiplier	61
2:12 Collision of ions outside the ion source . . . . .	64
2:13 Purification of gases . . . . .	69
2:14 Experimental procedure . . . . .	69

	<u>Page</u>
3. <u>PHYSICAL CONDITIONS IN THE ION SOURCE</u>	72
3:1 Recombination of ions and electrons in the beam . . . . .	73
i Steady-state concentration of ions under constant illumination . . . . .	73
ii Lifetime of an ion in the beam . . . . .	75
iii Time for removal of an ion from the beam by diffusion . . . . .	76
iv Charge density in volume sampled by the leak . . . . .	81
3:2 Processes occurring in the region from which ions were observed . . . . .	83
i The effect of first and second order loss mechanisms . . . . .	83
ii Analysis of the ion intensity curves by means of the Einstein equation . . . . .	87
iii Effect of mass flow . . . . .	92
iv Average lifetime of an ion in the ion source . . . . .	93
3:3 Conclusion . . . . .	94
4. <u>REACTIONS IN METHANE KRYPTON</u>	98
4:1 Introduction - purpose of studying CH <sub>4</sub> -Kr system and previous results . . . . .	98
4:2 Methane-Krypton experimental . . . . .	104

	<u>Page</u>
4:3 Results . . . . .	105
i Qualitative observations . . . . .	105
ii Preliminary estimate of rate constants . . . . .	107
iii Corrected values of rate constants . . . . .	111
iv Preparation of theoretical plots . . . . .	120
4:4 Observations and discussion . . . . .	123
5. <u>REACTIONS IN THE XENON-SENSITIZED IONIZATION OF ETHYLENE</u>	130
5:1 Discussion of previous investigations and the purpose of the present study . . . . .	130
5:2 Experimental . . . . .	133
5:3 Results and calculation of rate constants . . . . .	134
5:4 Discussion of the results . . . . .	145
6. <u>ION MOLECULE REACTIONS IN PURE OXYGEN AND PURE NITROGEN</u>	156
The attachment $O_2^+ + O_2 \rightarrow O_4^+$ and $N_2^+ + N_2 \rightarrow N_4^+$	
6:1 The importance of these reactions to various fields	156
6:2 The attachment of oxygen $O_2^+ + O_2 \rightarrow O_4^+$ . . . . .	158
i Previous work on this reaction . . . . .	158
ii Results . . . . .	163
iii Evaluation of the equilibrium constant . . . . .	171
iv Evaluation of the rate constant for the forward reaction . . . . .	175

	<u>Page</u>
v Evaluation of the rate constant for the reverse reaction . . . . .	183
vi Other reactions, possible interference . . .	185
vii Discussion of the results . . . . .	187
6:3 The attachment of nitrogen $N_2^+ + N_2 \rightarrow N_4^+$ . . . . .	188
i Previous work on this reaction . . . . .	188
ii The purpose of this study . . . . .	192
iii Other reactions involving $N_2^+$ and $N_4^+$ . . . . .	193
iv Results . . . . .	194
v Evaluation of the rate constants . . . . .	205
vi Evaluation of the equilibrium constant $K_p$ . . . . .	210
vii Further evaluation of $k_f$ . . . . .	217
6:4 Comparison of the oxygen and nitrogen reactions . . . . .	219
i Theoretical considerations of the reaction mechanism. The effect of temperature and bond energy on $k_f$ . . . . .	219
ii The effect of temperature and bond energy on $k_r$ . . . . .	226
iii Comparison of the equilibrium constants $K_p$ for oxygen and nitrogen . . . . .	231
6:5 The attachment $N^+ + N_2 \rightarrow N_3^+$ . . . . .	233
i Previous work . . . . .	233
ii Purpose of this study . . . . .	234
iii Results . . . . .	234
iv Discussion of the results . . . . .	241

	<u>Page</u>
7. <u>SUGGESTIONS FOR FURTHER RESEARCH</u>	244
7:1 Introduction . . . . .	244
7:2 Attachment reactions in $O_2-H_2O$ mixtures . . . . .	244
7:3 Preliminary investigation of $O_2-H_2O$ mixtures . . . . .	246
i Experimental . . . . .	246
ii Results . . . . .	246
7:4 Attachment reactions in $N_2-H_2O$ mixtures . . . . .	250
7:5 Further work on the attachment $N_2^+ + N_2 \rightarrow N_4^+$ . . . . .	253
7:6 The attachment reaction $CO^+ + CO \rightarrow C_2O_2^+$ . . . . .	254
 Bibliography . . . . .	 256
Appendix I . . . . .	266
Appendix II . . . . .	268

LIST OF FIGURES

<u>Figure</u>		<u>Page</u>
1:1	Schematic diagram of a mass spectrometer	4
2:1	Apparatus, showing ion source, electron gun quadrupole mass analyser and vacuum housing	26
2:2	Top view and section of the high pressure ion source	27
2:3	Gas inlet system and pressure measuring gauges	34
2:4	Cross section of deflection plates showing guard plates and electric field potential lines	37
2:5	Ion acceleration electrodes	40
2:6	Pulse generation circuit	48
2:7	Pulse sequence	49
2:8	Quadrupole rods	51
2:9	a. Plot of $U/V_0$ ratio versus $V_0/V_{0 \text{ max.}}$ b. Plot of relative intensity $I/I_{0.5}$ calculated by means of equation (2:xxi) versus $V_0/V_{0 \text{ max.}}$	55 55
2:10	Transmission factors versus mass for the quadrupole mass analyser	60
2:11	Amplification factors for the secondary electron multiplier	63
2:13	Total ion current as measured on the cone (electrode 16a) and by the quadrupole operated at $a/q = 0$ versus pressure of nitrogen in the ion source	65

<u>Figure</u>		<u>Page</u>
2:13	a. Ion signals produced by the auxiliary ion source as the vacuum chamber pressure $P_g$ was increased	67
	b. Ratio $N_2^+/O_2^+$ versus pressure	67
3:1	Detailed view of reaction region showing an approximated spread of the electron beam and the ion exit aperture	74
3:2	Plot of observed total ion signal $I_{obs}$ normalized to ion signal under constant irradiation $I_\infty$ , versus pulse width	78
3:3	a. Normalized ion signal $I_{obs}/I_\infty$ divided by the illumination fraction $f$ versus $f$	80
	b. Above data on log-log plot	80
3:4	Theoretical plot of ion concentration $I$ as the beam is switched on and a steady state condition develops	82
3:5	a. Schematic diagram of electron pulse and ion intensity curves at constant pulse width and variable repeat time $t_r$	84
	b. Normalized observed ion signal $I_{obs}/I_\infty$ divided by illumination fraction $f$ , plotted versus the pulse repeat time $t_r$	84
3:6	Observed total ion intensity versus time curves for pure $N_2$ at $380^\circ K$ $x = 0.67$ mm.	89

<u>Figure</u>		<u>Page</u>
3:7	Observed total ion intensity versus time curve for 1.55 torr N <sub>2</sub> at 385°K x = 1.67 mm.	90
3:8	Theoretical curves calculated from the Einstein equation (3:xviii)	91
4:1	CH <sub>4</sub> breakdown pattern from von Koch, reference 27	103
4:2	Raw data showing decay of Kr <sup>+</sup> , CH <sub>4</sub> <sup>+</sup> , CH <sub>3</sub> <sup>+</sup> and total ionization	106
4:3	Observed ion intensity curves for Kr <sup>+</sup> , CH <sub>4</sub> <sup>+</sup> , CH <sub>3</sub> <sup>+</sup> , CH <sub>5</sub> <sup>+</sup> , C <sub>2</sub> H <sub>5</sub> <sup>+</sup> , and total ionization for mixture of 1.2x10 <sup>-3</sup> torr CH <sub>4</sub> in 3.4 torr Kr	109
4:4	Ion intensity curves from (4:3) normalized to total ionization	112
4:5	Decay of i <sub>Kr</sub> <sup>+</sup> versus t	115
4:6	Decay of i <sub>CH<sub>4</sub><sup>+</sup></sub> versus t	117
4:7	Decay of i <sub>CH<sub>3</sub><sup>+</sup></sub> versus t	119
4:8	Theoretical ion intensity curves. Compare to figure (4:4)	122
4:9	Approximate schematic of potential energy functions of methane if the molecule is considered to be a diatomic H <sub>3</sub> C-H	128
5:1	Ion intensity curves for reaction of C <sub>2</sub> H <sub>4</sub> <sup>+</sup>	135
5:2	Ion intensity curves for reaction of C <sub>4</sub> H <sub>8</sub> <sup>+</sup>	137
5:3	Ion intensity curves for reaction of C <sub>6</sub> H <sub>12</sub> <sup>+</sup>	138



<u>Figure</u>		<u>Page</u>
5:4	Ion intensity curves for reaction of $C_3H_5^+$	139
5:5	Ion intensity curves for reaction of $C_5H_9^+$	140
5:6	Ion intensity curves for reaction of $C_7H_{13}^+$	141
5:7	Measured and calculated values of $k_6$ for the reaction (5:6) of $C_2H_4^+$ with $C_2H_4$ , versus xenon pressure	146
6:1	Observed ion intensity curves of $O_2^+$ and $O_4^+$ in $O_2$ at 298°K, pressures from 0.9 to 4 torr	161
6:2	Ion intensity curves from (6:1) normalized to total ion intensity (i.e. $O_2^+ + O_4^+$ ) 298°K	162
6:3 to 6:7	Normalized ion intensity curves of $O_2^+$ and $O_4^+$ , 297°K to 341°K	164 to 169
6:8	van't Hoff plot for equilibrium constant of $O_2^+ + O_2 \rightleftharpoons O_4^+$	172
6:9	Change of $K_p$ with oxygen pressure	174
6:10	Third and second order rate constants $k_f$ versus oxygen pressure for reaction (6:1a) a. preliminary values b. corrected values	177
6:11	Typical plot from which corrected values were obtained $O_2^+ + 2O_2 \rightleftharpoons O_4^+ + O_2$	180
6:12	Arrhenius plot of corrected values of $k_f$ for $O_2$	182
6:13	Observed ion intensity curves of $N^+$ $N_2^+$ $N_3^+$ $N_4^+$ in nitrogen at 381°K 2.65 torr	196

<u>Figure</u>		<u>Page</u>
6:14 to	Normalized ion intensity curves for the	197
6:21	nitrogen ions 300°K to 414°K	to 204
6:22	Third and second order rate constants $k_f$ , for reaction (6:2), versus pressure. Results at 380 and 381°K	206
6:23	Arrhenius plot of $k_f$ for reaction (6:2)	208
6:24	Plot from which "corrected" values of $k_f$ were obtained at 300°K	209
6:25	Variation of $K_p$ of reaction (6:2) $N_2^+ + N_2 \rightleftharpoons N_4^+$ versus pressure. Solid lines experimental. Dashed lines calculated from equation (6:xix).	212
6:26	Normalized ion intensity curves for $N_2$ -Ne mixture at 297°K	215
6:27	Normalized ion intensity curves for $N_2$ -Ne mixture at 376°K	216
6:28 to	Normalized ion intensity curves of $N^+$ and $N_3^+$	236
6:30	as fractions of $N^+ + N_3^+$	to 238
6:31	Plot of third and second order rate constants for the reaction $N^+ + nN_2 \rightarrow N_3^+ + (n-1) N_2$	240
7:1	Normalized ion intensities for $O_2$ - $H_2O$ mixture at 308°K, 2.28 torr $O_2$ , $3.82 \times 10^{-3}$ torr $H_2O$	248

LIST OF TABLES

<u>Table</u>		<u>Page</u>
2:1	Potentials on ion acceleration plates	42
2:2	Flight times of ions, acceleration voltage = -225 volts	45
2:3	Flight times of nitrogen ions, acceleration voltage = -67 volts	46
4:1	Rate constants for reactions 4:1 and 4:2 measured at low pressures (literature values)	100
4:2	Rate constants from decay of $\text{Kr}^+$ , $\text{CH}_4^+$ , $\text{CH}_3^+$ - preliminary values	110
4:3	Corrected values of rate constants from the decay of ions $\text{Kr}^+$ , $\text{CH}_4^+$ , $\text{CH}_3^+$	120
4:4	Thermal rate constants for reactions of $\text{Kr}^+$ , $\text{CH}_4^+$ and $\text{CH}_3^+$ with $\text{CH}_4$	121
5:1	Rate constants for the decay of $\text{C}_2\text{H}_4^+$	136
5:2	Rate constants for the decay of $\text{C}_4\text{H}_8^+$	142
5:3	Rate constants for the decay of $\text{C}_6\text{H}_{12}^+$	143
5:4	Rate constants for the decay of $\text{C}_3\text{H}_5^+$	143
5:5	Rate constants for the decay of $\text{C}_5\text{H}_9^+$	144
5:6	Rate constants for the decay of $\text{C}_7\text{H}_{13}^+$	144
6:1	Third order rate constants for the oxygen reaction	181
6:2	Constants for the attachment reaction $\text{O}_2^+ + \text{O}_2 \rightarrow \text{O}_4^+$	184
6:3	Constants for the attachment reaction $\text{N}_2^+ + \text{N}_2 \rightarrow \text{N}_4^+$	218

<u>Table</u>		<u>Page</u>
6:4	Rate constants for the reaction $N^+ + nN_2 \rightarrow N_3^+ + (n-1) N_2$	239
7:1	Rate constants for the forward reactions for hydration reactions	249

## INTRODUCTION

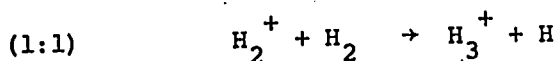
### 1:1 The Present Study

The present study was directed towards the investigation of the kinetics of ion-molecule reactions in gases at high pressures (1-10 torr) and at thermal energies. The temperature of the ion source could be varied from 300° to 450° K. The reaction times could be measured directly by means of a pulsing technique. These unusual reaction conditions were designed to fill a gap in the field of ion molecule reaction investigations. In the following few pages the development of the field of ion molecule reactions, and the need for measurements of ion molecule reactions under these conditions will be discussed.

### 1:2 Development of Ion-Molecule Reaction Studies

In an ordinary mass spectrometer used for analysis (isotope analysis, qualitative and quantitative analysis of vapours) the pressure in the ion source and mass analysis region is kept low so that the ions can leave the ion source and be mass analyzed without the occurrence of collisions with gas molecules. If the pressure of the ion source is increased, collisions of the ions with gas molecules begins to occur and these can lead to ion molecule reactions which change the nature of the primary ions. For example J.J. Thomson (1) with the first mass spectrograph observed ions of mass to charge ratio  $m/e = 3$  in

hydrogen gas and reasoned that these were due to  $H_3^+$ . This ion was also found by Dempster who observed that its intensity increased with hydrogen pressure (2). The origin of this ion was later correctly explained (3,4) as being due to the reaction (1:1):



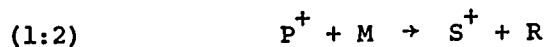
The presence of the  $H_3^+$  ion obviously interferes with isotopic determinations when the abundance of the ion  $HD^+$  has to be measured. Since at that time interest in mass spectrometric measurements was mostly centered on isotopic abundance measurements efforts towards improvement of the vacuum systems soon led to the elimination of the undesired ion molecule reactions. In subsequent mass spectrometric research which dealt with the measurements of ionization potentials, ionic heats of formation and analysis of vapours the occurrence of ion molecule reactions was not desired and thus low ion source pressures were maintained. Only during the early 1950's was it recognized that ion-molecule reactions might play a large role in radiation chemistry. With this in mind Talroze and Lyubimova (5), Stevenson and Schissler (6,7) started systematic studies. This early work caused a renewed interest in these reactions, and the field expanded rapidly. Many reactions were observed and their rates measured in

conventional mass spectrometers at ion source pressures of the order  $10^{-3}$ - $10^{-4}$  torr. The basis of these measurements will now be briefly described.

A typical mass spectrometer used for gas analysis is shown schematically in figure (1:1). Ions are produced in the ion source by bombardment of the gas by an electron beam. These primary ions which have the masses of the original molecules and fragments thereof are pushed out of the ion source by the small electric field  $E_x$  of the repeller. They are then accelerated by the potential  $V$  and analysed according to their mass to charge ratio  $m/e$  and detected. When the instrument is used for gas analysis the pressure in the ion source and analyser is kept very low (less than  $10^{-5}$  torr) so that no ion molecule collisions occur. When the ion source pressure is increased to  $10^{-4}$  torr, ion-molecule reactions become observable since some of the primary ions  $P^+$  suffer reacting collisions in their path  $\ell$  on their way to the ion exit slit (see Figure 1:1).

Considering the general reaction (1:2), one can write equation

(1:i) for



the attenuation of the primary ion, where  $I_p$  is the primary ion

$$(1:i) \quad I_p = I_p^0 e^{-Qn\ell}$$

intensity at distance  $\ell$ .  $I_p^0$  is the original primary ion intensity,

$Q$  is the experimental reaction cross section and  $n$  is the number

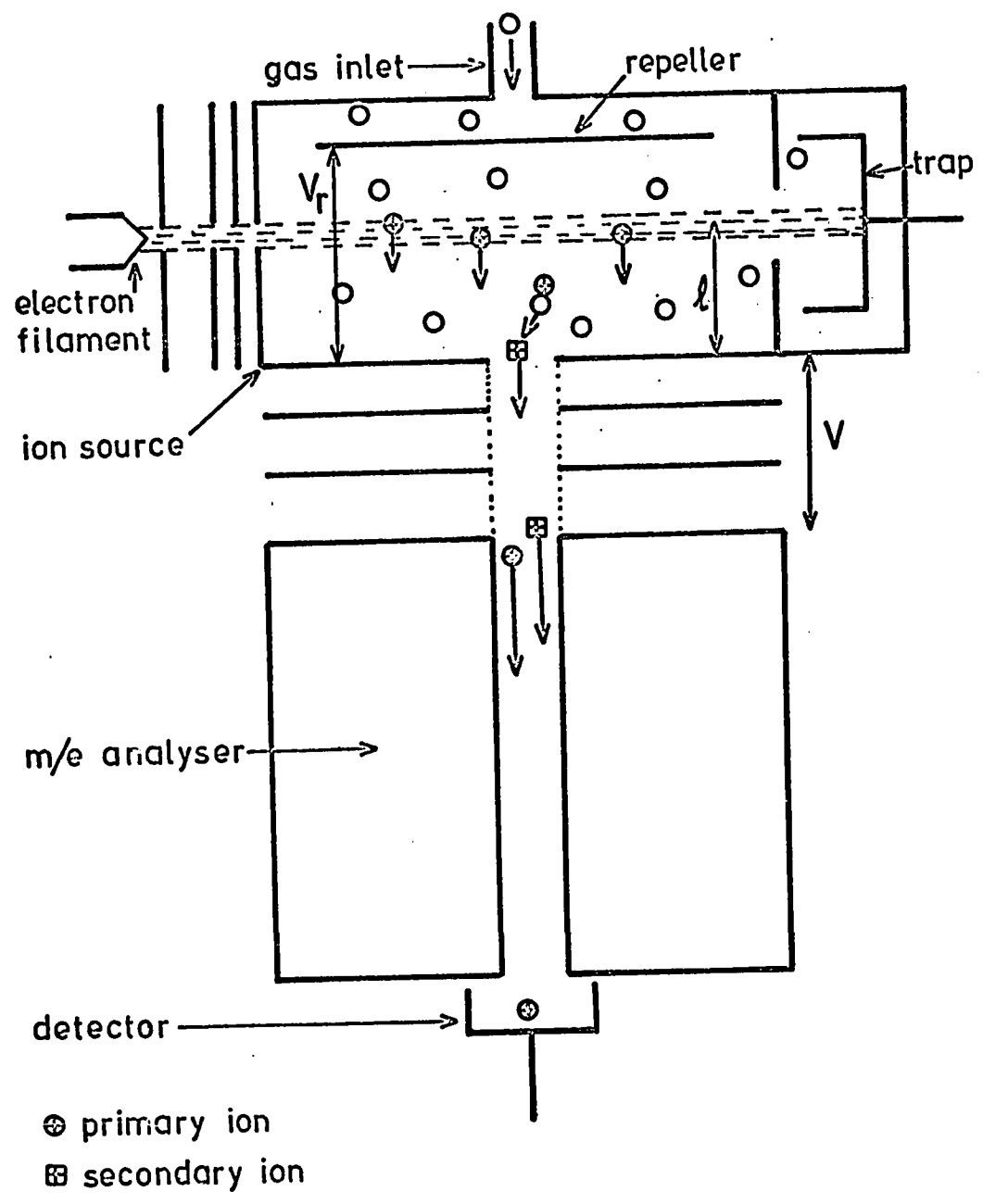


Figure 1:1 Schematic diagram of a mass spectrometer. Some secondary ion formation shown.



of molecules per cc in the ion source. Since  $I_p^0 - I_p = I_s$  where  $I_s$  is the intensity of the secondary ion  $S^+$  one can rearrange equation (1:i) to the form:

$$(1:ii) \quad \frac{I_s}{I_p} = e^{Qn\ell} - 1$$

At low pressures, where only a few of the primary ions react and the ratio becomes  $I_s/I_p < 0.05$  equation (1:ii) can be simplified to the form (1:iii):

$$(1:iii) \quad \frac{I_s}{I_p} = Qn\ell$$

All measurements by the early workers like Stevenson (6,7,8), Hamill (9), Field and Franklin (10,11) were done under low pressure conditions where equation (1:iii) holds.

These experiments were directed towards two different aspects of ion molecule reactions. One was to determine the types of reactions occurring when different reactants were present, the other was the dependence of the reaction cross section on the velocity of the primary ion.

Gioumoussis and Stevenson (12) developed the theory of velocity dependence for the reaction cross section. This was based upon a previous theory of Langevin who proposed that the cross section for collision of an ion and a molecule was dependent upon the polarizability  $\alpha$  of the molecule. The ion

and molecule converge with a relative velocity  $g$ . It is assumed that the ion induces a dipole in the molecule and the resultant force causes the trajectories to converge. If they pass within a certain distance the ion and molecule orbit around each other. The critical distance within which capture still occurs can be used to evaluate a capture cross section  $\sigma_g$  which is given in equation (1:iv).

$$(1:iv) \quad \sigma_g = \frac{2\pi e}{g} \sqrt{\frac{\alpha}{\mu}}$$

Where  $\mu$  is the reduced mass the other symbols having been defined previously.

The primary ion in the ion source of a mass spectrometer experiences continuous acceleration by the repeller field of strength  $E_r$ . In order to relate the experimentally observed cross section  $Q$  (equation 1:iii) to the Langevin equation (1:iv) Gioumoussis integrated the variable cross section  $\sigma_g$  over the total path  $\ell$  of the ion. Since the velocity of the ion due to the repeller field is very much larger than the velocity of the molecules, it is set equal to the relative velocity  $g$ . This averaging process leads to the relationship given in equation (1:v).

$$(1:v) \quad Q = 2\pi e \sqrt{\frac{\alpha}{\mu} \frac{2m_p}{eE_r \ell}}$$

where  $m_p$  is the mass of the primary ion. Gioumoussis in the above treatment assumed that reaction occurs at each capturing ion

molecule collision, i.e. that the reaction efficiency is unity. Using the Langevin cross section dependence (1:iv) Gioumouisis also derived an equation for the rate constant of an ion molecule reaction where both the ion and molecule moved with thermal (Maxwell) velocities. This relationship is given in equation (1:vi).

$$(1:vi) \quad k = 2\pi e \sqrt{\frac{\alpha}{\mu}}$$

Comparing (1:vi) and (1:v) one sees that the thermal rate constant  $k$  can be evaluated from the value of  $Q$ , experimentally determined in the presence of a repeller field, by the relationship (1:vii).

$$(1:vii) \quad k = \sqrt{\frac{eE_r \ell}{2m_p}} Q$$

It was shown for many reactions (e.g. 1:1) that the experimentally determined  $Q$  followed the  $1/E_r \ell$  dependence predicted by equation (1:v) and that the absolute magnitude corresponded very closely to that calculated by the same equation (8,13). The dependence on the reduced mass was also observed. Equation (1:v) does not predict a temperature dependence for  $Q$ . Indeed, it was eliminated by the assumption that the relative velocity  $g$  is only the velocity of the ion. The values of  $Q$  were found to be independent of temperature. The large values of  $Q$  ( $> 10^{-16} \text{ cm}^2$ , and up to  $10^3$  times larger than those of equivalent reactions of neutrals) and the lack of a temperature dependence, lead to the conclusion that the observed ion-molecule reactions were non-endothermic and had activation

energies close to zero (14). Thermal rate constants had large values ( $10^{-9}$  cc/molecule sec.) when calculated from (1:vii) and these corresponded with the predicted values (1:vi).

The validity of equation (1:vii) for thermal rate constants depends upon the assumed correctness of equations (1:v) and (1:vi). However, many reactions were found for which  $Q$  did not obey the  $1/E_r$  dependence of (1:v). It was pointed out by Stevenson (14) that the probability that a collision would lead to reaction may not be unity or constant. For complex reactions, the probability was not independent of the internal coordinates of the reactant ion or of the relative velocity  $g$  of the colliding pair. It was found to decrease with increasing velocity.

Thus equation (1:vii) and experiments done in the presence of a repeller field could not be used to determine rate constants for reactions occurring at thermal energies. Since ion molecule reactions occur at thermal energies in a large number of chemical systems, such as radiation chemistry, the ionosphere, flames and electrical discharges, it would be desirable to determine  $k$  under conditions where ions and molecules are in thermal equilibrium. The pulse technique was developed for this purpose.

### 1:3 Thermal Rate Constants of Ion Molecule Reactions at Low Pressures with Pulsed Instruments

The pulse technique for observing reactions at thermal energies

was first developed by Talroze (16,17). The ion source is pulsed as follows. The electron beam is switched on as a pulse for a very short time and ions are formed. After this there is a delay  $t_d$  during which equipotential conditions are maintained in the ion source and the ions may react under thermal conditions. The repeller potential is then applied in a pulse  $t_r$  repelling the ions. By varying the time  $t_d$  and measuring  $I_s/I_p$  as a function of  $t_d$  it is possible to find the rate constant  $k$  if the concentration of gas  $n$  is known. The equation given by Talroze (17) is (1:ix)

$$(1:ix) \quad \frac{I_s}{I_p} = knt_d + f(t_i, t_r)$$

where  $f(t_i, t_r)$  is a function of the pulse widths and is constant for constant  $t_i$  and  $t_r$ . This method is similar to most kinetic investigations in which the degree of conversion is determined as a function of elapsed time. The pulse technique has since been used by other workers notably Hand and Weysenhoff (18), Ryan and Futrell (19), and Harrison *et al* (20,21) to measure rate constants at thermal energies.

#### 1:4 Limitations of Low Pressure Studies

The study of ion-molecule reactions by the two low pressure techniques, the earlier method of continuous repulsion, and the later pulsed method, had certain limitations. Since the pressure was low (around  $10^{-4}$  torr) and the reaction time was short (about  $10^{-6}$  seconds) only reactions with large rate constants ( $10^{-9}$  to  $10^{-10}$  cc/molecule sec.) could be observed. The concentration of

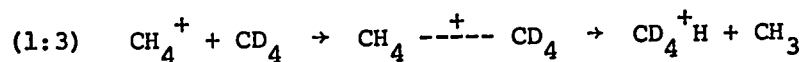
secondary ions was usually more than  $10^{-2}$  times smaller than that of the primary ions and thus further reactions could not be observed. However much useful information was obtained from observation of these fast reactions. It became possible to classify the reaction types as follows.

### 1:5 Types of Reactions Observed from Low Pressure

#### Experiments and the Need for High Pressures

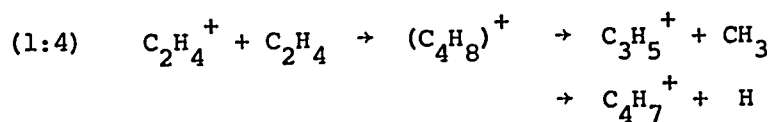
It is widely accepted now that low energy ion molecule reactions occur through the formation of a short-lived collision complex. It has been suggested that the transition complex takes one of two forms (22). One is a loose complex in which the ion-molecule system is held together by polarization forces. In the second the complex is considered to be covalently bonded.

For example reaction (1:3) involved a loose complex. It was shown (23) that the hydrogen atoms are not mixed, that the



product is  $\text{CD}_4^+ \text{H}$  rather than  $\text{CH}_3 \text{D}_2^+$  which would result from a complex of the form  $(\text{C}_2\text{H}_4\text{D}_4)^+$ .

The more strongly bonded complex is formed when it has the stoichiometry which corresponds to that of a stable ionic structure. In this case rearrangement does occur as in (1:4).

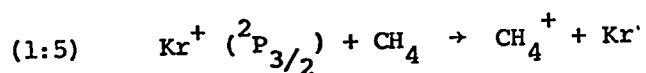


The intensities of the products  $C_3H_3^+$  and  $C_4H_7^+$  are similar to those of the fragment ions produced by electron impact ionization of butene molecules (11,24).

The types of ion molecule reactions are classified below more with respect to the product formed than to the type of complex involved.

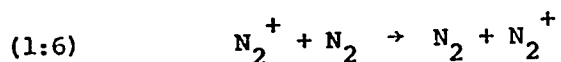
i Simple Charge Transfer

Superficially in charge transfer the ion abstracts an electron from the molecule during the collision and a new ion and molecule are formed as in reaction (1:5).

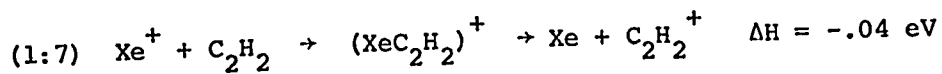


The requirement for charge exchange to occur at thermal energies is that the recombination energy of the ion be greater than the ionization potential of the neutral molecule. (In reaction (1:5)  $R E \quad Kr^+ (^2P_{3/2}) = 14.0 \text{ eV}$  and  $I_p(CH_4^+) = 13.12 \text{ eV}$ . The difference in energy  $-\Delta H$  is 0.88 eV and reaction occurs readily).

When the ion and molecule are the same species,  $\Delta H = 0$  and the reaction is called resonant charge transfer (25). Occasionally resonant conditions are imposed on reactions of different species (1:6),

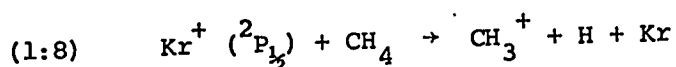


especially when the numbers of degrees of freedom of the ion and molecule are small. This was observed with xenon and ethylene (1:7) (26).



### ii Charge Transfer Induced Dissociation

When the change in enthalpy  $\Delta H$  is large because of large differences in ionization potentials, the new ion has a large excess energy and may dissociate (27) as in reaction (1:8).



In this case the recombination energy of  $\text{Kr}^+$  (14.67 eV) is 1.55 eV more than the ionization potential of  $\text{CH}_4^+$ . This large excitation energy causes a C-H bond to break. The rule for this to take place is that the recombination energy has to be larger than the appearance potential of the fragmentation. In this case the appearance potential equals the bond dissociation energy  $D(\text{CH}_3\text{-H})$  plus the ionization potential of  $\text{CH}_3$ .

By a suitable choice of the reactant ion the extent of fragmentation of the production may be specified. This is very useful if one wants to form only one or two types of ions for further reaction. The choice of ions is limited by the available recombination energies and appearance potentials of the ions and molecules.

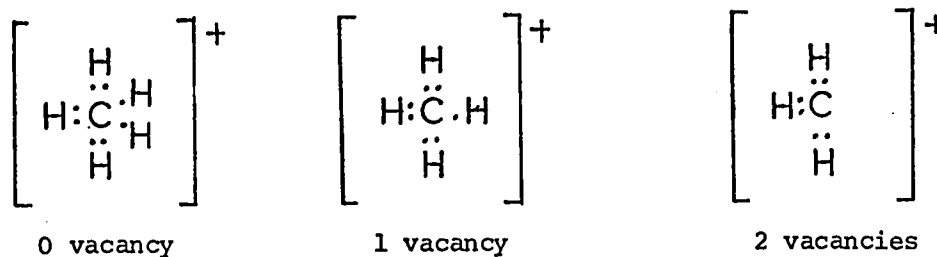
### iii Abstraction or Transfer of Atoms or Atomic Ions

A large majority of ion molecule reactions involve the abstraction by the ion of an ionic or neutral fragment from the



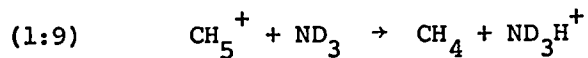
molecule, or the transfer by the ion of such a fragment to the molecule. Reactions in which the fragment is hydrogen have been categorized as shown below. Reactions in which the fragment is large are treated as condensation reactions.

Ion-molecule reactions of organic ions can be classified according to the electronic structure of the ion (28). Generally organic ions have zero, one or two electron vacancies in the valence shell. This can be illustrated by the methane ions.



a Proton Donation

Ions which have no vacancies would be expected to react by donating a proton (28).



These reactions have long been postulated in organic chemistry.

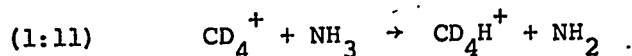
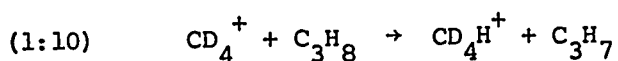
b Hydrogen Abstraction

Ions in which there is one vacancy and thus have an odd electron number are radical ions. Two reactions of radical

ions are hydrogen abstractions and addition to double bonds.

Addition will be considered later as a condensation reaction.

Hydrogen abstraction is shown in reactions (1:10) and (1:11) (29).

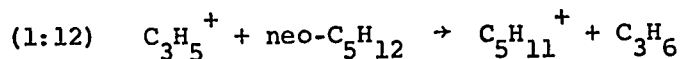


It was observed that when proton donation could be distinguished from hydrogen abstraction the rate constant of the former was about one order magnitude larger than that of the latter. This is probably due to the extremely electrophilic nature of  $\text{H}^+$ .

### c Hydride Ion Abstraction

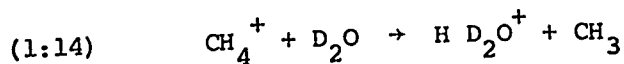
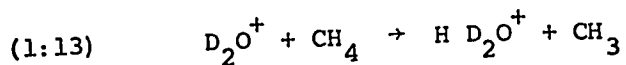
Ions in which there are two vacancies in the valence orbital tend to abstract  $\text{H}^-$  from saturated molecules (28).

Examples of such ions are  $\text{CH}_3^+$  and  $\text{C}_3\text{H}_5^+$  (30).



These ions can also react in condensation reactions.

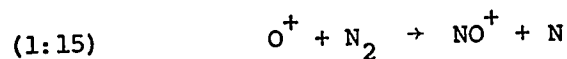
Using the above criterion of an ion having zero or one vacancy one cannot always predict whether proton donation will predominate over hydrogen abstraction or *vice versa*. Many of these reactions appear to involve a loosely bound complex and the most stable product ion results. Both reactions (1:13) and (1:14) give the same product (22), the former by hydrogen



abstraction and the latter by proton donation. One might expect hydrogen abstraction by  $\text{D}_2\text{O}^+$  and by  $\text{CH}_4^+$  since both ions have one electron vacancy.

#### d Atom-Ion Interchange Reactions

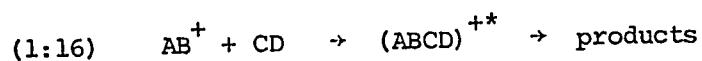
Certain reactions between inorganic diatomic gases have been labelled atom-ion interchange reactions and the exact mechanism left unspecified (17). In these reactions larger elements



than hydrogen are transferred.

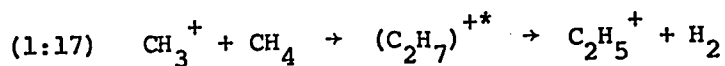
#### iv Condensation Reactions

The term condensation covers all those reactions in which covalent bonds (C-C and C-S) bind the complex and considerable rearrangement takes place so that units larger than atoms or atomic ions are transferred. The general reaction is given by (1:16)



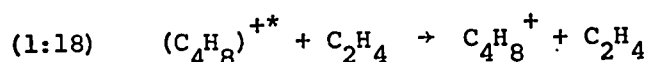
where  $\text{AB}^+$  is anion with one or two vacancies in the valence orbital. This group of reactions is probably the largest involving organic ions and molecules. Examples of these reactions are (1:4) in

which  $C_2H_4^+$  has one electron vacancy and (1:17) in which  $CH_3^+$  has two electron vacancies.

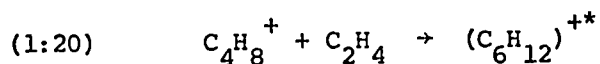
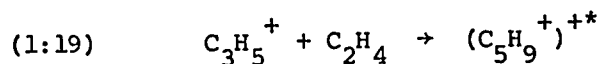


All the above types of reactions were observed at low pressures. One expects, however, that as the pressure is increased, these reactions will be modified and new reactions will appear.

At high pressures the intermediate complex of a condensation reaction may be stabilized by collision with the gas molecules. The complex has a large excitation energy due to bond formation. This energy is distributed in its vibrational and rotational modes, and is transformed into translational kinetic energy by collision with the gas molecules. Thus the complex becomes thermalized. The product of reaction (1:4) is observed to change at high pressures as  $(C_4H_8)^{+*}$  is stabilized as in (1:18).



Since at high pressures, the concentration of secondary ions becomes large, higher order reactions (consecutive reactions) are observed. The products of (1:4) or (1:18) can react further:

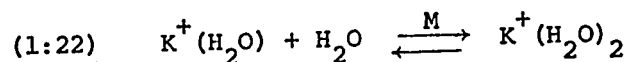
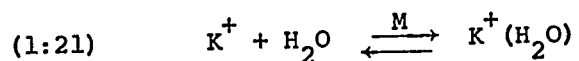


Ion-molecule reactions which have low reaction rates become

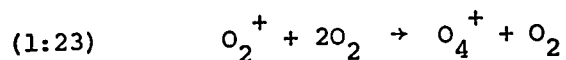
observable at higher pressures. A new type of reaction, which involves three body collisions and thus has a low rate, is the attachment reaction.

#### v Attachment Reactions

Reactions in which the bonding is mainly ionic, in which no rearrangement occurs and which involve the reactions of inorganic ions to form complexes bonded by covalent or ionic bonds, will be called attachment or clustering reactions. Examples of attachment reactions involving only ion-dipole forces are the clustering reactions of  $\text{H}_2\text{O}$  around  $\text{K}^+$  (31).



The reactions exhibit third order kinetics and are only observed at high pressures as the excess energy caused by bond formation must be removed by a third body to stabilize the complex. An example of a reaction in which the complex bonding may be partially covalent and partially ionic in character is the three body attachment of oxygen.



### 1:6 Previous Experimental Work at High Pressures

#### Instrumental Developments

Many workers recognized the desirability of obtaining results

at high pressures and mass spectrometers were modified accordingly. Field and Franklin and their co-workers were among the first to do so. The ion source of their mass spectrometer was modified to decrease the rate of escape of gas by making the electron entrance aperture and the ion exit slit smaller. The ion source pressure could be increased without increasing the analyzer pressure so that no collisions occurred outside the ion source. Thus Field and co-workers were able to observe high order reactions in methane (32) and in ethylene (33) at pressures of 0.3 torr. This apparatus was further improved and the ions produced in methane were observed at pressures up to 2 torr (34,35). These ions could then be compared with reactions proposed for conventional radiolysis of methane.

Disadvantages arise from the use of an electron beam in such apparatus. The electron beam may be intense, but the electrons are severely scattered and attenuated by the high pressure gas. The scatter can be decreased by collimating the beam with a magnetic field. However then, the beam, though collimated, travels in a distorted path and the beam to ion exit slit becomes uncertain.

The problem of attenuation can be overcome by use of more penetrating radiation than electrons. Rudolph and Melton used  $\alpha$  radiation from  $\text{Po}^{210}$  as source of ionization. The polonium was painted onto the repeller plate so that the

whole ion-source volume was irradiated. With this apparatus they were able to study high order reactions in ethylene (36) and acetylene (37) and observe charge exchange reactions between rare gas ions and organic molecules such as methane (38) and cyanogen. The problem of beam collimation is still present with this type of ion source as ions are formed at varying distances from the ion exit slit. Since the path lengths of primary and secondary ions are not known quantitative measurements are precluded.

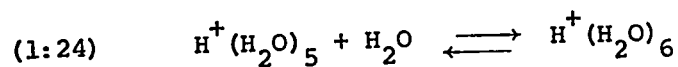
Wexler overcame the problem of penetration and collimation by using a beam of 2 m.e.v. protons from a Van de Graaf generator as the ionizing source (39). At pressures of 1.25 torr, high order consecutive ion-molecule reactions in ethylene were studied (e.g. reactions (1:19) and (1:20)). The ion  $C_4H_8^+$  was observed, which confirmed that at such pressures, collisional stabilization (1:18) took place. Similar polymerization reactions occurred in acetylene.

One common failure of these three types of instruments was that all used a repeller field to extract the ions. Consequently, even though high order reactions could be observed, the ions had energies larger than thermal.

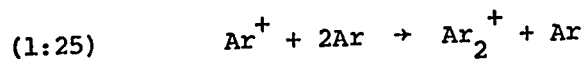
With the idea of simulating conventional gas radiolysis Kebarle and Godbole (40) built a mass spectrometer with a field free ion source which could be operated at pressures up to 200 torr.

The experiments of previous workers on the ionic polymerization of ethylene were extended to a pressure of 40 torr (41,42). However in this case the reactions occurred at thermal energies and one would expect the results to be applicable to the radiolysis of ethylene.

Attachment reactions involving ion-dipole interactions were also studied with this instrument (43). Such reactions were of the type shown in (1:24).



The instrument was also used to study attachment reactions of rare gas ions (44) e.g. (1:25):



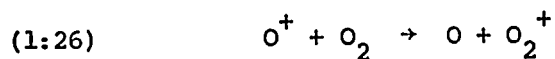
Since there is no repeller field in this type of ion source, one relies on mass flow and diffusion to remove ions. As with Melton's apparatus, the reactions times are poorly defined.

The time dependence of a reaction may be observed by means of a pulsed stationary afterglow. This technique was used by Fite *et al* (45) and Sayers and Smith (46). In this method a gas mixture is subjected to a short pulse of excitation and ions are formed in concentrations proportional to the constituent concentrations, and react with the neutrals. Ions emerging from an aperture in the side of the reaction chamber

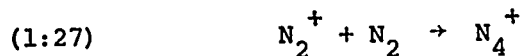


are analysed by a mass spectrometer.

The variation of each ion's intensity with time is recorded by an oscilloscope attached to the mass spectrometer. The ion-molecule reaction rate constants can be calculated directly from the time change of intensity of an ion and the neutral concentration. Unfortunately since the excitation pulse can excite and dissociate the neutral gas, the ions may not be reacting with ground state molecules. This technique was used to obtain the first values of aeronomic reactions. Sayers and Smith (46) observed the reaction of  $O^+$  ions in oxygen and obtained a rate constant which was

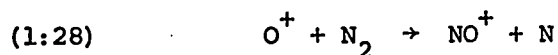


temperature dependent. Fite *et al* (45) observed the attachment of  $N_2$  to  $N_2^+$  and calculated a value for the rate constant.



The technique of a flowing afterglow was developed by Ferguson, Fehsenfeld and Schmeltekopf (47) to study ion-molecule reactions at thermal energies. In this technique, helium which has been ionized or excited by a microwave discharge flows through a tube at a pressure of about .5 torr. Reactant gases are injected downstream from the discharge. The He ions and excited He atoms ionize the reactant gas molecules. A second gas whose reactions with the primary ions are to be studied

is injected further downstream. The ions are sampled mass spectrometrically at the end of the flow tube. The reaction time can be calculated from the gas flow rate and path length. Since the reactant gas is injected below the discharge, most of the neutral molecules will be in the ground state. Ferguson *et al* developed the apparatus so that the reactant gases could be excited by a second discharge, just before they entered the stream, and so such unstable species as atoms could be added to the reaction in a very selective manner. They were able to study many ion-atom interchange reactions of aeronomic interest. These reactions had not been successfully investigated before. For example, the variation of the rate of reaction of (1:28) with the



vibrational temperature of  $\text{N}_2$  was measured (48).

Because the pressure of the carrier gas He is low  $\sim .5$  torr, and the partial pressures of the reactant gases even lower, only reactions with large rate constants ( $10^{-9}$  to  $10^{-11}$  cc/molecule sec.) may be studied. Fortunately most ion-atom interchange reactions have large reaction rates (49). The problems of mixing of the gas with the flow stream and the effect of ambipolar diffusion coefficients and ion detection efficiencies limit the accuracy of the rate constants to within a factor of two or three. However, this is the case for most reactions studied at high pressures.

### 1:7 The Development of the Present Instrument

The major limitation of the previous high pressure mass spectrometer built in this laboratory for the study of thermal ion-molecule reactions, was the uncertainty of the reaction time. Since the ions were removed by mass flow and diffusion, the time an ion remained in the ion source could only be estimated. The present instrument was designed so that reaction times could be measured accurately.

High energy electrons were chosen instead of  $\alpha$  particles for the source of ionization as an electron beam is conveniently pulsed. The energy used (4000v) provided a reasonable penetrating power. The pulse technique was similar to those used previously. Ions were formed by a short pulse of electrons. At a certain time later the ions leaving the ion source were admitted to the mass analyser by means of a second pulse and thus the time history of each ion intensity could be obtained by varying the time.

The ion-molecule reactions studied by this technique are described in chapters 4, 5 and 6. Since the actual reactions are not all related, the relevant background and survey of previous results will be given at the beginning of each chapter.

General reviews of ion-molecule reactions are given in the following references. Low pressure results are discussed in (13,15,16 and 22). Some of the recent reviews on high pressure mass spectrometry and thermal ion-molecule reactions are references

(39,42,49,50 and 51). The role of ion-molecule reactions in radiation chemistry has been reviewed by Ausloos (52).

## 2 EXPERIMENTAL

### 2:1 Requirements and Design of the Present Instrument

This instrument was designed with several requirements in mind. We wanted to operate the ion source at pressures of several torr and this required a large capacity pumping system to keep the mass analyser at low pressure.

A convenient source of ionizing radiation was required. A high energy beam of electrons was chosen as it was easy to pulse and reasonably safe to operate. Its use does not have the problems associated with the use of radioactive particle sources such as Polonium 210 which gradually spreads in vacuum and leads to contamination of the apparatus. An electron beam is conveniently pulsed by a pair of electrostatic deflection plates.

Finally a mass analyser was required. A quadrupole mass spectrometer was chosen as it has a high transmission and thus greater sensitivity than a magnetic instrument. The absence of a magnetic field makes ion beam collimation easier. The quadrupole unit also has a relatively low cost and is compact so that it is easily mounted in a vacuum chamber. The main components of the instrument are shown in figure (2:1).

### 2:2 The Ion Source

The high pressure ion source is shown in figure (2:2). It was made from a  $1\frac{1}{2}$  inch long, 3 inch diameter cylinder of non-magnetic stainless steel (type 304), through which a  $\frac{5}{8}$  inch

Figure 2:1

1. Electron filament.
2. Filament support plate.
- 3 & 4 Electron extraction electrodes..
5. Grounded cone (electron acceleration electrode).
6. Collimating electrode.
7. Solenoid coil providing axial magnetic field for electron focussing.
8. T.V. yoke for horizontal and vertical motion of the electron beam.
- 9a,b Deflection plates for electron pulsing.
10. Fluorescent beam focussing screen.
11. Electron entrance cone carrying slit leak.
12. Ion exit cone carrying circular leak.
13. Ion source with heaters.
14. Electron trap.
15. Cylindrical shielding screen.
- 16-20 Ion acceleration and focussing electrodes.
21. Quadrupole mass analyser.
22. Secondary electron multiplier.
- 23,24 Gas inlet tubes.

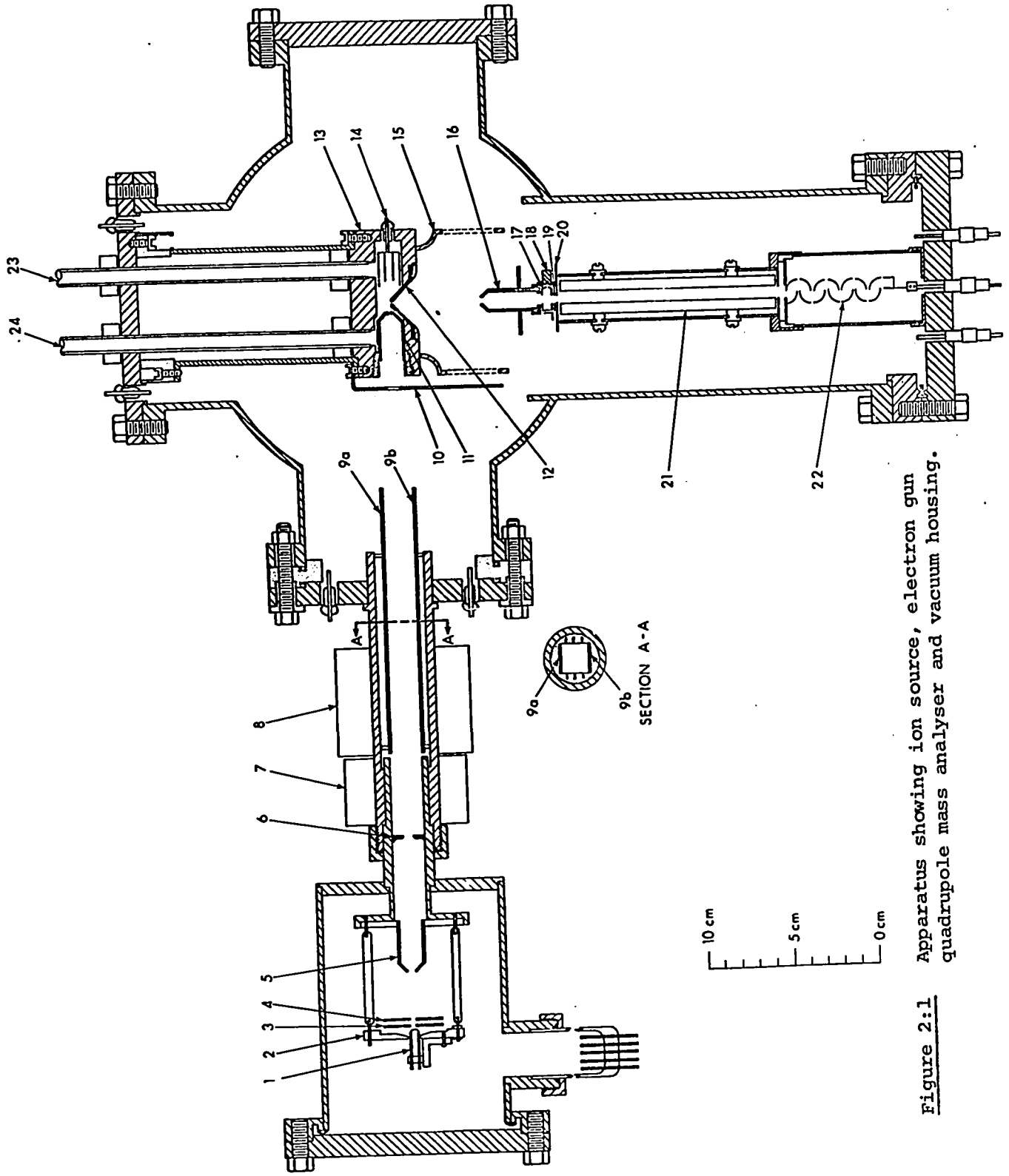


**Figure 2:1** Apparatus showing ion source, electron gun quadrupole mass analyser and vacuum housing.

Top View

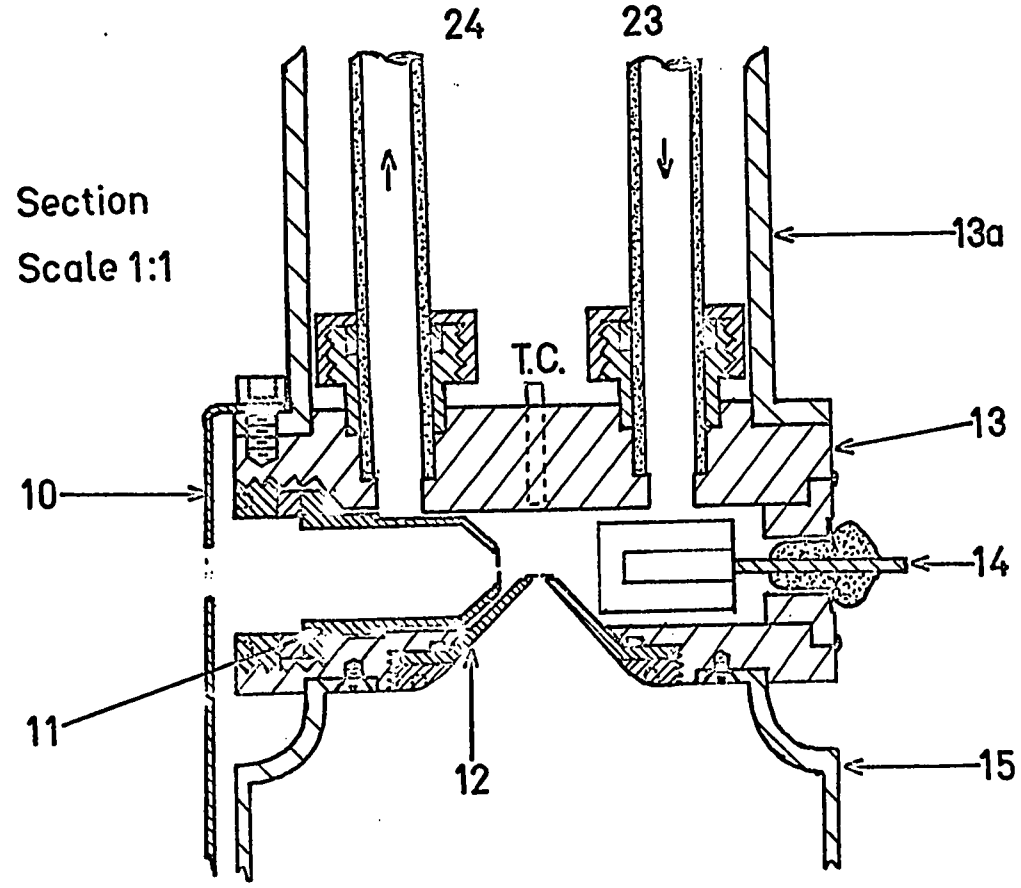
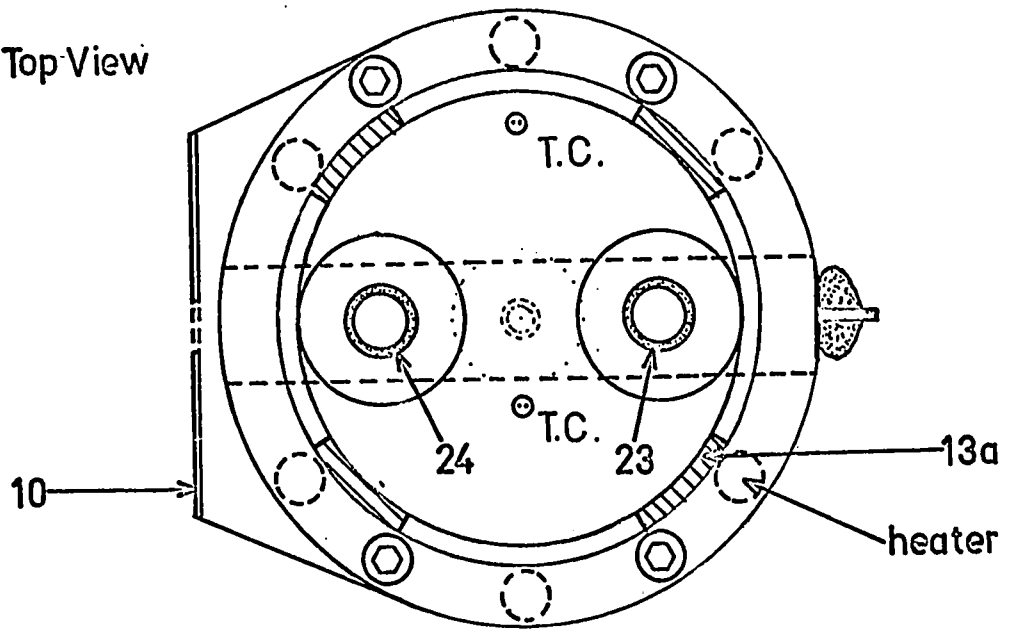


Figure 2:2 Top view and section of the high pressure ion source.



channel was bored perpendicular to the axis to provide a gas chamber. On the left-hand side was mounted a cylindrical electron entrance cone [11] which was sealed to the body of the ion source by a Viton "A" O-ring and held in place by a threaded steel ring. The right-hand end of the chamber was plugged by a steel insert which contained a Kovar glass high resistance electrical feed through [14] on which was mounted a Faraday cup electron trap. The trap was made from two concentric cylinders of .001" Tantalum spot welded. The trap was made from two concentric cylinders so that most of the secondary electrons emitted by impact of the primary electron beam, would not be able to escape from the trap.

Two gas inlet tubes [23,24] were sealed into the ion source (by an O-ring seal) so that gas could be flowed through. In most of these experiments, however, the exit tube [24] was sealed and gas flow was not used.

The electron beam entered the ion source through a small slit mounted on the cone [11]. The slit was made by welding stainless steel razor blades to a circular disc of .007" thick Tantalum which contained a 1.7 mm (1/16") hole. The final size of the slit was 1.70 mm x 0.040 mm. The Tantalum disc was welded to a narrow ring of platinum which in turn was soft soldered to the stainless steel electron entrance cone [11].

The ions left the ion source through a small hole mounted in a cone [12] which was sealed by an O-ring into

the bottom of the source. The ion exit hole was a 0.120 mm diameter hole drilled with a fine needle point in a 0.001" Tantalum disc. This in turn was spot welded onto a platinum washer which was soft soldered onto the top of the ion exit cone. The ion exit slit cone was held in place by a threaded ring. The inside of the ring was bevelled so that the high vacuum side of the ion exit cone consisted of a smooth conical surface with a solid angle of  $40^\circ$ .

Below the ion source was mounted an electrostatic shield [15] which provided a boundary for the electric field between the ion source and the ion acceleration electrodes (see figure 2:1). The shield was a thin wall cylinder slotted longitudinally so that the gas pumping speed was as high as possible, without deforming the electric field.

In front of the ion source entrance slit there was placed an electron beam focus plate [10]. This plate contained a 1/4" hole axial with the electron entrance cone. The plate was coated with a mixture of phosphor, sodium silicate, and sodium chloride. The electron beam caused the phosphor to glow so the beam could be focussed. The sodium chloride was added to make the phosphor coating conductive to prevent surface charging. The electron focus plate was extended down in front of the electrostatic shield [15] to prevent spurious ionization, caused by stray electrons from the electron beam.

The ion source was heated by six heaters made from 28 gauge nichrome wire, spiral wound on ceramic centres and insulated from the metal block by quartz tube insulators. Two iron-constantan thermocouples [T.C.] were inserted into the ion source. One was close to the heaters so that it could be used to control the temperature. The second was inserted in a well close to the gas chamber so that the gas temperature could be read. It was assumed that the gas reached the temperature of the walls of the ion source chamber. The thermocouples were mounted in short lengths of 1/8" copper tube which fit the wells tightly. The thermocouple joint was electrically insulated from the copper by thin strips of mica. The electrical insulation was only sufficient for a few hundred volts. However it provided electrical insulation between the ion source and the heater temperature controller.

The ion source was mounted on the vacuum chamber port flange by a cylindrical steel support [13a] which was electrically insulated by a disc of Araldite epoxy resin. The Araldite plastic could withstand a temperature of approximately 100°C before plastic deformation took place. The steel support was slotted to decrease heat conduction. The Araldite insulator was bolted directly to the flange which remained at room temperature and thus its temperature remained approximately the same. Nine electrical feed throughs were provided on the

flange. The gas lead-in tubes [23,24] were heated by nichrome wire heaters wrapped around the glass. An iron constantan thermocouple was attached to the inlet tube [23] by glass tape.

### 2:3 Temperature Control and Measurement

About 40 watts were required to heat the ion source to its maximum allowable temperature of 150°C. The temperature was controlled by manual setting of the heater voltage. It was found that this steady state method gave a much more constant temperature than when a temperature controller (A.P.I. Instrument Co. Model 905B) was used. The heater voltage was supplied by an auto transformer (Variac) connected to a constant voltage transformer.

The thermo-electric e.m.f. of the thermocouple close to the gas chamber was measured by a potentiometer. Ice water was used for the reference thermocouple. The temperature could be read to within one degree centigrade.

### 2:4 Vacuum Chamber

The main vacuum chamber was an 8 inch diameter stainless steel tube (figure 2:1) about 12 inches long. This was pumped by a National Research Corporation (HS6-1500) 6 inch, 1500 liters per second, diffusion pump through a water-cooled optical baffle. The pumping speed at the top of the baffle was quoted to be 750ℓ/second. One can calculate the pumping speed at the ion source (at the end

of the chamber) if the conductance of the lead is known by equation (2:i) from Dushman (53, p. 130)

$$(2:i) \quad \frac{1}{S} = \frac{1}{S_p} + \frac{1}{F}$$

where  $S$  is the pumping speed at the ion source and  $S_p$  is the speed at the pump (750ℓ/sec.).  $F$ , the conductance of the lead, may be obtained from a table as in reference (53, p.97) or (54, p.63). In this case  $F = 1000\ell/\text{sec.}$  and thus  $S = 400\ell/\text{sec.}$

At the top of the pumping lead four 4 inch pipes were welded into the 8 inch lead, mutually perpendicular, to provide mounting flanges (see figure 2:1). The one designed to hold the quadrupole probe was made "T" shaped. A second high capacity diffusion pump (NRC VHS-4) was mounted on this flange so that the quadrupole was differentially pumped. An ion gauge tube was mounted on the flange which is shown unused in figure (2:1).

The leakage of gas from the ion source was very high. Gas leaked through the ion exit hole and the electron entrance slit. Since the latter was larger most of the gas escaped through it. The conductance  $F_\ell$  of an aperture under molecular flow conditions is given by (2:ii) (53), where  $\bar{U}$  is the average velocity of the

$$(2:ii) \quad F_\ell = \frac{\bar{U}}{4} A$$

molecules, and  $A$  the area of the aperture. If  $A$  is in  $\text{cm}^2$ , and  $\bar{U}$  in  $\text{cm}/\text{sec.}$   $F_\ell$  is in units of  $\text{cc}/\text{sec.}$  The two apertures had

areas of  $1.1 \times 10^{-4} \text{ cm}^2$  (ion exit leak) and  $6.8 \times 10^{-4} \text{ cm}^2$  (electron entrance slit). At  $300^\circ\text{K}$  the velocity of  $\text{N}_2$  gas is  $4.77 \times 10^4 \text{ cm/sec}$ . The calculated conductance of both leaks would be  $9.3 \text{ cc/sec}$ . The measured conductance was  $8.5 \text{ cc/sec}$ . This indicates that the flow out of the ion source was essentially molecular.

The pumping speed at the ion source (actually at the ion gauge which was close to the ion source) can be calculated by use of equation (2:iii), where  $F_\ell$  is the total conductance of the leak,

$$(2:iii) \quad F_\ell P_s = S P_g$$

$P_s$  the source pressure and  $P_g$  the ion gauge pressure. At  $300^\circ\text{K}$   $F_\ell$  was measured as  $8.5$  for  $\text{N}_2$ ,  $P_g$  was  $1.7 \times 10^{-5}$  torr when  $P_s$  was  $1.1$  torr. If these values are substituted into equation (2:iii), then  $S = 560 \text{ l/sec}$ . which is close to the value of  $400 \text{ l/sec}$ . calculated before. Since the ion gauge is closer to the pump one would expect that the pumping speed obtained on the basis of the ion gauge reading will be somewhat larger than the actual value at the ion source.

## 2:5 Gas Inlet System

The gas inlet system is shown in figure (2:3). The construction materials were stainless steel and glass. The vacuum line was surrounded by an oven which could be heated up to  $150^\circ\text{C}$  to bake out impurities. The pressure in the ion source and the gas inlet

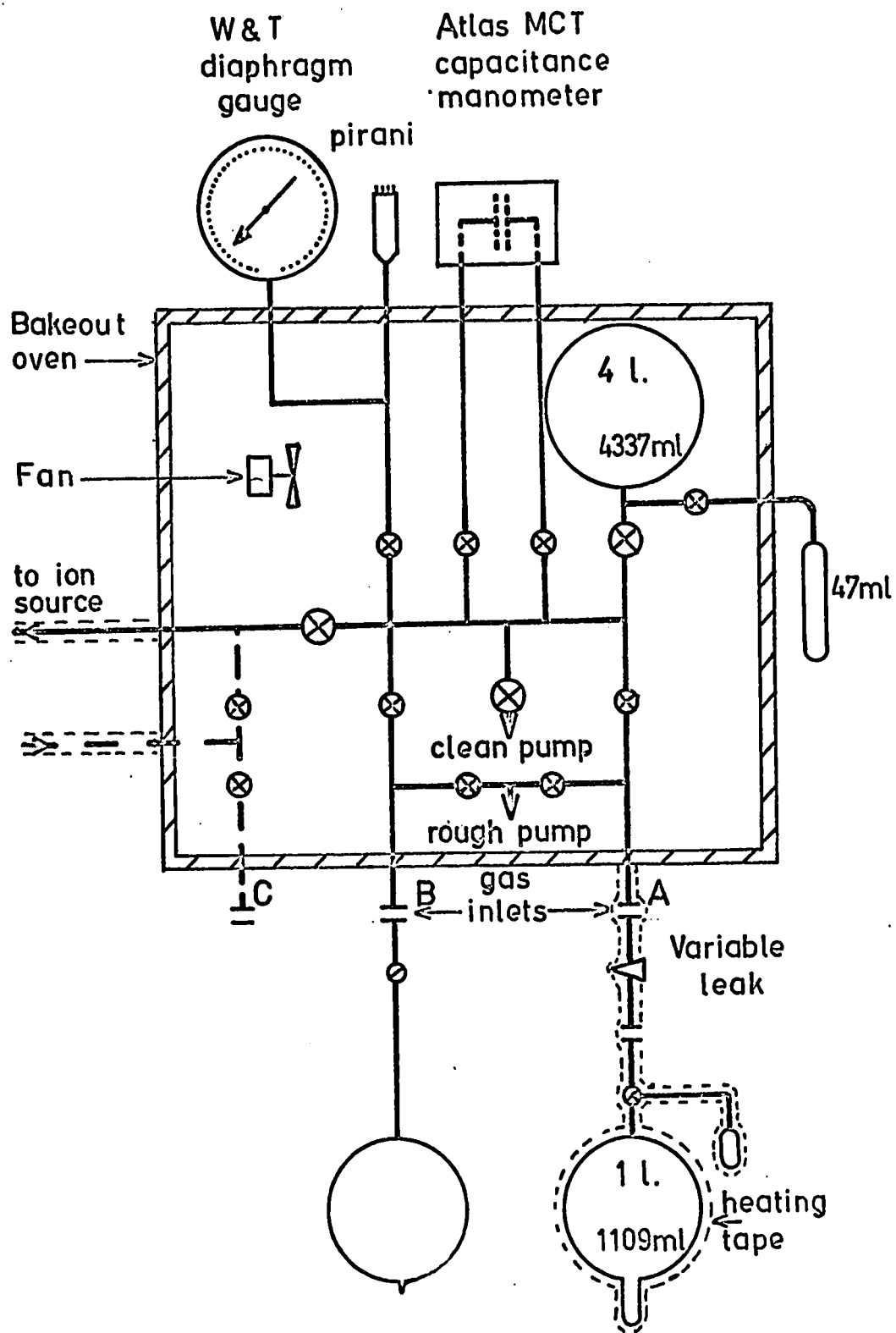


Figure 2:3 Gas inlet system and pressure measuring gauges.

system manifold was measured by means of an Atlas MCT manometer which read pressures up to 20 torr. Higher pressures up to 200 torr were measured by the Wallace Tiernan mechanical diaphragm gauge. The gas handling plant could be pumped by either of two pumping systems. The rough pump was used to remove large amounts of gas. The "clean" pump was used to remove the last traces of gas. Since the clean pump did not pass large quantities of gas, it had very low back streaming and thus the impurity levels in the gas inlet system and ion source could be kept very low. Large conductance valves were placed in the line between the storage bulb and the manifold and the manifold and the ion source so that there would not be any appreciable pressure drop between the bulb and the ion source. The diameter of the manifold and the tube to the manifold was 1.5 cm. The large conductance valves had 3/4 inch diameter cross sections. The small valves had about 3/16 inch diameter openings.

During construction of the inlet system the 4 liter bulb was calibrated by weighing the amount of water it could hold. The volumes of the other parts of the inlet systems were measured by expansion of gas from the 4l bulb. The calibration was required so that gas mixtures could be made.

## 2:6 The Electron Gun

The electron gun is shown in figure (2:1). Electrons emitted from the filament [1] were accelerated slightly by



the field between the filament support plate [2] and the extraction electrode [3]. They were then accelerated and focussed slightly by the focus electrode [4] and finally accelerated to the grounded cone [5]. The potentials on the electrodes were as follows. The filament support plate [2] potential was -4000 volts. The centre of the filament also had this potential. The extractor [3] potential was -3990 volts. The focus [4] potential could be varied from -3500 to -3900 volts. The gun was designed with a large distance between the group of electrodes at high voltage [1,2,3 and 4] and the grounded cone [5] so that it could be operated at voltages up to 25 kv. The electron beam was focussed by the solenoid coil [7] (1000 turns of 22 AWG copper wire with 0.2 to 1.5 amps generally required for focussing). Horizontal and vertical deflection of the beam was obtained from a television tube yoke which was also outside the vacuum envelope. The vacuum envelope at this point was made from brass so that the magnetic fields would not be seriously disturbed. The solenoid was controlled by a low voltage (7 volts) gas chromatograph dc supply modified so that two outputs were available.

The deflection plates are [9] and [9a]. A cross section of the tube at this point is shown figure (2:4). Electrostatic plots were made by means of conductive paper to find the required number of guard plates so that the field would be uniform. Three were required. The electrostatic potentials

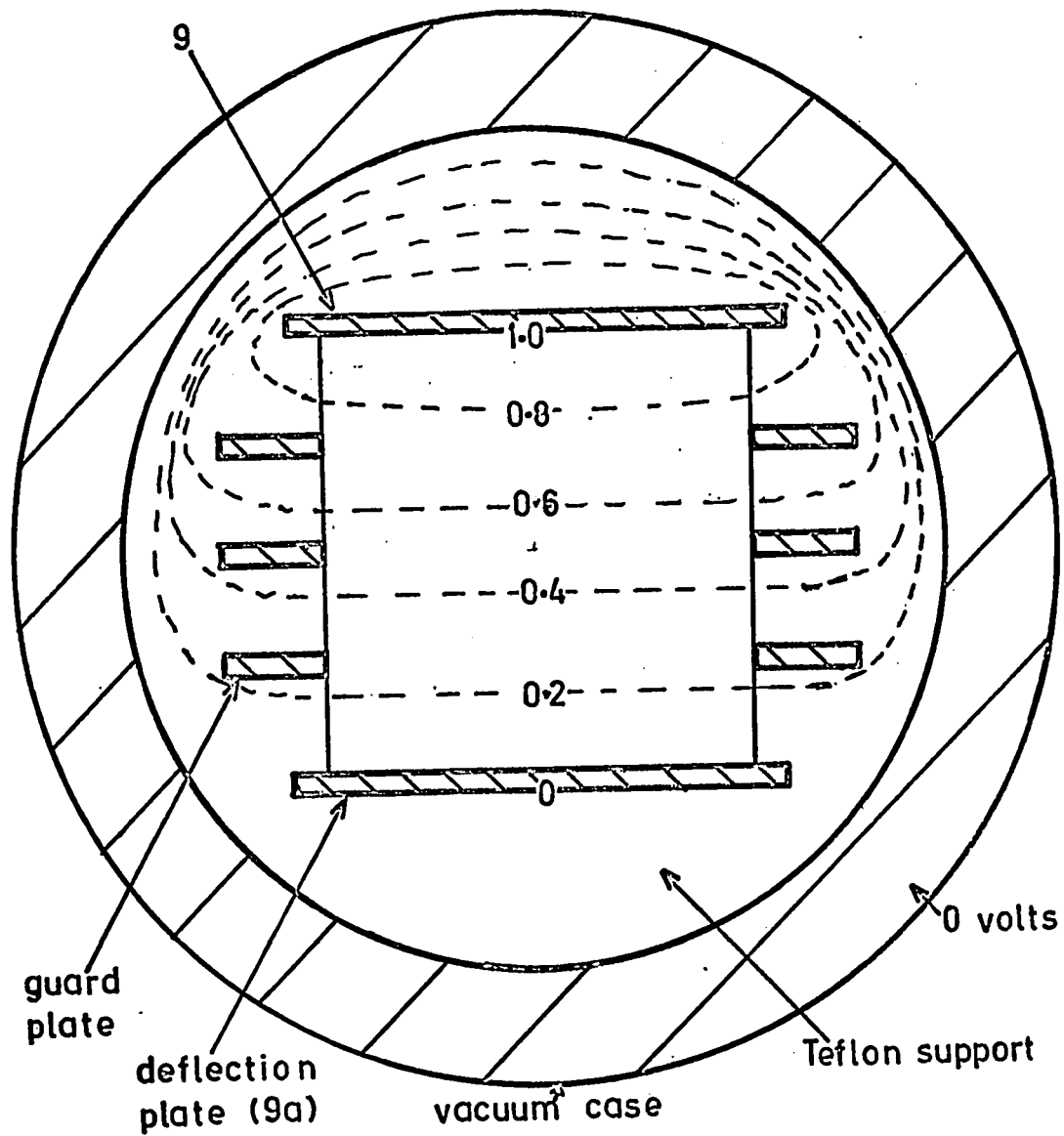
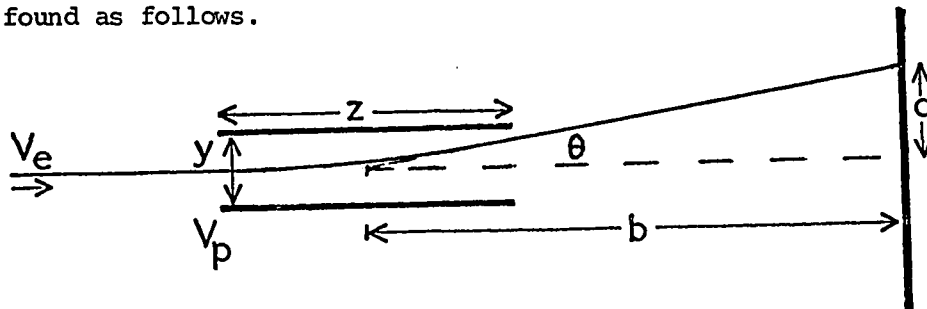


**Figure 2:4** Cross section of deflection plates showing guard plates and electric field potential lines. Section (A-A) of figure (2:1), Scale 4:1.

are shown in figure (2:4). One plate [9a] was kept at 0 potential and the pulse applied to the other. A network of resistors (total resistance  $10^4$  ohm) was placed across the guard plates so that there was a uniform voltage gradient across them. The  $10^4$  ohm resistance was also used to terminate the coaxial cable from the pulse generator so that the voltage pulses experienced by the plates were as square as possible. Electrode [6] was a collimation aperture to prevent stray electrons from hitting the deflection plates. Electrode [10] is the focus plate. The beam could be focussed to a spot from 2 to 5 mm in diameter (depending upon the position of filament used) and deflected about 8 mm from the centre.

The voltage required to deflect the electron beam is found as follows.



The angle is found from equation (2:iv) (55).

$$(2:iv) \quad \tan \theta = \frac{Z}{2y} \frac{V_p}{V_e}$$

where  $Z$  is the length of the plates and  $V_e$  the electron acceleration voltage across the plates and  $V_e$  the electron acceleration voltage.

Since  $\tan \theta$  is also related to the amount of deflection  $a$  and

the distance  $b$  from the centre of the plates to the focus plate,

$$(2:v) \quad \tan \theta = \frac{a}{b}$$

The voltage required to deflect the beam can be calculated from

(2:vi). If  $a = 1$  cm,  $b = 13$  cm,  $z = 15$  cm,  $y = 2$  cm,  $V_e = 4000$  volts,

$$(2:vi) \quad V_p = 2V_e \frac{a}{b} \frac{y}{z}$$

then  $V_p = 60$  volts. The pulse generator output could be varied from 0 to 40 volts and thus if the beam was centred on the focus plate hole 5 mm diameter it could be moved completely clear (about 8 mm).

Two materials were used for the electron gun filament. The first was tungsten ribbon  $\sim .005'' \times .030''$ . This was used for the experiments involving  $CH_4$  and  $K_r$ ,  $C_2H_4$  and  $X_e$ . The life of the filament was reduced drastically by oxygen. In this case a thoriated iridium filament was used. This filament material was very stable in oxygen. It also performed well with nitrogen although initially the presence of  $N_2$  decreased the emission.

### 2:7 Ion Acceleration and Gating

The ion acceleration electrodes are shown as [16] to [20] in figures (2:1) and (2:5). Two sets of electrodes were used. The first is shown in figure (2:5a) and the second in (2:5b). Ions leaving the high pressure ion source exit [12] were accelerated by a negative potential to the quadrupole entrance cone [16]. This

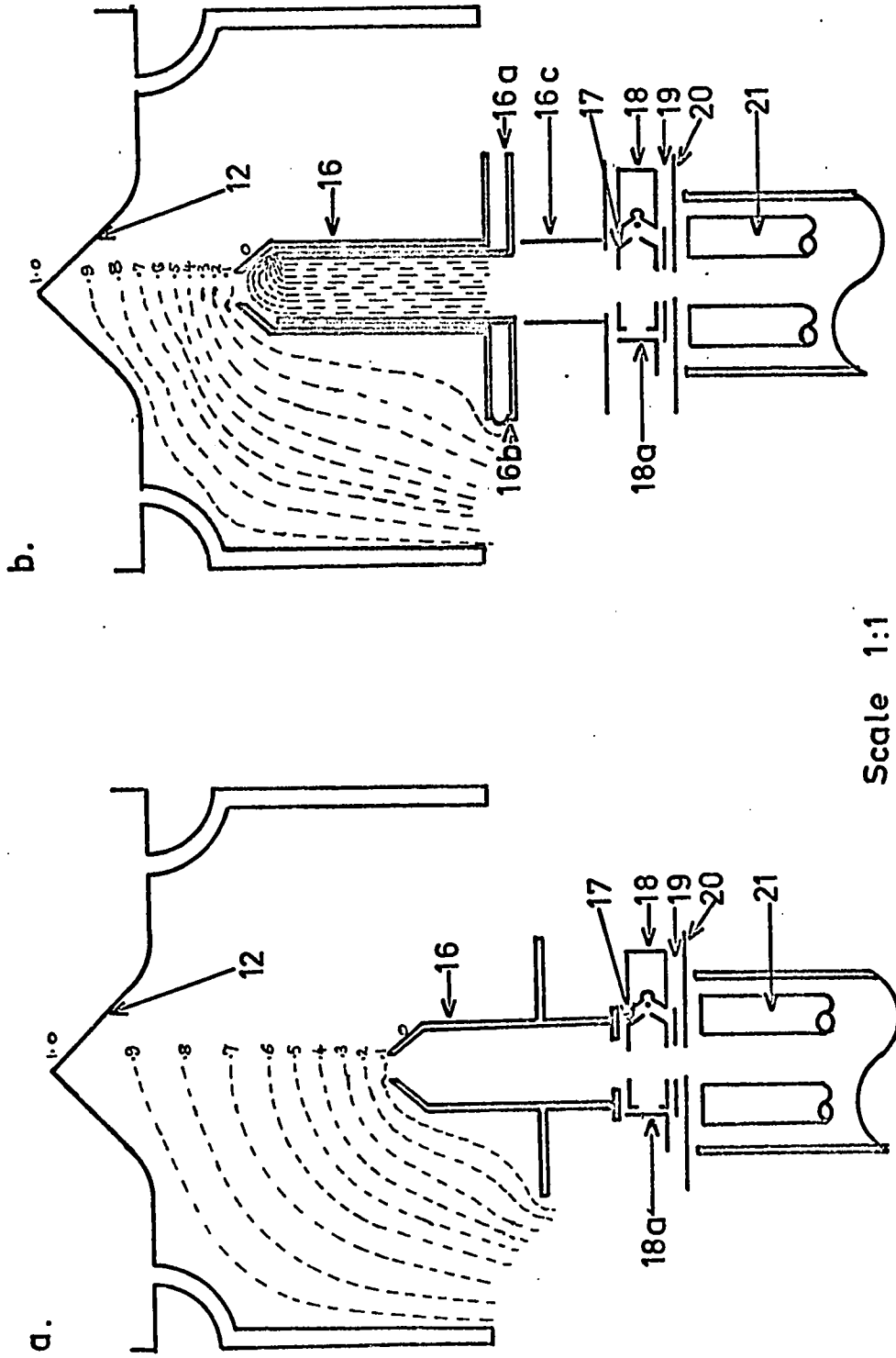


Figure 2:5 Ion acceleration electrodes.

(a) Electrodes 17, 18 and 19 used as the ion gate. (b) Electrode 16a, b used as the ion gate.

cone was mounted upon the existing quadrupole mass spectrometer ion source plates [17] to [20]. The ions passed through this auxiliary ion source into the quadrupole.

This auxiliary source was used for low pressure gas analysis. [17] is what is normally called the case of an ion source. [18] is the electron filament support and reflector (Pierce gun type) and [18a] the normal trap. The ion acceleration potential (about 7 volts) was applied between [17] and [20] the quadrupole entrance aperture. Electrode [19] was an ion focussing electrode.

The electrode potentials are shown in Table 2:1. The ion source potential was kept at +7.5 volts as this was the value which gave maximum signal on the high mass range of the quadrupole analyser.

For the earlier experiments, the studies on methane krypton, ethylene-xenon and oxygen, the electrodes in figure (2:5a) were used. In this case the electrodes [19] and the bottom half of [17] were pulsed to "gate" the entrance of ions into the mass analyzer. When the gate was closed electrodes [17] and [19] were at +40 V. The pulse from the generator (-40 V) returned this to zero so that the ions could pass through for the duration of the pulse.

Because of the presence of a battery (40 volts) in the pulse line it was found that the pulses were not square due to the large capacitance. The second group of electrodes shown

TABLE 2:1Potentials on Ion Acceleration Plates

Electrode	Electrode Potentials Volts
A. When auxiliary ion source used.	
16	0
17	+7.5
18	+7.5
19	-50
20	0 grounded
B. When high pressure source used as (2:5a)	
12,13	+7.5
14	+7.5
16	-90 to -225 v
17	0 gate open (pulsed)
18	+40 gate closed
19	
20	0 grounded
C. When high pressure source used as (2:5b)	
12,13	+7.5
14	+7.5
16	-67.5
16a	-67.5 gate open (pulsed)
	{ 0 gate closed
16c	0
17	0
18	0
19	0
20	0 grounded

in figure (2:5b) were designed so that the capacitance of the system could be reduced to obtain square pulses and also so that the flight time of the ion from the ion source to the ion gating position was reduced.

The ions could be deflected by the pair of plates [16a] and [16b]. These were two half cylinders mounted inside the cone. The electrode [16b] was kept at the cone potential (-67 volts) all other electrodes [16c] to [20] were kept at ground potential. During the interval between pulses, electrode [16a] was kept at zero potential. All ions would be deflected and discharged on [16b] or [16c]. A negative pulse (-67 volts) was applied to [16a] so that the space inside the cone became field free and the ions passed through into the quadrupole analyser.

#### 2:8 Travel Time of the Ion from the Ion Source to the "Gate" Electrodes

It was necessary to know the travel time of an ion from the ion source to the point at which the ion "gate" potential was applied. This travel time was calculated from the potentials of the electrodes.

A simple model was used at first for the electrodes in figure (2:5a). We assumed that the ion accelerated across a uniform field between the ion exit cone [12] and the quadrupole



entrance cone [16] and then travelled at constant velocity through the cone to the ion gate [17,19] where it was stopped. It was observed that the two distances were about the same. For an ion accelerating in a uniform field the terminal velocity  $U_t$  is given by (2:vii),  $e/m$  is the charge to mass ratio and  $V$  is

$$(2:vii) \quad U_t = \frac{2eV}{m}$$

the potential of the field. Since the average velocity is half the final velocity, the time is given by (2:viii) where  $s$  is the

$$(2:viii) \quad t = \frac{2s}{U_t}$$

distance between the cones. Since the ion travelled at constant velocity  $U_t$  through the quadrupole cone of length  $s'$ , this time is given by (2:ix). Since the two distances were equal,  $s' = s$ ,

$$(2:ix) \quad t' = \frac{s'}{U_t}$$

the total flight time  $t_f$  is given by (2:x). This formula was

$$(2:x) \quad t_f = 3s \sqrt{\frac{m}{2eV}}$$

used to find the flight times used for the methane-krypton results. The flight times are shown below in Table 2:2.

TABLE 2:2

Flight Times of Ions Calculated by Equation (2:x)  
for Electrodes Shown in Figure (2:5a). Acceleration voltage = -225 volts

Ion (m/e)	Flight time (micro sec.)	Value used
Kr <sup>+</sup> (84)	5.8	6
CH <sub>3</sub> <sup>+</sup> (15)	2.53	3
CH <sub>4</sub> <sup>+</sup> (16)	2.7	3
CH <sub>5</sub> <sup>+</sup> (17)	2.45	3
C <sub>2</sub> H <sub>5</sub> <sup>+</sup> (29)	3.4	3
O <sub>2</sub> <sup>+</sup> (32)	3.6	4
O <sub>4</sub> <sup>+</sup> (64)	5.0	5

$$s = 4.5 \text{ cm}, V = 232 \text{ volts}, e = 1.6 \times 10^{-12} (\text{g cm}^2/\text{sec}^2), m = g/6.023 \times 10^{23}$$

A second method was used to calculate the flight time. The assumption that the field was uniform was not correct as the field did not penetrate the ion exit cone evenly. The cross section of the ion source and electrodes was drawn with silver conductive paint upon conductance paper. Electrostatic plots were obtained for both electrode systems. These are shown on figure (2:5). The total potential was divided into ten equal units. The time the ion took to travel from one equipotential line  $n$  to the next  $(n+1)$  was calculated. The total time is given by the

summation of these times by equation (2:xi), where the voltages

$$(2:xi) \quad t_f = \sum_0^n \sqrt{\frac{2m}{e}} \frac{d_n (\sqrt{V_n} - \sqrt{V_{n-1}})}{\Delta V} \quad n=1 \text{ to } 10$$

at an equipotential level  $n$  is given by  $V_n$ , and distance between  $n$  and  $n-1$  is  $d_n$ .  $\Delta V$  is one tenth, in this case, of the total potential  $V$  and equals  $(V_n - V_{n-1})$ .

It was found that since the equipotential lines were more widely separated at the beginning of the ion's path, the times were slightly larger. The difference was less than 1 micro second. The travel times for nitrogen were calculated this way.

TABLE 2:3

Flight times of Nitrogen Ions Calculated by Equation (2:xi)

Electrode Arrangement Shown in Figure (2:5b)

Acceleration Voltage = -67 volts

Ion	Flight time (micro sec.)
$N^+$	3.2
$N_2^+$	4.5
$N_3^+$	5.4
$N_4^+$	6.4

## 2:9 Pulse Circuits

The order of the pulse generators is shown in figure (2:6). The order of the pulses is shown on figure (2:7). The first pulse generator (General Radio, Type No. 1217-C), was used to generate the pulse of width  $\Delta t_e$  applied to the electron beam deflection plates. The synchronization signal was fed into the oscilloscope (Tektronix 536), and generator number 2 (Datapulse Model 100). This was used as a variable delay, to change the times  $t''$  between the pulses. This delay time was the reaction time  $t$  plus the flight time  $t_f$ . The output of this generator (actually the delayed synchronisation pulse) was used to trigger the third generator (Datapulse Model 100) which produced the ion gate pulse of width  $\Delta t_i$ . The delay time  $t''$  was measured visually by means of the oscilloscope as the vernier scales on the pulse generators were not accurate. The technique of using an ion gate to establish the ion reaction time was chosen as it allowed the mass spectrometer to operate continuously. Since the signal amplifier had a slow response time, the signal indicated on the chart recorder was the integrated signal from many successive pulses.

## 2:10 Quadrupole Mass Analyser and Detection System

### The Measurement of the Transmission of the Analyser

The quadrupole mass spectrometer was an Electron Associates Inc. Model 200. Three mass ranges were provided, Low (1-50),

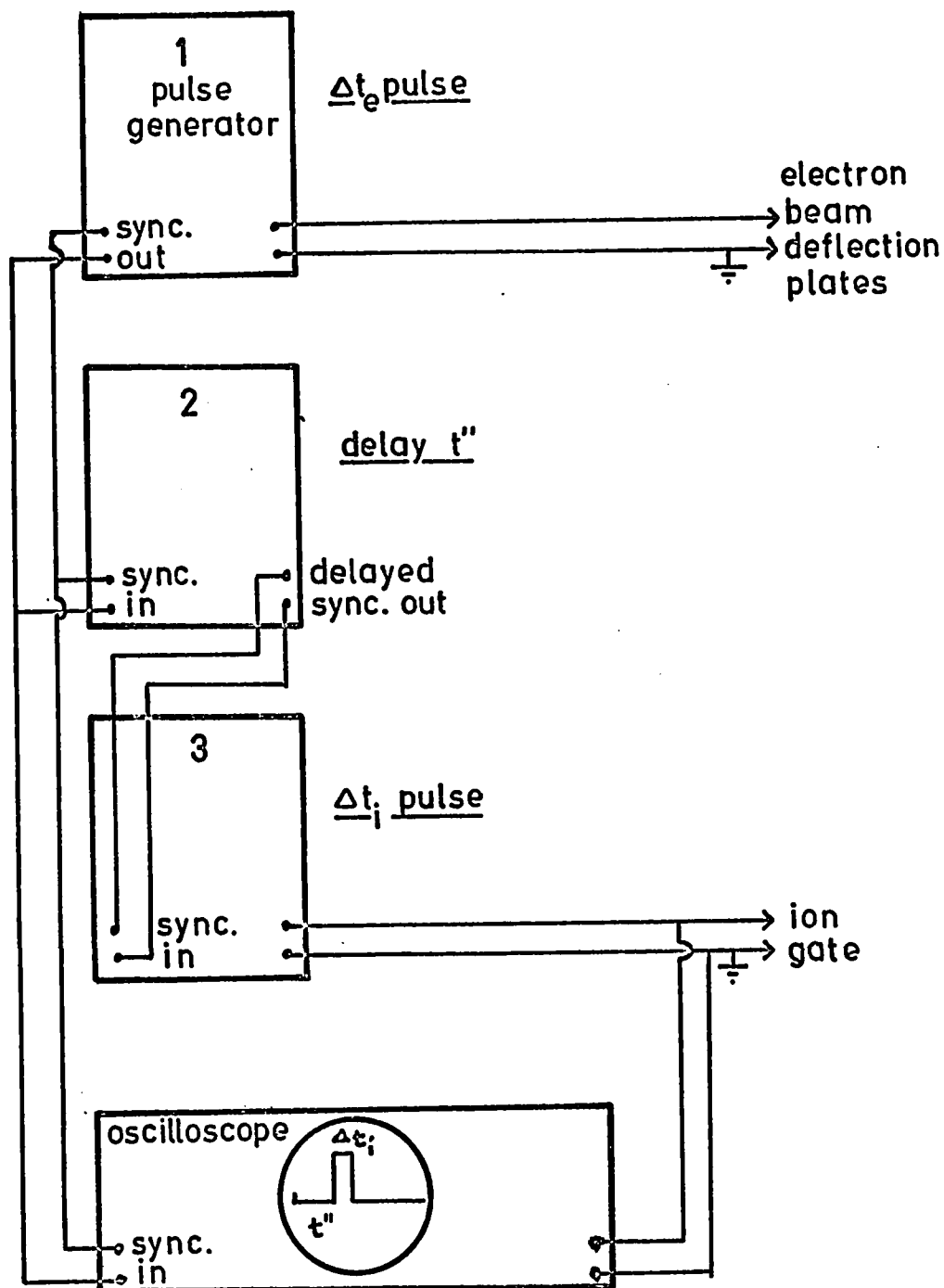


Figure 2:6 Pulse generation circuit.

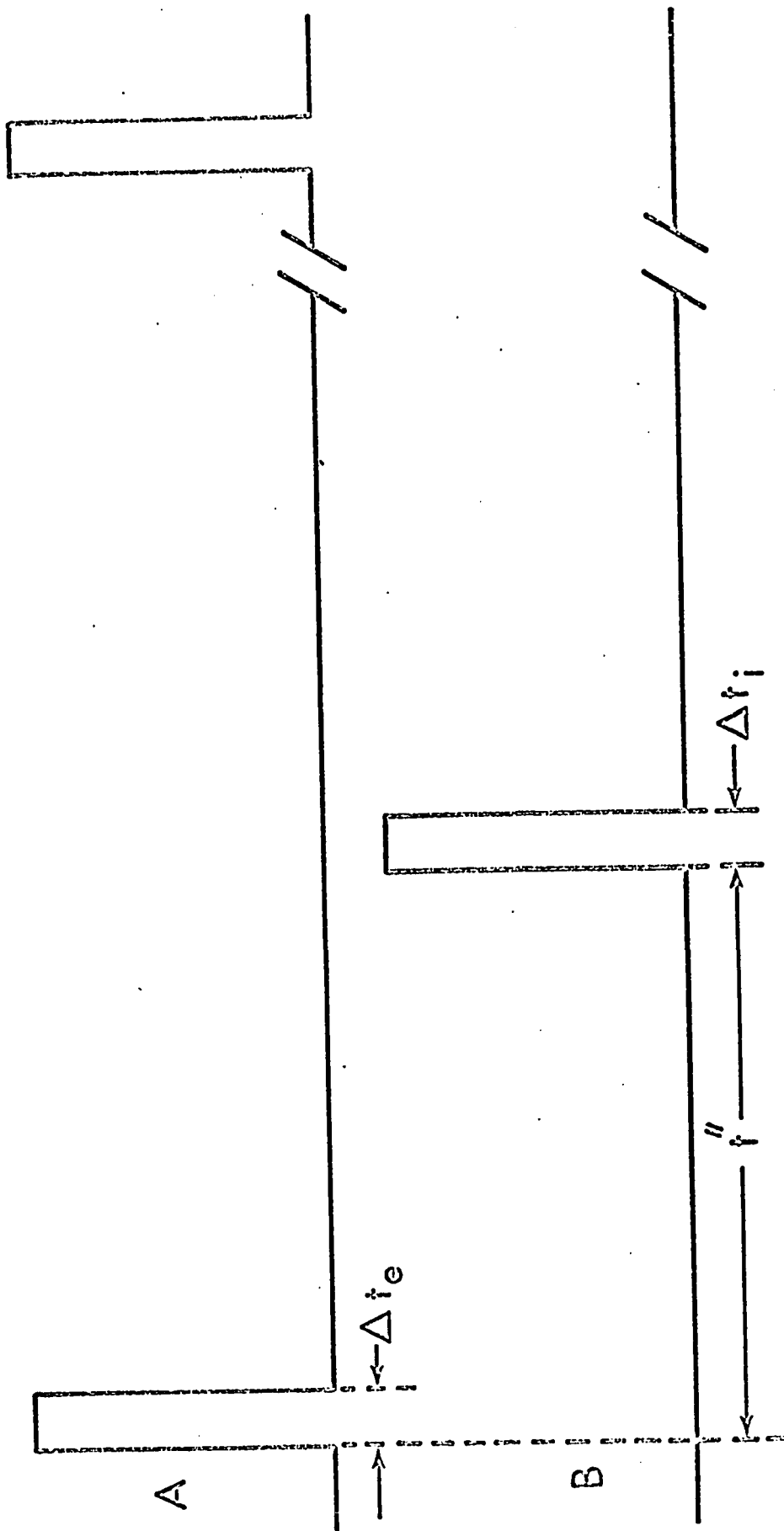


Figure 2:7 Pulse sequence.  $\Delta t_e$  electron pulse,  $\Delta t_i$  ion pulse,  $t$  delay time.

Medium (10 to 150) and High (10 to 500). The quadrupole probe was powered by an R.F./D.C. Generator which was part of the unit. Ion detection was by means of an electron multiplier from which the signal was fed into a Keithley Model 416 Picoammeter, and thence into a high speed oscillographic recorder (Sanborn 4500 series). Since the theory of operation of a quadrupole analyser may be required to explain the operation it is given below.

The quadrupole mass spectrometer was developed by Paul and co-workers (56,57,58). It consists of four long parallel rods (figure 2:8a). Theoretically the cross section of the rods should be hyperbolic, but a circular cross section may be used. Opposite pairs are connected together electrically. A dc voltage  $U$  and an rf voltage  $V_0 \cos \omega t$  are applied to the poles so that the positive pair of electrodes has a potential  $+(U + V_0 \cos \omega t)$  and the negative pair a potential  $-(U + V_0 \cos \omega t)$ . The electrodes are separated by a distance  $2r_0$  and the potential  $V$  at any point is then given by equation (2:xii), where  $x$  is the

$$(2:xii) \quad V = \left( \frac{x^2 - y^2}{r_0^2} \right) (U + V_0 \cos \omega t)$$

direction of the positive rods,  $y$  is that of the negative rods and  $z$  is the longitudinal axis. Ions are accelerated into the rf-dc field along the  $z$  axis. The motions of the ions are described by equations (2:xiii) to (2:xv).

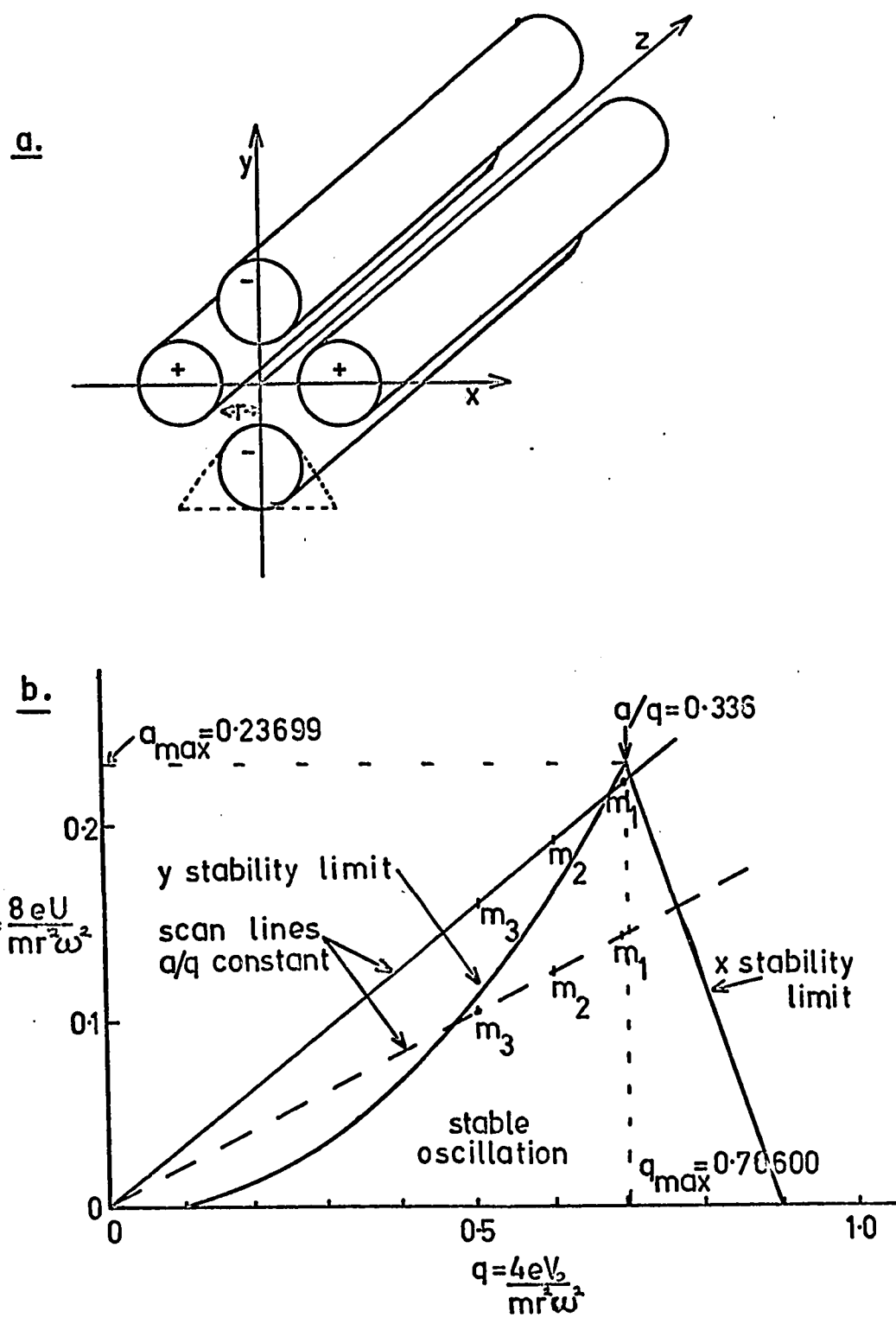


Figure 2:8 (a) Quadrupole rods. The hyperbolic cross section is approximated by a circular cross section.  
 (b) Stability diagram of the Mathieu parameters a and q.



$$(2:\text{xiii}) \quad m \frac{d^2 x}{dt^2} + \frac{2e (U + V_0 \cos \omega t)}{r_0^2} = 0$$

$$(2:\text{xiv}) \quad m \frac{d^2 y}{dt^2} - \frac{2e (U + V_0 \cos \omega t)}{r_0^2} = 0$$

$$(2:\text{xv}) \quad m \frac{d^2 z}{dt^2} = 0$$

(2:xv) is most easily integrated to give  $\frac{dz}{dt} = \text{constant}$ . This means that the ions travel at constant forward velocity through the quadrupole rod structure. Equations (2:xiii) and (2:xiv) are solved by use of a Mathieu function. The Mathieu equations of motion are (2:xvi) and (2:xvii).

$$(2:\text{xvi}) \quad \frac{d^2 x}{d\phi^2} + (a + 2q \cos 2\phi) x = 0$$

$$(2:\text{xvii}) \quad \frac{d^2 y}{d\phi^2} - (a + 2q \cos 2\phi) y = 0$$

Three dimensionless parameters are defined.

$$(2:\text{xviii}) \quad \phi = \frac{\omega t}{2}$$

$$(2:\text{xix}) \quad a = \frac{8eU}{mr_0^2 \omega^2}$$

$$(2:\text{xx}) \quad q = \frac{4eV_0}{mr_0^2 \omega^2}$$

When an ion enters the quadrupole structure its trajectory is controlled by these parameters. There is a region of stable

oscillations where the amplitude remains less than  $2r_0$ . This region is shown on the stability diagram shown in figure (2:8b). Ions with values for the parameters outside this region follow a trajectory of increasing amplitude and strike either the x rods when  $q$  is greater than the x stability limit or the y rods when  $a$  is greater than the y stability limit. Thus only ions with values of  $a$ ,  $q$ ,  $U$ ,  $V_0$ ,  $\omega$  and  $r_0$  will pass through and be detected. The number of ions with different masses which are detected depends upon the ratio  $a/q$ . If  $a/q$  is small (the dashed line  $a/q$ ), many ions of similar mass ( $m_1$ ,  $m_2$ ,  $m_3$ ) will be detected and the resolution is low. If  $a/q$  is large, as is shown by the scan line (the solid  $a/q$  line) on figure (2:8b), perhaps only one mass  $m_1$  will be stable at a time and the resolution will be high. Resolution increases with the  $a/q$  ratio and theoretically becomes infinite at  $a/q = 0.336$  ( $a = 0.23699$  and  $q = 0.70600$ ). The quadrupole is operated as a mass spectrometer with  $a/q$  just smaller than 0.336. Mass scanning may be accomplished in two ways,  $\omega$  is kept constant while  $U$  and  $V_0$  are varied so that the ratio  $U/V_0$  is kept constant, or  $U$  and  $V_0$  are kept constant while  $\omega$  is varied. The mass spectrometer used in this work used the first method. The transmission of the quadrupole is large because no ion defining apertures are required.

The transmission of an ion is dependent upon the  $U/V_0$  ratio ( $U/V_0 = a/2q$ ). Von Zahn *et al* (59) assumed that  $q$  was

kept constant, at the apex of the stability diagram (figure 2:8b) and that any deviations from  $a/q = \text{constant}$ , were then dependent upon  $a$ . He developed an equation (2:xxi) for the observed intensities  $I_1$  and  $I_2$  of two ions after mass analysis.

$$(2:xxi) \quad \frac{I_1}{I_2} = \frac{I_1^{\circ}}{I_2^{\circ}} \frac{(a_{\max} - a_1)}{(a_{\max} - a_2)} \quad \text{where } a_{\max} = .23699$$

$I_1^{\circ}$  and  $I_2^{\circ}$  are the original intensities of the two ions before analysis. Thus  $I_1/I_1^{\circ}$  and  $I_2/I_2^{\circ}$  are the transmission factors of the two ions. If the ratio  $U/V_0$  is constant as  $U$  and  $V_0$  are changed  $a/q$  will remain constant ( $a/q = 2U/V_0$ ) and thus one would expect constant transmission for all ions. The ratio  $U/V_0$  was measured for the low mass range of the present instrument. The ratio did not remain constant as  $U$  and  $V_0$  increased. Figure (2:9a) shows the variation of  $U/V_0$  as  $V_0$  was increased. The ordinate is expressed as a fraction of  $V_{0 \max}$  where  $V_{0 \max}$  is the highest rf voltage for the particular mass range. Since it was difficult to measure  $V_0$  accurately, the measured ratio  $U/V_0$  was normalized so that at  $.05 V_{0 \max}$ ,  $U/V_0 = a_{\max}/2q_{\max} = 0.16784$ . The variation of intensity with  $V_0$  was calculated by means of the von Zahn equation (2:xxi). The parameter  $a$  was calculated from the  $U/V_0$  ratio with  $q$  assumed to be constant at 0.7060. The intensity is shown as a relative intensity (with  $I$  at  $0.5 V_{0 \max}$  taken as unity) in figure (2:9b). One can see that the transmission of ions of low and high masses would be less than ions of

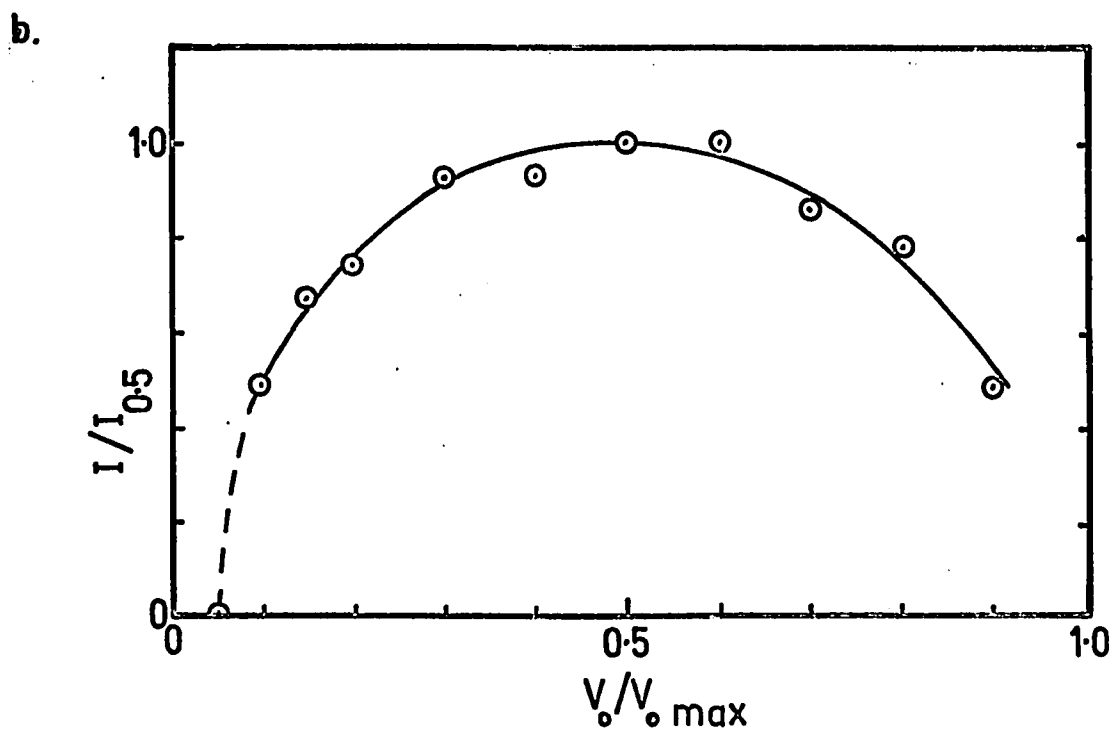
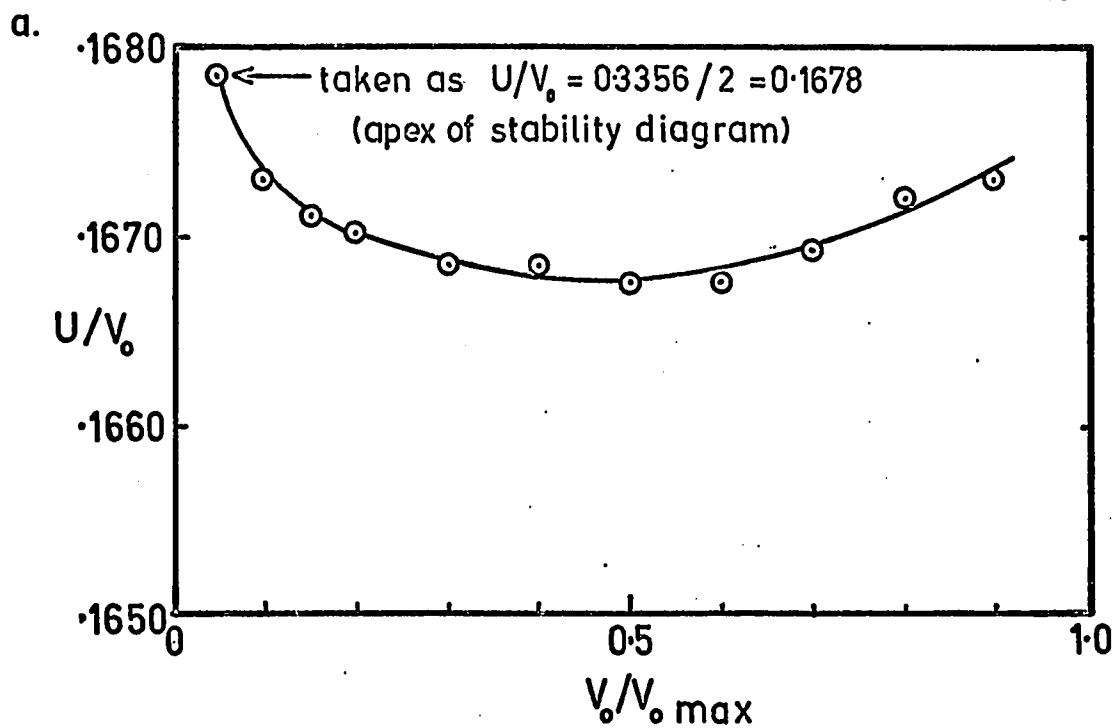


Figure 2:9 (a) Plot of  $U/V_0$  ratio versus  $V_0/V_{0 \text{ max}}$ .  
 (b) Plot of relative intensity.  $I/I_{0.5}$   
 calculated by means of equation (2:xxi)  
 versus  $V_0/V_{0 \text{ max}}$ .

$V_{0 \text{ max}}$  is r.f. voltage at high mass limit of each mass range.

intermediate mass. The equation (2:xxi) gives a linear relationship between transmission and  $a/q$  ( $q$  constant). Brubaker and Tuul (60) reported plots of transmission factors versus  $a/q$ . These plots show that for their instrument the transmission decreased slightly as  $a/q$  increased from 0 to perhaps 0.330 and then suddenly decreased as the ratio approached the maximum value 0.336. Thus small changes in  $a/q$  would change the transmission factor by a very large amount. This was found to be the case for the present instrument. The transmission was very dependent upon small changes in the ratio. Brunée *et al* reported (61) that even at constant  $U/V_0$  ratio the transmission decreased with increasing  $m/e$  and thus the equation (2:xvi), used to generate the theoretical transmission in figure (2:9b) is probably too simple.

Brunée *et al* (61) also described a method by which the quadrupole could be used to collect the total ionization. If the dc voltage  $U$  is switched off,  $a/q = 0$ , ( $a/q = 0$  is the ordinate of the stability diagram (figure 2:8b)), and there is no discrimination of ions. A certain small rf voltage  $V_0$  is required to focus the ions. All ions of mass greater than that corresponding to the small value of  $V_0$  are collected. The present instrument was modified to permit this method of operation.

The transmission factors were measured in the following manner. The ion source exit leak of .120 mm diameter was

replaced by a large leak  $\sim 1$  mm diameter. A repeller was welded to the electron trap so that the ion source could be operated as a conventional low pressure source. The only difference was that the electron energy was 4000 eV instead of 70 eV. The quadrupole entrance cone ([16] of figure 2:5a) was connected through a battery (-90 volts) to a sensitive amplifier (Keithley 610B electrometer). The ion current hitting the cone was measured. It was found that when the potential on the gate electrodes [17] and [19] was positive (+40 V) so that the gate was closed, the current measured on the cone increased. This change in current  $\Delta I$  was taken to be the current of the ions passing through the cone into the quadrupole analyser when the ion gate was open. The ion current at the exit of the analyser was divided by  $\Delta I$  to give a transmission factor. Only the results in which the transmission was constant as  $\Delta I$  was changed, by changing the ion source pressure, were used.

The gases used to calibrate the mass spectrometer were chosen so that electron impact produced ions of one mass or ions which were spread over a narrow mass range. The rare gases were used first. The intensity of the major ion was corrected for isotope ratios and for contributions due to doubly charged species. The cross sections for production by 4000 V electrons of multiply charged ions, relative to

singly charged ions were taken from tables in Schram (62). They were usually less than 10%. The diatomic gases  $O_2$ ,  $N_2$ , etc. were used next. The intensity of the molecular ion was corrected for the contribution of atomic ions to the total ion current  $\Delta I$ . Finally hydrocarbon gases were used. These were chosen such that a group of ions of similar mass were produced in large abundances. For example  $CH_4$  is ionized to  $CH_4^+$  and  $CH_3^+$  whose intensities total over 90% of the total ionization. Other hydrocarbon ions were used. The relative intensities of the major ions were taken to be essentially the same as those reported in the API tables for 70 eV electrons (Kearle and Godbole (63) showed that the fragmentation pattern remained essentially constant as the electron voltage was increased). By this method it was possible to establish transmission curves for the low and medium mass ranges.

The high mass range was calibrated by a slightly different technique. The transmission factors for three masses were found  $m/e$  84 ( $Kr^+$ ),  $m/e$  92 ( $C_6H_3-CH_3^+$ ) and 132 ( $Xe^+$ ). A spectrum of  $C_4Cl_6$  was run using the auxiliary low pressure ion source with the electron energy set at 70 eV. This was compared to a spectrum obtained by an A.E.I. MS-2 magnetic mass spectrometer. The relative factors of the ions of  $C_4Cl_6$  obtained by comparing the quadrupole spectrum to the MS-2 spectrum were normalized to the factors obtained for  $m/e$  84, 92 and 132.

The transmission curves for the three mass ranges are shown in figure (2:10). They were plotted in logarithmic form for convenience. These curves are remarkably similar to the theoretical curve, figure (2:9b).

The transmission factors were checked later when the ion acceleration electrodes shown in figure (2:5b) were installed. The ion current was measured on the deflection plate [16a]. The ion source potential was +7.4 V and the cone [16] potential -67.5 V. The deflection plate [16a] had a potential of -135 volts. The current was measured by the Keithley 610 B electrometer. Essentially the same results were obtained by this method and thus the use of  $\Delta I$ , as the current passing through the cone was verified.

The total ionization was collected by means of the quadrupole, when the dc voltage U was switched off. The transmission of the total ionization of  $N_2$ , with respect to the current measured on the deflection plate [16a] was about 30%, compared to 15% for  $N_2$  when the ions were mass analyzed. This could be interpreted two ways. The statement that when  $U = 0$  all ions are focussed by a small rf voltage  $V_0$ , may not be strictly true. Alternatively there could be a considerable loss of ions in the path from the cone [16] to the quadrupole entrance aperture [10]. This is more likely. It would mean that the transmission of the quadrupole analyzer itself



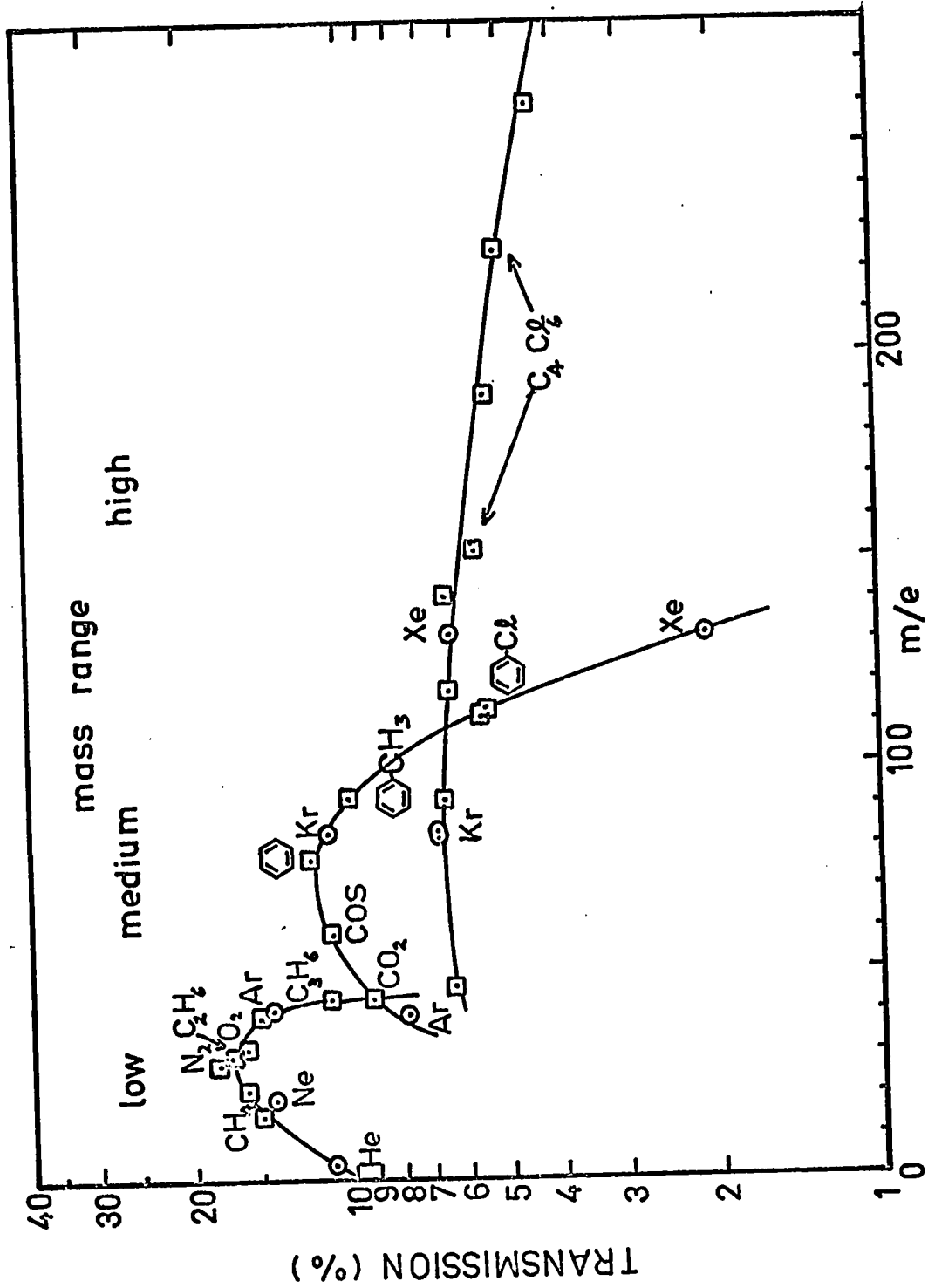


Figure 2:10 Transmission factors versus mass for the quadrupole mass analyser.  
 Ion acceleration voltage 7.4 volts. Resolution setting 500.

when run in the total collection mode was close to 50%. Probably the answer lies between, some ions were lost in transit from the cone [16] to the entrance aperture [20] and the quadrupole did not pass all ions in the total collection mode.

### 2:11 Discrimination in Detection by the Electron Multiplier

The ion signals in the present apparatus were detected by a 14 stage, copper beryllium secondary electron multiplier (SEM). Unfortunately an electron multiplier does not detect all ions with equal efficiency. The number of electrons ejected from the first dynode by the collision of the ion depends upon its mass and its chemical composition. The total amplification is proportional to the number of electrons from the first dynode. It has been reported (64) that the secondary electron current is proportional to the velocity of the ion. Now if ions of different masses are accelerated towards the first dynode by its negative potential, they all gain the same energies and thus their velocities will be proportional to  $1/\sqrt{\text{Mass}}$ . The relative electron currents for two ions of masses  $m_1$  and  $m_2$  will therefore be related by equation (2:xxii).

$$(2:xxii) \quad \frac{i_1}{i_2} = \sqrt{\frac{m_2}{m_1}}$$

Stanton, Chupka and Inghram (65) showed that the chemical

composition of the ion may affect the amplification. It appears that multi-atomic ions break apart on collision with the first dynode and act as a group of particles of the same energy. The amplification thus increases with the complexity of the ion. For example, Stanton *et al.* found  $C_{14}H_{10}^+$  had an amplification factor 2.2 times that of  $Hg^{204}$ .

The amplification factors for the various ions were measured in the present apparatus. First the amplified ion signal was recorded when the SEM was operated in the normal fashion. The signal was again recorded when the first dynode of the SEM had been connected to the recorder so that it acted as a Faraday cup. The ratio of the first signal to the second was the amplification factor. The amplification factors are shown plotted versus  $m/e$  in figure (2:11). One can see that the chemistry of the ion has a larger influence than does the mass upon the amplification factor. Equation (2:xxii) has been plotted so that it passes through  $Kr^+ m/e$  84. The atomic ions fit this line more closely than do the multi atomic ions.

An excellent discussion of the operation of secondary electron multipliers has been given by Beynon (64). The problem of amplification is discussed in detail.

The measured intensities of the ions were corrected for discrimination by the quadrupole analyser and the electron

composition of the ion may affect the amplification. It appears that multi-atomic ions break apart on collision with the first dynode and act as a group of particles of the same energy. The amplification thus increases with the complexity of the ion. For example, Stanton *et al.* found  $C_{14}H_{10}^+$  had an amplification factor 2.2 times that of  $Hg^{204}$ .

The amplification factors for the various ions were measured in the present apparatus. First the amplified ion signal was recorded when the SEM was operated in the normal fashion. The signal was again recorded when the first dynode of the SEM had been connected to the recorder so that it acted as a Faraday cup. The ratio of the first signal to the second was the amplification factor. The amplification factors are shown plotted versus  $m/e$  in figure (2:11). One can see that the chemistry of the ion has a larger influence than does the mass upon the amplification factor. Equation (2:xxii) has been plotted so that it passes through  $Kr^+$   $m/e$  84. The atomic ions fit this line more closely than do the multi atomic ions.

An excellent discussion of the operation of secondary electron multipliers has been given by Beynon (64). The problem of amplification is discussed in detail.

The measured intensities of the ions were corrected for discrimination by the quadrupole analyser and the electron

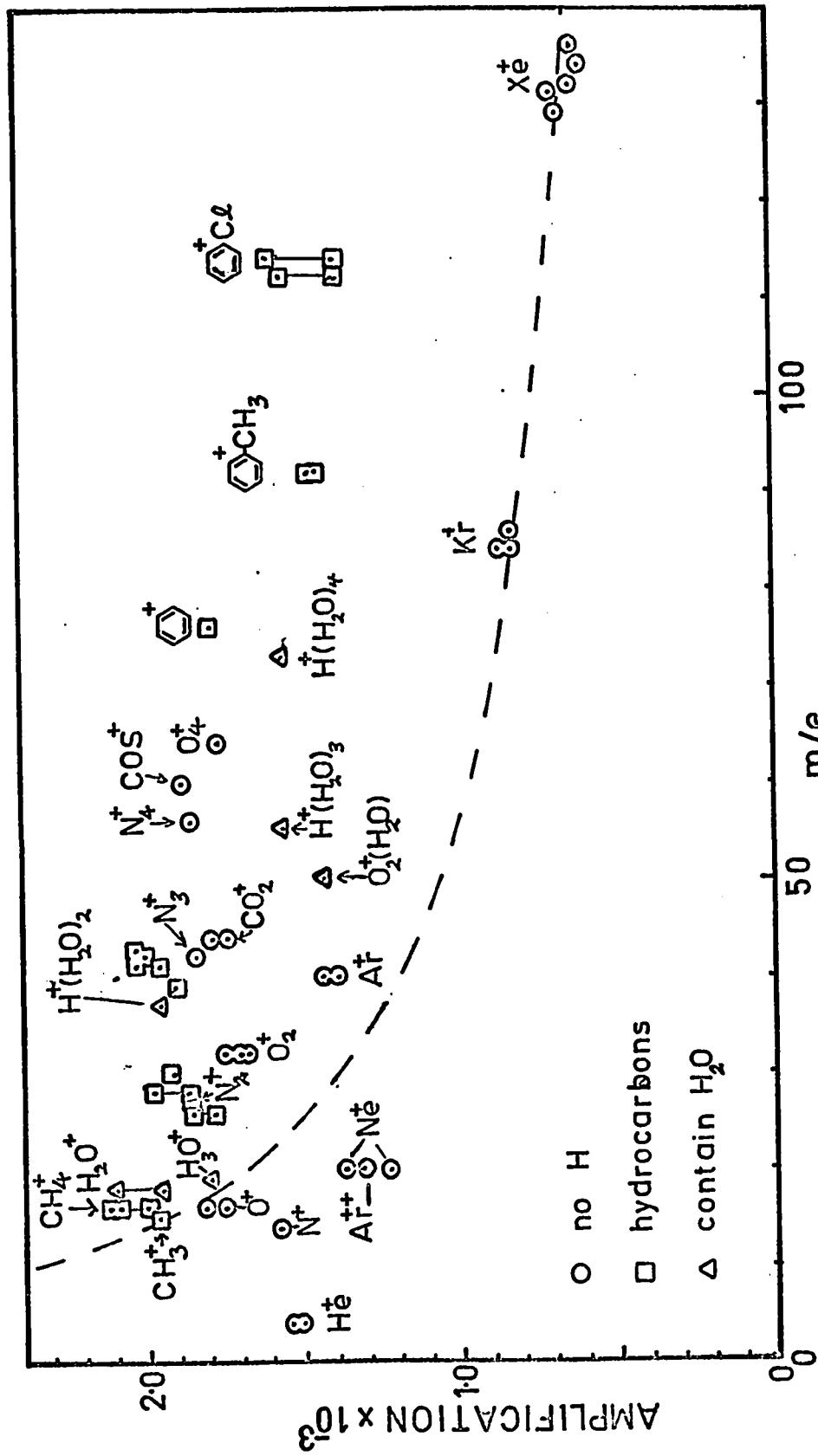


Figure 2:11 Amplification factors for the secondary electron multiplier. Multiplier potential = 3000 V.

multiplier. Each ion intensity  $I$  was multiplied by a factor  $F$ . This factor was calculated for each ionic species by equation (2:xxiii).

$$(2:xxiii) \quad F = \frac{1}{\text{Quadrupole Sensitivity Factor} \times \text{SEM Amplification}}$$

For most of the results relative factors rather than absolute factors were used. Consequently the absolute intensities are not given in figures in which the ion intensity is the ordinate.

#### 2:12 Collision of Ions Outside the Ion Source

The collision of ions along the trajectories from the ion source to the point of detection may cause discrimination. Two experiments were carried out to determine the extent of collision. The total ion current was measured as a function of the ion source pressure. It was measured on the cone deflection plate [16a] and by means of the quadrupole analyser operated in the total ionization mode. The results are shown in figure (2:12a). One would expect the signal would increase as the pressure increased provided that at all pressures the number of ions leaving the source was proportional to the number formed by electron impact. After the initial rise the cone signal became reasonably constant, and then rose slightly as the pressure outside the ion source i.e. in the vacuum chamber reached  $1 \times 10^{-4}$  torr. The signal measured by the quadrupole, however, decreased slightly. The decrease

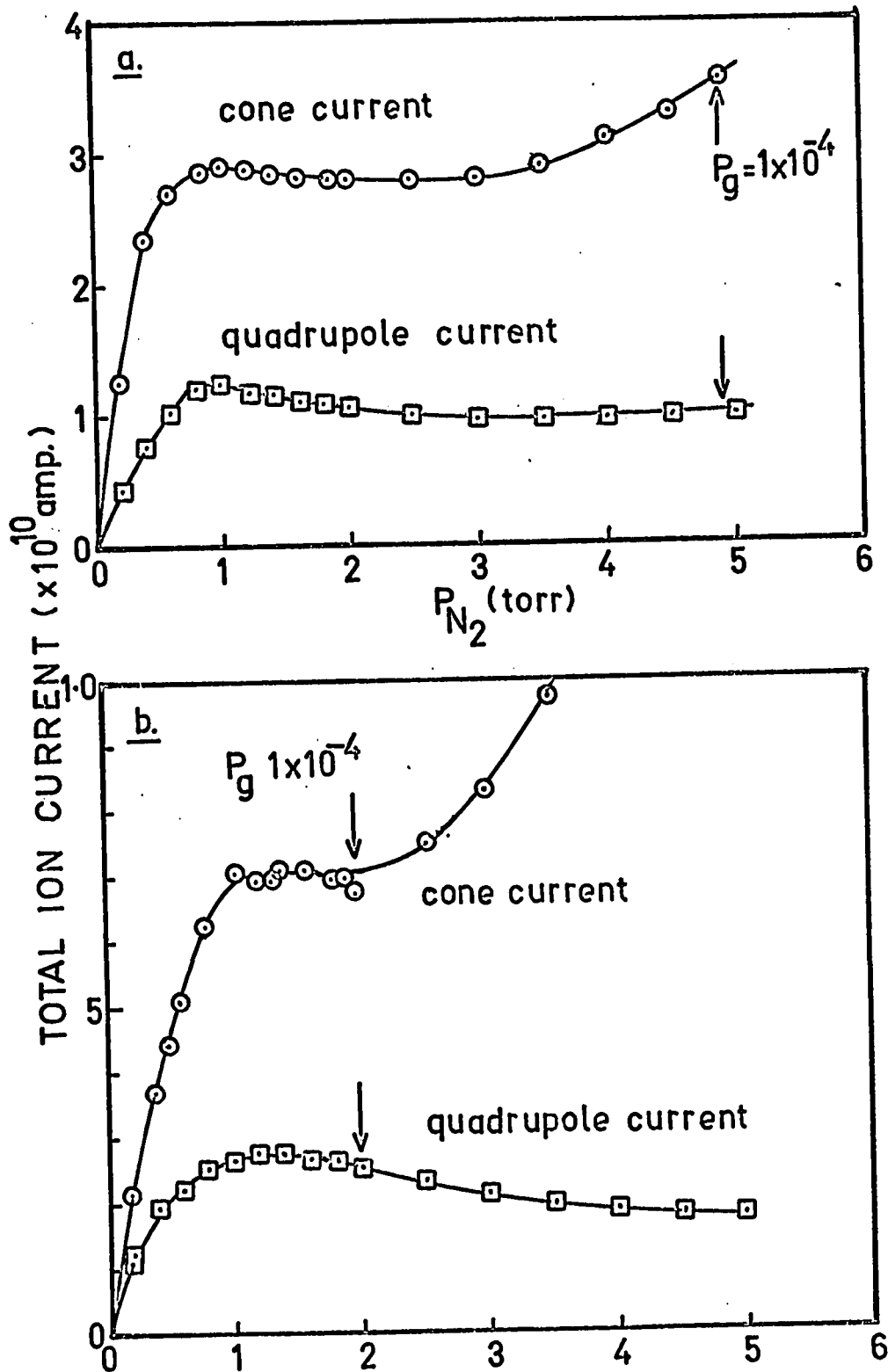


Figure 2:12 Total ion current as measured on the cone (electrode 16a) and by the quadrupole operated at  $a/q = 0$  versus pressure of nitrogen in the ion source.

a. Normal operating conditions.

b. Operation in the presence of unwanted gas leakage.

is probably due to collisions in the quadrupole tube as the flight time of an ion through the quadrupole analyser is relatively long. For  $N_2^+$ , with an ion source potential of +7.4 volts and a cone potential of -67 volts, the flight time of the ion from the ion source to the cone can be calculated as 4.5 micro seconds, while the flight time through the quadrupoles is 25 micro seconds. In figure 6:12b) are shown similar plots in which the leakage of gas from the ion source was much larger than normal ( $F = 25$  cc/sec. compared to 9 cc/sec.). This was due to an unwanted leak. In this case the exterior pressure increased much more rapidly as the ion source pressure increased. One can see that collisions inside the quadrupole tube reduced the signal by a larger factor than before. Also the pressure of  $1 \times 10^{-4}$  torr in the vacuum chamber was reached at a lower ion source pressure. Since the cone current shown in both diagrams (a and b) of figure (2:13) increase rapidly at pressures above  $1 \times 10^{-4}$  torr in the vacuum chamber, the increase is probably due to formation of ions in the region between the cone and the ion source by stray electrons from the electron beam. Normally the ion source operated under conditions where the pressure of  $1 \times 10^{-4}$  torr was not reached, and thus the only ions observed would be those produced in the ion source.

In the second experiment the ions  $N_2^+$  and  $O_2^+$  were produced



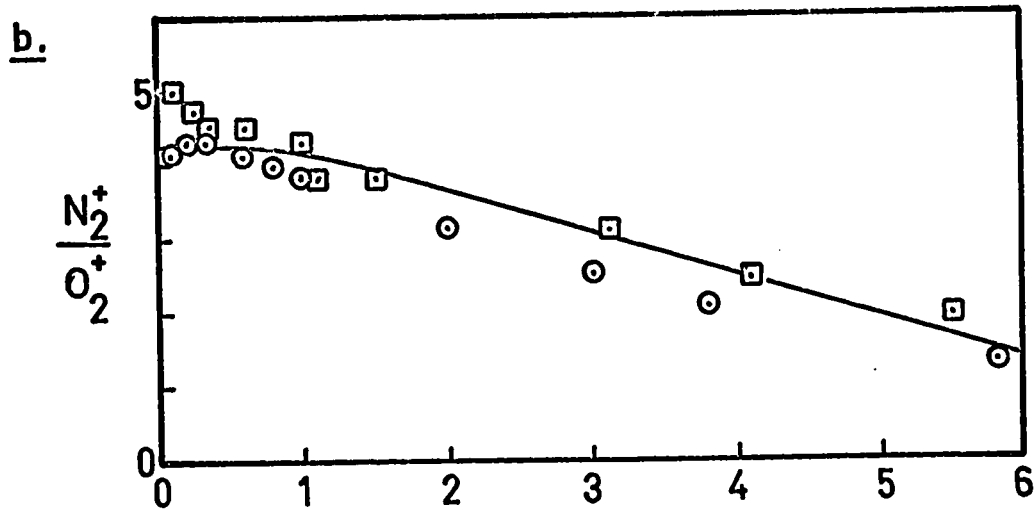
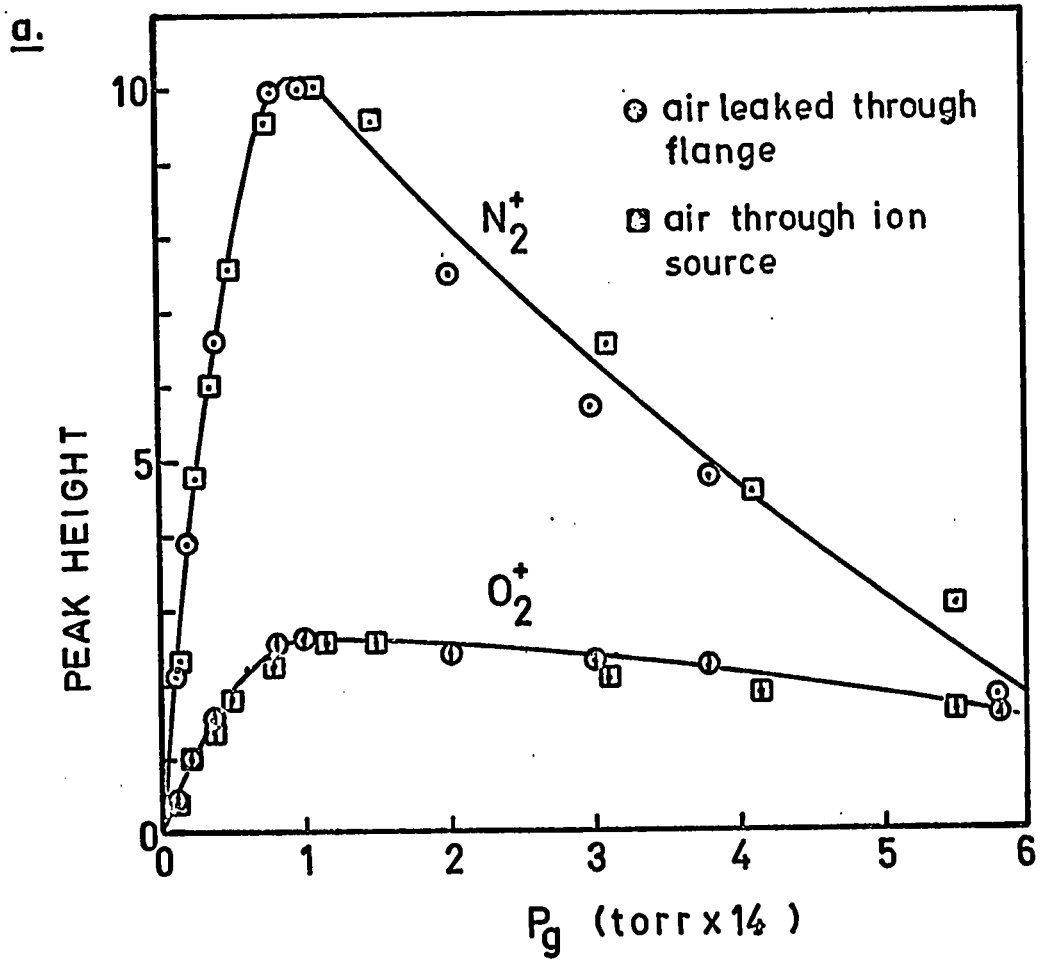


Figure 2:13

a. Ion signals produced by the auxiliary ion source as the vacuum chamber pressure  $P_g$  was increased.

b. Ratio  $N_2^+/O_2^+$  versus pressure.

in the low pressure ion source. The intensities of the two signals were observed as the vacuum chamber pressure was increased. Air was admitted to the chamber in two ways. It was admitted via the high pressure ion source and also by allowing it to leak through one of the mounting flanges. The results are shown in figure (2:13a). One can see that the ion signals increased until the pressure reached  $1 \times 10^{-4}$  and then decreased. This decrease must be due to collisions inside the quadrupole analyser. The ratio  $N_2^+/O_2^+$  is plotted versus pressure in figure (2:13b). The ratio remained reasonably constant as the pressure was increased to  $1 \times 10^{-4}$  torr above which it decreased rapidly. Since  $N_2^+$  has a larger ionization potential than those of the other major constituents of air, i.e.  $O_2$  and  $H_2O$ ,  $N_2^+$  would be lost by charge exchange collisions at a greater rate than would  $O_2^+$ . This is the cause of the decrease in the  $N_2^+/O_2^+$  ratio at the higher pressures. From this experiment it was concluded that discrimination of ions due to collision, were not important if the pressure in the vacuum chamber was kept below  $1 \times 10^{-4}$  torr. Most of the experiments reported later, were done under conditions in which the vacuum chamber pressure was kept below  $1 \times 10^{-4}$  torr.

### 2:13 Purification of Gases

Krypton, xenon, neon, oxygen and nitrogen were obtained from 1 liter bulbs manufactured by the Air Reduction Company. These contained very small amounts of impurities (about 10 ppm). Nitrogen was also obtained from other sources and purified. It was found that the nitrogen experiments were more consistent when  $N_2$  was continually flowed into the ion source. The Airco bulbs did not hold a sufficient amount for flow experiments. Nitrogen from a tank (containing 2 ppt  $O_2$  and 7 ppt  $H_2O$ ) was passed through a molecular sieve (Type 5A), to remove  $H_2O$ , through sodium-potassium alloy to remove  $O_2$  and again through molecular sieve (Type 3A), which was kept at  $-126^\circ C$  by a methyl cyclohexane-liquid nitrogen slush bath. It was possible to reduce the  $O_2$  and  $H_2O$  impurities to less than 50 ppm by this method.

Ethylene was obtained from a Phillips research grade cylinder of purity 99.94 mole percent. Methane, from a tank of Matheson "Ultra Pure" which was labelled to contain 50 ppm  $CO_2$ , 2.5 ppm  $O_2$ , 13 ppm  $N_2$ , < 5 ppm  $C_3H_8$  and 1.7 ppm  $C_2H_6$  was passed through a trap of 3A molecular sieve which was cooled to  $-196^\circ C$  by liquid nitrogen and stored in a 1l bulb.

### 2:14 Experimental Procedure

Appropriate gas mixtures were first made in the gas handling plant (figure 2:8). In the early experiments ( $CH_4$ -Kr, chapter 4)

and ( $C_2H_4$ -Xe, chapter 5), the mixture flowed from the 4 liter bulb into the ion source. It was found that the pressure decreased very rapidly and since it took several minutes to measure the intensity curve of each ion more reproducible results were obtained by remaking the mixture before measuring the next ion. The technique was improved by making large quantities of the gas mixture and storing it in an external bulb. This bulb was attached to the gas handling plant by a Granville Phillips variable leak so that the pressure in the G.H.P. was kept constant. The 4 liter bulb was used as a ballast volume. The gas mixture was analysed before and after the high pressure measurements by means of the auxiliary low pressure filament. It was found that gas mixtures of gases with widely different molecular weights (such as  $C_2H_4$  and Xe) did not fractionate while passing through the variable leak as they might be expected to do. Since for these mixtures one gas was only a fraction ( $\sim 1/10^3$ ) of the major constituent, the latter presumably controlled the flow characteristics. When the pure gases  $O_2$  and  $N_2$  were used, they were flowed at constant pressure directly from the source through the variable leak into the gas handling plant.

The ion intensity curves were obtained in the following manner. The gas was irradiated continuously by the electron beam and a spectrum was recorded. This spectrum was used to

establish which ions were present and whether there were impurities present. The electron beam was switched to the pulse mode and a second spectrum at constant ion collection was recorded. The ion gate was then switched to the pulse mode, the mass spectrometer was adjusted so that only one mass was recorded. The ion intensity was measured by increasing the delay time in steps. The time was measured by the oscilloscope. At each time, the chart recorder was moved forward and stopped, so that the curves appeared as step functions on the chart paper. This method of obtaining the intensity curves was used as the amplifier was slow and integrated the signal from many successive pulses. The ion intensity curves were replotted on graph paper (at times corrected for the flight time  $t_f$ ), with the appropriate factors applied to correct for the intensities for efficiency of collection.

3 PHYSICAL CONDITIONS IN THE ION SOURCE; THE LOSS OF IONS FROM ION-ELECTRON RECOMBINATION, FROM DIFFUSION TO THE WALLS AND FROM MASS FLOW OUT OF THE ION SOURCE.

The ions formed by the electron beam are lost by three mechanisms, by recombination with electrons, by diffusion to the walls and by removal from the ion source by flow of the gas. Each of these mechanisms has a different effect upon the ion intensity. The recombination of ions with electrons is a second order mechanism. Since the concentrations are equal, the loss of ionization will be second order and not pseudo-first order. The losses of ions by diffusion and mass flow are both first order.

Sampling of ions from any mass spectrometer ion source may involve discrimination against ions of different masses. This problem is especially complicated in sampling from high pressure ion sources since the ions are removed from a region at pressures of several torr into a region in which the pressure should be less than  $10^{-5}$  torr so that mass analysis is not affected by ion-molecule collisions. The ideal requirements are that the sample be representative of the ionic constituents and that the reaction system be undisturbed by the process of sampling. Unfortunately these cannot be fulfilled completely as the above processes, recombination, diffusion and mass flow affect the ions in different ways. The effect of these processes on ion sampling and on the suitability of the system for kinetic studies will be considered below.

### 3:1 Recombination of Ions and Electrons in the Beam

#### i Steady State Concentration of Ions Under Continuous Illumination

An estimate of the extent of ion-electron recombination may be obtained by an approximate calculation of the concentration of ions formed in the beam. Figure (3:1) shows an enlarged diagram of the ionizing region of the ion source. The ion current  $I_s$  may be calculated from the electron current  $I_p$  by means of equation (1:ii)

$$(1:ii) \quad \frac{I_s}{I_p} = e^{Qn\ell} - 1$$

where  $Q$  is the cross section,  $n$  the gas density and  $\ell$  the path length. The electron current  $I_p$  was measured on the trap at about 1  $\mu$ A when there was no gas in the ion source. This corresponds to  $6 \times 10^{12}$  electrons/sec. The cross section  $Q$  for  $N_2$  gas for 4000 volt electrons may be taken (62) as  $3 \times 10^{-17} \text{ cm}^2$ . At a pressure of 1 torr at 300°K,  $n = 3 \times 10^{16}$  molecules/sec. Since we want the concentration of ions,  $\ell$  may be taken as 1 cm. If these values are substituted into equation (1:ii)  $I_s$  is calculated as  $1.2 \times 10^{13}$  ion/sec. If the average thickness of the beam is about 1 mm, and its width is governed by the slit width 1.7 mm, the cross section of the beam is about  $2 \times 10^2 \text{ cm}^2$ . Thus the number of ions/cc  $I_s$  produced each second would be  $6 \times 10^{14}$ . This is a very high density of ions and many would be lost by

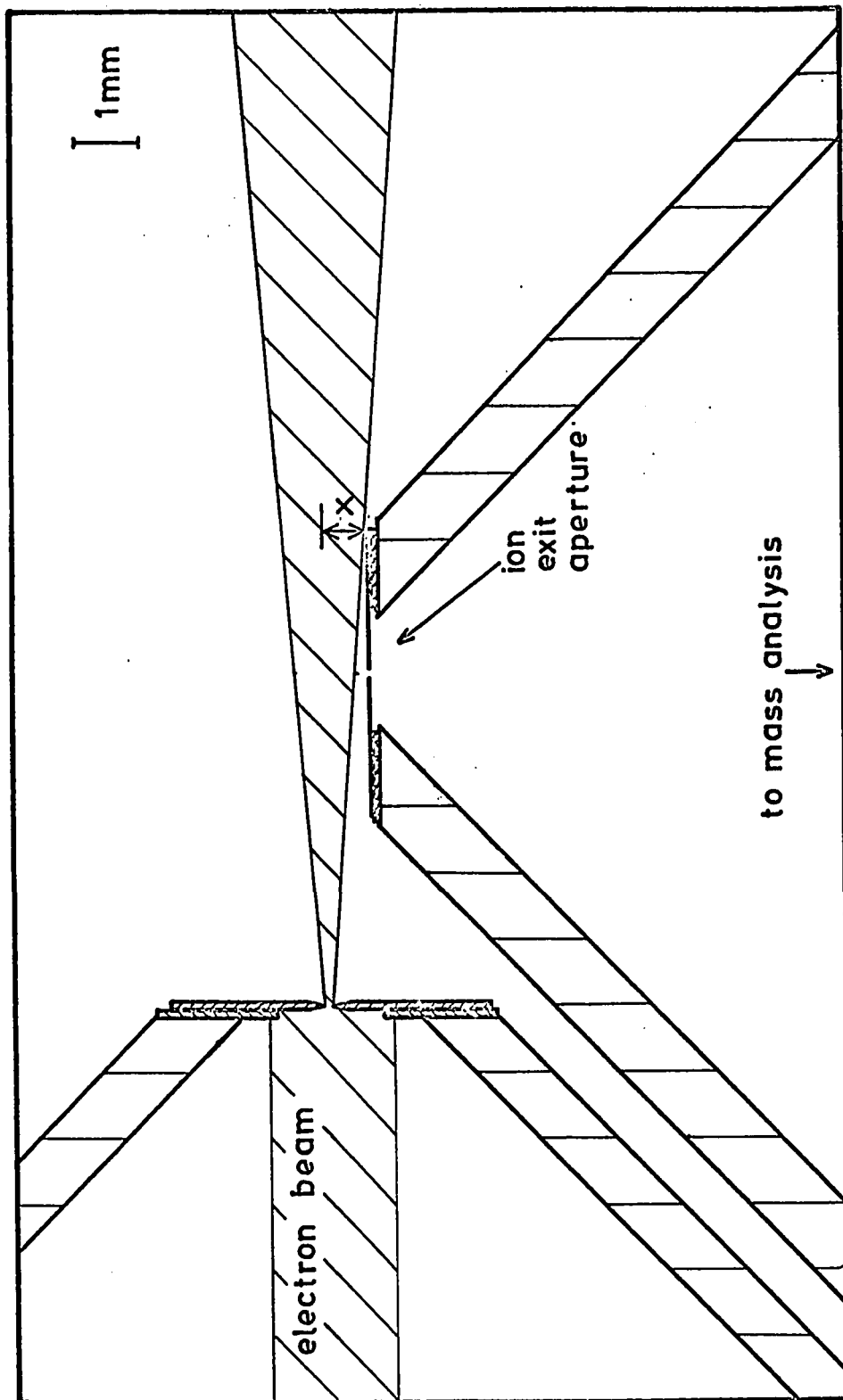


Figure 3:1 Detailed view of reaction region showing an approximated spread of the electron beam and the ion exit aperture. Two distances  $x$  were used, 0.67 mm and 1.67 mm.



recombination. Since the secondary electrons also cause ionization the actual density will be higher. The change in the ion concentration  $I$  due to recombination is given by (3:i) where  $\alpha$

$$(3:i) \quad \frac{dI}{dt} = -\alpha I [e] + I_s'$$

is the recombination coefficient which may be taken as  $3 \times 10^{-7}$  cc/ion sec. for  $N_2^+$  ions (66). Since the formation of an ion by electron impact produces a new electron, the electron concentration  $[e]$  may be taken to be equal to the ion concentration  $I$ . Under steady state conditions  $dI/dt = 0$  and equation (3:i) reduced to (3:ii).

$$(3:ii) \quad \alpha I_\infty^2 = I_s'$$

The concentration of ions under steady state conditions  $I_\infty$  is given by (3:iii).

$$(3:iii) \quad I_\infty = \sqrt{\frac{I_s'}{\alpha}}$$

If  $I_s' = 6 \times 10^{14}$  ions/cc sec. and  $\alpha = 3 \times 10^{-7}$  cc/ion sec. then the steady state concentration  $I_\infty = 4.5 \times 10^{10}$  ions/cc.

#### ii Lifetime of an Ion in the Beam

The average life of an ion in the beam is given by the ratio of the steady state concentration to the concentration of new ions produced each second. This is given by equation (3:iv). When the

$$(3:iv) \quad \tau = \frac{I}{I_s'}$$

above values for  $I$  and  $I'_s$  are substituted into this equation the average lifetime of an ion in the beam is calculated as  $\tau = 7 \times 10^{-5}$  seconds.

iii Time for Removal of an Ion from the Beam by Diffusion

At high ion densities (greater than  $10^8$  ions/cc) ions are removed from the beam by ambipolar diffusion (67, p.206). The time required for the removal of an ion from the beam is related to the ambipolar diffusion coefficient  $D_a$  and the distance  $d$  by equation (3:v) (67, p. 200, 68, p. 493).

$$(3:v) \quad \tau_{\text{diff}} \approx \frac{d^2}{D_a}$$

$d$  may be taken as 0.5 mm, half the width of the beam. The value of the ambipolar diffusion coefficient is somewhat unknown. We might take a value of  $100 \text{ cm}^2/\text{sec}$ . from a table given by McDaniel (68, p. 516).  $\tau_{\text{diff}}$  is then calculated as 25 micro seconds. This value has the same order of magnitude as the lifetime of the ion in the electron beam. Consequently one would expect that recombination would have an effect on the sampled ion intensity.

An experiment was carried out so that the effect of ion-electron recombination might be observed. The electron beam was pulsed and the ions leaving the ion source were collected continuously. The pulse length was changed while the pulse repeat frequency remained constant. The increase in intensity

$I_{obs}$  with the increase in pulse length was measured. The pulse repeat time was set at 2000 micro sec. for two runs and at 4000 for a third, as the ion intensity decayed after the pulse to very small values within 1000 micro seconds. Consequently the major effect on intensity would be brought about by the pulse length (from  $10\mu$  sec. to  $1000\mu$  sec.) The results are shown on figure (3:2). The observed intensity  $I_{obs}$ , as a fraction of the intensity under constant illumination  $I_{\infty}$ , is plotted versus the pulse width which is expressed as a fraction  $f$  of the pulse repeat time. This is called the illumination fraction where the value  $f = 1.0$  corresponds to constant illumination. The plots are shown in log form (figure 3:2) as the solid lines a, b and c. If the ions in the beam were lost only by first order processes, the intensity would increase directly proportional to the illumination time. The dashed line d indicates this situation. It can be seen however that the ion signal increased at a rate, such that the log-log slope is less than one. This indicates that processes greater than first order are responsible for loss of ions. The part of the time fraction scale between about 0.3 and 1.0, where the slope increases, corresponds to the situation where the ion signal does not decay between pulses. This would cause an overlap and the change in intensity would not be due to the increase in pulse length. The data of 0.92 torr with 4000 micro second

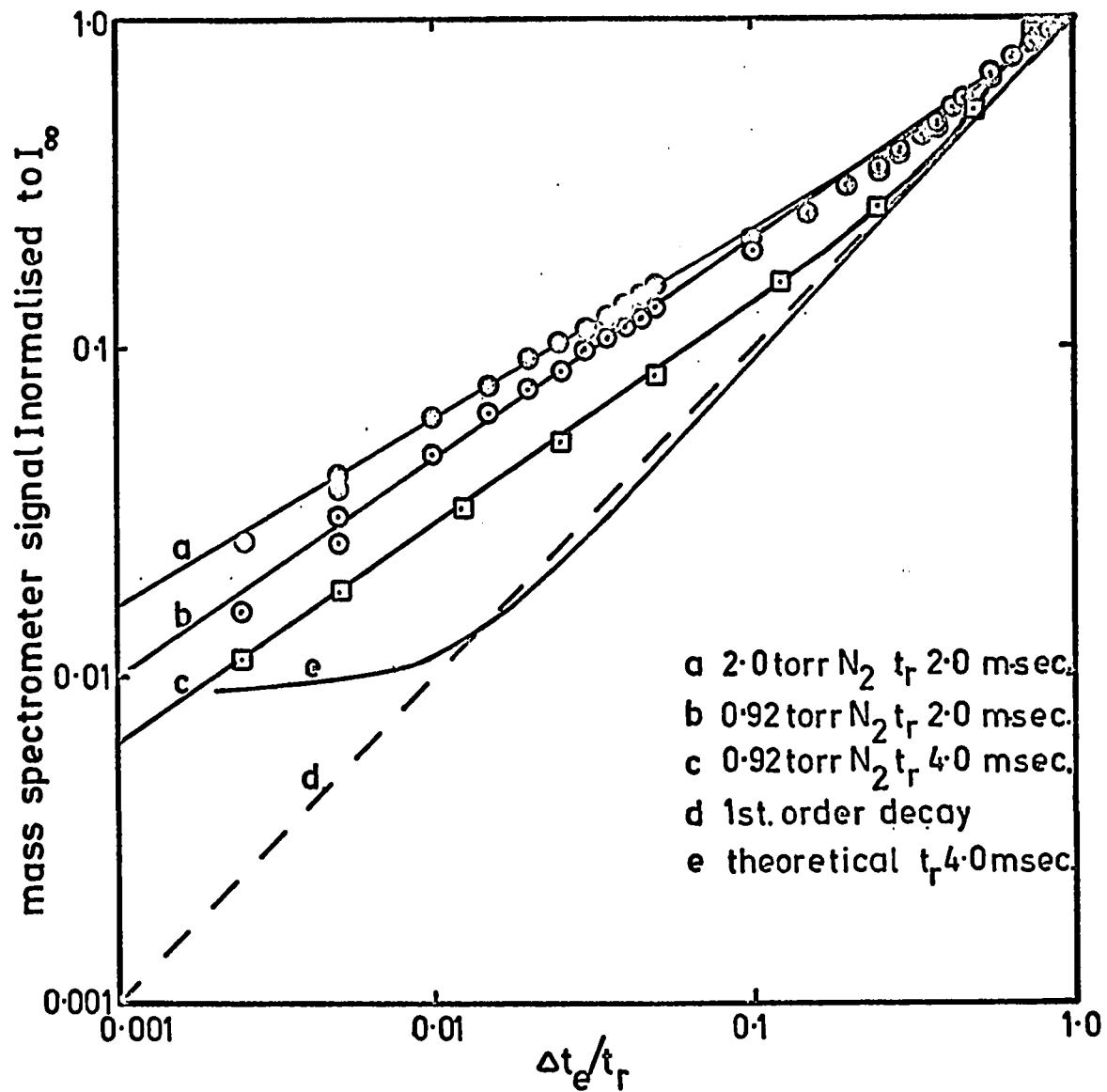


Figure 3:2 Plot of observed total ion signal  $I_{obs}$  normalized to ion signal under constant irradiation  $I_{\infty}$  versus pulse width expressed as a fraction ( $f = \Delta t_e / t_r$ ) of the pulse repeat time.

repeat time line c of figure (3:2) was plotted in a slightly different manner in figure (3:3a). The normalized intensity was divided by the time fraction f. When the pulse widths were short this time-normalized intensity was much larger than when the pulse widths were long. This same data is shown in a log form figure (3:3b).

A theoretical calculation was carried out. It was assumed that equation (3:i) held that ions were only produced by a linear relationship ( $I_s t$ ) and lost by a second order process ( $-\alpha I^2 t$ ). Equation (3:i) may be integrated to give the following equation (3:vi) (67, p. 79) where  $I_t$  is the intensity at time t and  $I_\infty$

$$(3:vi) \quad I_t = \frac{I_\infty (e^{2 I_\infty \alpha t} - 1)}{(e^{2 I_\infty \alpha t} + 1)}$$

the steady state intensity given by equation (3:iii).

$$(3:iii) \quad I_\infty = \sqrt{\frac{I_s}{\alpha}}$$

Equation (3:vi) was used to generate the curve showing the change in intensity with time, after the beam was switched on. This is shown in figure (3:4) as the solid line. The beam was considered to decay by a second order process after the pulse ended. The equation used is (3:vii). The decay of the intensity I after

$$(3:vii) \quad I = \frac{I_t}{(1 + \alpha I_t t)}$$

each pulse is shown as dashed lines. The areas under the curves,

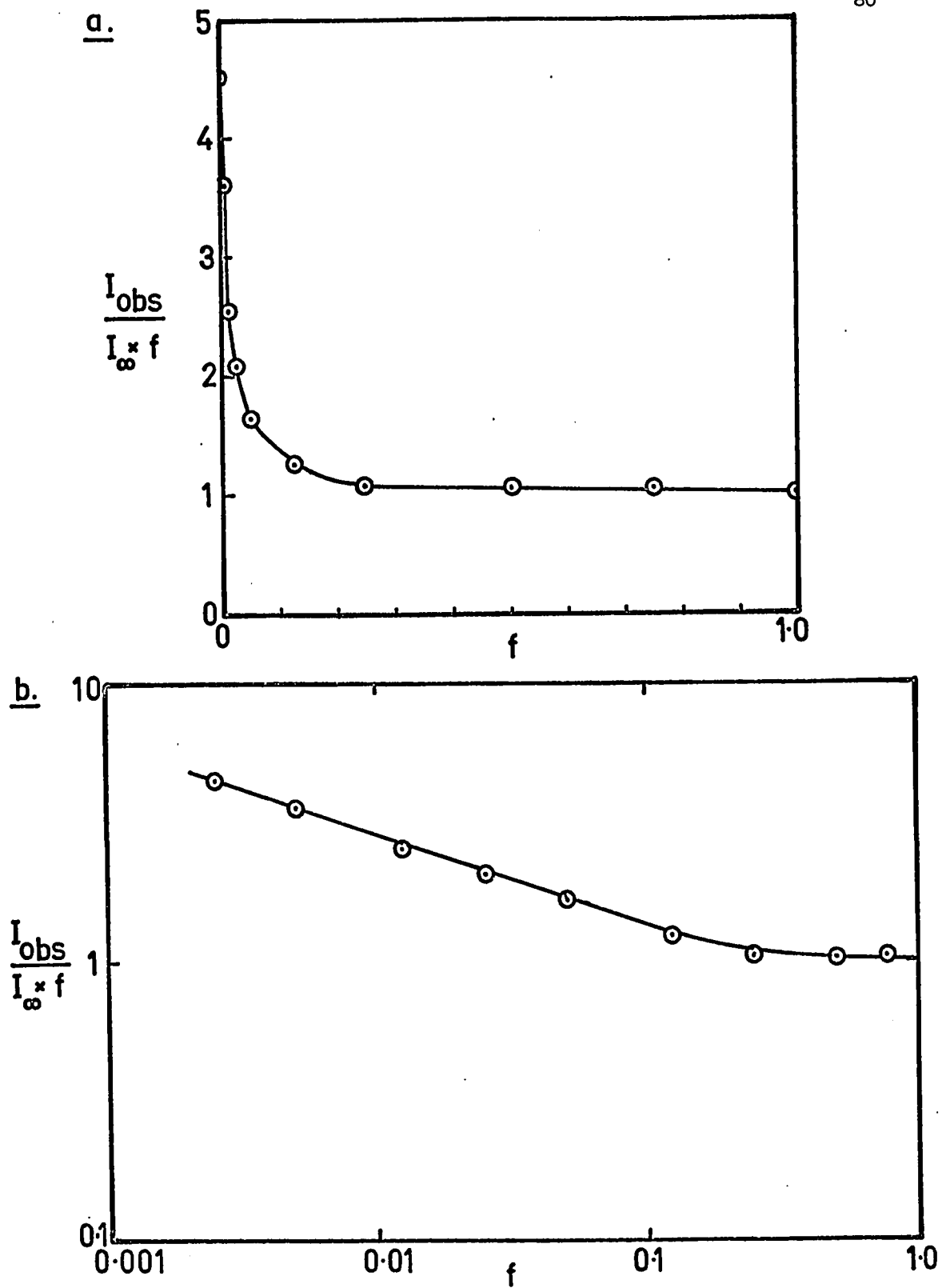


Figure 3:3 a. Normalized ion signal  $I_{obs}/I_{\infty}$  divided by the illumination fraction  $f$  versus  $f$ .

b. Above data on log-log plot.

which show the increase in intensity during the pulse, and the decrease after the pulse, were measured geometrically. These areas would normally correspond to the ion signal received by the mass spectrometer. These areas were normalized to the area of constant illumination. The results were plotted versus pulse length (as a fraction of the pulse repeat time) and are shown by line e in figure (3:2). One can see that the general shape of the curve is similar to the observed values. One would not expect it to agree exactly as many approximations were made in the calculations. The decay was assumed to be entirely second order and the geometric areas were only measured approximately.

Figure (3:4) also shows that the steady state condition was not established until the electron beam had been on about 200 micro seconds. This time is much longer than the pulse width (10 micro seconds) used in the later experiments.

#### iv Charge Density in Volume Sampled by the Leak

The density of charges in the sample leaving the leak may be calculated from the current measured at the ion acceleration cone. The density is given by equation (3:viii).  $n$  is the charge

$$(3:viii) \quad n = \frac{I_c}{F_l}$$

density,  $I_c$  the cone current and  $F_l$  the conductance of the leak. The cone current was measured as  $1 \times 10^{-9}$  amps which corresponds

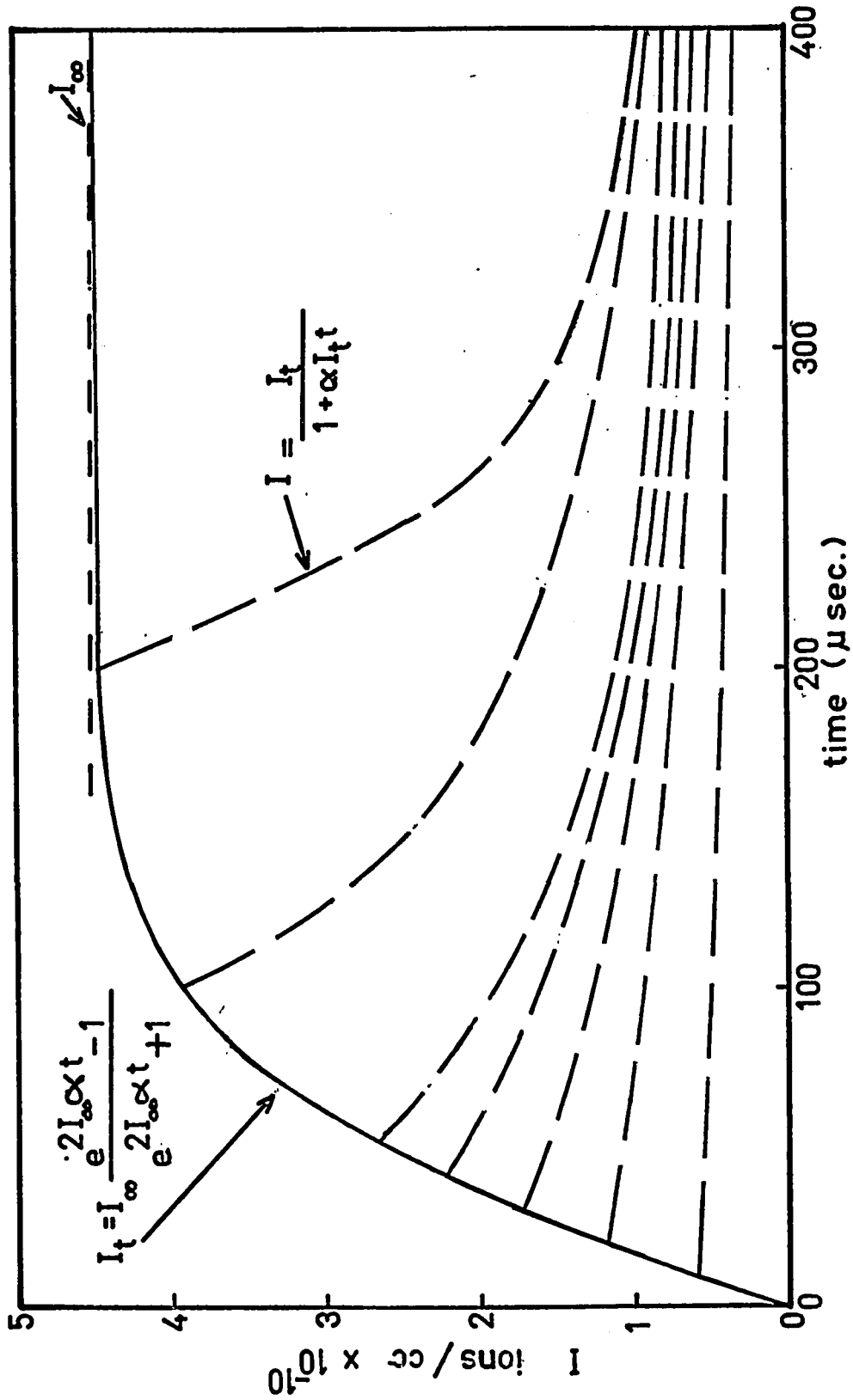


Figure 3:4 Theoretical plot of ion concentration  $I$  as the beam is switched on and a steady state condition develops. Decay curves at the end of each pulse if second order decay occurs.



to  $6 \times 10^9$  ions/second. The conductance of the leak was about 1.1 torr cc/second. The charge density is then calculated as  $n = 5 \times 10^9$  ions/cc at 1 torr. This is only one order of magnitude less than the calculated steady state concentration of ions in the beam. It indicates that the ions are probably not sampled directly from the beam but from just outside.

### 3:2 Processes Occurring in the Region From

#### Which Ions Were Observed

##### i The Effect of First and Second Order Loss Mechanisms

Each short pulse of electrons produces a group of ions which decay during the time between electron pulses. It would be interesting to determine the mode of this decay. A schematic diagram of the ion decay after each ionizing pulse is shown in figure (3:5a).

First consider that the decay occurs by a first order mechanism. On each pulse an initial ionization  $I_0$  is produced and it decays according to (3:ix) where  $I_t$  is the intensity at

$$(3:ix) \quad I_t = I_0 e^{-kt}$$

time  $t$  after the pulse and  $k$  the rate constant for decay. The pulse width  $\Delta t_e$  is assumed to be infinitely narrow, i.e.  $\Delta t_e \rightarrow 0$ . Let the residual intensity remaining from the previous pulse =  $C$ . The total intensity at each pulse is  $A$ .

$$(3:x) \quad A = I_0 + C$$

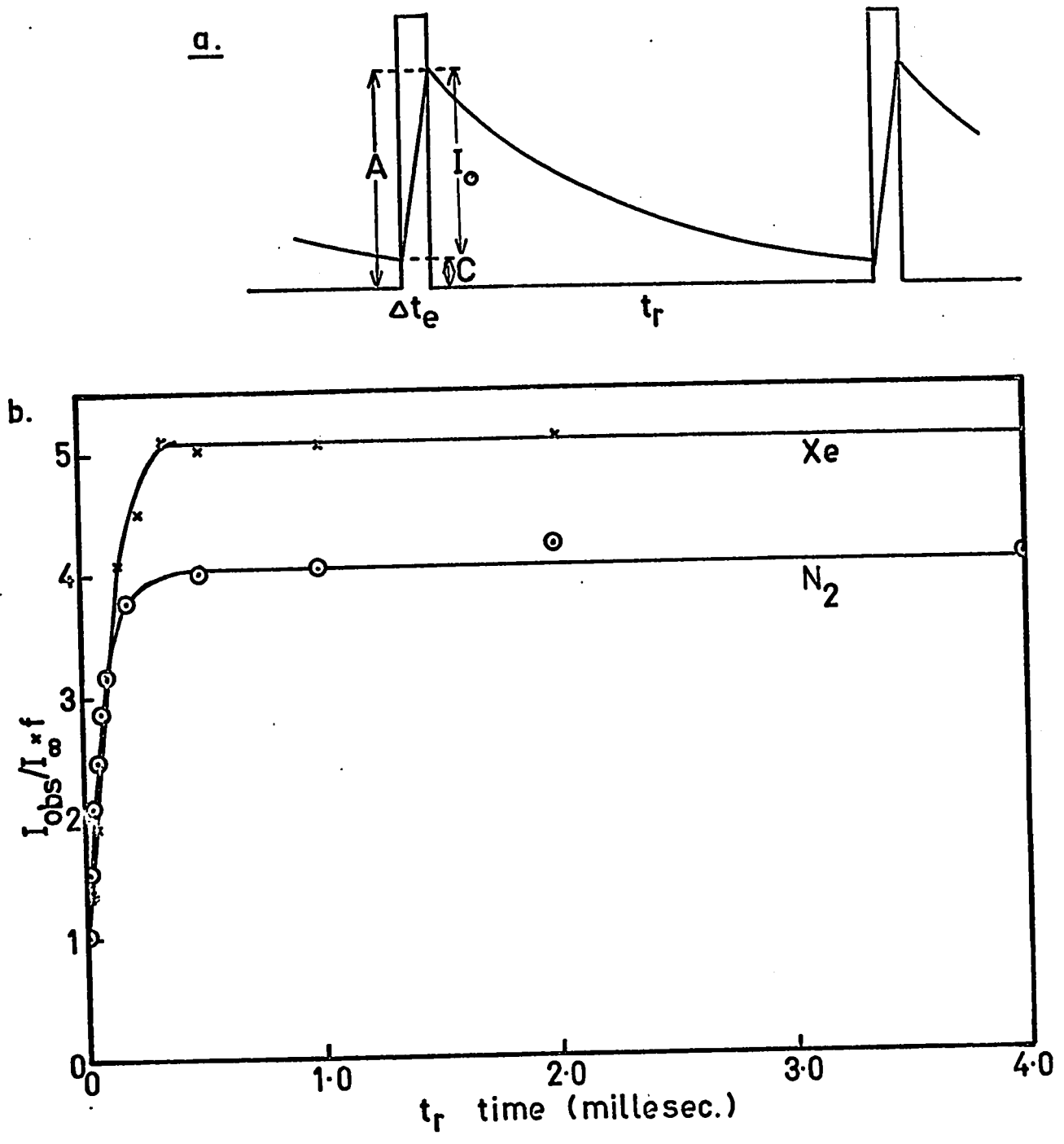


Figure 3:5 a. Schematic diagram of electron pulse and ion intensity curves at constant pulse width and variable repeat time  $t_r$ .  
b. Normalized observed ion signal  $I_{obs}/I_o$ , divided by illumination fraction  $f$ , plotted versus the pulse repeat time  $t_r$ .

Thus the observed intensity  $I_t'$  at any time  $t$  is given by (3:xi).

$$(3:xi) \quad I_t' = A e^{-kt}$$

The value of  $C$  is given by (3:xii) where  $t_r$  is the time between pulses.

$$(3:xii) \quad C = A e^{-kt_r}$$

If equations (3:ix) and (3:xii) are substituted into (3:xi) the observed intensity is given by equation (3:xiii).

$$(3:xiii) \quad I_t' = \frac{I_o}{(1 - e^{-kt_r})} e^{-kt}$$

Under conditions of continuous collection, the ion signal is proportional to the area under the decay curve. This may be found by integrating equation (3:xiii) between the limits 0 and  $t_r$  equation (3:xiv).

$$(3:xiv) \quad \int_0^{t_r} I_t' = \frac{-I_o}{(1 - e^{-kt_r})} \left[ \frac{1}{k} e^{-kt} \right]_0^{t_r}$$

$$(3:xv) \quad \therefore \text{Area} = \frac{I_o}{k}$$

Thus when the decay is first order the area is independent of the pulse repetition rate. However the observed signal is dependent upon the initial intensity  $I_o$ , and the intensity of the electron beam which is proportional to  $1/t_r$ . If one corrects the observed intensity to constant illumination then the signal is again independent of  $t_r$ .

This calculation may be repeated for the situation in which the decay of ionization is second order. The general equation for second order decay is given by (3:xvi). The parameters were defined earlier. The integrated equation which

$$(3:xvi) \quad I_t = \frac{I_o}{I_o \alpha t + 1}$$

is proportional to the area is given by (3:xvii).

$$(3:xvii) \quad \text{Area} = \frac{1}{\alpha} \ln \left[ \left( \frac{I_o}{2} + \sqrt{\frac{I_o^2}{4} + \frac{I_o}{\alpha t_r}} \right) \alpha t_r + 1 \right]$$

In this case the area is dependent upon  $t_r$  and increases as  $t_r$  increases.

The ion signal from 0.92 torr  $N_2$  in which the major ions were  $N_2^+$  and  $N_4^+$  was measured. The pulse width  $\Delta t_e$  was kept constant at 10 micro seconds. The results are shown on figure (3:5b). The observed ion intensity was normalized to constant illumination by dividing by the fraction of time  $f = (\Delta t_e / t_r)$ . The initial rise indicates that the decay of the pulses at times less than 200 micro seconds is second order, whereas at long reaction times the decay has decreased to first order. A plot of the normalized ion signal from Xe gas ( $Xe^+$  and  $Xe_2^+$ ) at 3.90 torr, with 20 micro seconds pulse width, also shown in figure (3:5b), demonstrates that the behaviour was constant for different gases.

ii Analysis of the Ion Intensity Curves by  
Means of the Einstein Equation

The total ion intensity curves obtained for  $N_2$  gas were analysed by means of the Einstein equation (3:xviii) (68, p. 492, 67, p. 199). This equation is for the spreading of a cloud of

$$(3:xviii) \quad N = \frac{N_0}{\sqrt{2\pi Dt}} e^{-x^2/4Dt}$$

particles by diffusion in one dimension through a gas.  $N_0$  is the number of particles located at the origin of a one dimensional coordinate system at time  $t=0$ .  $N$  is the number of ions at a point  $x$  some time  $t$  later,  $D$  is the diffusion coefficient. At any time  $t$  a plot of  $N$  as a function of  $x$  has the shape of a Gaussian error curve.

For the purpose of this calculation the electron beam was considered to be an infinitely thin plane. The ions would diffuse from the plane effectively only in one dimension and thus the above equation may be used. The distance  $x$  remains constant in the present situation. The variation of  $N$  with time was determined, by means of equation (3:xviii). Various combinations of  $D$  and  $x$  were used in the calculations. The results were plotted in semi log form as the initial intensity  $N_0$  was not known and the plots could be moved up or down until the maxima had the same height. These were compared with the experimental ion intensity curves which were also plotted in semi log form.

Figure (3:6) shows some of the measured total ionization curves and figure (3:8) some theoretical curves. It can be seen that the results do not agree very well. The ion curve obtained for 1.55 torr  $N_2$  at 385°K is the only one which has the same general shape. Very large values of the diffusion coefficient  $D$  were required to obtain ion intensity plots even close to the experimental ones. The position of the maximum of the ion intensity curve deserves some comment. The maximum time  $t_m$  is found by taking the derivative with respect to  $t$ , of equation (3:xvi). The maximum time is given by equation (3:xix). Since the diffusion coefficient  $D$  is

$$(3:xix) \quad t_m = \frac{x^2}{2D}$$

inversely proportional to pressure (67, p. 201). One would expect that as the pressure increased that the time would increase proportionally. The time of the maximum of the experimental ion intensity curves were found to increase slightly, but certainly not proportionally to the pressure. If the measured distance  $x$ , between the plane of the slit and the ion exit aperture, is substituted into equation (3:xvii), large values of  $D$  (500  $cm^2/sec.$  to 1500  $cm^2/sec.$ ) are predicted by the values of the time  $t_m$ .

These calculations confirm that at short times, the loss of ions was by means other than diffusion, i.e. recombination,

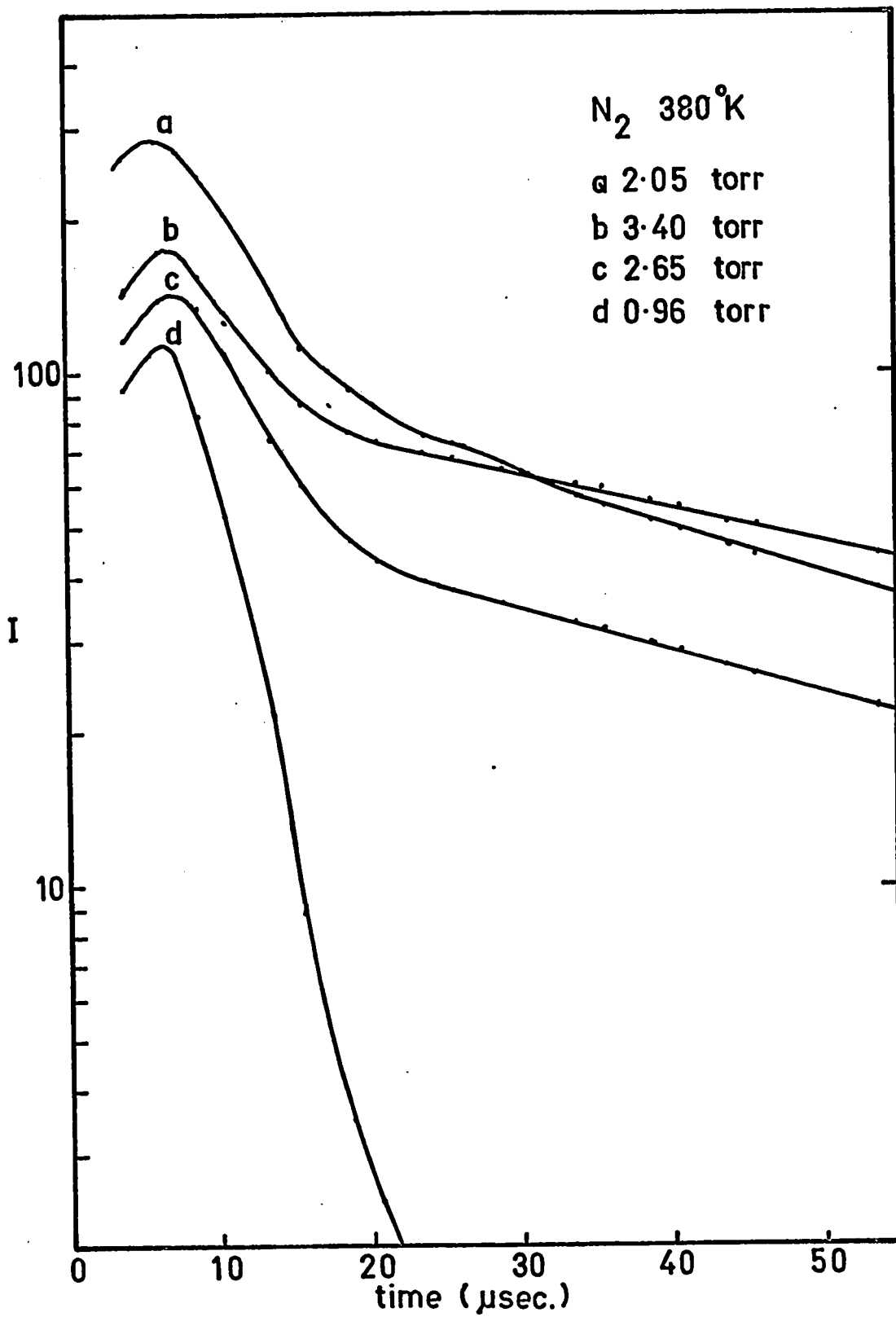


Figure 3:6 Observed total ion intensity versus time curves for pure N<sub>2</sub> at 380°K, x = 0.67 mm.

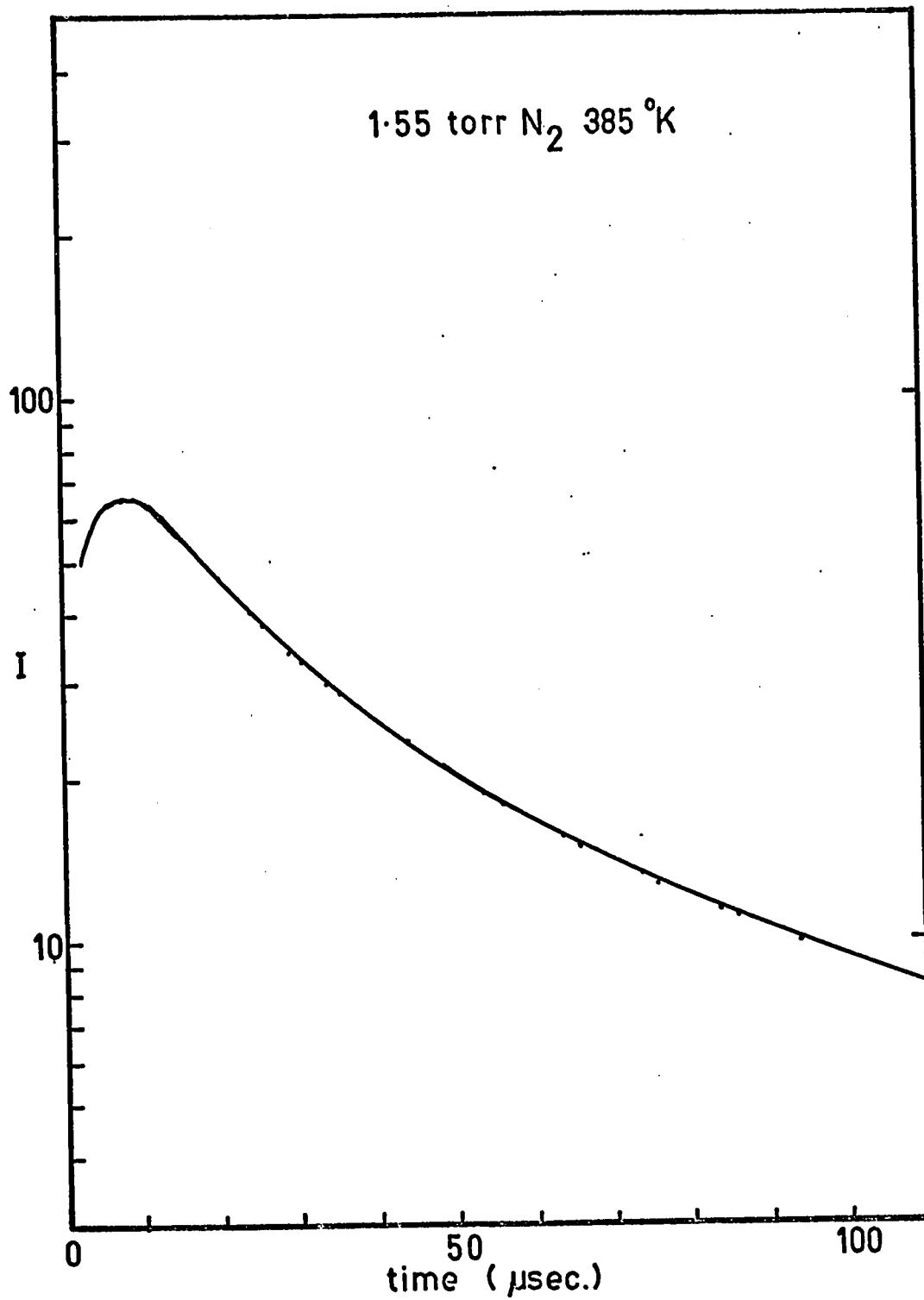


Figure 3:7 Observed total ion intensity versus time curve for  
1.55 torr N<sub>2</sub> at 385°K, x = 1.67 mm.



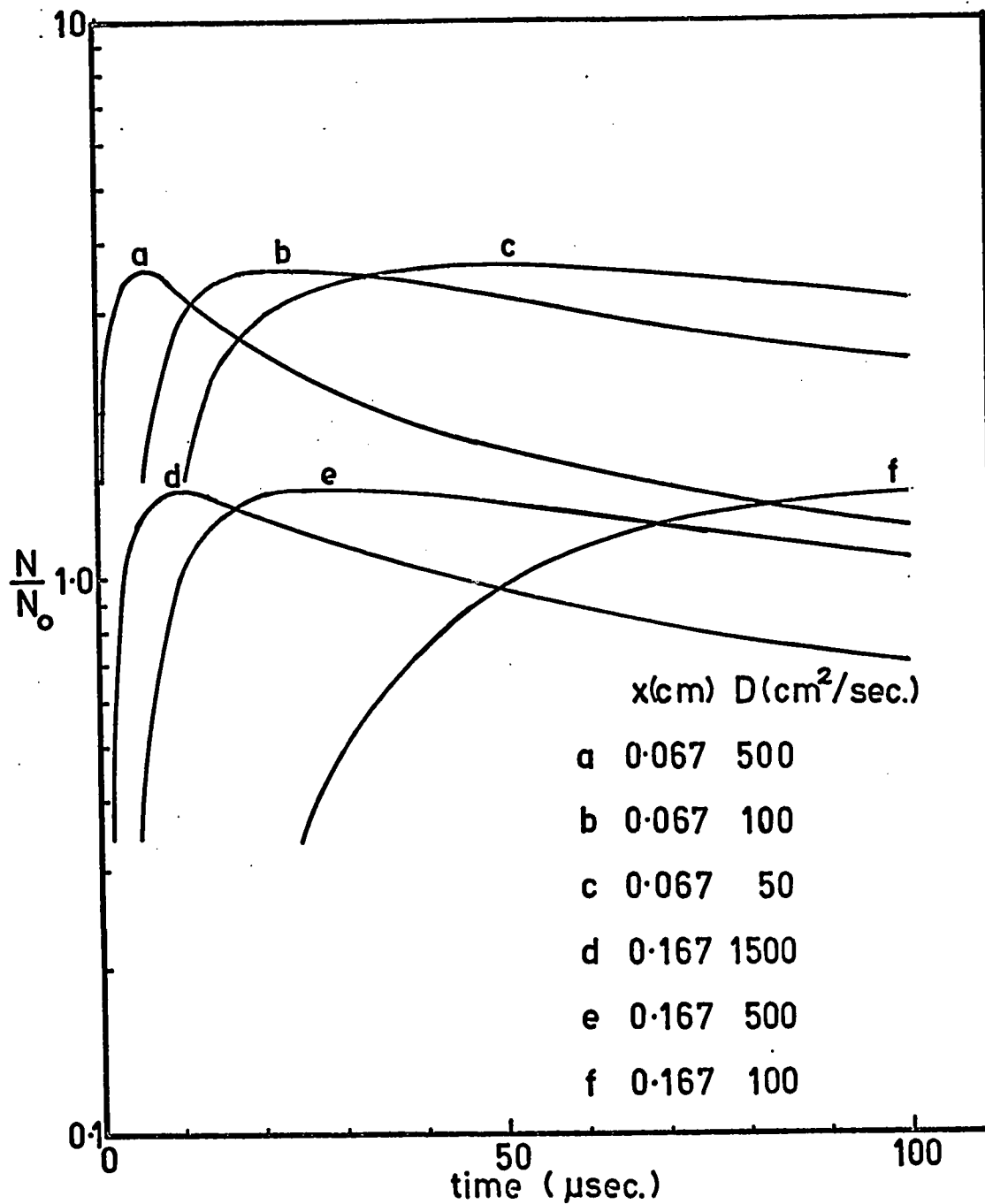


Figure 3:8 Theoretical curves calculated from the Einstein Equation (3:xviii)

as the initial loss was very rapid. At long reaction times > 30 micro seconds (from figure 3:6) the decrease appeared to be due to diffusion, as the log plots (figure 3:6) show almost a linear decrease in intensity.

### iii Effect of Mass Flow

If the ion is removed from the ion source entirely by mass flow, the time required for an ion to travel from its point of origin to the ion exit aperture may be calculated by means of an equation (3:xx) developed by Kebarle *et al* (42).

$$(3:xx) \quad t = \frac{2\pi}{3F_{\ell}} (r^3 - r_0^3)$$

This is the equation for flow from a hemisphere above the leak. The leak conductance  $F_{\ell} = 1.13$  cc/sec. for nitrogen.  $r$  is the radius of the hemisphere and  $r_0$  the radius of the leak. If  $r$  is taken as 0.67 mm and  $r_0$  as .060 mm, the time  $t$  is calculated as 560 micro seconds. When  $r = 1.67$  mm  $t = 8.5$  milli seconds. This would indicate that the effect of mass flow towards the removal of ions is not as effective as recombination or diffusion of the ions. Since a large amount of gas flowed out of the electron entrance slit, one might expect some ions to be removed also. The same equation may be used.  $r = 5$  mm and  $r_0$  is negligible in comparison. At a distance of 5 mm the time for outflow will not be

affected by the length of the slit, and the flow pattern will be essentially spherical and equation (3:xx) may be used.

When  $F_g = 8.1$  cc/sec. and  $r = 5$  mm,  $t = 30$  milli seconds which is also a long time with respect to the ion decay time.

#### iv Average Lifetime of an Ion in the Ion Source

The average life of an ion was calculated from the ion intensity curve. This curve was obtained for  $N_2$  gas at 1.55 torr at a temperature of 395°K. The average time  $\bar{t}$  was calculated from the values of the intensity  $I_i$  measured at many times  $t_i$ . The time axis was divided into time intervals  $\Delta t$  each 5 micro seconds long. At each time interval  $\Delta t$ , the height  $I_i$  was measured. The average value of the function where  $I = f(t)$  is given by (3:xxi).

$$(3:xxi) \quad \bar{I} = \frac{\sum \Delta t_i I_i^2}{\sum \Delta t_i I_i}$$

Since  $I = f(t)$  the average time  $\bar{t}$  times the average height  $\bar{I}$  equals the area under the curve i.e. equation (3:xxii).

$$(3:xxii) \quad \bar{t} \cdot \bar{I} = \sum \Delta t_i I_i$$

Thus the average time is given by (3:xxiii).

$$(3:xxiii) \quad \bar{t} = \frac{(\sum \Delta t_i I_i)^2}{\sum \Delta t_i I_i^2}$$

The values of  $I_i$  and  $\Delta t_i$  for the ion intensity curve of

1.55 torr  $N_2$  (figure 3:7) were tabulated and the value for  $\bar{t}$  was found to be 160 micro seconds.

### 3:3 Conclusion

The above order of magnitude calculations and experiments show that the ion intensity was affected by three loss mechanisms recombination, ambipolar diffusion and mass flow.

Under continuous illumination it appeared that the majority of the ions were lost by recombination in the beam. Since this is a second order process, ions undergoing first order chemical reactions in the beam would exhibit a kinetic order which is not first order. The average lifetime of an ion in the beam was calculated to be 70 micro seconds, at 1 torr. The time for diffusion out of the beam was calculated at about 25 micro seconds. Since these are the same order, a considerable concentration of ions would diffuse from the beam. It was shown however, that the ion density in the region sampled by the leak was an order of magnitude less than the steady state concentration of ions in the beam. The observed ions must therefore have been sampled from a region just outside the beam and consequently one would expect that recombination of ions and electrons in the beam would not adversely affect the kinetic studies. At higher pressures the average lifetime of an ion in the beam would decrease

whereas the time for the ions to diffuse from the beam would increase. Consequently even though the ion concentration in the beam increased the number diffusing out may not increase. This might explain the observed ion intensity versus pressure plot (figure 2:12a). The ion intensity increased up to about 1 torr and then remained constant. The loss in signal, from a predicted continual increase with pressure could not be explained completely by loss through ion-molecule collisions outside the ion source. Thus the ion intensity measured outside the ion source was probably representative of the ion concentration in the sampled volume.

When the electron beam was pulsed, the processes occurring appeared to be somewhat different. If the rate of production of ions is  $6 \times 10^{14}$  ions/cc sec. then  $6 \times 10^9$  ions/cc would be produced in 10 micro seconds (the usual time used in most of these experiments). This is less than the steady state concentration. The ion intensity plots (3:6) indicate that the loss of ions occurs initially at a rate greater than first order and then decays to a first order rate. This was also indicated by figure (3:5b). One might estimate from figure (3:6) that the change of rate took place at perhaps  $20 \mu$  seconds, or from figure (3:6), that it took place at 200 micro seconds. Since figure (3:6) shows the ions intensity curves directly the value of 20 micro seconds is probably the better one. The ions were

removed from the ion source by the first order processes, diffusion and mass flow. The diffusion coefficients obtained from the time of maxima of the ion intensity curves were extraordinarily high consequently the Einstein equation probably does not describe the situation properly. Since the maxima were independent of pressure one might conclude that ions were formed close to the leak and that these were removed in a very short time. Since the travel time of the gas was large the ions were probably removed mostly by diffusion. Unfortunately the diffusion coefficient is mass dependent. Equation (3:xxiv) (67, p. 201) shows the relationship between the diffusion coefficient of an ion and the masses  $m$  of the ion and  $M$  of the gas.

$$(3:xxiv) \quad D \propto \sqrt{\frac{M + m}{M}}$$

Thus  $D$  will increase with the mass of the ion and decrease with increasing mass of the gas. Consequently there would be some mass discrimination and this will affect the kinetic measurements.

The decay of the total ionization will affect the kinetic measurements only if the decay is second order. If the decay is first order the kinetic measurements will be correct.

Consider that the total number of ions per pulse =  $I_0^0$ . Since this decays by a first order mechanism the observed intensity at time  $t$ , with no reactions occurring is  $I_0^t$ . The

presence of a reactant gas, which reacts with the ions by a first order mechanism, will cause the decrease in ions to be faster. If one takes the measured concentration of  $I_o^o$  at some time,  $t$  i.e.  $I_o^t$ , and adds a small concentration of reactant gas the intensity will fall to  $I_c^t$ . Since the mechanism is first order the intensities may be expressed by equation (3:xxv)

$$(3:xxv) \quad \ln\left(\frac{I_o^t}{I_c^t}\right) = kct$$

where  $k$  is the reaction rate constant and the concentration of reactant gas. To measure  $k$  take times  $t_1$  and  $t_2$ .

$$(3:xxvi) \quad kc(t_2 - t_1) = \ln\left(\frac{I_o^{t_2}}{I_c^{t_2}}\right) - \ln\left(\frac{I_o^{t_1}}{I_c^{t_1}}\right)$$

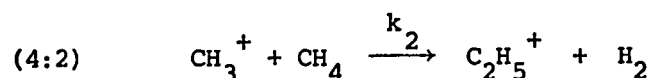
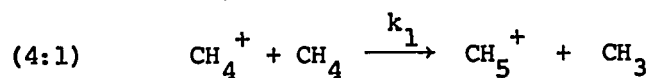
$$(3:xxvii) \quad kc(t_2 - t_1) = \ln\left(\frac{I_o^{t_2}}{I_c^{t_2}} \cdot \frac{I_c^{t_1}}{I_o^{t_1}}\right)$$

If the ion intensities are normalized by dividing out by the total ionization  $I_o$  at all times the fractional ion intensities  $i$  will give the correct rate constant since  $i_t = I_c^t / I_o^t$ . Thus the decay of the total ionization by a first order mechanism will not disturb the kinetic studies. This technique was used in most of the kinetic studies described in the next sections.

#### 4. REACTIONS IN METHANE - KRYPTON

##### 4.1 Introduction - Purpose of Studying CH<sub>4</sub>-Kr System, and Previous Results

The technique of using a pulsed electron beam and gates ion beam to observe the rate of decay of intensity, of ions produced at very high pressures was new, and consequently some chemical verification of the method was required. Since the pulse technique was designed to measure absolute reaction rates, an ionic reaction with a well known rate constant was needed. All well known ion-molecule reaction rate constants are in the order of  $10^{-9}$  to  $10^{-10}$  cc/molecule second and were measured at low pressure. Probably the most frequently measured rate constants are those for reactions (4:1) and (4:2) in methane. These reactions are frequently used for calibration purposes(69).



They were first observed by Talroze and Lyubimova (5) and by Stevenson and Schissler (6,7) who measured their cross sections. Similar measurements were made by many other workers in conventional mass spectrometers. These early results are contained in a review by Field *et al* (33). Unfortunately since the ions were reacting under the influence of a repeller field they did not have thermal energies. Rate constants for thermal ions, calculated from these



cross sections by the equation (1:vii) (see section 1:2), were found to be slightly dependent upon the repeller field strength,

$$(1:vii) \quad k = Q \sqrt{\frac{eE_r l}{2mp}}$$

and therefore the use of these values for thermal conditions is somewhat ambiguous.

Values of the rate constants at thermal energies have since been determined at low pressures by means of a pulsing technique (16,18,70,71,72,73). This technique was described earlier in section (1:3).

The results for  $k_1$  (reaction 4:1) and  $k_2$  (reaction 4:2) are summarized in Table 4:1. One can see that the different workers have obtained very similar results, since those values for  $k_1$  obtained by pulse methods agree within 10%. Fewer values of  $k_2$  are available. When  $\text{CH}_4$  is ionized by electron impact the intensity of  $\text{CH}_3^+$  is less than that of  $\text{CH}_4^+$ . Thus  $k_2$  is more difficult to measure and the uncertainty of its measurement is larger than that of  $k_1$ . However the value of 0.79 for  $k_2$  compared to 0.99 for  $k_1$  from the repeller method (reference 33) shows that the two reactions have about the same rates.

From the data in Table 4:1, one can calculate a suitable pressure at which the reactions may be conveniently observed.

TABLE 4:1  
Rate Constants for Reactions (4:1) and (4:2)  
Measured at Low Pressures (Literature Values)

Technique	Rate constants (cc/molecule sec.)x10 <sup>9</sup>		Reference
	k <sub>1</sub>	k <sub>2</sub>	
Repeller	0.99	0.79	(33) other values are quoted in this reference
Pulsed	1.16		(16)
	1.25		(70)
	1.25	0.70	(71)
	1.11		(18)
	0.96		(72)
		0.86	(73)

The half life of a bimolecular reaction such as (4:1) is given by equation (4:i) (74).

$$(4:i) \quad \tau = \frac{1}{k_1 [\text{CH}_4]}$$

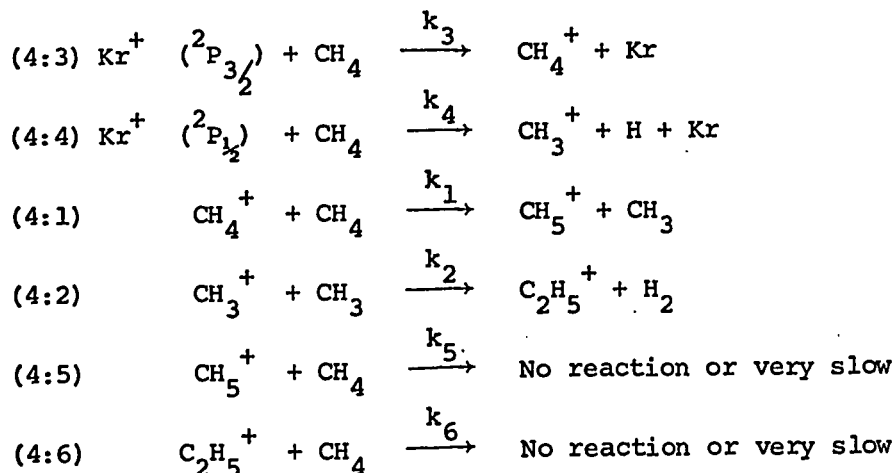
where [CH<sub>4</sub>] is the concentration (in molecules/cc, if k<sub>1</sub> is in cc/molecules sec.) In this instrument it was most convenient to set the electron pulse duration at 10 micro seconds. Since the pulse width must be short with respect to the reaction time a convenient half life of the reaction might be set at

50 micro seconds. Using equation (4:i) and a value of  $1 \times 10^{-9}$  for  $k_1$ , one obtained a  $\text{CH}_4$  concentration of  $2 \times 10^{13}$  molecules/cc. At  $300^\circ\text{K}$  this is about  $10^{-3}$  torr.

Our intention was to calibrate the ion source at high pressures, of the order of 1 to 5 torr. To get such pressures, and yet still have the pressure of  $\text{CH}_4$  about  $10^{-3}$  torr a charge exchange dilution technique (which is also termed inert gas sensitization (42)) was used. The reactant gas is mixed with a large excess of the inert gas. A rare gas or one of the diatomic gases such as nitrogen is used as the inert gas sensitizer. If the ionization cross sections of the two gases are not too different, the concentration of ions produced from the reactant and the inert gas will be approximately proportional to their partial pressures when the mixture is irradiated. In our example these pressures are  $10^{-3}$  and 1 torr and would lead to the ion ratio of 1:1000. However if the recombination energy (R.E.) of inert sensitizer gas is larger than the ionization potential ( $I_p$ ) of the reactant gas most of the ionization will be transferred to the latter through charge transfer reactions (Section 1:5, i,ii).

Krypton was chosen as the inert gas. The  $\text{Kr}^+$  ion has two states. The  $^2\text{P}_{3/2}$  with a recombination energy of 14.00 eV and the  $^2\text{P}_{1/2}$  with a R.E. of 14.67 eV. These react with  $\text{CH}_4$  to produce  $\text{CH}_4^+$  and  $\text{CH}_3^+$  respectively (27). The overall

reaction scheme may then be written as follows:



The unreactivity of  $\text{CH}_5^+$  and  $\text{C}_2\text{H}_5^+$  ions in methane was previously established by Field *et al* (34), by Kebarle (75) and by Wexler (39). This then sets a limit to the reaction sequence.

The presence of both  $\text{CH}_4^+$  and  $\text{CH}_3^+$  is unfortunate since it complicates the kinetics. Two other gases with recombination energies larger than the ionization potential of methane, and which might have been conveniently used, are xenon and argon. The choice of sensitizer gas was made by referring to several studies of charge transfer reactions of the rate gases with methane (27,38,76,77). The results of von Koch (27) were the most useful. Figure (4:1A) shows a breakdown curve for  $\text{CH}_4^+$  taken from this paper. This curve indicates relative concentrations of the ions that are produced by charge exchange, as the recombination energy of the primary ion is increased.

The use of xenon (R.E.  ${}^2\text{P}_{1/2} = 13.44$  eV) would appear ideal, since by exchange only  $\text{CH}_4^+$  is produced. Unfortunately

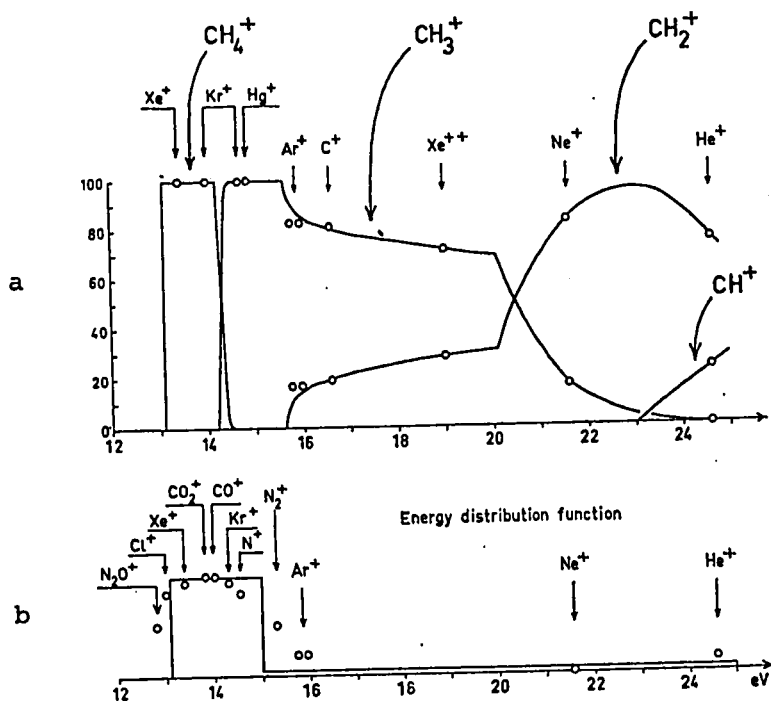


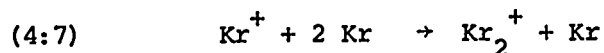
Figure 4:1 From von Koch reference (27).

- (a) Breakdown curve of methane; the mass spectrum as a function of the energy absorbed.
- (b) Distribution of energies given  $\text{CH}_4^+$  by electron impact.

however Field and Franklin (78) have reported that in mixtures of xenon and methane the ions  $\text{XeCH}_3^+$ ,  $\text{XeCH}_2^+$ ,  $\text{XeCH}^+$ ,  $\text{XeC}^+$  and  $\text{XeH}^+$  are observed. These ions would complicate the kinetics exceedingly. Argon might have been chosen since it produces a large intensity of  $\text{CH}_3^+$ , but the rate constant for reaction (4:2) is less well known and  $\text{CH}_2^+$  is also produced.

As was mentioned earlier, the break down curve indicates that of the two states of  $\text{Kr}^+$ , the  $^2\text{P}_{3/2}$  reacts with  $\text{CH}_4$  to give  $\text{CH}_4^+$  and the  $^2\text{P}_{1/2}$  to give  $\text{CH}_3^+$ . Cermak and Herman (77) reported the relative yields to be 0.65 and 0.35 respectively.

Krypton ions react with krypton atoms to form a molecular ion, by means of a three body reaction (4:7).



This reaction is not expected to interfere, since at a relative pressure of methane to krypton of 1:1000,  $\text{Kr}^+$  ions will be removed much more quickly by the charge exchange reactions (4:3) and (4:4).

#### 4.2 Methane-Krypton Experimental

The variation with time, of the intensities of the ions  $\text{Kr}^+$ ,  $\text{CH}_3^+$ ,  $\text{CH}_4^+$ ,  $\text{CH}_3^+$  and  $\text{C}_2\text{H}_5^+$  was measured for mixtures of methane and krypton. The methane concentration was varied over a range of  $0.68 \times 10^{-3}$  to  $3.4 \times 10^{-3}$  torr in a constant pressure of 3.4 torr krypton. All experiments were done at room temperature

(i.e. 297 to 300°K). The electron pulse and ion gate widths were set at 10 micro seconds. The pulse repeat time was set at 2000 micro seconds so that the ionization produced by each electron pulse had decayed completely between pulses. All other conditions were the same as described previously (section 2).

### 4.3 Results

#### i Qualitative Observations

The variation of intensity of the major ions observed in a mixture of  $1.4 \times 10^{-3}$  torr  $\text{CH}_4$  in 3.4 torr Kr is shown in figure (4:2). This represents a set of typical results. The plot also shows the change of total ion intensity with time. As can be seen, the decrease of total ion intensity was very rapid for the first 50 micro seconds. The decrease then slowed down so that the ion signal became negligibly small after 2000 micro seconds. This decrease in total ionization in the ion source was due to ion-electron recombination, ion diffusion to the wall, and mass outflow through the leak. These factors and their significance to the kinetic measurements were described earlier in section (3:3).

One can see qualitatively in this figure how the reaction sequence is carried. The  $\text{Kr}^+$  ions initially formed travelled towards the ion source exit and there was an initial increase in the  $\text{Kr}^+$  intensity, and hence the total ion intensity, since

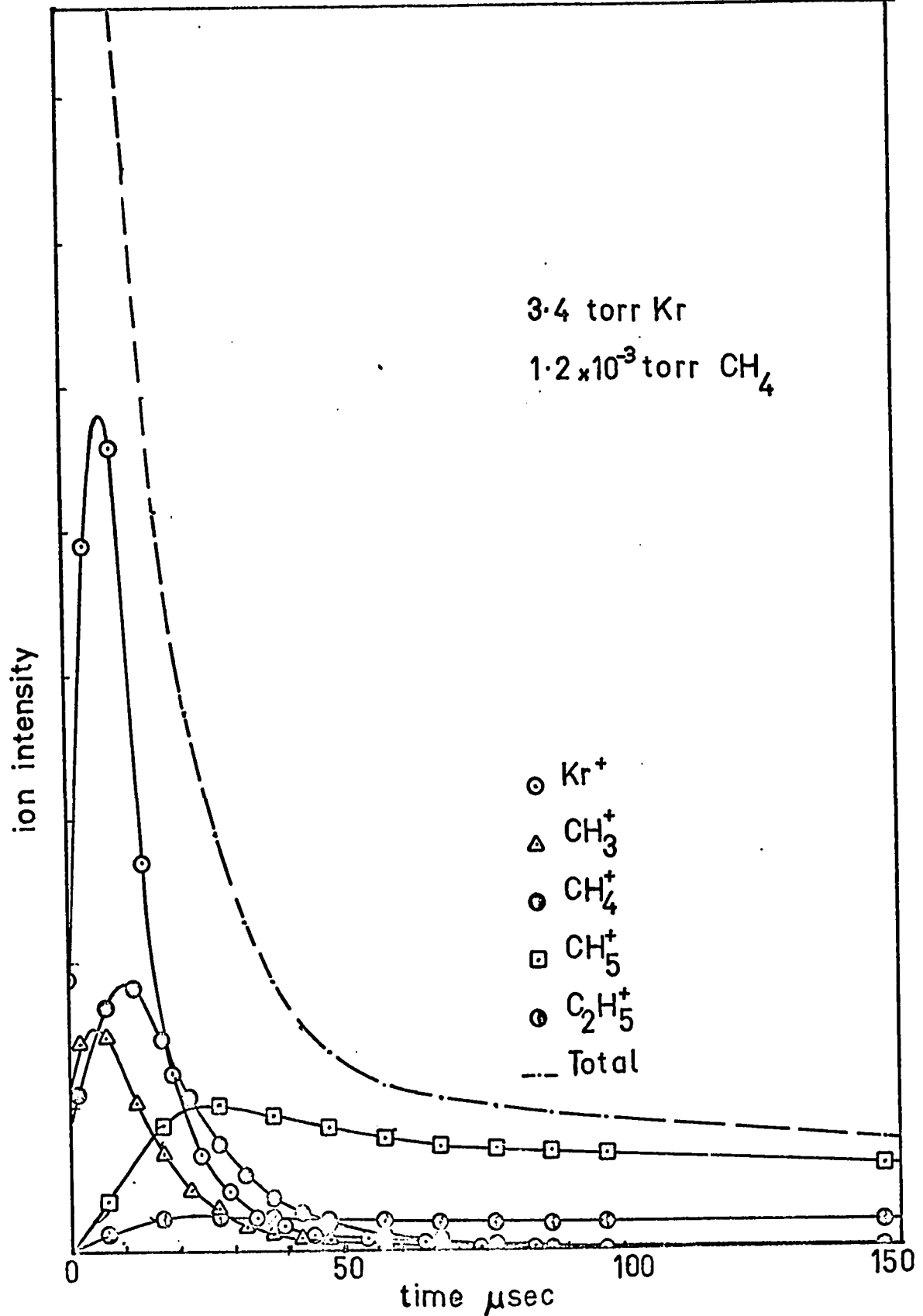


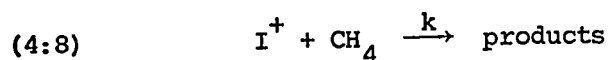
Figure 4:2 Raw data showing decay of  $\text{Kr}^+$ ,  $\text{CH}_4^+$ ,  $\text{CH}_3^+$  and total ionization.



at short times (0-10 micro sec.)  $Kr^+$  was the major ion.  $Kr^+$  was also being produced in this time by the 10 micro sec. electron pulse. As the  $Kr^+$  ions reacted they disappeared more rapidly than the total ionization and  $CH_4^+$  and  $CH_3^+$  appeared. These in turn decreased as  $CH_5^+$  and  $C_2H_5^+$  were formed.

### ii Preliminary Estimate of Rate Constants

In order to gain a preliminary set of values for the rate constant one may try to select conditions where the decrease of an ion intensity due to reaction is faster than the decrease due to diffusion and mass outflow. It was assumed that this was the case for the reactions of  $Kr^+$ ,  $CH_3^+$  and  $CH_4^+$ . One may derive an equation for the loss of  $Kr^+$  as follows. For the general bimolecular reaction (4:8)



$$(4:ii) \quad \frac{d[I^+]}{dt} = -k [I^+] [CH_4]$$

Since the concentration of ions is much less than the neutral concentrations i.e.  $[CH_4] \gg [I^+]$ , we may consider that  $[CH_4]$  is constant, so that the reaction becomes pseudo-first order. We can rearrange (4:ii) and integrate (4:iii). Let  $[I^+]$  be written as  $I^+$ .

$$(4:iii) \quad \frac{dI^+}{I^+} = -k [CH_4] dt$$

$$(4:iv) \quad \ln \frac{I^+}{I_0^+} = -k [CH_4] t$$

This can be written alternatively in an exponential form.

$$(4:v) \quad I^+ = I_o^+ e^{-k[CH_4] t}$$

From equation (4:iv), if  $\log_{10} [I^+]$  is plotted versus  $t$  the slope becomes  $-k[CH_4]/2.303$ . The equation used in practice then becomes (4:vi), if equation (4:iii) is integrated between times  $t_1$  and  $t_2$ .

$$(4:vi) \quad k = \frac{-2.303 \log_{10} (I_{t_2}/I_{t_1})}{[CH_4] (t_2 - t_1)}$$

One may also use this equation for the loss of  $CH_4^+$  and  $CH_3^+$  if an additional assumption is made; that reactions (4:3) and (4:4) had gone essentially to completion before reactions (4:1) and (4:2) occurred so that these ions were not being produced at a time when their decrease due to reaction gave a linear log plot.

The log plots of the intensities (corrected for mass spectrometer sensitivities) of the ions  $Kr^+$ ,  $CH_4^+$  and  $CH_3^+$  for a mixture of  $1.4 \times 10^{-3}$  torr  $CH_4$  and 3.4 torr  $Kr$  are shown in figure (4:3). The respective rate constants are calculated as  $1.97 \times 10^{-9}$ ,  $1.50 \times 10^{-9}$  and  $1.64 \times 10^{-9}$  cc/molecule seconds. The rate constant measured from the decrease of  $Kr^+$  is a composite of those for reactions (4:3) and (4:4) as the two states of  $Kr^+$  were indistinguishable experimentally.

The preliminary values for the rate constants for three

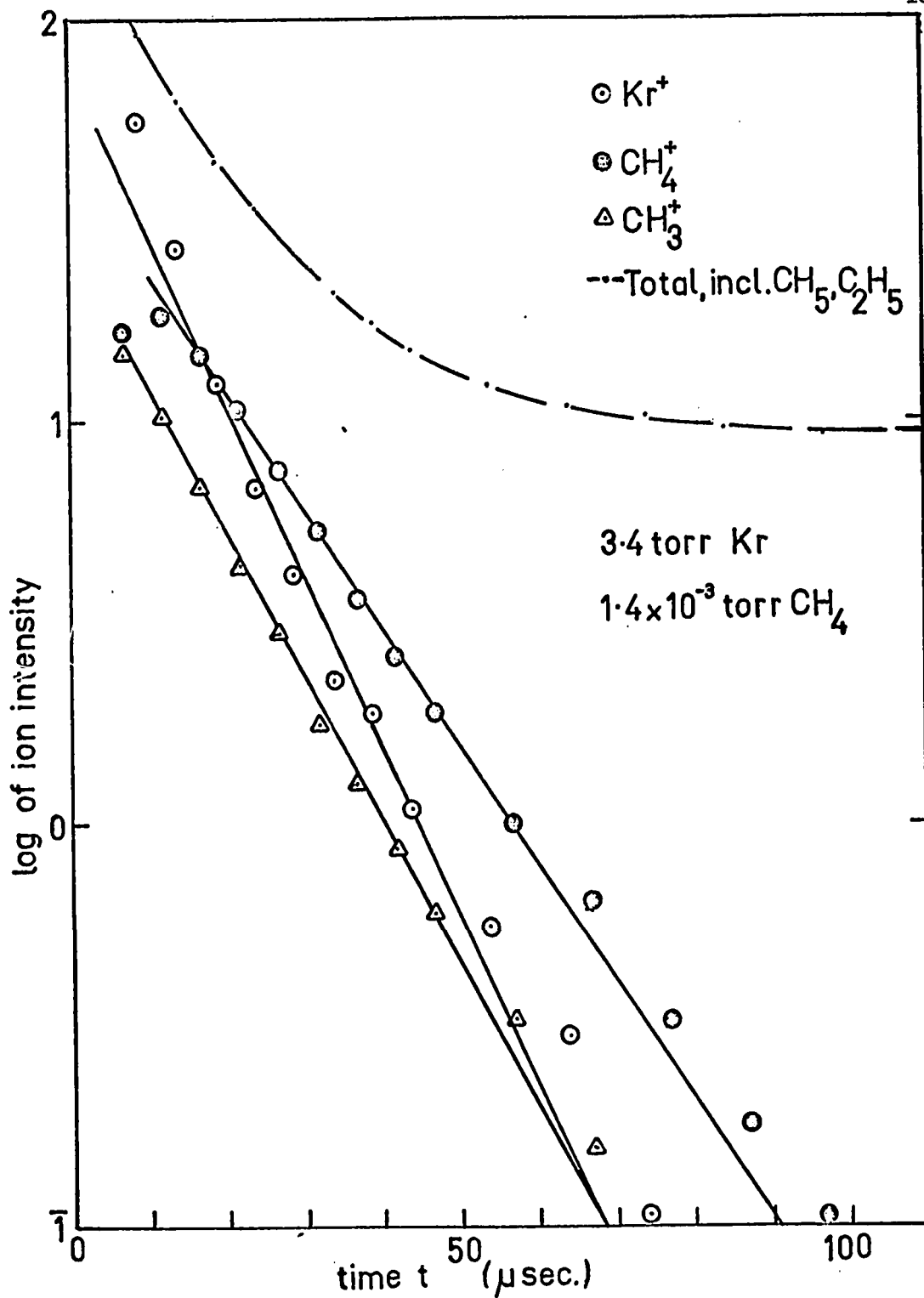


Figure 4:3 Observed ion intensity curves for  $\text{Kr}^+$ ,  $\text{CH}_4^+$ ,  $\text{CH}_3^+$ ,  $\text{CH}_5^+$ ,  $\text{C}_2\text{H}_5^+$ , and total ionization for mixture of  $1.2 \times 10^{-3}$  torr  $\text{CH}_4$  in 3.4 torr Kr.

methane concentrations are given in Table 4.2.

TABLE 4:2  
Rate constants from the decay of  
Kr<sup>+</sup> CH<sub>4</sub><sup>+</sup> CH<sub>3</sub><sup>+</sup> - preliminary values

P Kr = 3.4 torr	Rate constants (cc/molecule sec.)x10 <sup>9</sup>			
	P CH <sub>4</sub> x10 <sup>3</sup> torr	k (Kr <sup>+</sup> ) Rx (4:3), (4:4)	k CH <sub>4</sub> <sup>+</sup> Rx (4:1)	k CH <sub>3</sub> <sup>+</sup> Rx (4:2)
	0.68	2.21	1.60	1.94
	0.68	2.15	1.53	1.85
	1.4	1.97	1.50	1.64
	3.4	1.71	1.27	1.48

The values have the same order of magnitudes as those measured by other techniques (Table 4:1) but are different by almost a factor of two. The two runs at  $0.68 \times 10^{-3}$  torr CH<sub>4</sub> show that the reproducibility was good, as the difference in duplicate runs is less than 10%.

The total ionization is also plotted on figure (4:3), taken from figure (4:1). One can see that the decrease with time is almost as large as the decrease of the individual ion intensities, and since this will make each ion intensity decrease appear to be faster than that from reaction alone,

these rate constants will be too large.

One can see also that these rate constant rates are not independent of methane pressure. There were two possible explanations; firstly that the reactions were not really pseudo first order, or secondly that the decrease of ion intensity due to mass flow was not the same at each methane concentration. Careful comparison of total ionization curves at different  $\text{CH}_4$  pressures (not shown) showed this was the case. Consequently a normalization procedure was applied as follows.

### iii Corrected Values of Rate Constants

The data shown in figure (4:3) were normalized by plotting each ion intensity at a time  $t$  as a fraction of the total ion intensity at that time. The normalized curves are shown in figure (4:4). The reaction sequence can be seen quite clearly in this figure.

Plots similar to (4:2) and (4:4) were prepared for other data resulting from the irradiation of mixtures  $0.68 \times 10^{-3}$  and  $3.4 \times 10^{-3}$  torr methane in 3.4 torr Kr (these are not shown) subsequently the fractioned intensities will be labelled with a small  $i$  (e.g.  $i_{\text{Kr}}^+$ ).

The data in figure (4:4) represents a system of consecutive (pseudo) first order reactions, since the concentration of  $\text{CH}_4$

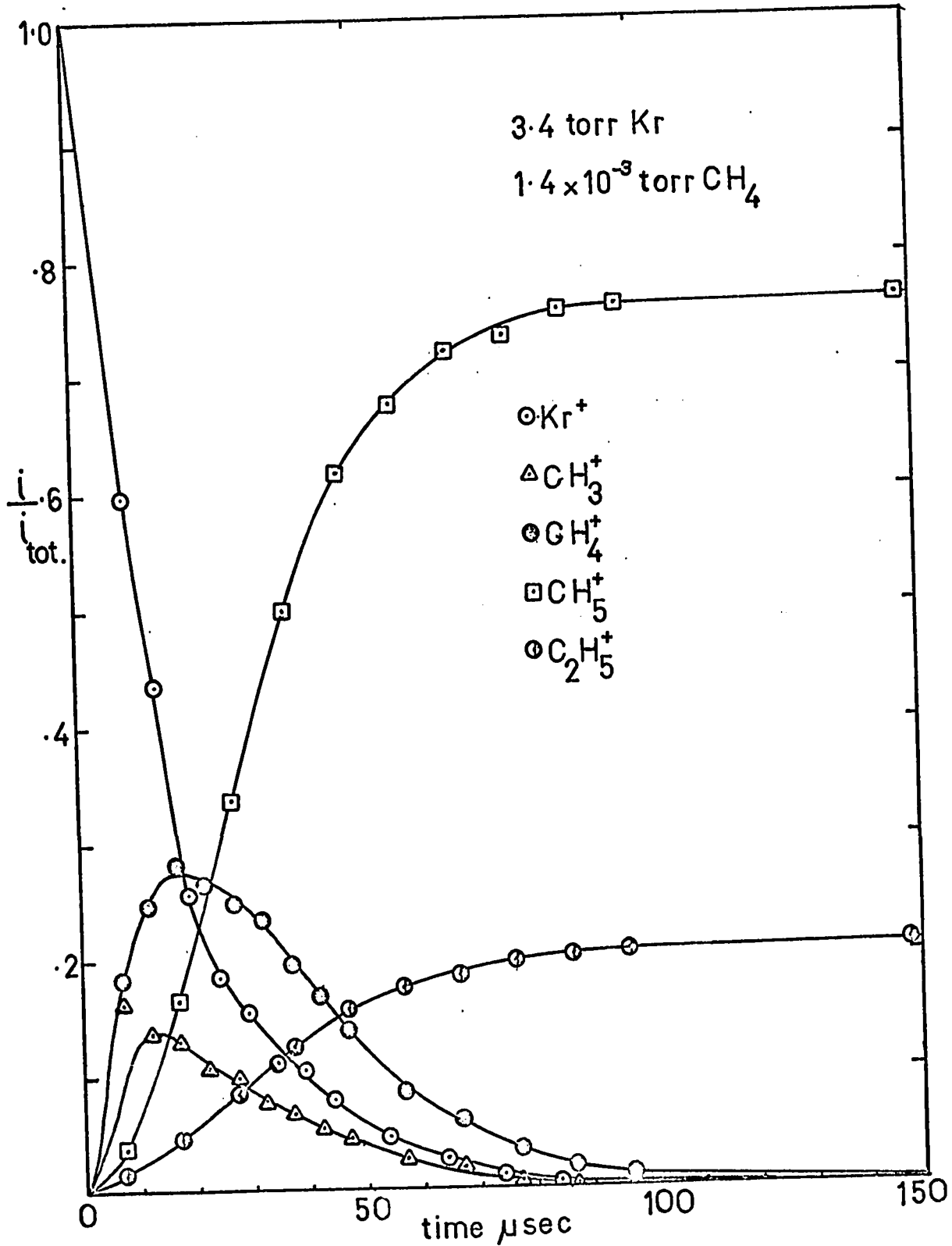
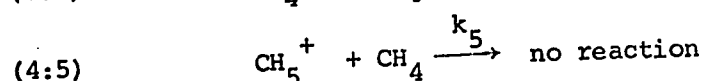
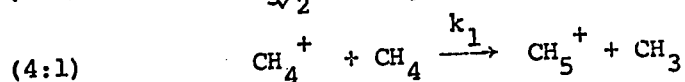
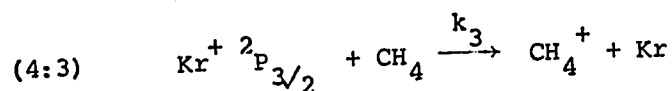


Figure 4:4 Ion intensity curves from (4:3) normalized total ionization.

is constant. Reactions (4:3), (4:1) and (4:5) and reactions (4:4), (4:2) and (4:6) can be treated as two parallel reaction chains. Mathematical formulae are readily available (79). First consider one of the chains. This is a single two stage reaction with a single starting substance  $\text{Kr}^+$ .



The concentrations of the ions are given at any time  $t$  by equations (4:vii) to (4:ix).

$$(4:\text{vii}) \quad i_{\text{Kr}^+ 3/2} = i_{\text{Kr}^+ 3/2}^{\circ} \cdot e^{-k_3[\text{CH}_4]t}$$

$$(4:\text{viii}) \quad i_{\text{CH}_4^+} = i_{\text{Kr}^+ 3/2}^{\circ} \left[ \frac{k_3}{(k_1 - k_3)} e^{-k_3[\text{CH}_4]t} + \frac{k_3}{(k_3 - k_1)} e^{-k_1[\text{CH}_4]t} \right]$$

$$(4:\text{ix}) \quad i_{\text{CH}_5^+} = i_{\text{Kr}^+ 3/2}^{\circ} - (i_{\text{Kr}^+ 3/2} + i_{\text{CH}_4^+})$$

A similar set of reactions may be written for the chain starting with  $\text{Kr}^+ \text{ } ^2\text{P}_{1/2}$ .

The initial abundances of  $\text{Kr}^+$  in the  $^2\text{P}_{3/2}$  and the  $^2\text{P}_{1/2}$  may be expressed as fractions  $f_1$  and  $f_2$  of the total  $\text{Kr}^+$  intensity  $i_{\text{Kr}^+}^{\circ}$ . At  $t = 0$  the intensity  $i_{\text{Kr}^+}^{\circ} = i_{\text{total}} = 1$  and thus

$i_{\text{Kr}}^{\text{O}+({}^2\text{P}_{3/2})} = f_1 \times 1$  and  $i_{\text{Kr}}^{\text{O}+({}^2\text{P}_{1/2})} = f_2 \times 1$ . At any time  $t$ ,  $i_{\text{Kr}}^+$  is given by (4:x).

$$(4:x) \quad i_{\text{Kr}}^+ = i_{\text{Kr}}^+({}^2\text{P}_{3/2}) + i_{\text{Kr}}^+({}^2\text{P}_{1/2})$$

Since one cannot differentiate between the two states of krypton with the mass spectrometer, one can obtain  $i_{\text{Kr}}^+$  by substituting the two form of (4:vii) into (4:x).

$$(4:xi) \quad i_{\text{Kr}}^+ = f_1 e^{-k_3[\text{CH}_4]t} + f_2 e^{-k_4[\text{CH}_4]t}$$

The values for  $f_1$  and  $f_2$  will be given by the relative abundances at long times of the ions  $\text{CH}_5^+$  and  $\text{C}_2\text{H}_5^+$  (see figure (4:4)). The observed relative abundances, when averaged over several runs, were found to be in the ratio 0.75 to 0.25. These relative abundances for  $\text{CH}_4^+$  and  $\text{CH}_3^+$  produced initially by charge exchange from  $\text{Kr}^+$  are similar to expected values. The theoretical ratio depends upon the transition probabilities. These are given by  $(2S+1)$  where  $S$  is the spin ( $\frac{3}{2}$  or  $\frac{1}{2}$ ). The ratio then is  $i_{\text{Kr}}^+({}^2\text{P}_{3/2}) : i_{\text{Kr}}^+({}^2\text{P}_{1/2}) = 4:2 = 0.67 : 0.33$  similar to that obtained by Cermak and Herman (77) of 0.65 and 0.35.

If  $k_3 = k_4$  equation (4:xi) can be reduced to (4:v). Plots of  $\log i_{\text{Kr}}^+$  versus  $t$  for the three methane concentrations are shown in figure (4:5). From the straight line portions of the plots values for the rate constant for the disappearance of  $\text{Kr}^+$  are obtained. Now from equation (4:xi)  $\log i_{\text{Kr}}^+$  would only give a straight line over the whole range of  $\text{Kr}^+$  if  $k_3 = k_4$ .



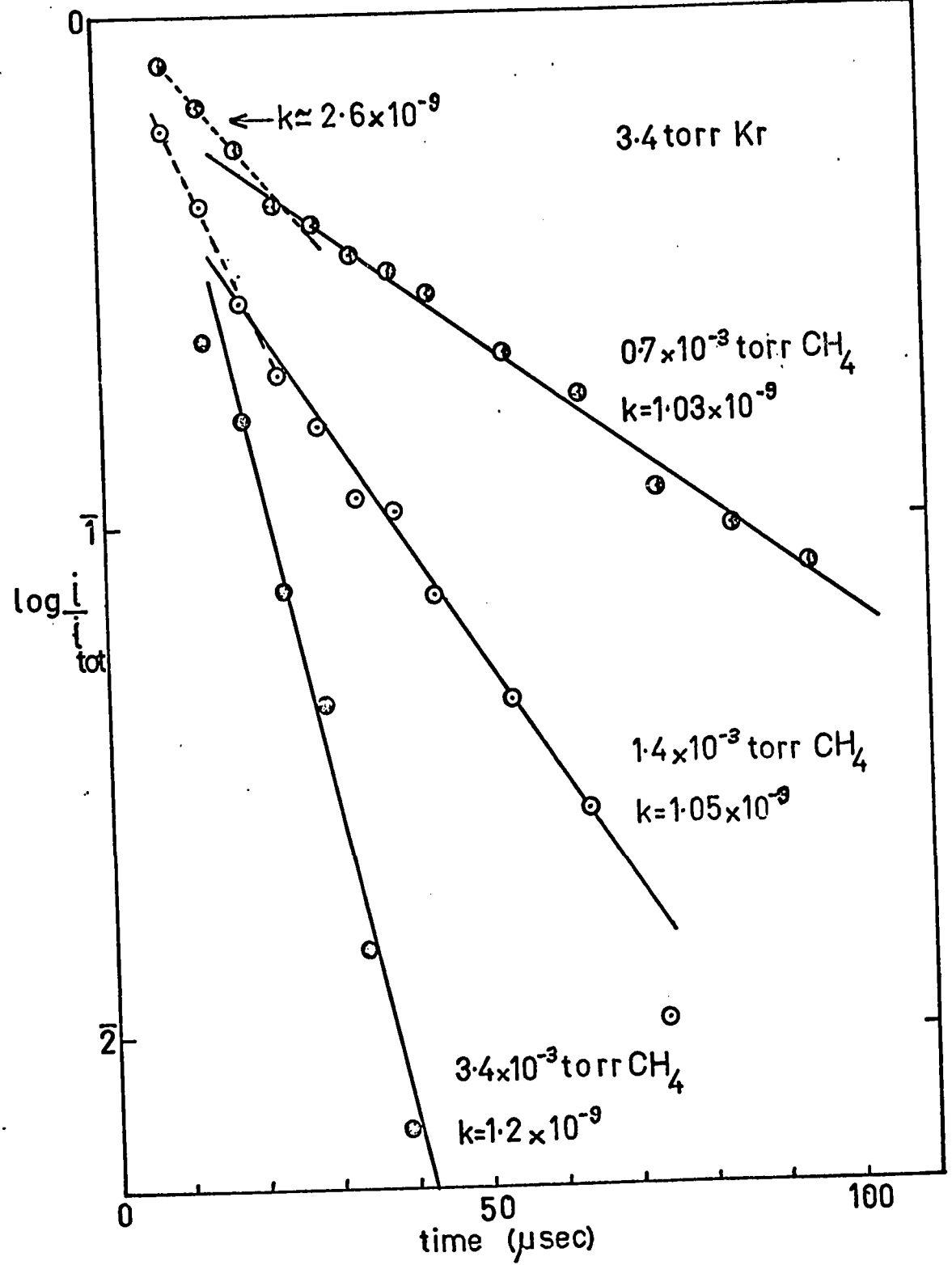


Figure 4:5 Decay of  $i_{Kr^+}$  versus t.

However the linear portion in figure (4:5) does not extend over the whole  $\text{Kr}^+$  range, but from perhaps 50% to 1%. This is consistent with either  $k_3 = k_4$  or  $k_3 < k_4$  since if reaction (4:4) were faster it would be complete in a shorter time than reaction (4:3) i.e. in the range of  $\text{Kr}^+$  from 100% to 50%. In figure (4:5) the initial slope on the 0.7 and  $1.4 \times 10^{-3}$  torr  $\text{CH}_4$  runs is approximately twice that of the linear portions. The maximum for the time dependent curve of  $\text{CH}_3^+$  always appeared at a delay time shorter than that of  $\text{CH}_4^+$  (see for example figure (4:3) or figure (4:4)). Both of these observations are consistent with  $k_3 < k_4$ . Thus the value of the rate constant calculated from the linear portions of the plots of figure (4:5) should be that of reaction (4:3) (i.e.  $k_3 = 1.1 \times 10^{-9}$  cc/molecule sec.)  $k_4$  appears to be approximately twice  $k_3$  ( $\sim 2.6 \times 10^{-9}$  cc/molecule sec.) but a reliable value could not be obtained. Runs at lower concentrations (than 0.7 millitorr) of  $\text{CH}_4$  where the portions 100% to 60% of  $i_{\text{Kr}^+}$  should have lasted longer gave unreliable results since under these conditions the decrease of  $\text{Kr}^+$  intensity due to reaction became much too slow compared with the decrease due to other processes (diffusion, etc.). Thus there were large errors in the fractional intensities.

Equation (4:viii) for the concentration of the second ion in the consecutive reaction sequence is used for the  $\text{CH}_4^+$  ion. The intensity of  $\text{CH}_4^+$  is given by equation (4:xii).

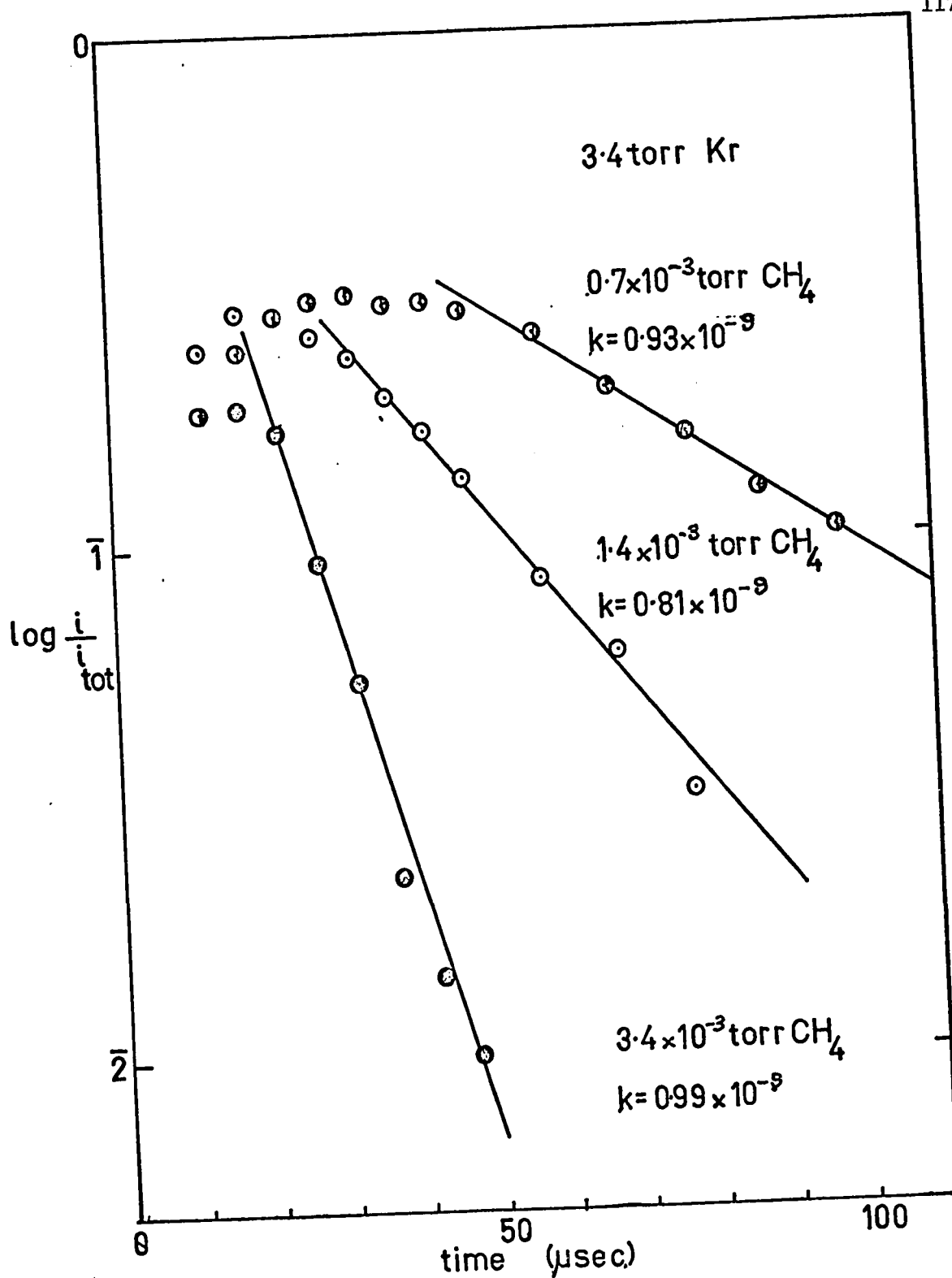


Figure 4:6 Decay of  $i_{\text{CH}_4}^+$  versus  $t$ .

$$(4:xii) \quad i_{CH_4^+} = f_1 \frac{k_3}{k_1 - k_3} \left[ e^{-k_3[CH_4]t} - e^{-k_1[CH_4]t} \right]$$

which is derived from (4:viii) where  $i_{Kr^+}^{o3/2} = f_1 x_1$ . The factor  $f_1 = 0.75$  is that used in equation (4:xi) as the initial concentration of  $Kr^{+2}P_{3/2}$ . A similar equation (4:xiii) for  $CH_3^+$  is used where  $f_2 = 0.25$ .

$$(4:xiii) \quad i_{CH_3^+} = f_2 \frac{k_4}{k_2 - k_4} \left[ e^{-k_4[CH_4]t} - e^{-k_2[CH_4]t} \right]$$

The rate constant for reaction (4:1) can be obtained from the time dependence of  $i_{CH_4^+}$  through equation (4:xii). The simplest evaluation of  $k_1$ , arises when  $k_1$  is less than  $k_3$ . Then the term  $e^{-k_3[CH_4]t}$  is very small; that is reaction (4:3) may be considered to be essentially complete. In this case a plot of  $\log(i_{CH_4^+})$  versus  $t$  should give a linear portion with slope  $= -\frac{k_1[CH_4]}{2.303}$ . Such logarithmic plots of  $i_{CH_4^+}$  for the three pressures of methane are shown in figure (4:6).

Using a similar argument for  $CH_3^+$ , that reaction (4:4) is essentially complete before (4:2) is observed, the term  $e^{-k_4[CH_4]t}$  in equation (4:xiii) becomes very small and a plot of  $\log i_{CH_3^+}$  versus  $t$  will have a slope approximately  $-\frac{k_2[CH_4]}{2.303}$ . These plots are shown in figure (4:7).

The rate constants obtained from plots such as those in figures (4:5), (4:6) and (4:7) are summarized in Table 4.3. Duplicate runs of each methane pressure are shown.

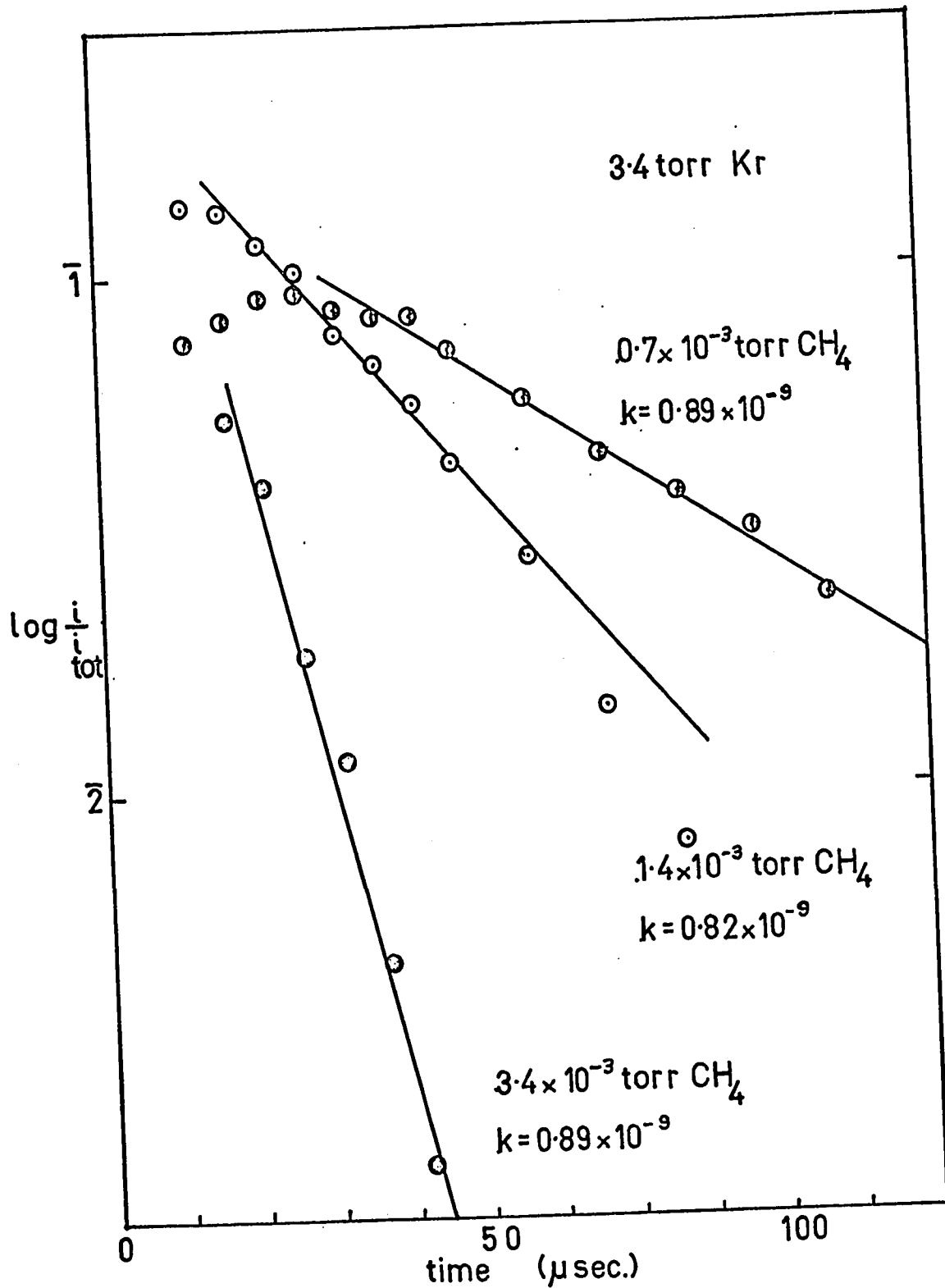


Figure 4:7 Decay of  $i_{\text{CH}_3^+}$  versus  $t$ .

TABLE 4:3

Corrected Values of Rate Constants From the  
Decay of the Ions  $Kr^+ CH_4^+$  and  $CH_3^+$

$CH_4$ (millitorr)	Pressures		Rate constants (cc/molecule sec.) $\times 10^9$		
	Kr torr		k ( $i_{Kr^+}$ )	$k_1$ ( $i_{CH_4^+}$ )	$k_2$ ( $i_{CH_3^+}$ )
0.68	3.4		a 1.04	b 0.94	c 0.89
0.7	3.4		0.9	0.8	0.8
1.4	3.4		a 1.05	b 0.87	c 0.82
1.4	3.4		1.04	0.96	0.95
3.4	3.4		a 1.20	b 0.99	c 0.89
3.4	3.4		1.23	0.95	1.03
Average values			d 1.1	0.9	0.9

a from figure (4:5)

b from figure (4:6)

c from figure (4:7)

d Average values transferred to Table 4.4.

#### iv Preparation of Theoretical Plots

As a final check the equations (4:xi) to (4:xv) were used to generate theoretical ion concentration curves for  $Kr^+ CH_4^+ CH_3^+$

$\text{CH}_5^+$  and  $\text{C}_2\text{H}_5^+$ . From equation (4:ix) one may obtain the two new equations (4:xiv) and (4:xv) required for  $i_{\text{CH}_5^+}$  and  $i_{\text{C}_2\text{H}_5^+}$ .

$$(4:\text{xiv}) \quad i_{\text{CH}_5^+} = f_1 - \left[ f_1 e^{-k_3[\text{CH}_4]t} + i_{\text{CH}_4^+} \right]$$

$$(4:\text{xv}) \quad i_{\text{C}_2\text{H}_5^+} = f_2 - \left[ f_2 e^{-k_4[\text{CH}_4]t} + i_{\text{CH}_3^+} \right]$$

Curves with various combinations of values of  $k_1, k_2, k_3, k_4, f_1$  and  $f_2$  were prepared. These were then compared with figure (4:4). Figure (4:8) shows the curve which fitted the best. The values used to obtain figure (4:8) are listed in column b of Table 4:4.

TABLE 4:4

Thermal Rate Constants for Reactions  
of  $\text{Kr}^+, \text{CH}_4^+$  and  $\text{CH}_3^+$  with  $\text{CH}_4$ .

Reaction	Rate constant (cc/mol.sec.) $\times 10^9$		
	a	b	c
$\text{Kr}^+ (^2\text{P}_{3/2}) + \text{CH}_4 \xrightarrow{k_3} \text{CH}_4^+ + \text{Kr}$		1.1	
$\text{Kr}^+ (^2\text{P}_{1/2}) + \text{CH}_4 \xrightarrow{k_4} \text{CH}_3^+ + \text{Kr} + \text{H}$		2.0	
$\text{CH}_4^+ + \text{CH}_4 \xrightarrow{k_1} \text{CH}_5^+ + \text{CH}_3$	0.9	1.0	1.15 $\pm$ .1
$\text{CH}_3^+ + \text{CH}_4 \xrightarrow{k_2} \text{C}_2\text{H}_5^+ + \text{H}_2$	0.9	1.0	0.8 $\pm$ .1

a Values from averages in Table 4:3.

b Values used for theoretical plot figure (4:8).

c Averages of literature values Table 4:1.

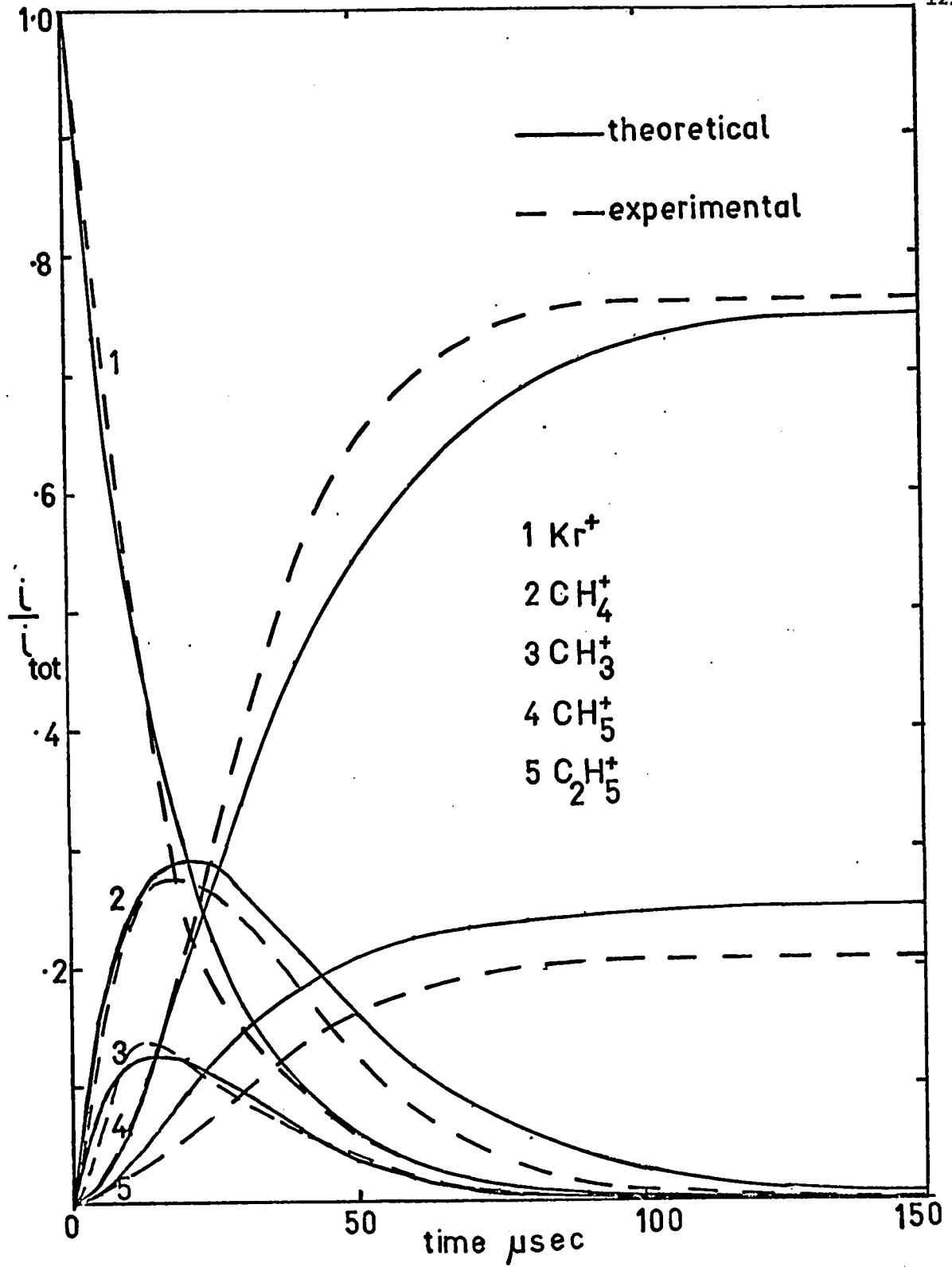


Figure 4:8 Theoretical ion intensity curves. Compared to figure (4:4).



#### 4.4 Observations and Discussion

The values of the rate constants obtained from the theoretical plot are probably the most accurate since they correspond to the most complete use of the experimental data. The values for  $k_1$  and  $k_2$  of  $0.9 \times 10^{-9}$  cc/molecule second of column a of Table 4:4 will be low since they were calculated without accounting for the rates of formation of the reactant ions  $\text{CH}_4^+$  and  $\text{CH}_3^+$ .

The present results for  $k_1$  and  $k_2$  (column b) agree very well with the previous results (column c). This agreement is not necessarily to be expected even if both sets of data are correct since the ions reacting in the two systems have different excitation energies. Consider  $\text{CH}_4^+$  in reaction (4:1) for example. When  $\text{CH}_4$  is ionized by 50 to 100 volt electrons, as in the low pressure studies, the  $\text{CH}_4^+$  ion is produced with a distribution of excitation energies. Von Koch (27) has estimated this distribution function which is shown in figure (4:1 b). The distribution function was determined by comparing the relative intensities of the ions produced by electron impact (50 to 100 volt electrons) to the "breakdown curve" (figure 4:1 a) which shows the mass spectrum of  $\text{CH}_4$  as a function of the energy absorbed by the molecule. Since the energy required to produce  $\text{CH}_3^+$  is 1.2 eV (14.3 - 13.12) above that required to produce  $\text{CH}_4^+$ , the distribution function shows that the  $\text{CH}_4^+$  ions

involved in the reaction studied (by electron impact) at low pressure, would have, on the average, an excitation energy of perhaps 0.6 eV.

The  $\text{CH}_4^+$  ion, produced by charge exchange from  $\text{Kr}^{+2} \text{P}_{3/2}$  would have an excitation energy of 0.88 eV (14.00 - 13.12). However under the high pressure conditions used in the present work the  $\text{CH}_4^+$  ion will undergo about 1000 collisions with Kr atoms before meeting a  $\text{CH}_4$  molecule. It is not certain that 1000 collisions will remove all the excitation energy, as the efficiency of energy transfer in a  $\text{CH}_4^+$  - Kr collision is not known. One would expect that since the collision complex would be held together by polarization, it would be long-lived and allow energy exchange to occur. The rate of exchange would be much larger than that for collisions of neutral species for which the collisions are short lived. Very small concentrations of an ion of mass corresponding to  $(\text{KrCH}_4)^+$  were observed. Thus it is likely that in the present experiments the  $\text{CH}_4^+$  ions were thermalized. It is remarkable therefore that the values for  $k_1$  agree exactly. If the assumption, that the  $\text{CH}_4^+$  ion is thermalized at high pressure, is correct, it indicates that the rate of reaction (4:1) to produce  $\text{CH}_5^+$  is not affected by the presence of some internal excess energy. This situation was implied by the Gioumonsis-Stevenson equation (equation 1:vi) which defines the rate constant in terms of the polarization forces and not

on the internal energies of the ion and molecule. The complex between  $\text{CH}_4^+$  and  $\text{CH}_4$  was shown earlier (section 1:5) to be held together by polarization forces.

The values in Table 4:4 indicate that the measured rate constant for the reaction (4:2) of  $\text{CH}_3^+$  was larger from the present high pressure determination than from the previous low pressure determinations. This appears when the rate constants  $k_1$  and  $k_2$  are compared. At high pressure the data indicates  $k_1 = k_2$ , whereas at low pressure  $k_1 > k_2$ . If one assumed that this difference is real, and is not due to the limits of experimental accuracy, one might explain it as follows. One might assume that the same conditions existed for  $\text{CH}_3^+$  as for  $\text{CH}_4^+$ , that is, at low pressure the reacting  $\text{CH}_3^+$  had some excitation energy, but at high pressure was thermalized. It was previously remarked (section 1:5) that the complex  $(\text{CH}_3-\text{CH}_4)^+$  was different from  $(\text{CH}_4-\text{CH}_4)^+$ , that it was bound by covalent bonds as well as polarization forces. The presence of excess energy might inhibit the formation of a covalently bound complex and thus decrease the rate constant.

It is interesting that the rate constant for the charge exchange reaction (4:4) in which  $\text{Kr}^{+2}P_{1/2}$  reacts to give  $\text{CH}_3^+$  is almost twice as large as the reaction (4:3) in which  $\text{Kr}^{+2}P_{3/2}$  produces  $\text{CH}_4^+$ . It may be possible to explain this in terms of the Massey near-adiabatic hypothesis (80). This hypothesis

states that for charge exchange from an ion to a molecule, having a low relative velocity, the rate will be small unless the change in excess energy  $\Delta E$  is small.  $\Delta E$  is the energy that must be converted into translational energy during the collision. For atoms and atomic ions,  $\Delta E$  would be due to the difference in electronic levels. However when molecules are involved, the vibrational and rotational levels would be used, so that  $\Delta E$  would depend upon them as well as upon the electronic levels. Consequently, some knowledge of the  $\text{CH}_4^+$  electronic and corresponding vibrational levels is needed, so that the Massey adiabatic hypothesis may be applied.

Baker *et al* (81) measured the photoelectron spectrum of methane and observed it contained two maxima at approximately 13.7 and 14.7 eV (compared to 12.70 eV, the adiabatic ionization potential of  $\text{CH}_4^+$ ). They attributed the results to "transitions from the methane molecular ground state to ionic states of symmetries lower than  $T_d$ , i.e.  $C_{3v}$  and  $C_{2v}$ , formed by the removal of an electron from the highly bonding  $(p_t)_6^6$  orbital." The  $C_{3v}$  state is that in which there are three equivalent C-H bonds, and one non-equivalent C-H bond lying on the rotation axis. Baker *et al* also state that the  $\text{CH}_3^+$  appears when the critical amount of vibration energy is supplied to the  $C_{3v}^2A$  ground state so that the non-equivalent C-H bond breaks. Since charge exchange from  $\text{Kr}^+$  to methane produced two

different ions we might consider that two distinct processes occur, that  $\text{Kr}^{+2}\text{P}_{3/2}$  produces initially a  $\text{CH}_4^+$  ion in the  $T_d$  state, while  $\text{Kr}^{+2}\text{P}_{3/2}$  produces initially a  $\text{CH}_4^+$  ion in the  $C_{3v}$  state, which since it is also vibrationally excited breaks down to  $\text{CH}_3^+$  and H. The rates of these two reactions would depend upon the probability of transition from the methane molecule ground state ( $T_d$  symmetry) to the two ionic states  $T_d$  and  $C_{3v}$ , both vibrationally excited. One must therefore expand the application of the Massey hypothesis by considering also Franck-Condon factors.

In order to explain the results, one might propose a simple potential energy schematic diagram for methane, figure (4:9). The methane is considered, for simplicity, to be a diatomic molecule  $\text{H}_3\text{C-H}$ . One would expect that since the  $\text{CH}_4^+ T_d$  and the  $\text{CH}_4^+ C_{3v}$  have the same symmetry that the bond length  $\text{H}_3\text{C-H}$  would be essentially the same. The potential energy functions are shown vertically above one another. The transition of highest probability would then be between the lowest levels. Since, the  $\text{CH}_4^+ C_{3v}$  ion has a non-equivalent C-H bond, and since it more easily absorbs vibrational energy one might expect it to be larger than the C-H bonds of the  $T_d$  state. This one is shown in figure (4:9). The probability would be large for transition from the low vibrational level of  $\text{CH}_4^+ T_d$  to quite high vibrational levels of  $\text{CH}_4^+ C_{3v}$ .

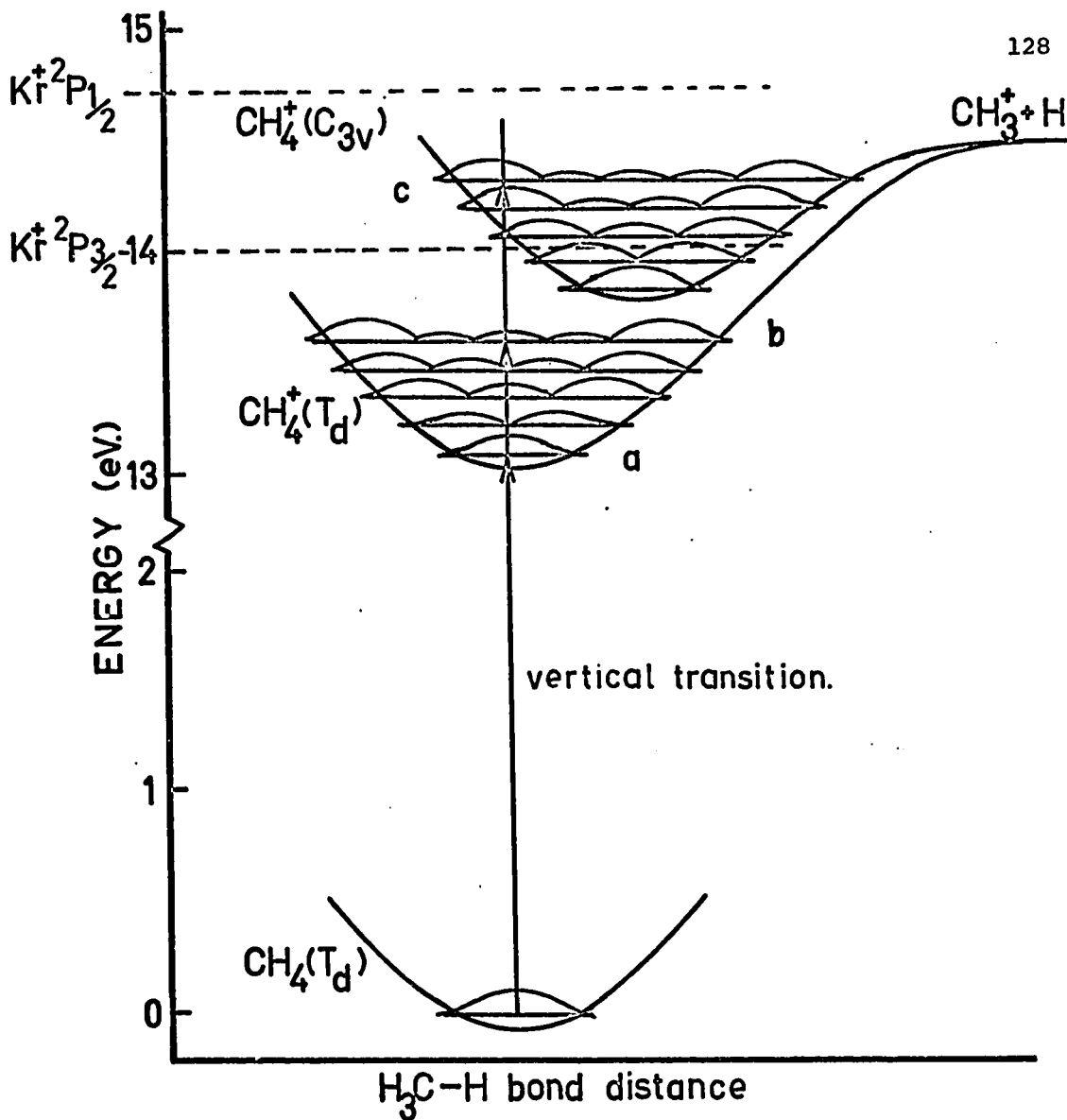


Figure 4:9

Approximate schematic of potential energy functions of methane if the molecule is considered to be a diatomic H<sub>3</sub>C-H

- (a) large overlap from CH<sub>4</sub>(T<sub>d</sub>) lowest level to lowest level of CH<sub>4</sub><sup>+</sup>(T<sub>d</sub>).
- (b) low overlap from CH<sub>4</sub>(T<sub>d</sub>) lowest level to higher levels of CH<sub>4</sub><sup>+</sup>(T<sub>d</sub>).
- (c) large overlap from CH<sub>4</sub>(T<sub>d</sub>) lowest level to higher levels of CH<sub>4</sub><sup>+</sup>(C<sub>3v</sub>).

When  $\text{Kr}^{+2}\text{P}_{3/2}$  charge exchanges to give  $\text{CH}_4^+\text{T}_d$ , the difference between the recombination energies (14.00 eV) and the energy of the lowest state of  $\text{CH}_4^+\text{T}_d$  (13.12 eV) is 0.88 eV. However since this may not be taken up as vibrational energy (according to the present hypothesis) the excess energy  $\Delta E$  which must be transformed into translational energy is large. For the case of  $\text{Kr}^{+2}\text{P}_{1/2}$  exchanging to give  $\text{CH}_4^+\text{C}_{3v}$ , the difference between the R.E. and the lowest level of  $\text{CH}_4^+\text{C}_{3v}$  is even larger (1.0 eV). However since the transition would more likely be to a high vibrational level, most of this energy would become vibrational energy, and  $\Delta E$  would be small. Consequently, by the Massey hypothesis, this latter reaction would have the larger rate constant. This agrees with the experimental observation. Figure (4:9) could also be used to explain why  $\text{Kr}^{+2}\text{P}_{3/2}$ , with a recombination energy of 14.0 eV, would not produce  $\text{CH}_4^+\text{T}_d$  in the lowest vibrational level (about 3.7 eV). Since the transition would not be vertical, it would not be allowed by the Franck-Condon restriction.

One might make one final comment concerning the reliability of the present pulse technique. We have shown that the results were consistent, and agreed with expectation from the results of other workers, and thus the pulse technique may be considered sufficiently reliable to be applied to kinetic studies of unknown systems.

When  $\text{Kr}^{+2}\text{P}_{3/2}$  charge exchanges to give  $\text{CH}_4^+\text{T}_d$ , the difference between the recombination energies (14.00 eV) and the energy of the lowest state of  $\text{CH}_4^+\text{T}_d$  (13.12 eV) is 0.88 eV. However since this may not be taken up as vibrational energy (according to the present hypothesis) the excess energy  $\Delta E$  which must be transformed into translational energy is large. For the case of  $\text{Kr}^{+2}\text{P}_{1/2}$  exchanging to give  $\text{CH}_4^+\text{C}_{3v}$ , the difference between the R.E. and the lowest level of  $\text{CH}_4^+\text{C}_{3v}$  is even larger (1.0 eV). However since the transition would more likely be to a high vibrational level, most of this energy would become vibrational energy, and  $\Delta E$  would be small. Consequently, by the Massey hypothesis, this latter reaction would have the larger rate constant. This agrees with the experimental observation. Figure (4:9) could also be used to explain why  $\text{Kr}^{+2}\text{P}_{3/2}$ , with a recombination energy of 14.0 eV, would not produce  $\text{CH}_4^+\text{T}_d$  in the lowest vibrational level (about 3.7 eV). Since the transition would not be vertical, it would not be allowed by the Franck-Condon restriction.

One might make one final comment concerning the reliability of the present pulse technique. We have shown that the results were consistent, and agreed with expectation from the results of other workers, and thus the pulse technique may be considered sufficiently reliable to be applied to kinetic studies of unknown systems.



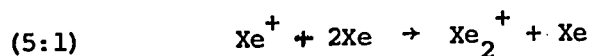
## 5 REACTIONS IN THE XENON-SENSITIZED IONIZATION OF ETHYLENE

### 5:1 Discussion of Previous Investigations and the

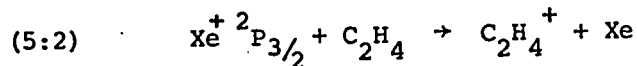
#### Purpose of the Present Study

Ion-molecule reactions in ethylene have been studied by many workers (39,41,42,82,83) who wanted to obtain information to explain the processes occurring in ethylene radiolysis. Of great interest was the ionic polymerization of ethylene to form large ions of the type  $C_nH_{2n}^+$  (83,84). Electron impact of ethylene produces many primary fragment ions (32), a large number of reactions occur to form secondary and higher order ions. The reactions are simplified when xenon-sensitized ionization is used, as the number of different primary ions is reduced (42,85).

At pressures of several torr of xenon the majority of the ions are  $Xe^+$  and  $Xe_2^+$ .  $Xe_2^+$  is formed by the third order attachment reaction (5:1). Both of these ions can ionize ethylene. Since

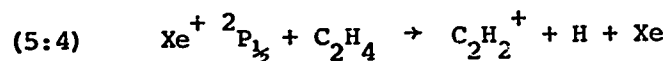
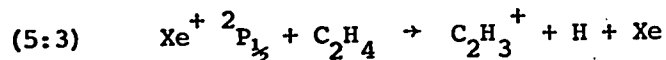


$Xe^+ 2P_{3/2}$  has a recombination energy (12.16 eV) which is larger than the ionization potential for the formation of  $C_2H_4^+$  (10.51 eV), the latter are produced by the charge exchange reaction (5:2).



Charge transfer studies (17,77,86) have shown that  $Xe^+ 2P_{1/2}$ , with a recombination energy of 13.44 eV, reacts with ethylene

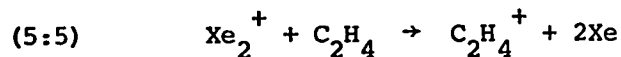
to form  $C_2H_3^+$  (Ip 13.93 eV) and  $C_2H_2^+$  (Ip 13.5 eV) by reactions (5:3) and (5:4). Both reactions are endothermic. These studies



were done with ions with energies slightly above thermal.

Karachevtsev *et al* (87) observed that charge transfer from  $Xe^+$  ions at close to thermal energies produced the ions in the following concentrations  $C_2H_4^+$  0.71,  $C_2H_3^+$  0.05 and  $C_2H_2^+$  0.24. At slightly higher energies Cermak and Herman (77) quoted the relative abundances as 0.68; 0.09 and 0.23. Szabo (86) found similar values 0.60; 0.09 and 0.31. The theoretical prediction for the intensities of  $Xe^+ 2P_{3/2}$  and  $Xe^+ 2P_{1/2}$  produced by electron impact are 0.67 and 0.33. The relative intensity of  $C_2H_4^+$  to the sum of the intensities of  $C_2H_3^+$  and  $C_2H_2^+$  observed by these workers thus supports the reaction mechanisms given above.

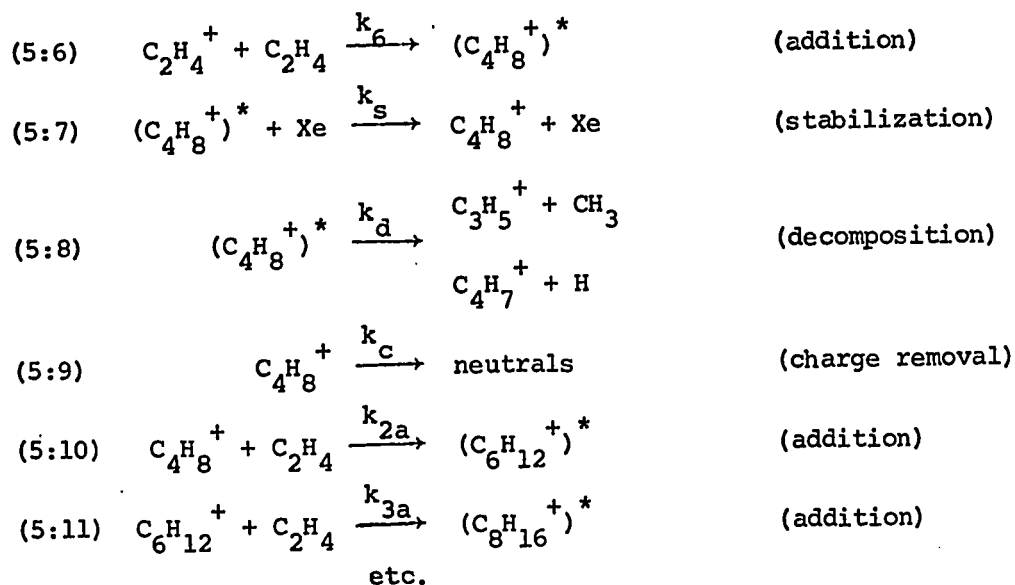
The molecular ion  $Xe_2^+$  (R.E. 11.16 eV) may also produce  $C_2H_4^+$  by reaction (5:5).



Kebarle *et al* (42,85) observed that, under thermal conditions at high xenon pressures (up to 40 torr), charge transfer to ethylene produced essentially only  $C_2H_4^+$ . This would indicate that the exothermic reactions (5:2) and (5:5)

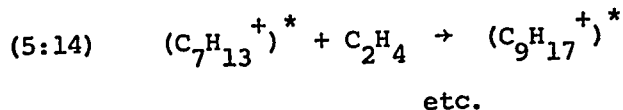
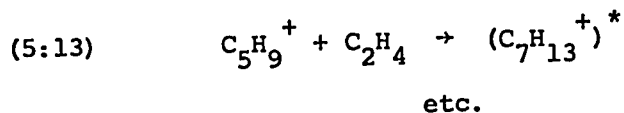
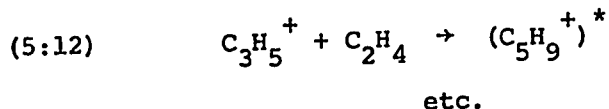
occurred and that the endothermic reactions (5:3) and (5:4) did not occur. Thus at high xenon pressures reaction sequences originating from  $C_2H_4^+$  may be investigated.

The following reaction sequence, for reactions of ethylene in xenon, based upon a similar sequence proposed by Field (32) for reactions in pure ethylene, was proposed by Kebarle *et al* (42).



Kebarle *et al* (42) observed that, as the ion size increased, the reaction rate constants for further addition decreased. They estimated the ratios of the rate constants as  $k_{2a}/k_a \approx 0.002$  and  $k_{3a}/k_{2a} \approx 0.4$  by an indirect method of measurement. The values for  $k_{2a}$  and  $k_{3a}$  were then calculated by assuming that  $k_a$  had the Gioumouisis Stevenson value of  $1 \times 10^{-9}$  cc/molecule sec.

The ion  $C_3H_5^+$ , which is the major ion formed on decomposition of  $(C_4H_8^+)^*$ , may react further with  $C_2H_4$  and undergo addition reactions.



These ions  $C_3H_9^+$  and  $C_2H_{13}^+$  could also result from decomposition of the excited intermediates  $(C_6H_{12}^+)^*$  and  $(C_8H_{10}^+)^*$  by reactions parallel to (5:8). The rate constants for the reactions (5:12) to (5:14) could not be measured by Kebarle *et al* (42,85). The present study was undertaken to measure directly the rate constants for reactions (5:6) and (5:10) to (5:14).

## 5:2 Experimental

The time dependencies of the intensities of the ions  $C_2H_4^+$ ,  $C_4H_8^+$ ,  $C_6H_{12}^+$ ,  $C_3H_5^+$ ,  $C_5H_9^+$  and  $C_7H_{13}^+$  were measured for various mixtures of xenon and ethylene. For the study of  $C_2H_4$  the ethylene pressure was varied over the range 0.74 to  $8 \times 10^{-3}$  torr, and the xenon pressure over the range 0.42 to 7.4 torr.  $C_3H_5^+$  was studied at xenon pressures around 3.8 torr and methane pressures from 1.5 to  $4.7 \times 10^{-3}$  torr. The reactions of  $C_2H_4^+$  and  $C_3H_5^+$  were fast and consequently the ethylene pressure had to be low. For the ions which had lower rate constants the ethylene pressure was increased up to almost 1 torr

while the total pressure was kept constant at about 4.0 torr.

All runs were made at room temperature (297 to 300°K). The pulse widths  $\Delta t_e$  and  $\Delta t_i$  were set at 10 micro seconds and the pulse repeat time at 2000 micro seconds so that the ion intensity decayed essentially to zero between pulses.

The experimental work was done before the normalization technique described previously (section 4) had been developed. Consequently only the intensities of the reactant ions were measured and two assumptions were made; firstly, that the rate of decrease of intensity of the ion through reaction was much faster than the decrease in total ionization by diffusion and mass flow, and secondly, that the formation of an ion by a previous reaction was completed before the time during which the decrease of its intensity was observed. The results obtained were similar to those shown in figure (4:3) for the methane ions. It was shown in the methane study that the rate constants calculated when these assumptions were made, were within a factor of two of the corrected values.

### 5:3 Results and Calculation of Rate Constants

The decrease of  $C_2H_4^+$  intensity with time for several pressures is shown in figure (5:1). The reaction was assumed to be pseudo first order since the concentration of  $C_2H_4$  was much larger than that of  $C_2H_4^+$ . The rate constants were

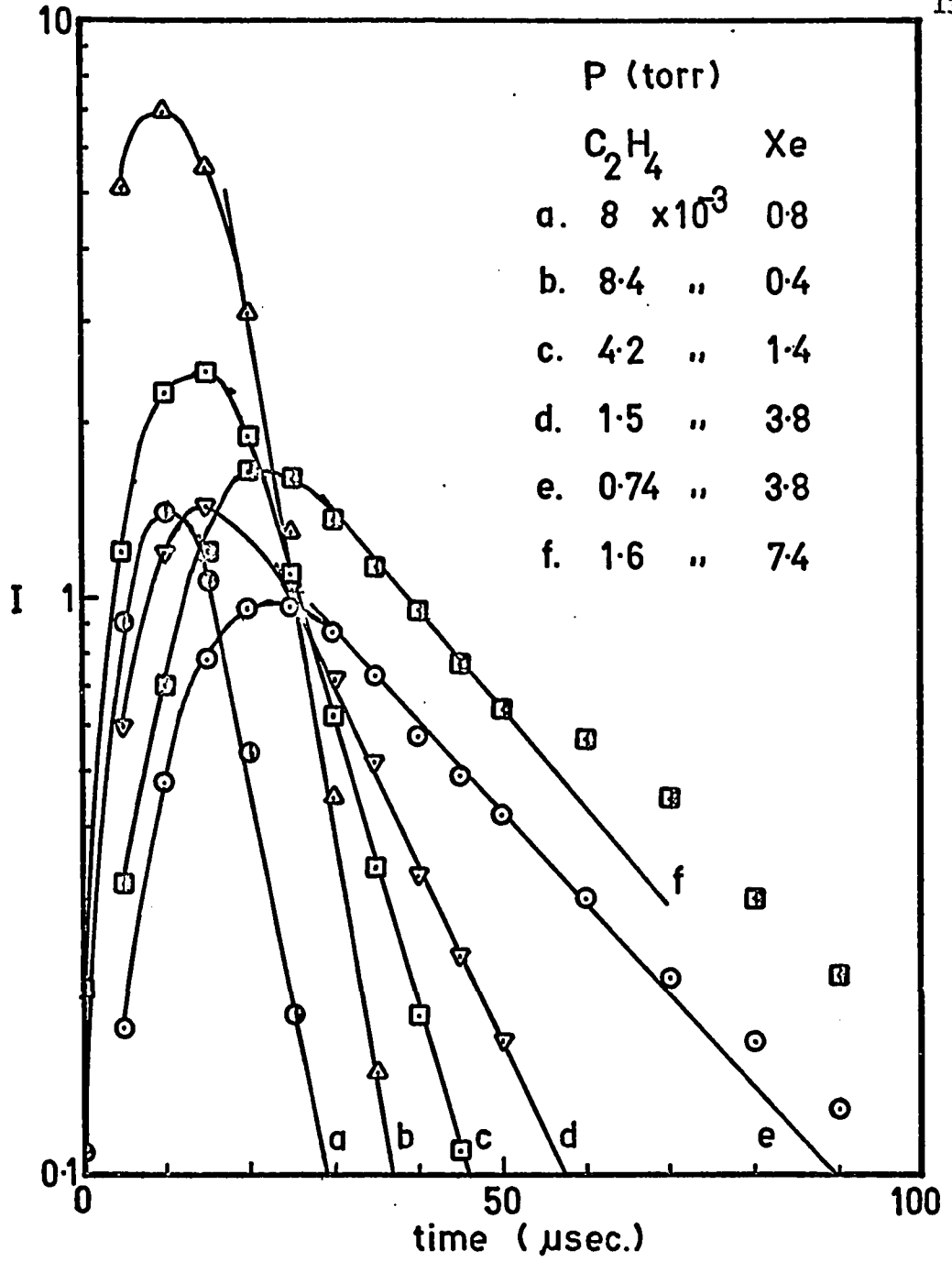


Figure 5:1 Ion intensity curves for reaction of C<sub>2</sub>H<sub>4</sub><sup>+</sup>.

calculated by means of the first order equation (5:i) in

$$(5:i) \quad k = \frac{2.303 \log (I_{t_2}/I_{t_1})}{(t_2 - t_1) [C_2H_4]}$$

which the ion intensities  $I_{t_2}$  and  $I_{t_1}$  were measured from the log plots figure (5:1). The values for  $k_6$ , the calculated rate constant for the decay of  $C_2H_4^+$  by reaction (5:6), are given in Table 5.1.

The ion intensity curves for the other ions are given in figures (5:2) to (5:6). The rate constant values, tabulated in Tables 5.2 to 5.6, were also calculated by means of equation (5:i).

TABLE 5:1

Rate Constant  $k_6$  for the Decay of  $C_2H_4^+$   
 (5:6)  $C_2H_4^+ + C_2H_4 \xrightarrow{k_6} (C_4H_8^+)^*$

Xe pressure (torr)	$C_2H_4$ pressure (torr x $10^3$ )	$k_6$ (cc/molecule sec. x $10^9$ )
0.42	8.4	0.77
0.8	8.0	0.74
1.4	1.4	0.87
1.4	4.2	0.91
3.8	0.74	1.7
3.8	1.5	1.5
4.9	1.0	1.3
7.4	1.55	2.1

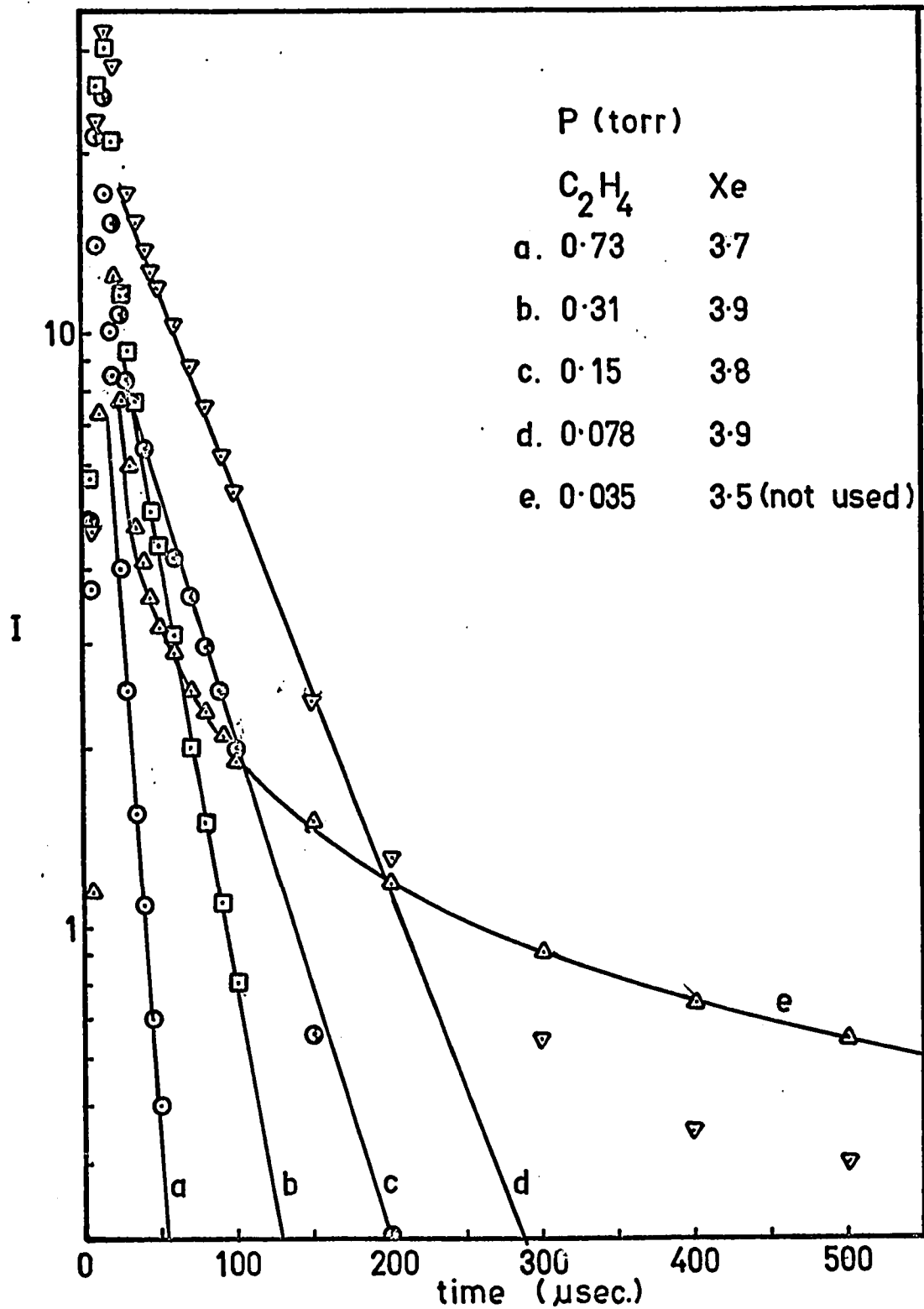


Figure 5:2 Ion intensity curves for reaction of  $C_4H_8^+$ .



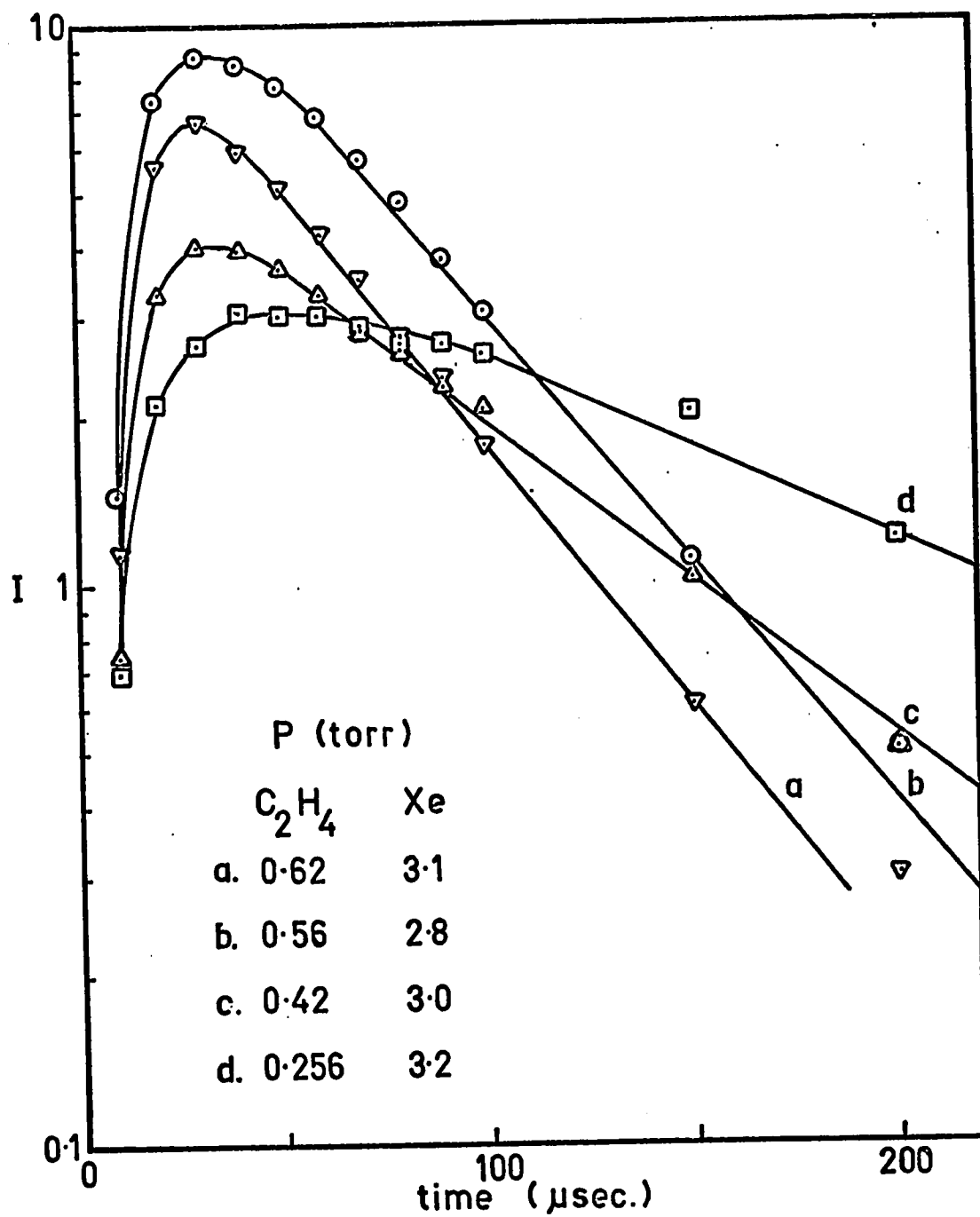


Figure 5:3 Ion intensity curves for reaction of  $C_6H_{12}^+$ .

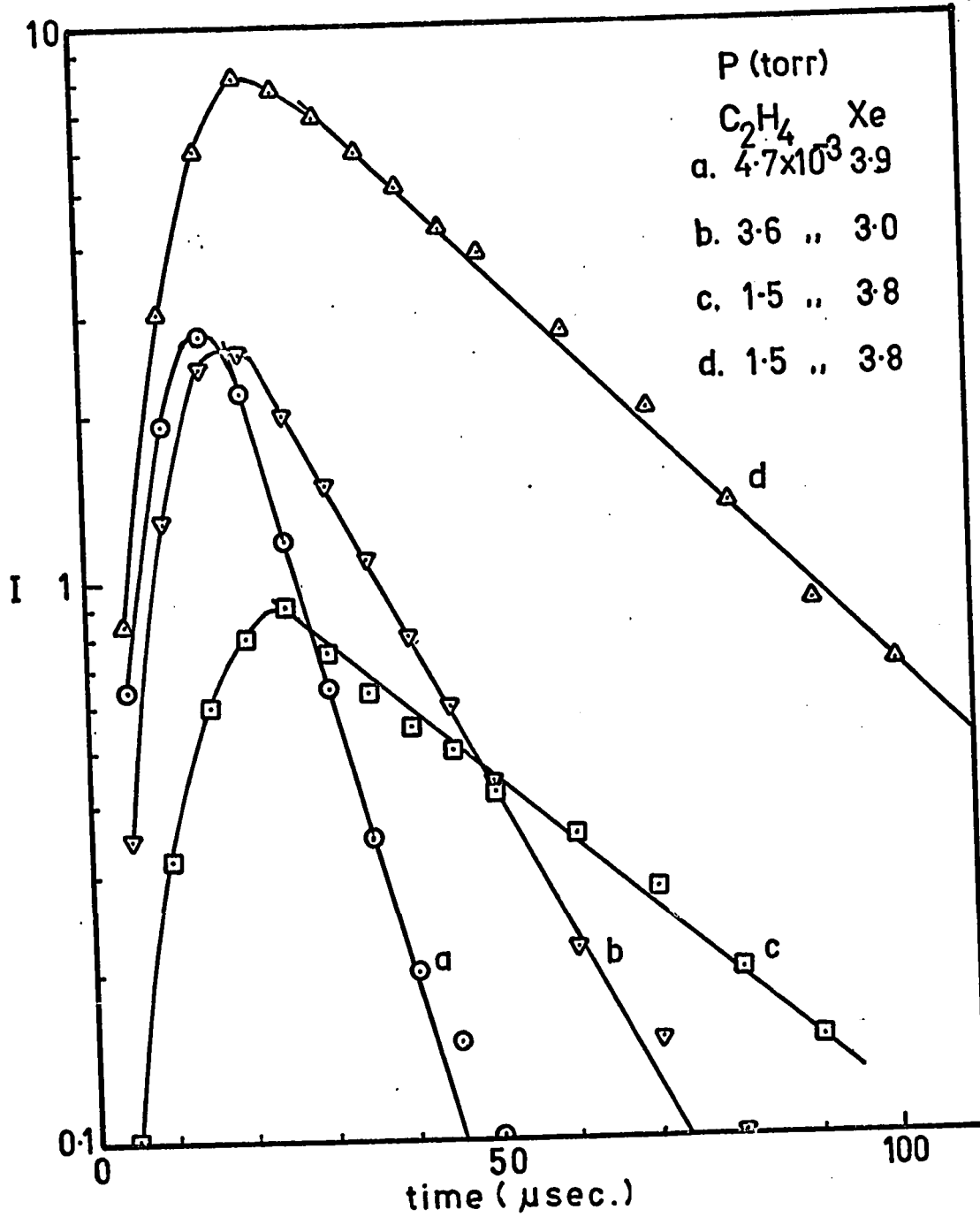


Figure 5:4 Ion intensity curves for reaction  $C_3H_5^+$ .

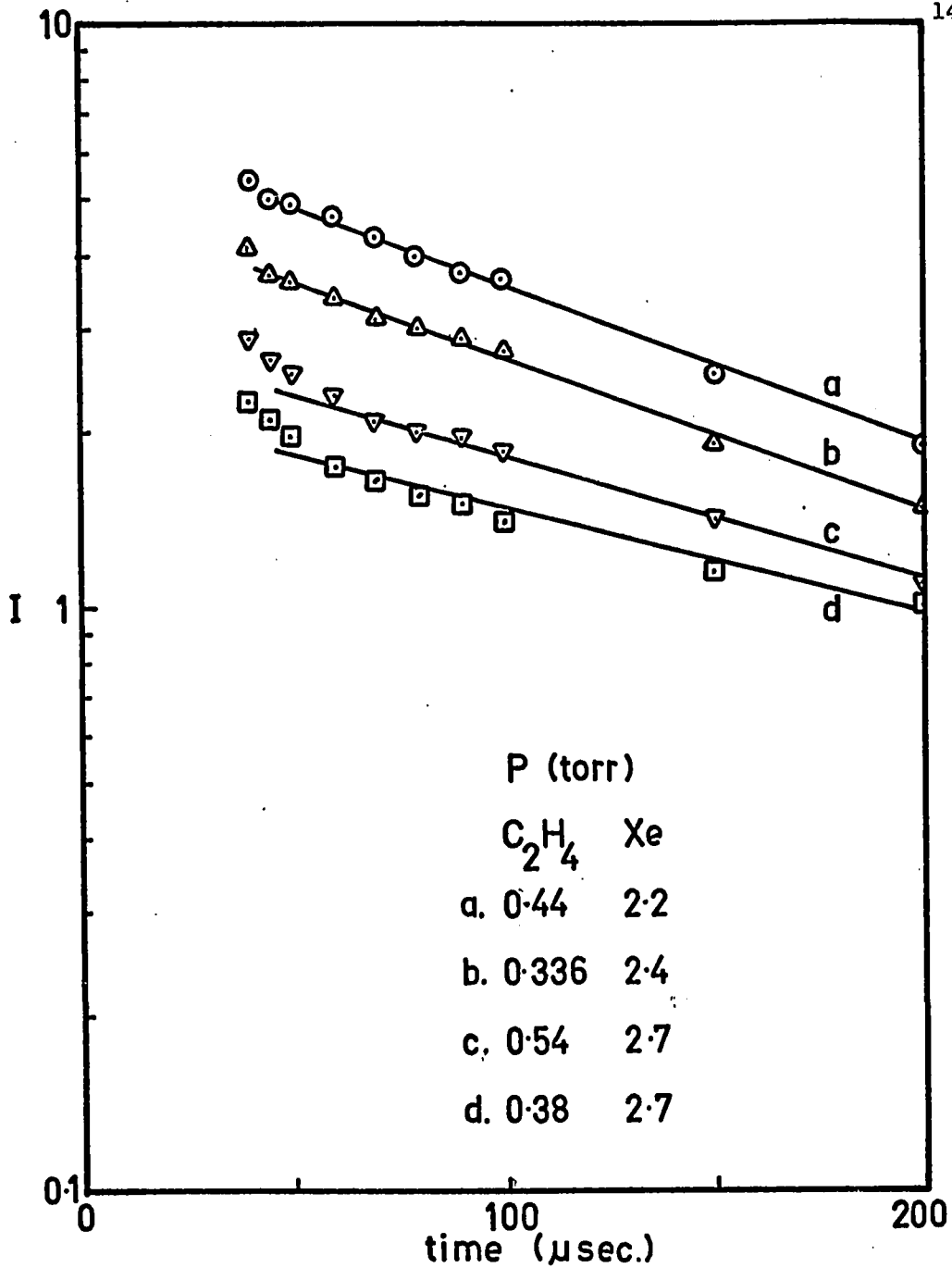


Figure 5:5 Ion intensity curves for reaction of  $C_5H_9^+$ .

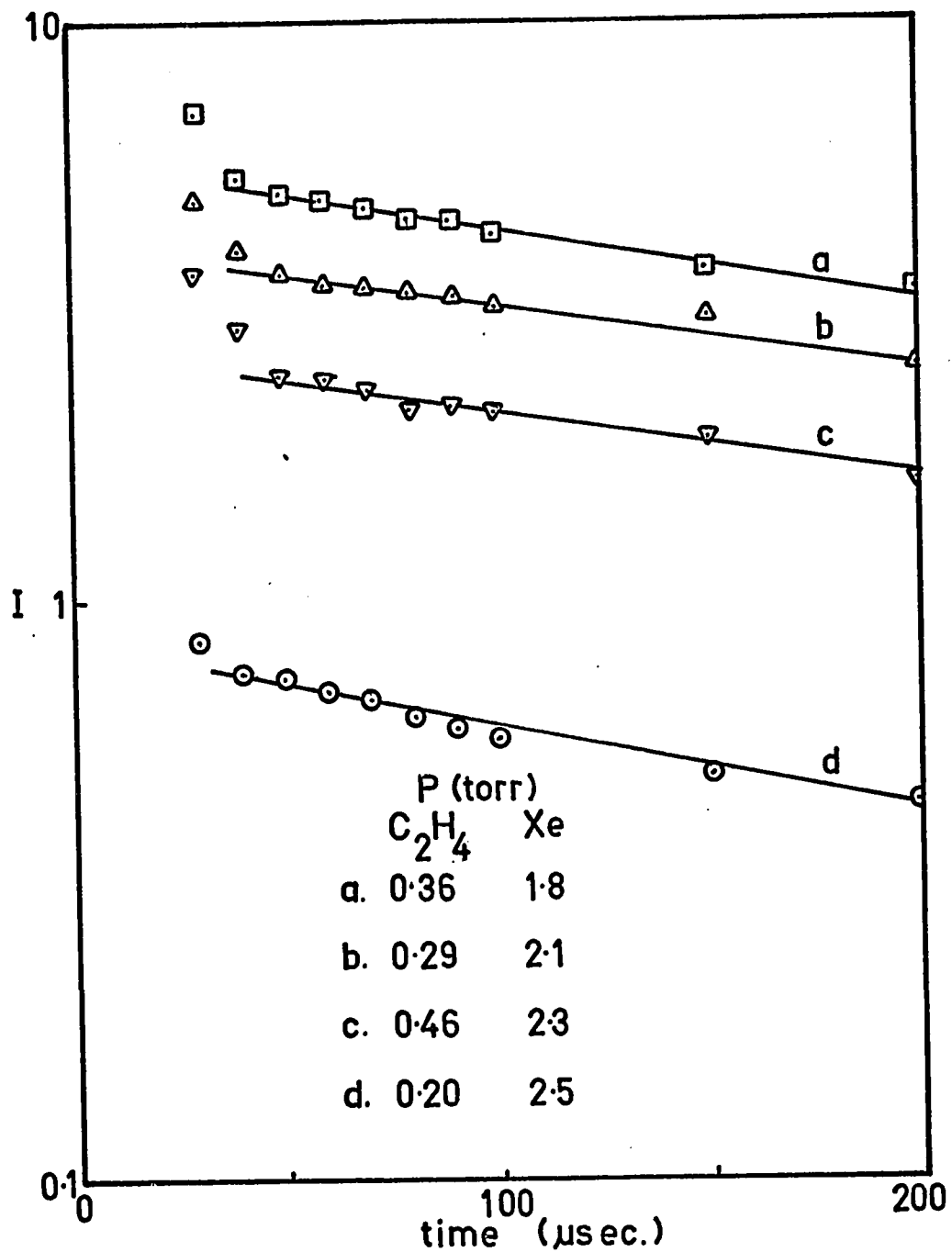
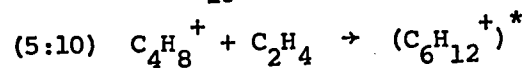


Figure 5:6 Ion intensity curves for reaction  $C_7H_{13}^+$ .

TABLE 5.2

Rate Constant  $k_{10}$  for the Decay of  $C_4H_8^+$

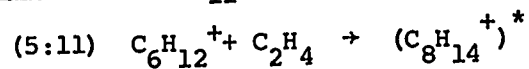


Xe pressure (torr)	$C_2H_4$ pressure (torr)	$k_{10}$ (cc/molecule sec. x $10^{12}$ )
1.4	0.035	7.1
1.5	0.13	4.0
1.55	0.28	2.8
3.0	0.42	3.27
3.2	0.64	3.39
3.3	0.66	3.83
3.5	0.49	4.22
3.5	0.70	3.92
3.6	0.288	5.02
3.6	0.288	3.6
3.7	0.73	4.5
3.9	0.078	7.0
3.9	0.31	3.7
4.5	0.15	4.5

Average value of  $k_{10} = 4.35 \times 10^{-12}$  cc/molecule sec.

TABLE 5.3

Rate Constant  $k_{11}$  for the Decay of  $C_6H_{12}^+$

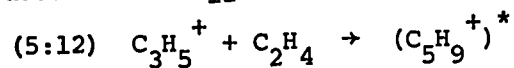


Xe pressure (torr)	$C_2H_4$ pressure (torr)	$k_{11}$ (cc/molecule sec. x $10^{12}$ )
2.7	0.38	1.01
2.8	0.56	1.22
3.0	0.42	1.07
3.1	0.62	1.17
3.2	0.256	1.24

Average value of  $k_{11} = 1.14 \times 10^{-12}$  cc/molecule sec.

TABLE 5.4

Rate Constant  $k_{12}$  for the Decay of  $C_3H_5^+$

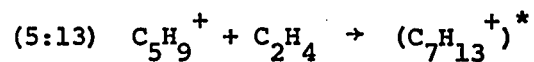


Xe pressure (torr)	$C_2H_4$ pressure (torr x $10^3$ )	$k_{12}$ (cc/molecule sec. x $10^9$ )
3.0	3.6	0.60
3.8	1.5	0.62
3.8	1.5	0.75
3.9	4.7	0.90

Average value of  $k_{12} = 0.76 \times 10^{-9}$  cc/molecule sec.

TABLE 5:5

Rate Constant  $k_{13}$  for the Decay of  $C_5H_9^+$

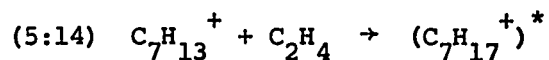


Xe pressure (torr)	$C_2H_4$ pressure (torr)	$k_{13}$ (cc/molecule sec. $\times 10^{12}$ )
2.2	0.44	0.49
2.4	0.336	0.60
2.5	0.50	0.41
2.5	0.50	0.39
2.7	0.38	0.35
2.7	0.54	0.33
2.8	0.224	0.63

Average value of  $k_{13} = 0.46 \times 10^{-12}$  cc/molecule sec.

TABLE 5:6

Rate Constant  $k_{14}$  for the decay of  $C_7H_{13}^+$



Xe pressure (torr)	$C_2H_4$ pressure (torr)	$k_{14}$ (cc/molecule sec. $\times 10^{12}$ )
1.8	0.36	0.31
2.1	0.294	0.30
2.15	0.43	0.21
2.25	0.45	0.21
2.3	0.46	0.17
2.35	0.33	0.26
2.5	0.20	0.44

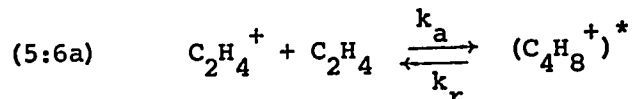
Average value for  $k_{14} = 0.27 \times 10^{-12}$  cc/molecule sec.

#### 5:4 Discussion of the Results

The measured rate constant  $k_6$  was found to be dependent upon the pressure of xenon. The rate constant increased with xenon pressure as can be seen from figure (5:7). This may be explained in the following manner.  $k_6$  was calculated from the assumption that the change in  $C_2H_4^+$  concentration only depended upon its loss by reaction (5:6) and could be represented by equation (5:ii). However perhaps the reverse of reaction (5:6)

$$(5:ii) \quad \frac{d[C_2H_4^+]}{dt} = -k_6 [C_2H_4] [C_2H_4^+]$$

should be included, as in (5:6a).



The change in concentration of  $C_2H_4^+$  is given by equation (5:iii).

$$(5:iii) \quad \frac{d[C_2H_4^+]}{dt} = -k_a [C_2H_4] [C_2H_4^+] + k_r [C_4H_8^{+*}]$$

The concentration of  $(C_4H_8^+)^*$  is unknown. The change in concentration of  $(C_4H_8^+)^*$  is given by equation (5:iv), since  $(C_4H_8^+)^*$  is involved in

$$(5:iv) \quad \frac{d[C_4H_8^{+*}]}{dt} = k_a [C_2H_4] [C_2H_4^+] - k_r [C_2H_4^{+*}] - k_d [C_4H_8^{+*}] - k_s [Xe] [C_4H_8^{+*}]$$

reactions (5:6a), (5:7) and (5:8).  $k_r$  is the rate constant for decomposition back to  $C_2H_4^+$  whereas  $k_d$  is the constant for decomposition to  $C_3H_5^+$  and  $C_4H_7^+$ . If the excited ion  $(C_4H_8^+)^*$



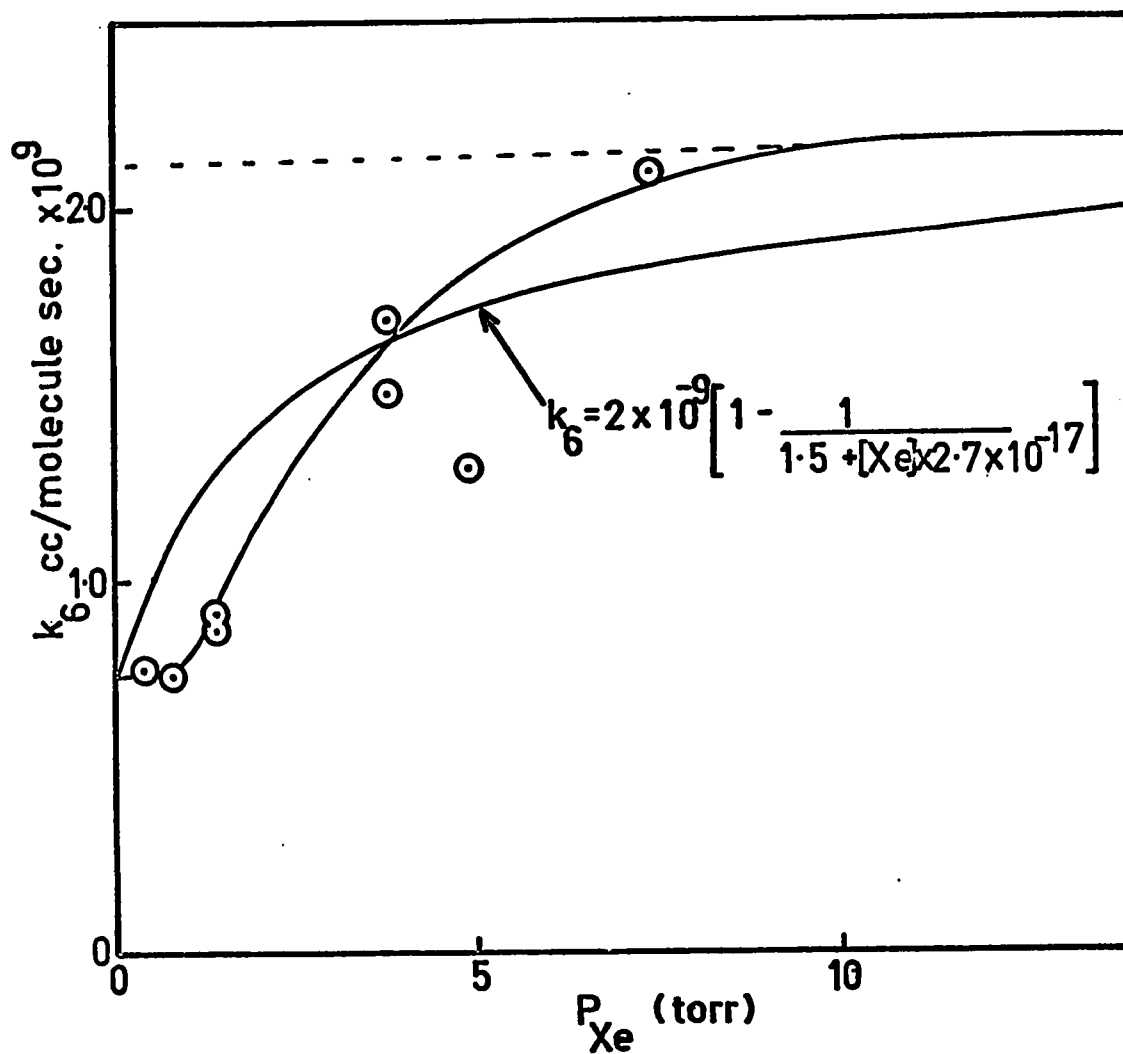


Figure 5:7 Measured and calculated values of  $k_6$  for the reaction (5:6) of  $\text{C}_2\text{H}_4^+$  with  $\text{C}_2\text{H}_4$ , versus xenon pressure.

is assumed to be in a steady state concentration, i.e.

$d[C_4H_8^{+*}]/dt=0$  equation (5:iv) may be rearranged so that  $[C_4H_8^{+*}]$  is expressed by (5:v).

$$(5:v) \quad [C_4H_8^{+*}] = \frac{k_a [C_2H_4^+] [C_2H_4]}{k_d + k_r + k_s [Xe]}$$

This may be substituted into equation (5:iii) which is rearranged.

$$(5:vi) \quad \frac{d[C_2H_4^+]}{dt} = -k_a \left( 1 - \frac{k_{-a}}{k_d + k_r + k_s [Xe]} \right) [C_2H_4] [C_2H_4^+]$$

Thus the experimentally measured  $k_6$  is given by equation (5:vii).

$$(5:vii) \quad k_6 = k_a \left( 1 - \frac{k_r}{k_d + k_r + k_s [Xe]} \right)$$

When the xenon pressure is large we may assume  $k_s [Xe] \gg (k_d + k_r)$ .

Thus  $k_a$  becomes defined by (5:viii) where  $p$  is the xenon pressure.

$$(5:viii) \quad k_6 = k_a$$

$p \rightarrow \infty$

From figure (5:7)  $k_6$  at high Xe pressure is  $2.1 \times 10^{-9}$  cc/molecule sec. which is the value of  $k_a$ .

When the xenon pressure is zero, equation (5:vii) reduces to (5:ix)

$$(5:ix) \quad k_6 = k_a \cdot \frac{k_d}{k_d + k_r}$$

$p \rightarrow 0$

This can be rearranged to give (5:x).

$$(5:x) \quad \frac{k_a}{k_6} = 1 + \frac{k_r}{k_d}$$

$p \rightarrow 0$

When  $p \rightarrow 0$   $k_6$  from figure (5:7) has a value of about  $0.7 \times 10^{-9}$  cc/molecule sec. Thus equation (5:x) can be used to find the ratio of  $k_r/k_d$  equation (5:xii).

$$(5:xi) \quad \frac{2.1 \times 10^{-9}}{0.7 \times 10^{-9}} = 3 = 1 + \frac{k_r}{k_d}$$

$$(5:xii) \quad \frac{k_r}{k_d} = 2$$

This indicates that at low pressures, twice as much  $(C_4H_8^+)^*$  decomposes back to  $C_2H_4^+$ , as decomposes to form  $C_3H_5^+$  and  $C_4H_7^+$ .

An approximate theoretical prediction of the change of the experimental  $k_6$  with xenon pressure may be obtained by substituting the values for  $k_a$ ,  $k_r/k_d$  and  $k_s$  back into equation (5:vii). First a value of  $k_s$  is required. Equation (5:vii) may be rewritten as (5:xiii).

$$(5:xiii) \quad k_6 = k_a \left( 1 - \frac{1}{\frac{k_d}{k_r} + 1 + \frac{k_s}{k_r} [Xe]} \right)$$

If the values are substituted into (5:xiii),  $k_6$  is given as follows.

$$(5:xiv) \quad k_6 = 2.1 \times 10^{-9} \left( 1 - \frac{1}{1.5 + \frac{k_s}{k_r} [\text{Xe}]} \right)$$

Arbitrarily, the experimental value of  $k_6$  (of  $1.66 \times 10^{-9}$ ) at 4 torr Xe was substituted into this equation, and the ratio  $k_s/k_r$  calculated as  $2.7 \times 10^{-17}$  cc/molecule sec. The curve on figure (5:7) was calculated from (5:xv).

$$(5:xv) \quad k_6 = 2.1 \times 10^{-9} \left( 1 - \frac{1}{1.5 + 2.7 \times 10^{-17} [\text{Xe}]} \right)$$

Since the accuracy of the data is probably not better than a factor of two, the agreement of the theoretical and the experimental curves is acceptable in that it shows that at low xenon pressures a large amount of the excited  $(\text{C}_4\text{H}_8^+)^*$  returned to  $\text{C}_2\text{H}_4^+$ , whereas at higher pressures it was stabilized to  $\text{C}_4\text{H}_8^+$ . Values for  $k_d$ ,  $k_r$  and  $k_s$  could not be determined from the present data. A value for  $k_d$ , from which  $k_r$  and  $k_s$  could be calculated, might be obtained from the increase in intensity of  $\text{C}_3\text{H}_5^+$ . However in the present study the increase was at short reaction times when the increase in total ionization was rapid. Even if this problem was not present the rapid reaction of  $\text{C}_3\text{H}_5^+$  with  $\text{C}_2\text{H}_4^+$  would interfere with the calculation of  $k_d$ , as the rate of loss of  $\text{C}_3\text{H}_5^+$  is almost as large as the rate of formation. The ratio  $k_s/k_d$ , calculated as  $1.35 \times 10^{-17}$  cc/molecule from the ratios  $k_d/k_r$  and  $k_s/k_r$ , is close to the previously obtained

value (42,85), which was estimated as 2 to  $3.4 \times 10^{-17}$  cc/molecule for larger ions i.e. the  $C_6, C_8, C_{10}$  homologs.

Values for  $k_d$  have been estimated by other workers (32)  $k_d = 4 \times 10^7 \text{ sec}^{-1}$  and (80)  $k_d = 5 \times 10^7 \text{ sec}^{-1}$ . These would give values of  $k_s$   $1.2 \times 10^{-9}$  cc/molecule sec. Tiernan and Futrell (83) calculated  $k_s$  as  $1.1 \times 10^{-9}$  cc/molecule sec. by the means of the Gioumoussis-Stevenson equation (12). Values of  $10^7 \text{ sec}^{-1}$  for  $k_d$  mean that at pressures of the order of 1 torr ( $C_4H_8^+$ )\* would have a lifetime large enough for a portion of the molecules to be stabilized. This was observed previously (42,85,88,89) and in the present study (figure 5:7).

For the following discussion it is assumed that the measured rate constants for reactions of the larger ions were equal to the rate constants for the addition of  $C_2H_4^+$  ion by reaction i.e.  $k_{10} = k_{2a}$  and  $k_{11} = k_{3a}$ . This would occur at the high pressure limit and consequently the assumption may not be completely correct as the xenon pressures were not very large i.e. <4 torr. The present study confirms the observation by Kebarle *et al* (42,85) that the rate constants for the addition of  $C_2H_4$  decrease as the size of the ion increases. The observed values were, for  $C_2H_4^+$   $k_a = 2.1 \times 10^{-9}$ , for  $C_4H_8^+$   $k_{2a} = 4.35 \times 10^{-12}$  and for  $C_6H_{12}^+$   $k_{3a} = 1.14 \times 10^{-12}$  (all cc/molecule sec.). The ratio  $k_{2a}/k_a = 0.002$  is the same as that estimated by Kebarle *et al* (42, ). The ratio  $k_{3a}/k_{2a} = 0.26$  also agrees

with the previously determined value of  $\sim 0.4$ .

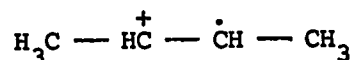
It was suggested (42,85) that the large decrease in rate constants for the addition reactions must be due to structural effects, the largest decrease occurs in the reactivity of  $C_4H_8^+$  compared to  $C_2H_4^+$  ( $k_{2a}/k_a = 0.002$ ). One would expect the transition state of  $(C_4H_8^+)^*$  to have a linear structure.



This could be converted into a stable 1-butene ion by two 1,2 hydride ion shifts or one 1,3 hydride ion shift.



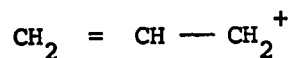
Since the  $(C_4H_8^+)^*$  is highly excited a 2-butene might result.



The reaction of a stable 2-butene ion with  $C_2H_4$  would produce an ion  $(C_6H_{12}^+)^*$  with the charge on a terminal  $CH_2$  group. Since a primary carbonium ion is less stable than a tertiary or secondary ion, this transition state would have a high energy, and thus the rate for reaction of the stable  $C_4H_8^+$  would be expected to be low. Kebarle *et al* (42) measured the cross section for the reaction of 2-butene ions with  $C_2H_4$  in a conventional low pressure mass spectrometer and observed the value was about 500 times smaller than the cross section for reaction of  $C_2H_4^+$  with  $C_2H_4$  under similar conditions. Tiernan *et al* (83) recently

confirmed this measurement. They found the 2-butene ions reacted at a rate 1200 times smaller than did the ethylene ions. They supported the proposal that the decrease in reactivity appears to be due to the tendency of the charge on the ion to seek a secondary or tertiary position. The ions larger than  $C_4H_8^+$  would thus become large branched polymers.

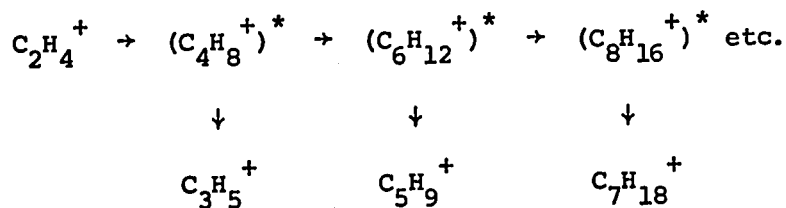
The rate constants for the further reaction of the ions  $C_3H_5^+$ ,  $C_5H_9^+$  and  $C_7H_{13}^+$  showed a parallel decrease in value as the complexity of the ion increased. The values were  $C_3H_5^+$   $k_{12} = 0.76 \times 10^{-9}$ , for  $C_5H_9^+$   $k_{13} = 0.46 \times 10^{-12}$  and for  $C_7H_{13}^+$   $k_{14} = 0.27 \times 10^{-12}$ . The ratios are thus  $k_{13}/k_{12} = 0.0006$  and  $k_{14}/k_{13} = 0.6$ . The reactivity of  $C_3H_5^+$  is almost as high as that of  $C_2H_4^+$ . This was predicted by Kebarle *et al* (42,85). The  $C_3H_5^+$  ion resulting from the fragmentation of the 1-butene structure would probably have the charge on a terminal  $CH_2$  group. Consequently, there would not be a large energy increase



in the formation of the excited  $(C_5H_9^+)^*$  in which the charge would initially also be on a terminal  $CH_2$  group, and the reactivity of  $C_3H_5^+$  might be expected to be of the same order as that of  $C_2H_4^+$ . However  $(C_5H_9^+)^*$  could rearrange and be deactivated like  $(C_4H_8^+)^*$  to form a secondary carbonium ion and thus have a low rate for further reaction.

Because the rate constants for the reaction of the ethylene

primary ions with ethylene were observed to be large, Lampe (90) suggested that ion-molecule reactions could play a role in the radiolysis of ethylene. Ausloos *et al* (91) considered the contribution of ion-molecule reactions to the formation of the small molecular products  $H_2$  and  $C_2H_2$  and concluded that ion-molecule reactions were only partly responsible. Wagner (84) found that when  $C_2H_4$  was irradiated at  $-196^\circ C$ , low molecular weight branched polymers were formed. He suggested the polymerization was initiated by  $C_2H_4^+$ , propagated by ionic condensation reactions giving large molecular ions  $(C_nH_{2n})^+$ , and terminated by ion electron recombination. This is similar to the reaction sequence suggested by Field (32) for pressures less than one torr.

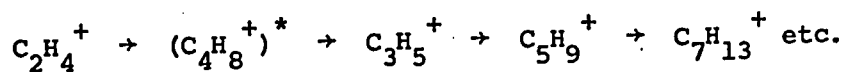


In this case the chain propagation is by the molecular ions  $C_nH_{2n}^+$  (n even), and the carbonium ions  $C_kH_{2k-1}^+$  (k odd) are produced by decomposition. Kebarle *et al* (42,85) supported this mechanism in their study of ethylene at pressures of less than 1 torr, in the presence of xenon up to 40 torr.

On the other hand, Wexler and Marshall (82) proposed that, initially the carbonium ion  $C_3H_5^+$  was formed by the



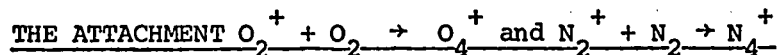
decomposition of  $(C_4H_8^+)^*$  and then chain propagation occurred through the carbonium ions  $C_k H_{2k-1}^+$  (k odd).



Since in the present study we found that the rate constants for the addition of  $C_2H_4$  to the carbonium ions were similar in magnitude to the rate constants for addition of  $C_2H_4$  to the molecular ions, it appears that the low pressure (.1 to 10 torr) gas phase polymerization of ethylene involves both mechanisms. That is, that the chain propagation occurs through the molecular ions and, some of these break down to the carbonium ions which also propagate the polymerization. Kebarle *et al* (42,85) observed that the rate constants for the larger ions  $C_8$  and  $C_{10}$  were smaller (less than  $10^{-14}$  cc/molecule sec.) than those for the  $C_4$  and  $C_6$  ions, reported here, and that the high pressure spectrum of ethylene appeared to terminate close to  $m/e$  200. If the rate constant is taken as  $10^{-14}$  cc/molecule sec. and the concentration as  $3 \times 10^{17}$  molecules/cc (10 torr) the half life ( $t_{1/2} = 1/k [C_2H_4]$ ) becomes about  $3 \times 10^{-4}$  seconds. The average life time of a charge would be about  $10^{-3}$  seconds. Since these are of the same order of magnitude the polymer size would be prevented from increasing as ions would be lost by charge neutralization. At a pressure of one atmosphere, ( $3 \times 10^{19}$  molecules/cc) the half life of a

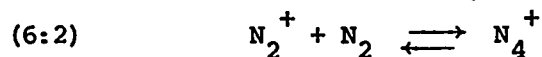
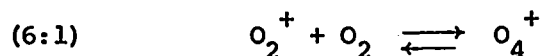
reaction with a rate of  $10^{-14}$  cc/molecule sec. would be about  $3 \times 10^{-6}$  seconds and if the charge lifetime were  $10^{-3}$  seconds, the polymerization could continue.

## 6. ION-MOLECULE REACTIONS IN PURE OXYGEN AND PURE NITROGEN



### 6.1 The Importance of These Reactions to Various Fields

In this section, studies of the attachment reactions (6:1) and (6:2) in pure oxygen and pure nitrogen will be discussed.



The formation of  $O_4^+$  and  $N_4^+$  have previously been studied quite extensively for several reasons: to provide data from which theoretical predictions of the structures of the complexes could be made, to determine the charge carriers in gas discharge and mobility experiments and in atmospheric electricity, and to establish reaction sequences occurring in the ionosphere. A brief description of the role attachment reactions, such as these, play in the determination of ion mobilities and in the ionosphere will be given to illustrate their importance.

The mobility of an ion is determined by measuring its velocity as it drifts, under the influence of an electric field, through a gas at high pressure ( $\sim 1$  torr). Mobility is defined as the ratio of velocity to field strength. The mobility is dependent upon the mass of the ion and upon the ratio of field strength to gas pressure,  $E/p$ . In the early experiments the ions were not mass analysed and the identities were guessed

or deduced from other information such as quantum mechanical predictions. Consequently there arose apparently inconsistent results. The drift velocities of many ions increase in a uniform manner as  $E/p$  is changed. However it was found that this did not occur for  $N_2^+$  in  $N_2$  gas. Varney (92) proposed that reaction (6:2) took place as it would explain his results. This was later confirmed when the ions from a drift tube containing nitrogen were analysed mass spectrometrically and  $N_4^+$  was observed.

Since the mobility of an ion which may undergo attachment reactions depends upon the time spent as the original ion or as a complex the rates of formation of the complex must be known before accurate mobilities can be determined. Knowledge of these rates is also necessary to formulate and explain ion mobility theories.

The products of attachment reactions have also been observed in the Earth's ionosphere by sampling its ionic constituents with a rocket-borne mass spectrometer (40). The ions  $H_3O^+$ ,  $H_5O_2^+$  and ions with masses greater than  $m/e = 45$  were present in the D region of the ionosphere. The D region is the lowest region of the ionosphere in which there is an appreciable concentration of ions and electrons (93). The pressure in this region is high (from approximately .01 to several torr) and thus attachment reactions, which frequently involve three body

collisions become as important as two body collisions in changing the ionic composition. The identities of the major ions in the ionosphere are required for calculation of ion-electron recombination rates. These rates are used to correlate the measured electron density with the observed ion densities and rates of production from the Sun's radiation. The rates of ion-electron recombination reactions depend upon the structure of the ions. Since large ions e.g. complex ions, can release the energy of ion-electron recombination by dissociation they have larger recombination coefficients than do smaller ions. For example, at 300°K the dissociative recombination rate of  $N_4^+$  is a factor of 10 larger than that of  $N_2^+$  (94).

Attachment reaction studies provide essential information about the structures, stabilities, rates of formation and rates of loss of ion complexes in the atmosphere and can provide useful data to assist in the construction of ionosphere models. These models in turn may be used to predict the effect of chemical reactions on changes in electron density. The electron density is a basic property of the ionosphere and controls many physical phenomena such as the propagation of radio waves.

## 6.2 The Attachment of Oxygen $O_2^+ + O_2 \rightleftharpoons O_4^+$

### i Previous Work on this Reaction

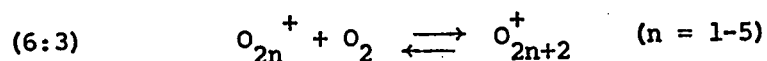
Ion molecule attachment reactions of oxygen have been

less extensively studied than those of other small molecules, especially nitrogen. It is not exactly clear why  $N_4^+$  has been studied more than  $O_4^+$  but it is probably due to short lifetimes of the filament in oxygen. Oxygen is much more reactive than nitrogen towards electron filament materials such as tungsten. Because of our instrumental design the exposure of the filament to gas escaping from the ion source is minimized and this makes experiments with high ion source pressures possible.

Brederlow (95) first detected the ion  $O_4^+$  in the positive column of an electric discharge in oxygen at high pressure and current densities (2.5 torr, 100 mA) by means of a low resolution mass spectrometer (resolution 1 in 6). Since Brederlow was studying ionic diffusion, specifically the transition from free diffusion to ambipolar diffusion as oxygen pressure and discharge currents were changed, the kinetics of reaction (6:1) were not studied. In another oxygen discharge experiment Knewstubb *et al* (96) observed the ions in the negative column and measured very small concentrations of  $O_4^+$ . In this experiment the pressure and current were low (0.4 torr and 0.4 mA) and thus reaction (6:1) was not a major reaction.

The only previous extensive study of the oxygen system was done by Conway and Yang who studied the equilibrium but not the kinetics of reaction (6:1). These authors studied the formation of  $O_4^+$  by reaction (6:1) (97) and also the

formation of larger clusters (98)  $O_6^+$  to  $O_{10}^+$  by the general reaction (6:3). In Conway's apparatus purified oxygen was



flowed through the ion source and ionization was caused by beta radiation from a titanium tritide source. This source overcame the problems of using an electron filament. The ions diffused towards the wall and passed through two 25 micron diameter holes into the evacuated mass analyzer region. The ions were then accelerated and analysed. Conway estimated that the reaction time was about  $10^{-3}$  sec. and that the reaction (6:1) had reached equilibrium. The equilibrium constant for reaction (6:1) was calculated for pressures from 1 to 9 torr of oxygen, over a temperature range of 259 to 344°K. The equilibrium constant  $K_p$  was evaluated by equation (6:i) where  $P_{O_2}$  is the pressure of oxygen in torr, and  $i_{O_4}$  and  $i_{O_2}$

$$(6:i) \quad K_p = \frac{i_{O_4}^+}{i_{O_2}^+ \cdot P_{O_2}}$$

the observed ion currents, which were assumed to be proportional to the partial pressures of the ions.

From a van't Hoff plot (of  $\log K_p$  versus  $10^3/T$ ) Conway and Yang obtained values for the enthalpy and entropy, i.e.

$$\Delta H = -9.60 \text{ kcal/mole} \quad \Delta S = -20.6 \text{ kcal/mole } ^\circ K.$$

Theoretical calculations were made of the structure of  $O_4^+$ .

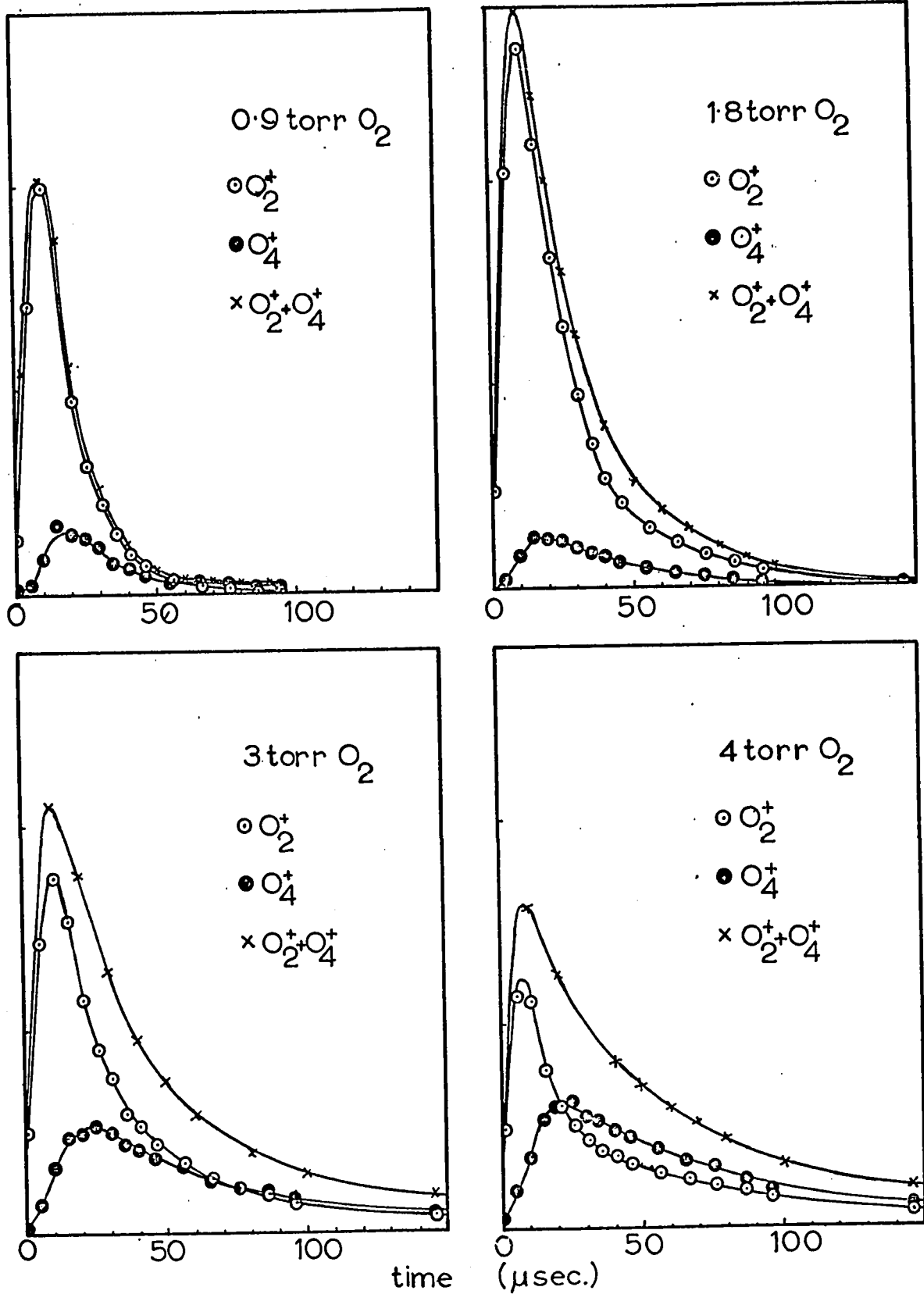


Figure 6:1 Observed ion intensity curves of  $O_2^+$  and  $O_4^+$  in  $O_2$  at 298°K, pressures from 0.9 to 4 torr.



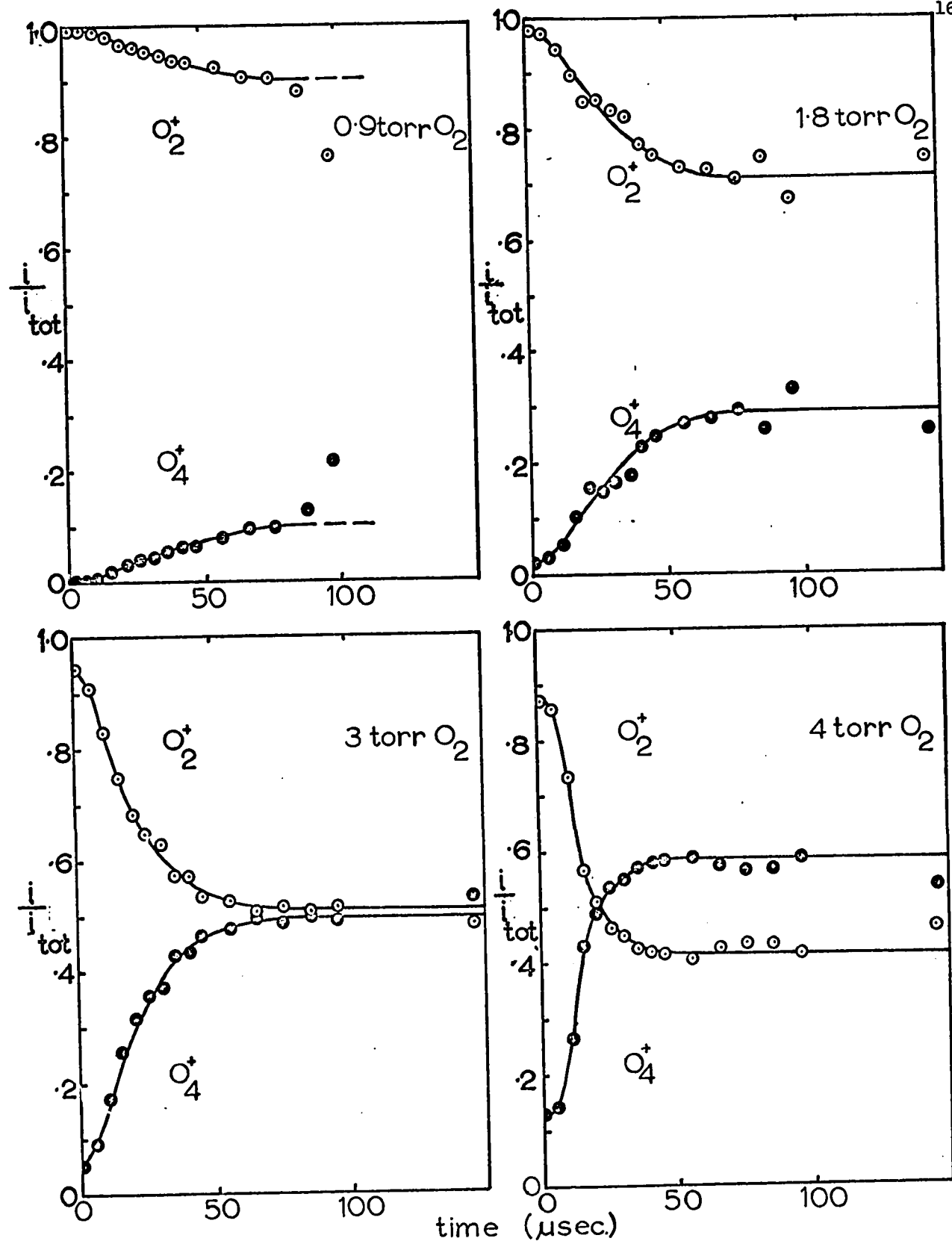


Figure 6:2 Ion intensity curves from (6:1) normalized to total ion intensity (i.e.  $\text{O}_2^+ + \text{O}_4^+$ ) 298°K.

Three possible structures were proposed which gave values of the entropy in agreement with the experimental value.

The present study was made to measure the kinetics of reaction (6:1) and to establish its kinetic order.

### ii Results

The changes of ion intensities with time were measured for pressures from 1 to 8 torr over a temperature range 298 to 341°K. Figure (6:1) shows such time dependence curves obtained in oxygen at 298°K at pressures from .9 to 4 torr. The total ionization curve was determined by summing the  $O_2^+$  and the  $O_4^+$  intensities. (The  $O^+$  and  $O_3^+$  contributions were negligible and not measured). The intensities of  $O_2^+$  and  $O_4^+$  were then replotted as fractions  $i$  of the total ionization, by the general procedure which was validated earlier in section (4:4). These normalized curves of the same data are shown in figure (6:2).

Data obtained for reaction (6:1) at several higher temperatures are shown as normalized ion intensity curves in figures (6:3) to (6:7). The results for several pressures at each temperature have been superimposed to reduce the number of figures.

Inspection of the graphs figure (6:2) shows qualitatively how the reaction progressed with time. Initially the intensity of  $O_2^+$  decreased rapidly while that of  $O_4^+$  increased, since the

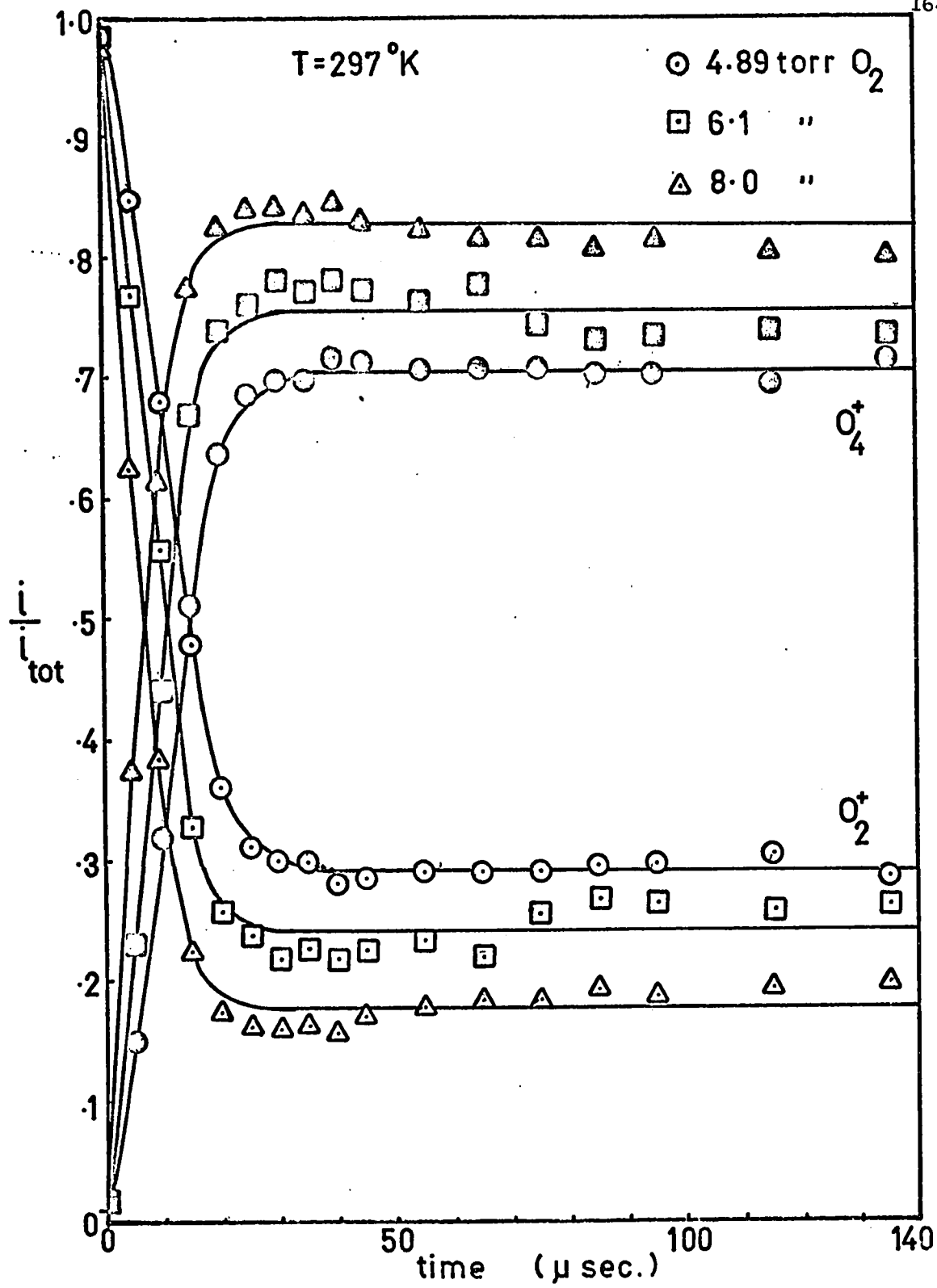


Figure 6:3 Normalized intensity curves of  $O_2^+$  and  $O_4^+$ . Oxygen at  $297^\circ K$ , 4.89 to 8.0 torr.

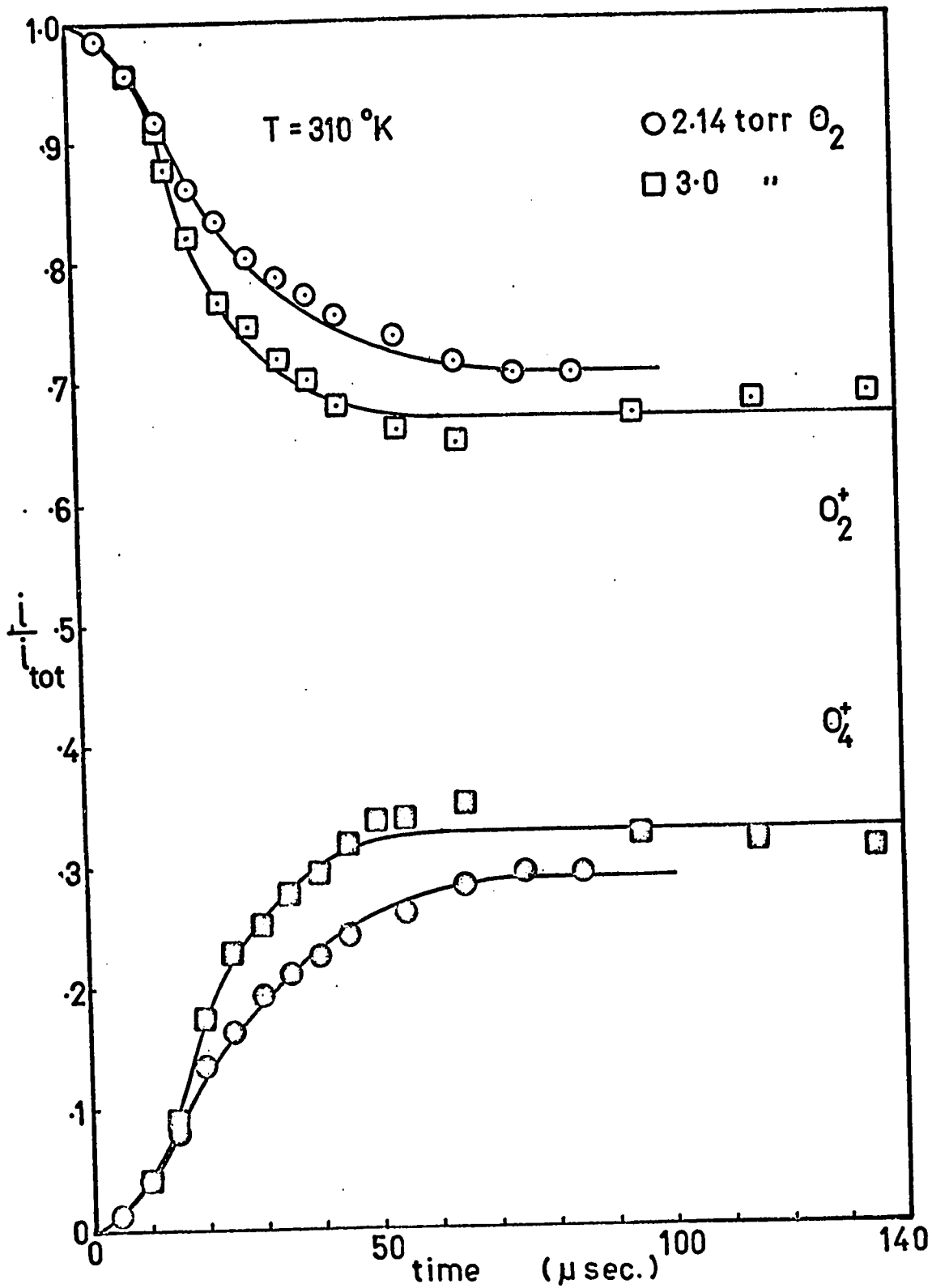


Figure 6:4a Normalized intensity curves of  $O_2^+$  and  $O_4^+$ . Oxygen at  $310^\circ K$ , 2.14 and 3.0 torr.

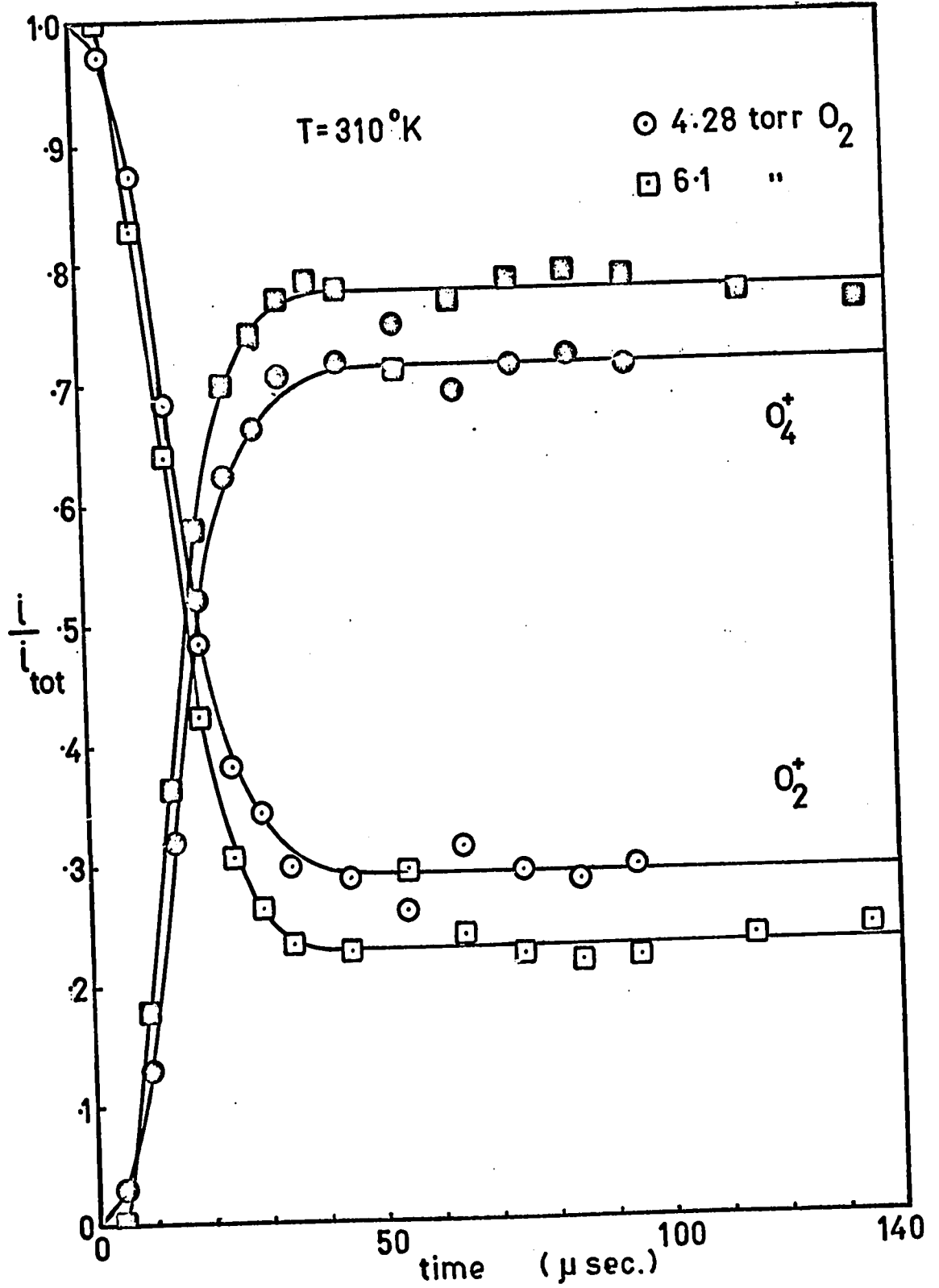


Figure 6:4b Normalized intensity curves of  $O_2^+$  and  $O_4^+$ . Oxygen at  $310^\circ K$ , 4.28 and 6.1 torr.

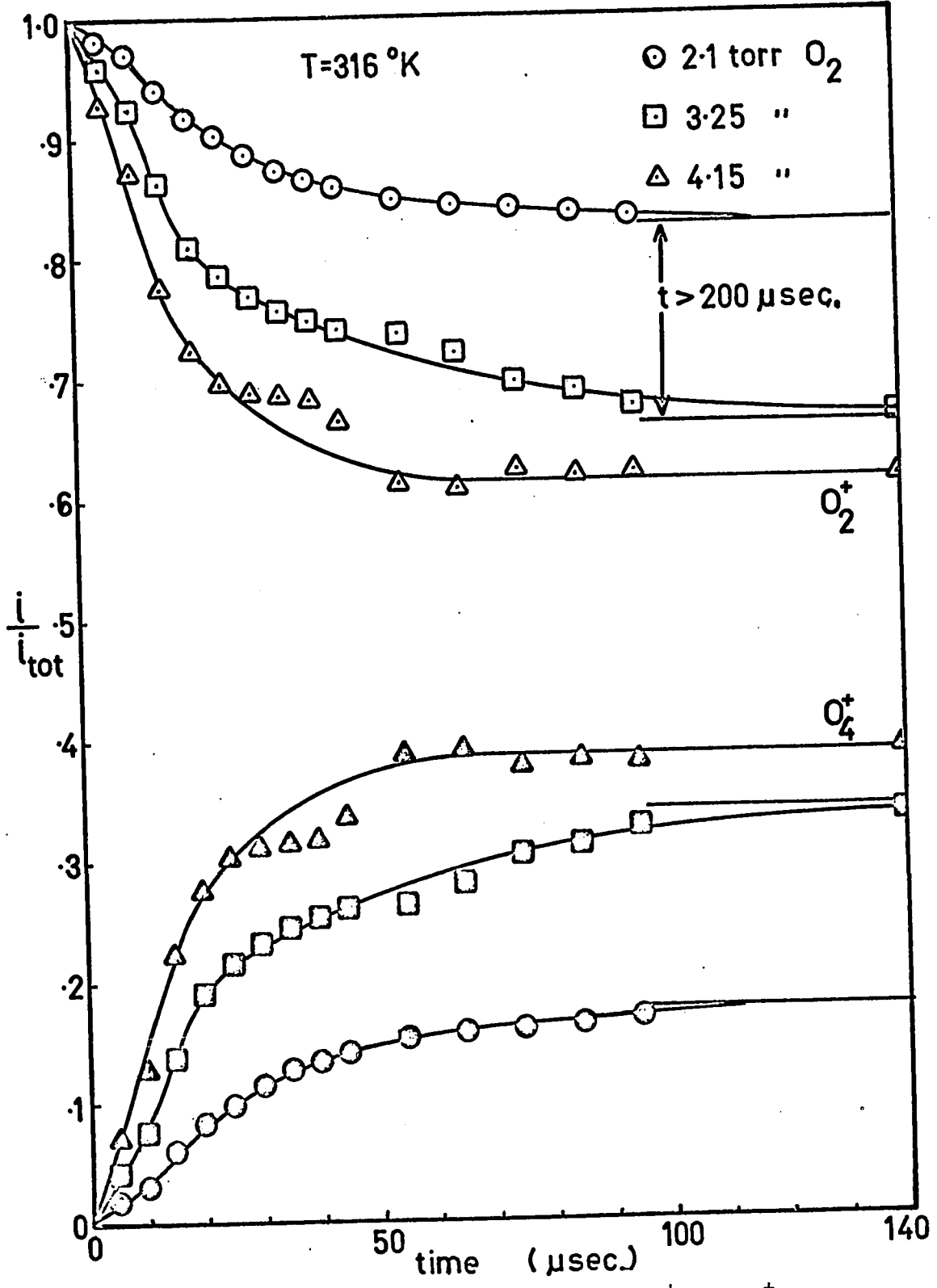


Figure 6:5 Normalized intensity curves of  $\text{O}_2^+$  and  $\text{O}_4^+$ . Oxygen at  $316^{\circ}\text{K}$ , 2.1 to 4.15 torr.

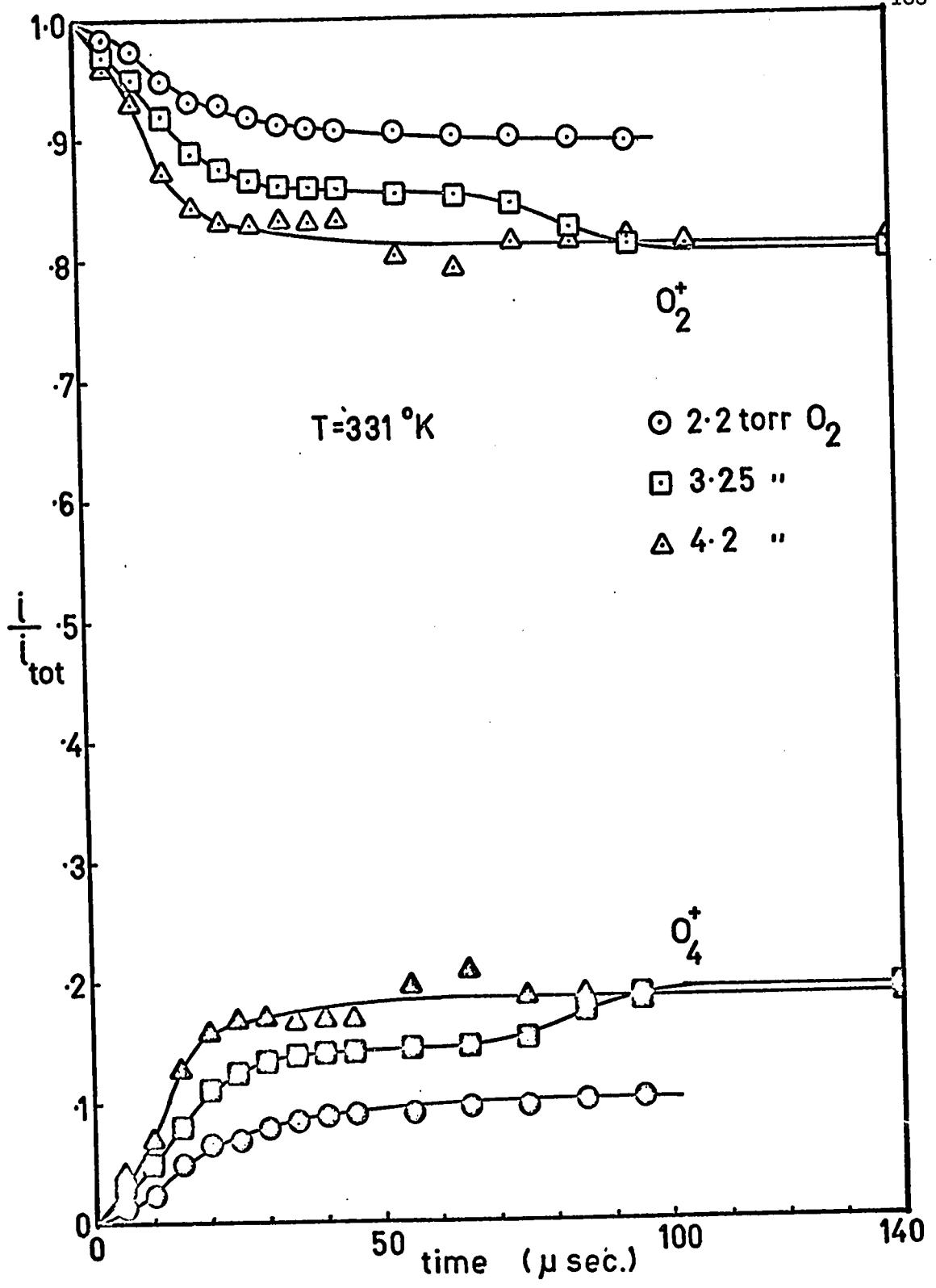


Figure 6:6 Normalized intensity curves of  $\text{O}_2^+$  and  $\text{O}_4^+$ . Oxygen at  $331^\circ\text{K}$ , 2.2 to 4.2 torr.

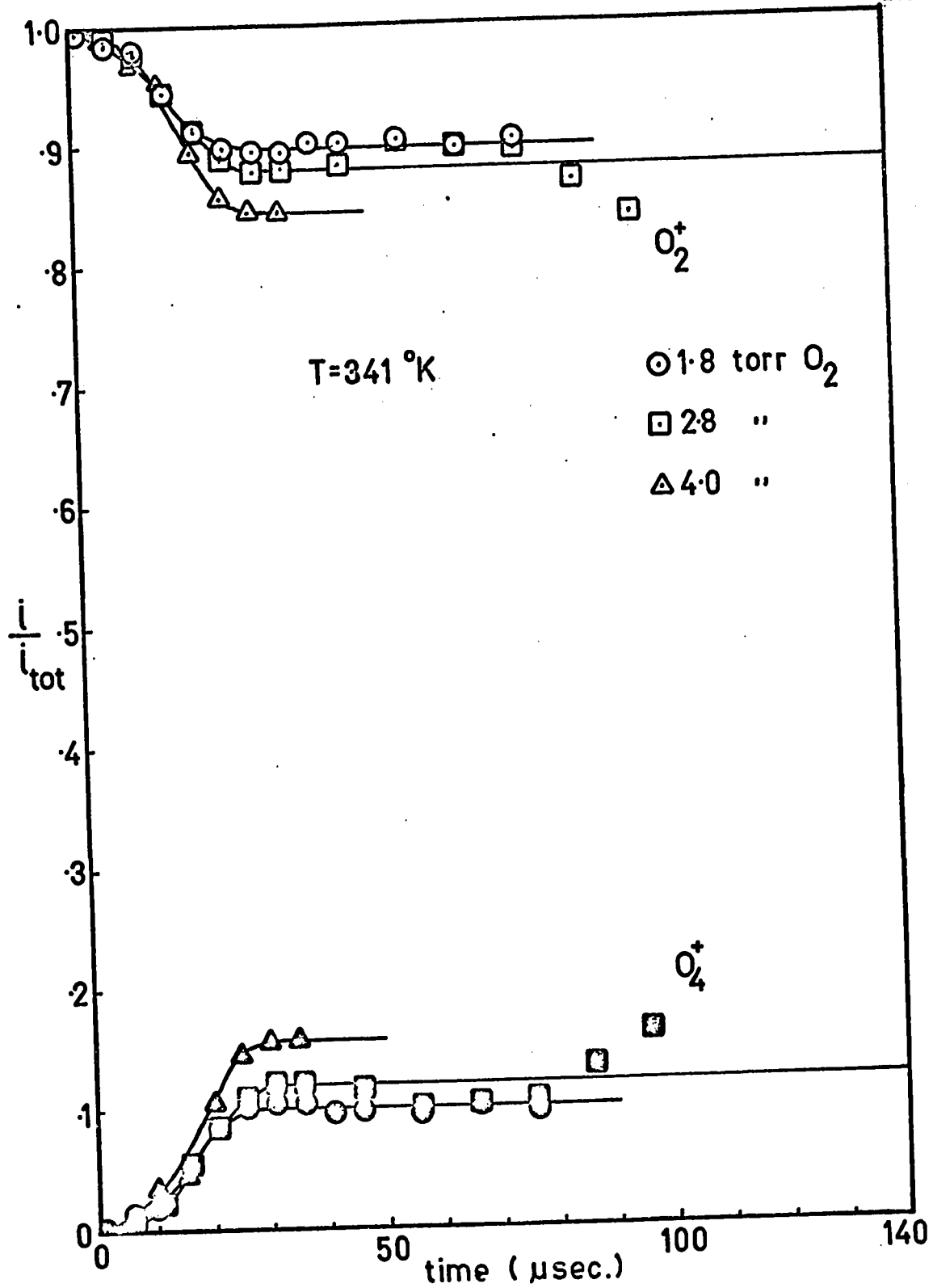


Figure 6:7 Normalized intensity curves of  $\text{O}_2^+$  and  $\text{O}_4^+$ . Oxygen at  $341^\circ\text{K}$ , 1.8 to 4.0 torr.



forward reaction was predominant. As the reaction time increased the effect of the reverse reaction began to decrease the rate of the overall forward reaction until equilibrium was reached, and then the ion intensities remained constant. As the pressure increased the equilibrium went to the right i.e. more  $O_4^+$  was formed. Also the effect of the reverse reaction became greater so that equilibrium was reached in a shorter time.

The higher temperature runs, (figures (6:4) to (6:7), show that the equilibrium shifted to the left i.e.  $K_p$  decreased with increasing temperature. The smaller rate of decrease of  $i_{O_2}$  showed that the forward rate constant decreased. Finally equilibrium was reached at shorter times and thus the reverse reaction must have increased as the temperature increased.

An experimental problem occurred in that at long reaction times the total ion intensity was quite small and thus a large error is present in the normalized  $i_{O_2}^+$  and  $i_{O_4}^+$ . This is not immediately apparent when the data is presented in the normalized form, but it accounts for the experimental scatter of the results at long reaction times ( $> 100 \mu \text{ sec.}$ ). At the higher pressures (figure (6:2) 3 torr and 4 torr) this problem was less acute. To reduce the error the signal at long reaction times was increased by increasing the width of the ion gate. Since the ratio  $i_{O_2}^+/i_{O_4}^+$  was constant at long reaction times, increasing the width should not have altered the ratio, as it

would at short times where  $i_{O_2}^+ / i_{O_4}^+$  was time dependent.

### iii Evaluation of the Equilibrium Constant

From the figures one can immediately evaluate the equilibrium constant, and this was done first so that the results could be compared to Conway's. The intensities  $i_{O_2}^+$  and  $i_{O_4}^+$  taken at long reaction times ( $> 100 \mu \text{ sec.}$ ) where the reaction was at equilibrium were substituted into equation (6:i). A van't Hoff plot was prepared by plotting  $\log K_p$  versus  $10^3/T$ , figure (6:8). The solid line is a least squares line while the dashed line represents the data of Yang and Conway (97). The results are in very good agreement.

Thermodynamic properties can be calculated from the change of  $K_p$  with temperature from the following equations. The Gibbs free energy is related to the equilibrium constant by equation (6:ii) and to the enthalpy and entropy by (6:iii). These two

$$(6:ii) \quad \Delta G = - RT 2.3 \log K_p$$

$$(6:iii) \quad \Delta G = \Delta H - T \Delta S$$

equations can be combined to give the relationship between  $\Delta H$ ,  $\Delta S$  and  $K_p$  (6:iv).

$$(6:iv) \quad \Delta S = \frac{\Delta H}{T} + 2.303R \log K_p$$

$\Delta H$  was obtained from the van't Hoff plot by setting the slope equal to  $-\Delta H/2.303R$ .  $\Delta S$  was calculated from (6:iv) at

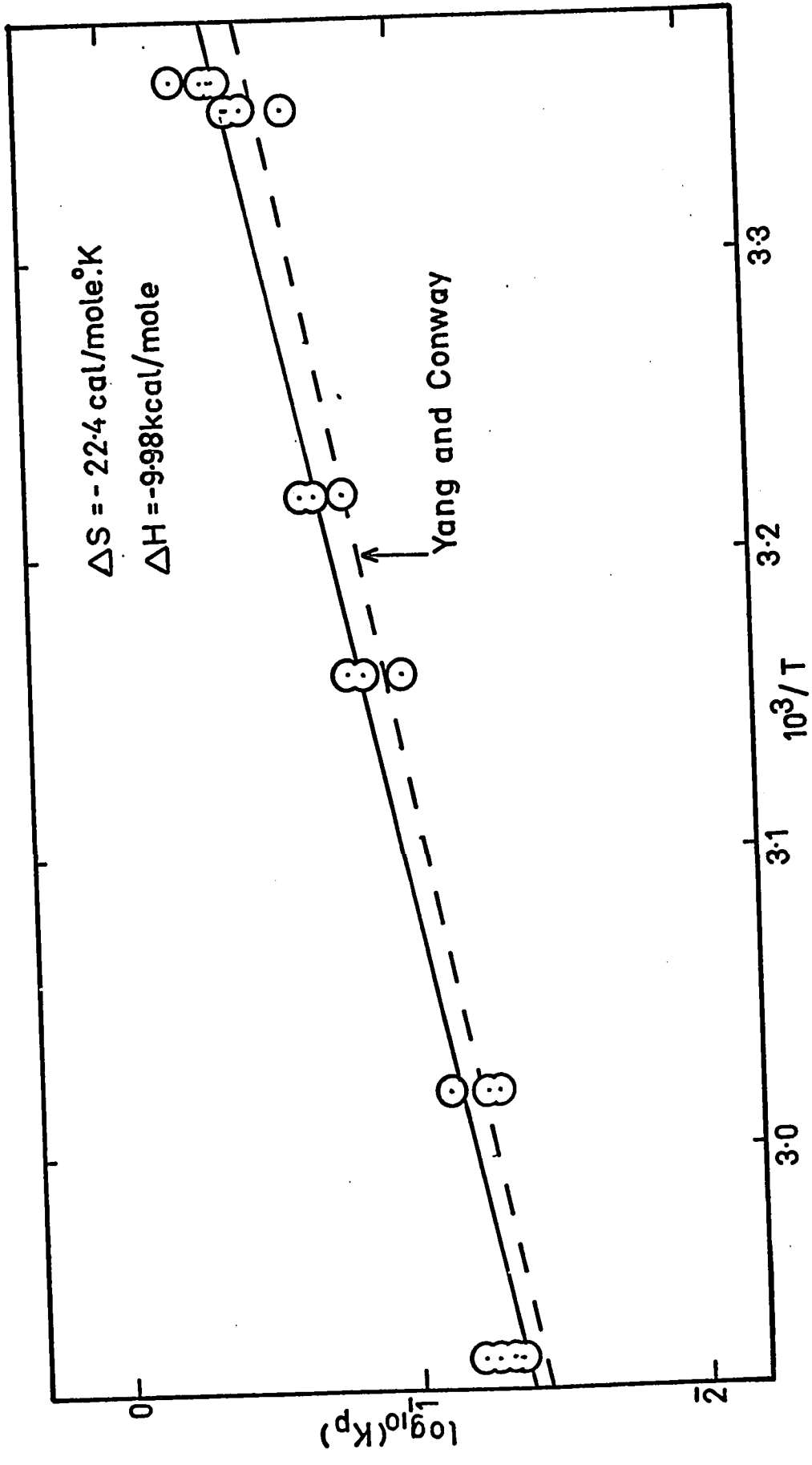


Figure 6:8 van't Hoff plot for equilibrium constant of  $O_2^+ + O_2 \rightleftharpoons O_4^+$ .

$T = 298^\circ\text{K}$ . Equation (6:i) gave  $K_p$  in units of  $\text{torr}^{-1}$  i.e. the standard state was 1 torr. To get  $\Delta S^\circ$  in units based upon one atmosphere as the standard state  $K_p$  in  $\text{torr}^{-1}$  must be multiplied by 760 torr/atmosphere. Since  $\Delta H$  is taken from the slope, the units of  $K_p$  do not affect its units.

From figure (6:8) the following values were obtained,  $\Delta H = 9.98 \text{ kcal/mole}$ ,  $\Delta S = -22.4 \text{ cal/mole } ^\circ\text{K}$ . These are very close to those obtained by Yang and Conway (97). ( $\Delta H = -7.60 \text{ kcal/mole}$ ,  $\Delta S = -20.6 \text{ cal/mole } ^\circ\text{K}$ ).

The  $K_p$  values, measured here, were slightly dependent upon pressure. Figure (6:9) shows the pressure dependence of  $K_p$  at room temperature ( $\sim 298^\circ\text{K}$ ). One can see that the values increased with pressure up to about 3 torr and were then constant with increasing pressure. The first four points were taken from the data of figure (6:2) at  $298^\circ\text{K}$  and the later four points from the data of figure (6:3) at  $297^\circ\text{K}$ . The points may not agree exactly as one would expect the  $297^\circ\text{K}$  points to be slightly higher. However one can see that at the lower pressures, 0.9 and 1.8 torr, equilibrium has not really been established when the ion intensities had decayed to small values. One might speculate that since at low pressures the ion signal decayed very rapidly the ions were removed by diffusion and mass flow in a time shorter than that required for equilibrium to be established. If  $\text{O}_2^+$  and  $\text{O}_4^+$  were

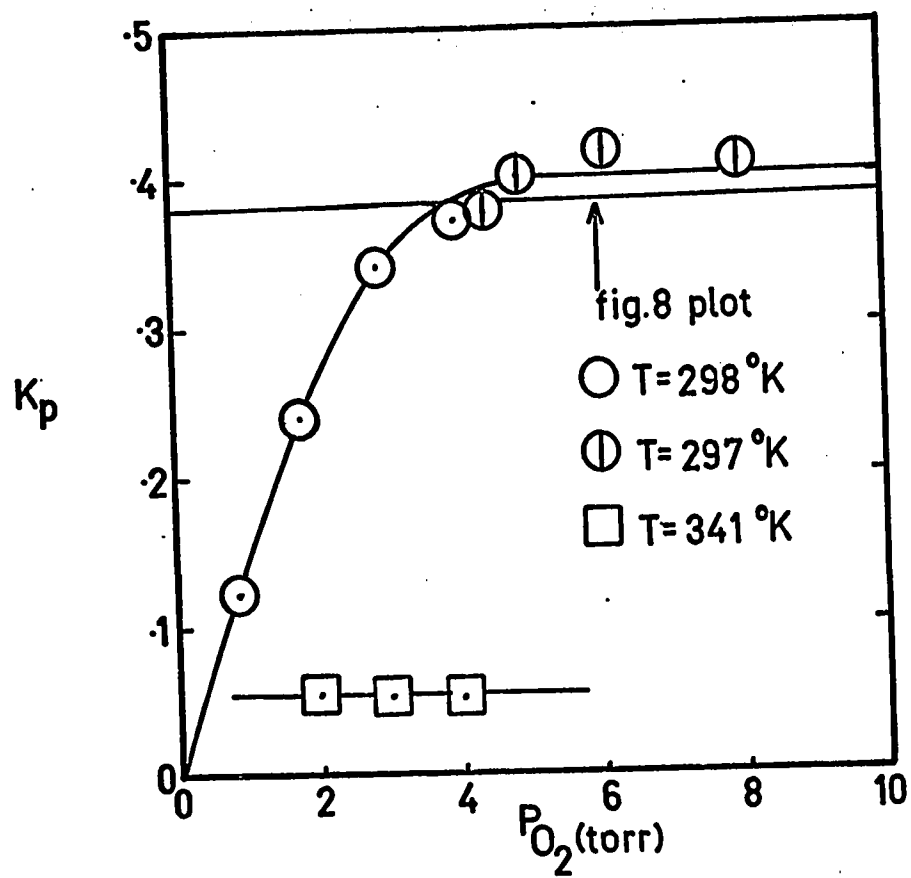
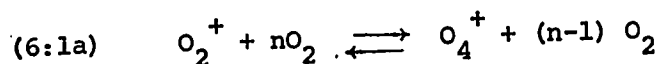


Figure 6:9 Change of  $K_p$  with oxygen pressure.

removed at about the same rates (by mass flow) it would appear that equilibrium had been established. These two values were not used on the van't Hoff plot of figure (6:8). At higher temperatures the values of  $K_p$  were constant over the range 2 to 4 torr as equilibrium was achieved in shorter times than at lower temperatures. Curves at 1 torr were not measured as equilibrium conditions were not expected.

#### iv Evaluation of the Rate Constant for the Forward Reaction

Values of the rate constant for the forward reaction were calculated from the decay of  $i_{O_2^+}$  at short reaction times (from the normalized curves). We wanted to establish the order of reaction (6:1). The reaction may be rewritten in the general form (6:1a)



where  $n = 1$  or  $2$  for the second order and third order cases respectively. The change in  $O_2^+$  is given by (6:v). At short reaction times  $[O_4^+]$  is small and one may assume that the change

$$(6:v) \quad \frac{d[O_2^+]}{dt} = -k_f [O_2^+] [O_2]^n + k_r [O_4^+] [O_2]^{n-1}$$

in  $O_2^+$  is only produced by the forward reaction. If  $[O_4^+] = 0$ , equation (6:v) may be rewritten. This equation may be integrated

$$(6:vi) \quad \frac{d[O_2^+]}{[O_2^+]} = -k_f [O_2]^n dt$$

(from  $t_1$  to  $t_2$ ) and rearranged. Substituting  $2.303 \log x$  for  $\ln x$  we get the equation which was used to evaluate  $k_f$ .

$$(6:vii) \quad k_f = \frac{2.303 \log (i_{O_2^+} t_2 / i_{O_2^+} t_1)}{(t_2 - t_1) [O_2]^n}$$

We have also made the assumption that the ion intensifies  $i_{O_2^+}$  and  $i_{O_4^+}$  were proportional to the concentrations  $[O_2^+]$  and  $[O_4^+]$ .

Preliminary values for  $k_f$  were calculated from  $i_{O_2^+}$  on figure (6:2), at the steepest part of its decay by use of equation (6:vii). The second and third order values ( $n=1$  and  $n=2$  respectively) are shown on figure (6:10). Since the second order constant varies linearly with pressure and is zero for zero pressure the reaction is clearly third order up to at least 4 torr. Third order rate constants were then calculated for all the temperatures given in the data on figures (6:2) to (6:7).

The preliminary values for the third order rate constant were plotted as an Arrhenius plot. The Arrhenius equation (6:viii) may be rewritten in a logarithmic form (6:ix) for the forward

$$(6:viii) \quad k = A e^{- (E_a/RT)}$$

$$(6:ix) \quad \log k_f = \log A - E_f/2.303 RT$$

reaction. A plot of  $\log k_f$  versus  $1/T$  will give a straight line of slope  $-E_f/2.303 R$ . An activation energy  $E_f = -5.2$  kcal/mole was calculated from the least squares line. This value is rather

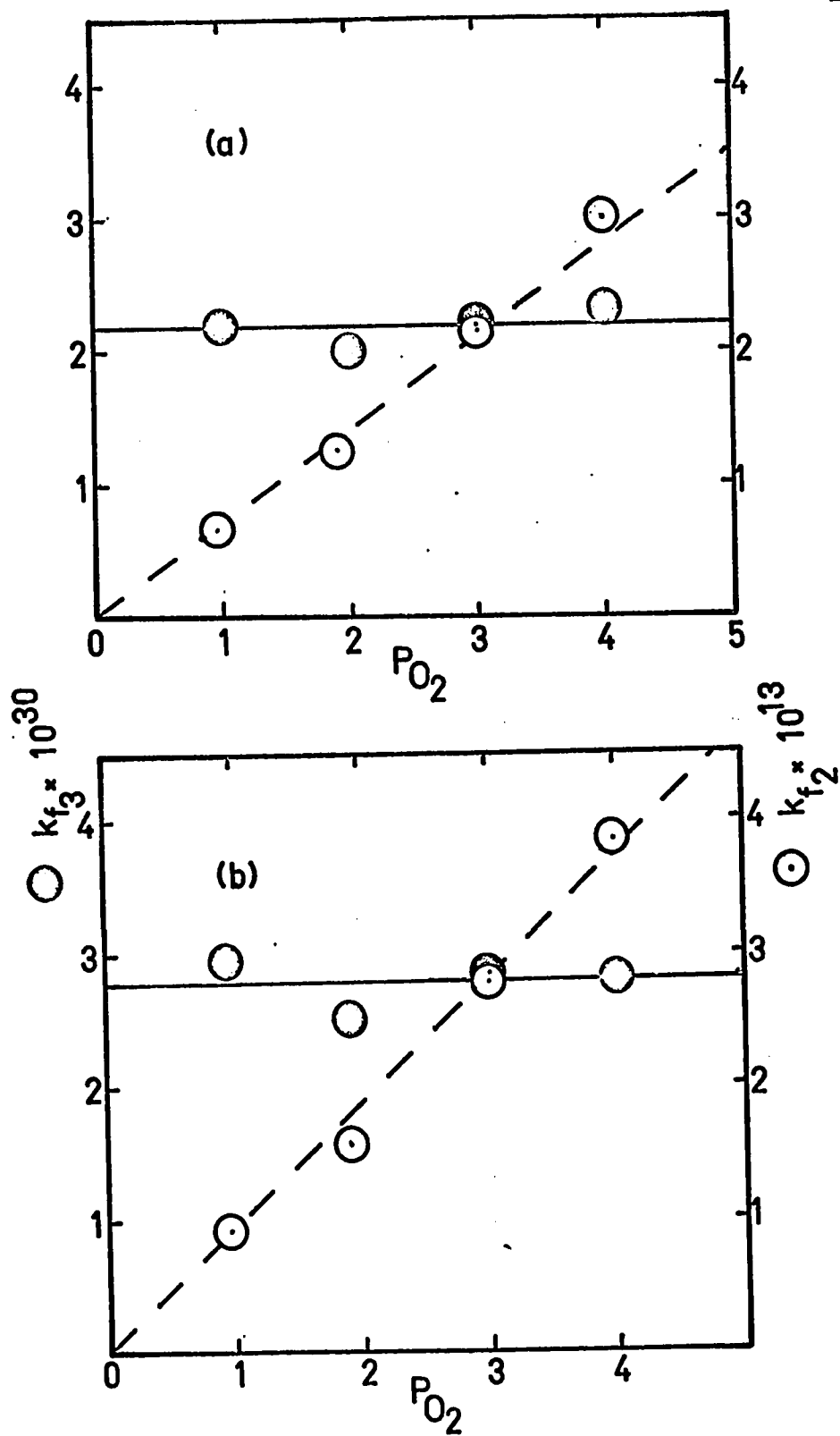


Figure 6:10 Third and second order rate constants  $k_f$  versus oxygen pressure for reaction (6:1a).  
 (a) preliminary values  
 (b) corrected values.



large for an ion-molecule reaction, especially since most second order reactions have zero activation energy.

Several experimental effects may explain the large magnitude. Firstly, since the ionization pulse had a duration of 10 micro seconds,  $O_2^+$  was still being produced after zero reaction time. Theoretically the steepest part of the  $iO_2^+$  decrease curve should have been at zero time. However since  $O_2^+$  was still produced at this time, the steepest part of the curve did not occur until after a time of about 15 micro seconds. However at this time the reverse reaction began to contribute significantly since  $O_4^+$  was not zero. Thus the measured preliminary values of  $k_f$  at any temperature would be smaller than the actual values. At higher temperatures (341°K) the reverse reaction had an even greater effect than at lower temperatures 298°K, since the equilibrium was reached more quickly, in 30 micro seconds rather than in 100 micro seconds and the values of  $k_f$  would be even smaller. The  $\log k_f$  (preliminary) versus  $1/T$  plot would then have a steeper slope than that of the true values and thus give a large value of  $E_f$ . A lesser problem also occurred which caused the reaction time of 15 micro seconds to be chosen. The change in total ionization intensity was rapid in the first 10 micro seconds and thus the relative values of  $iO_2^+$  and  $iO_4^+$  had large errors.

The rate constant  $k_f$  was re-evaluated by taking into

account the effect of the reverse reaction. The equation (6:x), for  $k_f$  is developed in Appendix I.

$$(6:x) \quad k_f = \frac{2.303}{(1+C)} \frac{\log [i_{O_2}^+ (1+C) - C]}{t [O_2]^n}$$

The constant  $C = i_{O_2, eq}^+ / i_{O_4, eq}^+$  taken at long reaction times i.e. when the reaction has reached equilibrium. A plot of

$\frac{2.303}{1+C} \log [i_{O_2}^+ (1+C) - C]$  versus time has a slope of  $k[O_2]^n$  where  $n=1$  for the second order rate constant and  $n=2$  for the

third order constant. Such plots were prepared for all the data in figures (6:2) to (6:7). As predicted by the theory, the plots are straight lines. Such a plot for the data at 298°K (figure 6:2) is shown in figure (6:11). The line should pass through 0 at  $t=0$ . However since  $O_2^+$  was still being produced during the first 10 micro seconds the line did not always do so. This should not affect the value of  $k_f$  as it was taken from the slope of a line through many points. The corrected values of  $k_f$  at 298°K, for the second and third order case were plotted versus pressure, figure (6:10b), and the third order mechanism was confirmed.

The preliminary and corrected values for the third order constant are shown in Table 6:1. One can see that when the effect of the reverse reaction was taken into account the values of  $k_f$  became slightly larger.

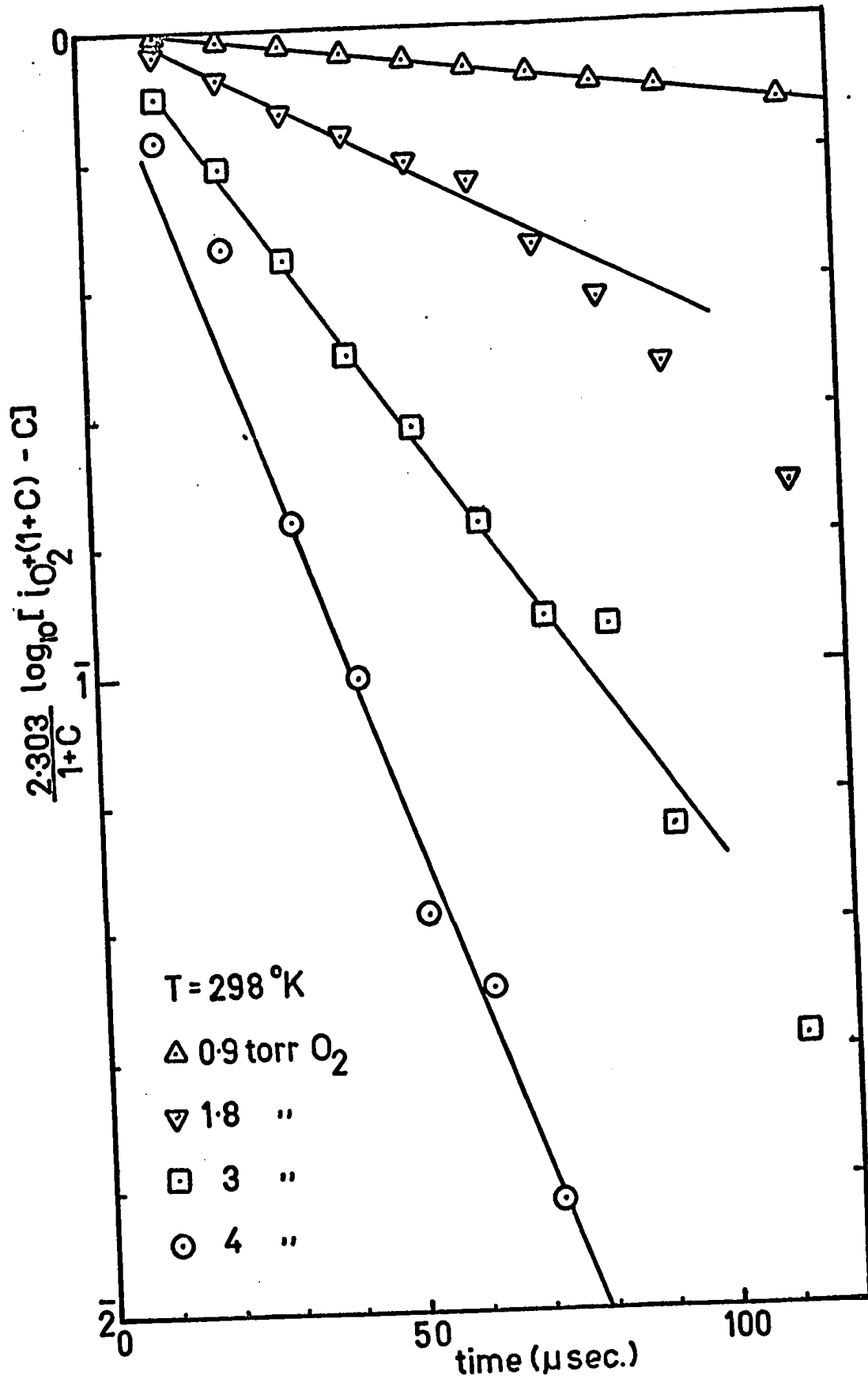
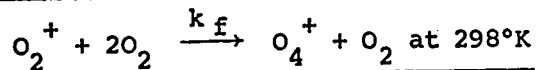


Figure 6:11 Typical plot from which corrected values were obtained  $O_2^+ + 2O_2 \rightleftharpoons O_4^+ + O_2$ .

TABLE 6:1

## Third Order Rate Constants for the Reaction



O <sub>2</sub> Pressure torr	Rate constants (cc <sup>2</sup> /molecule <sup>2</sup> sec.)x10 <sup>30</sup>	
	k <sub>r</sub> by (6:vii)	k <sub>f</sub> by (6:x)
0.95	2.21	2.79
1.9	2.03	2.50
3.0	2.20	2.84
4.0	2.32	2.81

An Arrhenius plot, figure (6:12), was prepared from the rate constants obtained by the second method and equation (6:x). The least squares line gave an activation energy of -2.0 kcal/mole. This is consistent with values obtained for radical recombination reactions involving stabilization by a third body.

Not all the graphs in figures (6:2) to (6:7) could be recalculated using the plot of  $\frac{2.303}{1+C} \log[i_{\text{O}_2^+} (1+C) - C]$  since in the cases where equilibrium was reached quickly the ratio  $C = i_{\text{O}_2^+}(\text{eq})/i_{\text{O}_4^+}(\text{eq})$  was large and the corresponding correction to  $i_{\text{O}_2^+}$  became large. Some of these plots did not give straight lines from which values of  $k_f$  could be calculated. These were discarded. The points used on figure (6:12) are quite

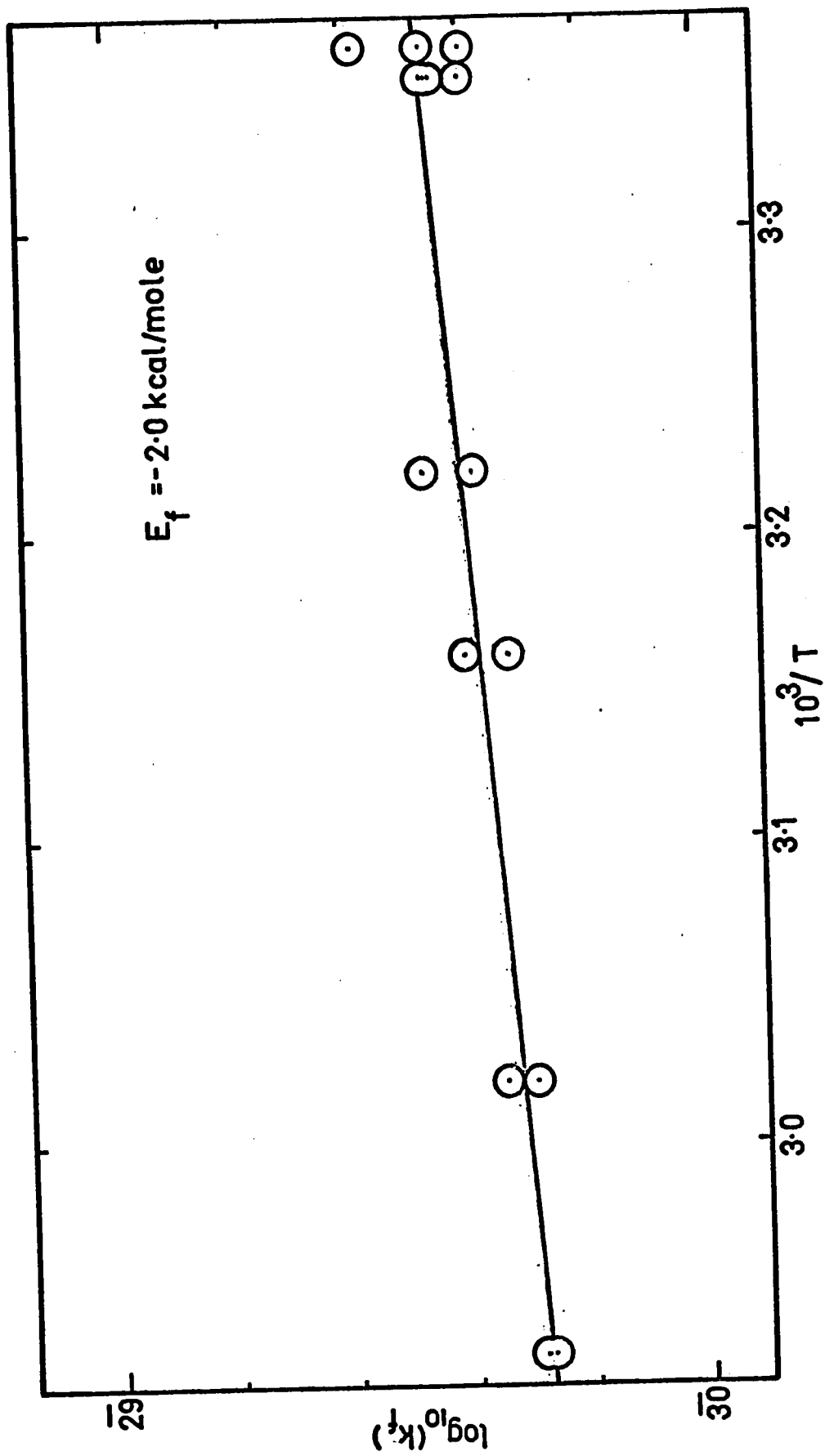


Figure 6:12 Arrhenius plot of corrected values of  $k_f$  for  $O_2$ .

representative of the data.

v Evaluation of the Rate Constant for the Reverse Reaction

The forward and reverse rate constants are related to the equilibrium constant  $K$ , which is expressed in terms of concentrations rather than in terms of pressure, as is  $K_p$ . The relationship between

$$(6:xi) \quad K = \frac{k_f}{k_r}$$

the two equilibrium constants is given by (6:xii) where  $\Delta v$  is the change in the number of moles ( $\Delta v = 1$  for reaction 6:1) and  $R$  in

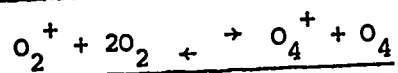
$$(6:xii) \quad K = K_p (RT)^{\Delta v}$$

appropriate units is  $1.034 \times 10^{-19}$  torr cc/molecule °K. The reverse rate constant can then be calculated from (6:xiii).  $k_r$  calculated

$$(6:xiii) \quad k_r = \frac{k_f}{K_p T \times 1.034 \times 10^{-19}} \text{ cc/molecule sec.}$$

at  $298^\circ \text{K}$  and  $314^\circ \text{K}$ , then has the values  $2.44 \times 10^{-13}$  cc/molecule<sup>-1</sup> sec<sup>-1</sup> and  $1.25 \times 10^{-12}$  cc/molecule<sup>-1</sup> sec<sup>-1</sup>. These lead to a value of the activation energy of the reverse reaction of 7.50 kcal/mole.

A summary of the results is given in Table 6.2.

Constants for the Attachment Reaction (6:1)EXPERIMENTAL RESULTS

$$\Delta H = -9.98 \pm .5 \text{ kcal/mole. at } 298^\circ\text{K}$$

$$\Delta S = -22.4 \text{ cal/mole deg.}$$

$$E_f = -2.0 \text{ kcal/mole}$$

$$E_r = 7.5 \text{ kcal/mole}$$

$$k_f = 2.90 \times 10^{-30} \text{ cc}^2/\text{molecule}^2 \text{ sec. at } 298^\circ\text{K}$$

$$= 1.27 \times 10^{-30} \text{ cc}^2/\text{molecule}^2 \text{ sec. at } 400^\circ\text{K (extrapolated)}$$

$$k_r = 2.44 \times 10^{-13} \text{ cc/molecule sec. at } 298^\circ\text{K}$$

$$= 6.54 \times 10^{-12} \text{ cc/molecule sec. at } 400^\circ\text{K (extrapolated)}$$

$$K = 1.19 \times 10^{-17} \text{ (standard state 1cc/molecule) at } 298^\circ\text{K}$$

$$= 1.94 \times 10^{-19} \text{ (standard state 1cc/molecule) at } 400^\circ\text{K}$$

$$K_p = 3.85 \times 10^{-1} \text{ (standard state 1 torr) at } 298^\circ\text{K}$$

$$= 4.7 \times 10^{-3} \text{ (standard state 1 torr) at } 400^\circ\text{K}$$

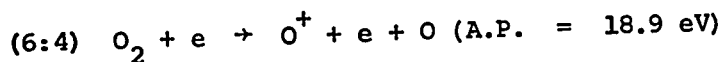
PREVIOUS RESULTS (Yang and Conway)

$$\Delta H = -9.60 \text{ kcal/mole at } 298^\circ\text{K}$$

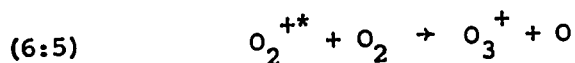
$$\Delta S = -20.6 \text{ cal/mole deg.}$$

vi Other Reactions, Possible Interference

The ions  $O^+$  and  $O_3^+$  were also observed. It was possible that they might interfere with the rate constant measurement for reaction (6:1).  $O^+$  was produced from  $O_2$  by reaction (6:4).



At lower pressures i.e. 0 to 0.4 torr  $O_3^+$  was a major ion in the spectrum. Its formation has been studied by Curran (99). Since he measured its appearance potential as  $17.0 \pm 0.05$  eV as compared to 13.61 (R.E.) for  $O^+$  and 12.06 eV (I.P.) for  $O_2^+$  he suggested that it would be formed from an excited state of  $O_2^+$  by reaction (6:5). The energy of an excited state, in



excess of the  $O_2^+$  lowest ionization potential (12.06 eV) would be required to break an O-O bond. The appearance potential of 17.0 eV measured by Curran corresponds quite closely to that of the  $O_2^+$  excited state  $^2\pi_u$  (16.8 eV) measured by Winters *et al* (100).

Curran observed an appearance potential of 17.0 eV for  $O_4^+$  also and suggested it came from the same state. One would expect that this ion could be formed from several of the  $O_2^+$  states ( $^2\pi_g = 12.06$  eV,  $^4\pi_u = 16.0$  eV,  $^2\pi_u = 16.8$  eV or  $^4\Sigma_g^- = 18.0$  eV) as the excess energy of  $O_4^{+*}$  could be



removed by collision. The lowest state, however, would be expected to contribute the most since firstly it is the state of highest abundance (76 Lindholm) and also it would produce  $O_4^{++}$  with the least excitation energy to be removed by collision. The excitation energy would be less than that required by reaction (6:6). That is, the high energy excited states could produce  $O_4^+$  and  $O_3^+$  depending upon the lifetime of the excited complex, but the lower  $O_2^+$  could only produce  $O_4^+$ .

In this work the observed  $O^+$  and  $O_3^+$  intensities were extremely small at oxygen pressures from 1 to 8 torr, about 1 to 2% of the  $O_2^+$  and  $O_4^+$  intensities under constant irradiation conditions. An attempt was made to measure  $O^+$  and  $O_3^+$  but their intensities were at the lower limit of detection under pulse irradiation. Consequently we assumed that (Rx 6:6) did not affect the intensity of  $O_2^+$  and accordingly only measured the  $O_2^+$  and  $O_4^+$  intensities.

In a few of the runs an impurity ion  $m/e$  50 ( $O_2(H_2O)^+$ ) was observed. This was due to water. In such cases a new oxygen sample was prepared. The mass spectrometer gas handling plant and ion source were baked out until the water was removed such that only the oxygen ions were observed.

## vii Discussion of Results

It was very gratifying to get values for  $\Delta H$  and  $\Delta S$  very close to those of Yang and Conway (97). The latter were corrected for the effects of ambipolar diffusion as it was felt that this did have an effect upon the rate of ion removal from their type of ion source. The values of  $K_p$  calculated by them were not independent of pressure. A close examination of the van't Hoff plot in reference (97) reveals that the values increased with increasing pressure. Because of this Yang and Conway felt that the results obtained at the low pressure limit of their apparatus, 1 torr gave the most meaningful results when corrected for the different diffusion rates of the ions.

The equilibrium constants calculated from our data were constant above a certain pressure of oxygen. The ions were probably removed more by mass flow than by ambipolar diffusion. In this case there would be no discrimination in the sampling of ions and the values obtained for  $K_p$  should be correct. The ion source exit leaks used by Yang and Conway had a total area which is about 1/15 of the area of the exit slit used on the present instrument. The outflow of gas would have been smaller by this factor. It is, therefore, quite possible to have the ion extraction diffusion controlled in the former and mass flow controlled in the present apparatus.

It is usual to equate the  $\Delta H$  for a dissociation reaction

to the bond energy of the dissociated bond. The  $\Delta H$  value of the attachment reaction is the reverse for that of dissociation. We can then write for the  $O_4^+$  ion:

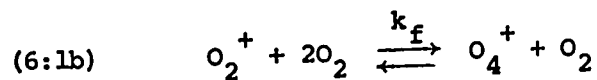
$$(6:xiv) \quad -\Delta H = D(O_2^+ - O_2)$$

Thus the dissociation energy of  $O_4^+$  is 10.0 kcals. Also if the change in volume is small one can equate  $\Delta H \sim \Delta E$  and thus

$$(6:xv) \quad \Delta H \sim E_f - E_r \\ -10 \sim -2 - 7.5 = 9.5 \text{ kcals/mole}$$

(The change in volume  $P\Delta V$  gives the difference 0.5 kcal/mole).

It was observed that the rate constant for the forward reaction of oxygen was approximately thirty times smaller than that of the corresponding reaction in nitrogen (101). This will be discussed, along with the energy transfer theory, in the next chapter. Since data indicates that the reaction is third order we may then write the reaction as below (6:1b).



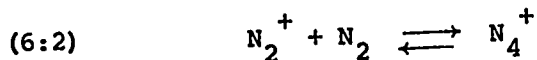
The two rate constants  $k_f$  and  $k_r$  may be composite rate constants.

### 6:3 The Attachment of Nitrogen, $N_2^+ + N_2 \rightarrow N_4^+$

#### i Previous Work on this Reaction

A reaction which parallels the oxygen reaction studied above is the attachment of  $N_2$  molecules to  $N_2^+$  ions. This is represented

by reaction (6:2)



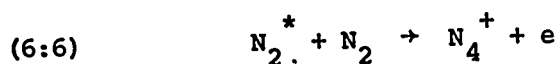
This reaction is considered to cause the low mobility of  $N_2^+$  ions in nitrogen gas and it has been studied extensively with respect to mobility problems (102,103,104). The equilibrium constant and the rate constants have been measured at energies higher than thermal in electric drift fields and at thermal energies in the absence of an electric field.

Varney studied the mobility of  $N_2^+$  and  $N_4^+$  in nitrogen in a drift field apparatus (92,105-108) operated at pressures up to 35 torr and field strength 200 volts/torr. He calculated the extent of dissociation of  $N_4^+$  from the change of ionic mobility with the variation of  $E/P_0$  (electric field strength/normalized pressure where  $P_0 = px273/T$ ). From the extent of dissociation he deduced a value for an equilibrium constant  $K$ . He also proposed a relationship between the ion temperature  $T_i$  and the  $E/P_0$  ratio ( $T_i = T_{\text{gas}} + aE/P_0$  where  $a$  is a constant). A van't Hoff plot ( $\ln K$  versus  $1/T_i$ ) was used to calculate a value for the dissociation energy  $D(N_2^+ - N_2) = -\Delta H$ . His value for  $\Delta H$  was  $-0.50$  eV ( $\sim 11.5$  kcal/mole).

An apparent equilibrium constant was obtained under thermal conditions at a pressure of 1 torr  $N_2$  by Knewstubb (109). His value was 75 (standard state 1 torr) at  $300^\circ\text{K}$ . If Varney's

van't Hoff plot (108) is extrapolated to a value of  $1/T_i = 1/300^\circ\text{K}$  the  $K_p$  value obtained is about  $5 \times 10^5$ . This is extremely large compared to the values previously obtained for the oxygen reaction (6:1).

A value for the dissociation energy can be calculated from another set of data.  $N_4^+$  is also formed by a second reaction, the Hornbeck-Molnar process (6:6). Asundi, Schultz and Chantry (103) measured the appearance potentials of  $N_4^+$  and  $N_2^+$  in nitrogen

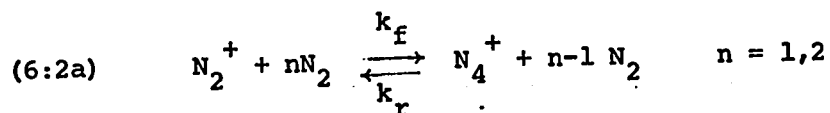


by means of a mono-energetic electron beam technique. They took the appearance potential of  $N_2^+$  to be 15.6 eV as the reference point of the electron energy scale. (The spectroscopic value is 15.58 eV. Saporoschenko (110) obtained a value of  $15.5 \pm 0.2$  eV). The appearance potential of  $N_4^+$  was  $15.0 \pm 0.1$  eV). This value is the energy of the excited neutral  $N_2^*$ . It was also measured by Curran (111) as  $15.04 \pm 0.5$  eV. The difference between the energies of the two methods of formation of  $N_4^+$  gives a minimum for the bond energy  $D(N_2^+ - N_2)$ . This is given by (6:xvi).

$$(6:xvi) \quad D(N_2^+ - N_2) \geq (15.6 - 15.0) \pm 0.1 \text{ eV} \\ \geq 13.8 \pm 2.3 \text{ kcal/mole}$$

The two values of  $-\Delta H$ , 11.5 and 13.8 kcal/mole agree within the experimental error of 0.1 eV (2.3 kcal/mole).

The rate constant for the forward reaction (6:2) has been measured under drift field and thermal conditions. Since the kinetic order has been under contention(112), we will write the reaction as (6:2a) in accordance with the reaction (6:1a) for oxygen.



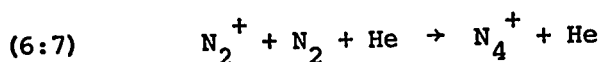
$n=1$  for a second order reaction and  $n=2$  for a third order reaction.

Warneck (101) measured  $k_f$  by means of a drift field technique and obtained a third order value of  $8.5 \times 10^{-29} \text{ cc}^2/\text{molecule}^2 \text{ sec.}$

The pressure was varied from .09 to 0.2 torr. The constant appeared to be independent of  $E/P_0$  as well as pressure. McKnight *et al* (104) measured drift field velocities of the nitrogen ions  $N^+$ ,  $N_2^+$ ,  $N_3^+$  and  $N_4^+$  at pressures from 0.5 to 1.0 torr and calculated a third order constant for reaction (6:2a) which was dependent upon  $E/P$ . Their values ranged from  $7 \times 10^{-29}$  at low  $E/P_0$  to  $2 \times 10^{-29} \text{ cc}^2/\text{molecule}^2 \text{ sec.}$  at high  $E/P_0$ .

Knewstubb (109) reported a third order value of  $8 \times 10^{-29} \text{ cc}^2/\text{molecule}^2 \text{ sec.}$  measured under thermal conditions at pressures up to 1 torr. He reported a temperature coefficient of "close to -1 percent per degree at 298°K." This gives an activation energy of about -3.6 kcal/mole. Fite *et al* (45) observed the formation of  $N_4^+$ , by means of a pulsed afterglow technique. They estimated a second order  $k_f$  value of approximately

$5 \times 10^{-13}$  cc/molecule sec. and this corresponds to  $3 \times 10^{-29}$  cc<sup>2</sup>/molecule<sup>2</sup> sec. (third order) at the pressure of 0.5 torr used. More recently Fehsenfeld (113) reported a reaction (6:7) similar to (6:2a), observed by means of the flowing afterglow technique. Since the pressure of helium (about 1 torr) was approximately 100 times



that of nitrogen, helium acted as the third body. Rate constants were reported,  $1.9 \times 10^{-29}$  cc<sup>2</sup>/molecule<sup>2</sup> sec. at 280°K and  $1 \times 10^{-28}$  cc<sup>2</sup>/molecule<sup>2</sup> sec. at 80°K. The activation energy can be calculated to be -0.37 kcal/mole from these two values.

#### ii The Purpose of This Study

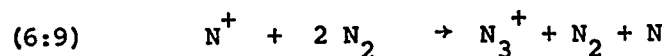
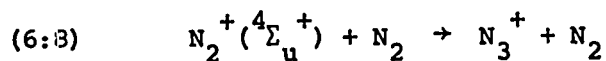
We decided to look at the nitrogen reaction under the same conditions as used for oxygen for several reasons. Firstly, the measurement of the rate constant for the forward reaction in nitrogen would provide a check on the value for oxygen. It has been noticed that these values were different by a factor of approximately thirty which would appear to be exceptionally large. The order of the reaction occurring in the pressure region 0.2 to 5 torr was under contention. Secondly both Varney's values for the equilibrium constant  $K_p$  and Warneck's value of the rate constant  $k_f$  for the forward reaction were calculated from ion intensities which had been measured under the influence of an electric field, in which the ions

were not at thermal energies. In the present work, the ion source was essentially field free and thus the ion temperature should have become the same as the gas temperature after the ion had undergone several collisions. Knewstubb's value for the equilibrium constant was very different from that obtained by an extrapolation of Varney's data (75 compared to  $5 \times 10^5$ ). We hoped to check these data.

We also hoped to obtain the temperature dependences of both the rate constant  $k_f$  and the equilibrium constant  $K_p$  so that they could be compared with those obtained for the oxygen reaction.

### iii Other Reactions Involving $N_2^+$ and $N_4^+$

$N_3^+$  ions are formed in nitrogen by two mechanisms. At low pressures  $N_3^+$  is formed from an excited state of  $N_2^+$ , (reaction 6:8), whereas, at high pressures, it is formed by a third order reaction from  $N^+$ , (reaction 6:9). The relative effect of reaction (6:8) compared to reaction (6:2) on the removal of  $N_2^+$  ions depends

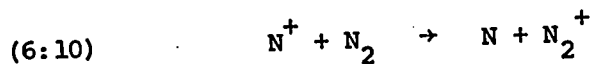


upon the amounts of  $N_2^+$  in the excited state  $^4\Sigma_u^+$  and in the ground state. Asundi *et al* (103) showed that the excited ion is deactivated by collisions with  $N_2$  molecules at pressures above  $10^{-2}$  torr and thus one would expect that reaction (6:8) would



not be important in the pressure range 0.4 to 3.6 torr used in this work. Reaction (6:9) will be considered later in section (6:5).

One would not expect that  $N_2^+$  ions would be formed by collision with  $N^+$  as the reaction (6:10) is endothermic



(R.E.  $N^+ = 14.54$  eV) ( $I_p N_2^+ = 15.58$  eV). Since the concentration of N atoms would be small the reverse of this reaction is probably insignificant in depleting the  $N_2^+$  concentration.

The ion  $N_4^+$  may be formed from excited  $N_2$  molecules by the Hornbeck-Molnar process reaction (6:6) as mentioned earlier. The importance of this reaction compared to reaction (6:2a) depends upon the ratio of  $N_2^*$  to  $N_2^+$ . Asundi *et al* showed that  $N_2^*$  was deactivated by collision with  $N_2$  at pressures greater than  $10^{-2}$  torr, and that when the electron energy was greater than 17.5 eV, the production of  $N_4^+$  was essentially only by the third order reaction from  $N_2^+$  (reaction 6:2a,  $n=2$ ). In the present experiment the gas pressure and electron energy were high and the contribution of the H-M process to  $N_4^+$  formation was expected to be small.

#### iv Results

The intensity curves for the ions  $N^+$ ,  $N_2^+$ ,  $N_3^+$  and  $N_4^+$  were measured for pressures ranging from 0.4 to 3.60 torr and

temperatures from 300°K to 420°K. Most of the results were done at pressures 0.6 to 1.50 torr. In some of the runs, only  $N_2^+$  and  $N_4^+$  were measured. The results for 2.65 torr  $N_2$  at 380°K are shown in figure (6:13). The ion intensities replotted as fractions of the total ionization are shown in figure (6:14). Similar plots for different pressures at the same temperature are shown in figures (6:15) to (6:17).

The sum of the fractional intensities of  $N_2^+$  and  $N_4^+$  is shown on figures (6:14) to (6:17). The sum remained reasonably constant as the time increased. This was found to occur in many of the runs in which all ions were measured. The sum ( $i_{N_2}^+ + i_{N_4}^+$ ) also remained essentially constant. Deviations from constancy did not exhibit any trends. It was therefore concluded that the ions  $N_2^+$  and  $N_4^+$  reacted independently from the ions  $N^+$  and  $N_3^+$ ; that  $N_2^+$  was lost only by reaction (6:2) to give  $N_4^+$  and that the concentration of  $N_2^+$  in the excited state  $^4\Sigma_u$  was low. The intensity curves obtained when only  $N_2^+$  and  $N_4^+$  were measured are shown in figures (6:18) to (6:21).

When there were small amounts of water or oxygen impurities present the ions  $N_2H^+$ ,  $H_2O^+$ ,  $H_3O^+$  and  $O_2^+$  were observed. Since all the nitrogen ions have ionization potentials much larger than the impurities ( $I_{pH_2O^+} = 12.61$  eV) ( $I_{pO_2^+} = 12.06$  eV) the impurities would remove nitrogen ions by charge exchange. Much effort was expended to remove the impurities. If the impurity

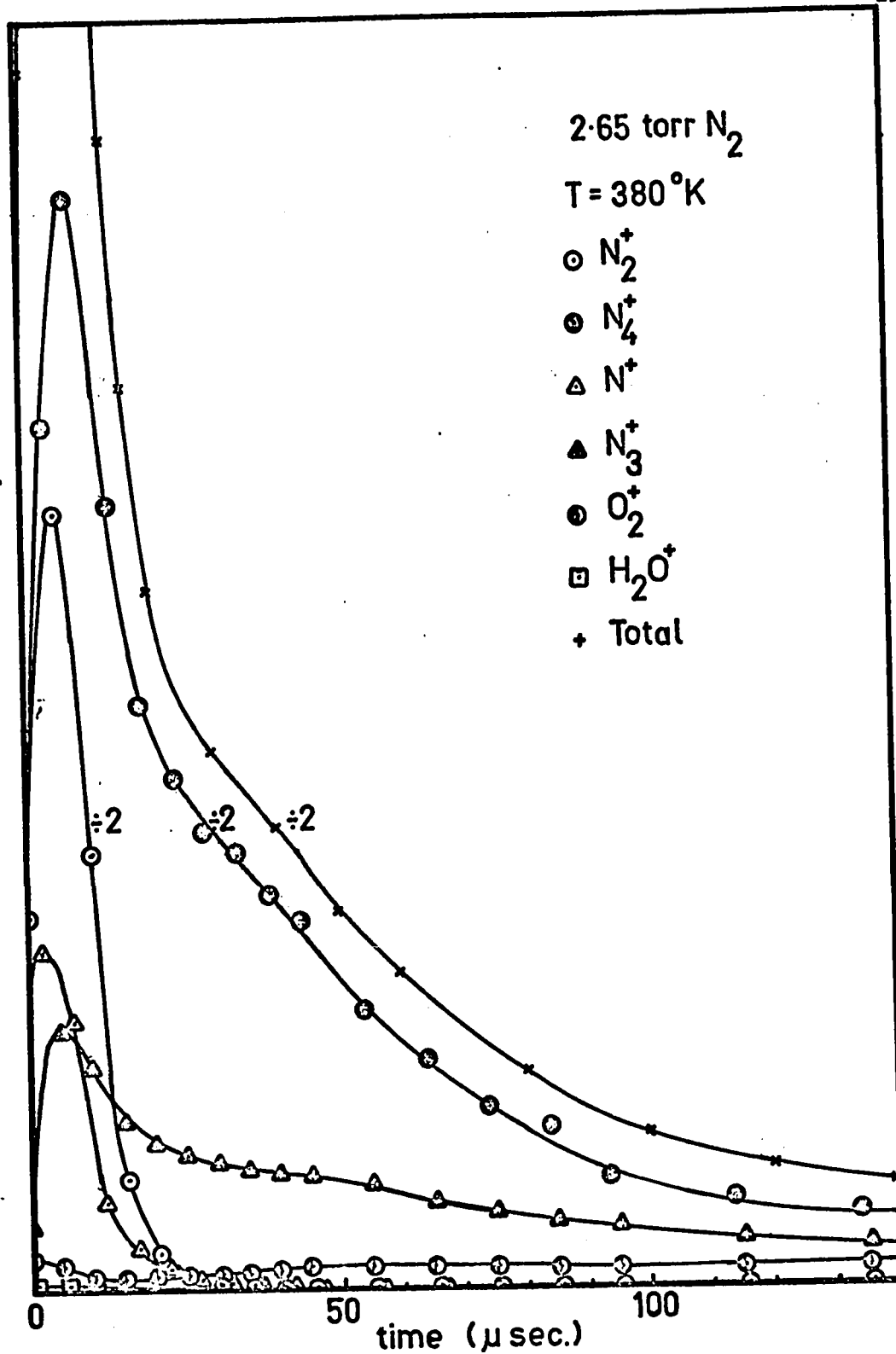


Figure 6:13 Observed ion intensity curves of  $N^+$   $N_2^+$   $N_3^+$   $N_4^+$   
 in nitrogen at  $381^\circ K$ , 2.65 torr.

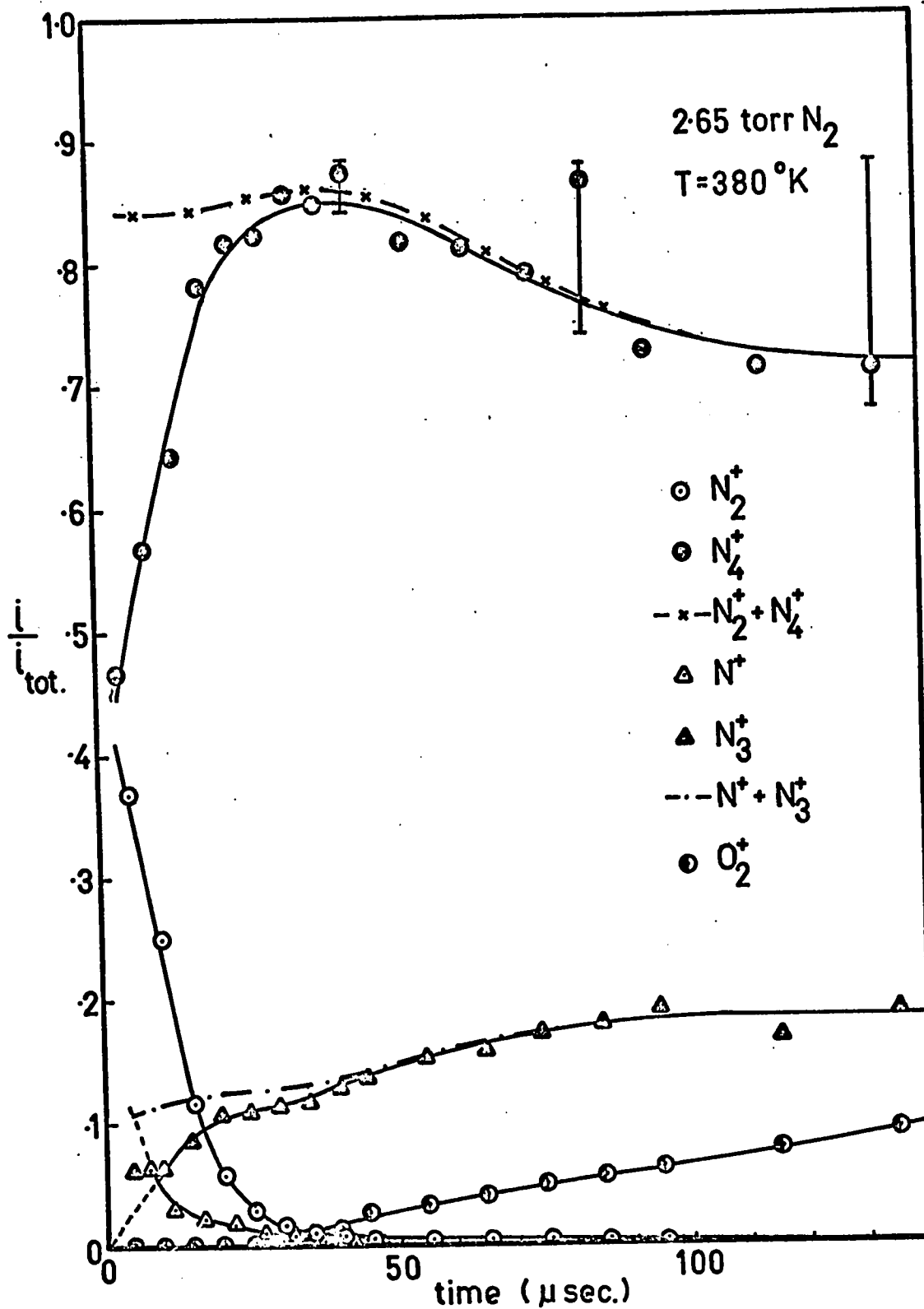


Figure 6:14 Ion intensity curves normalized to total ionization nitrogen at 381°K, 2.65 torr.

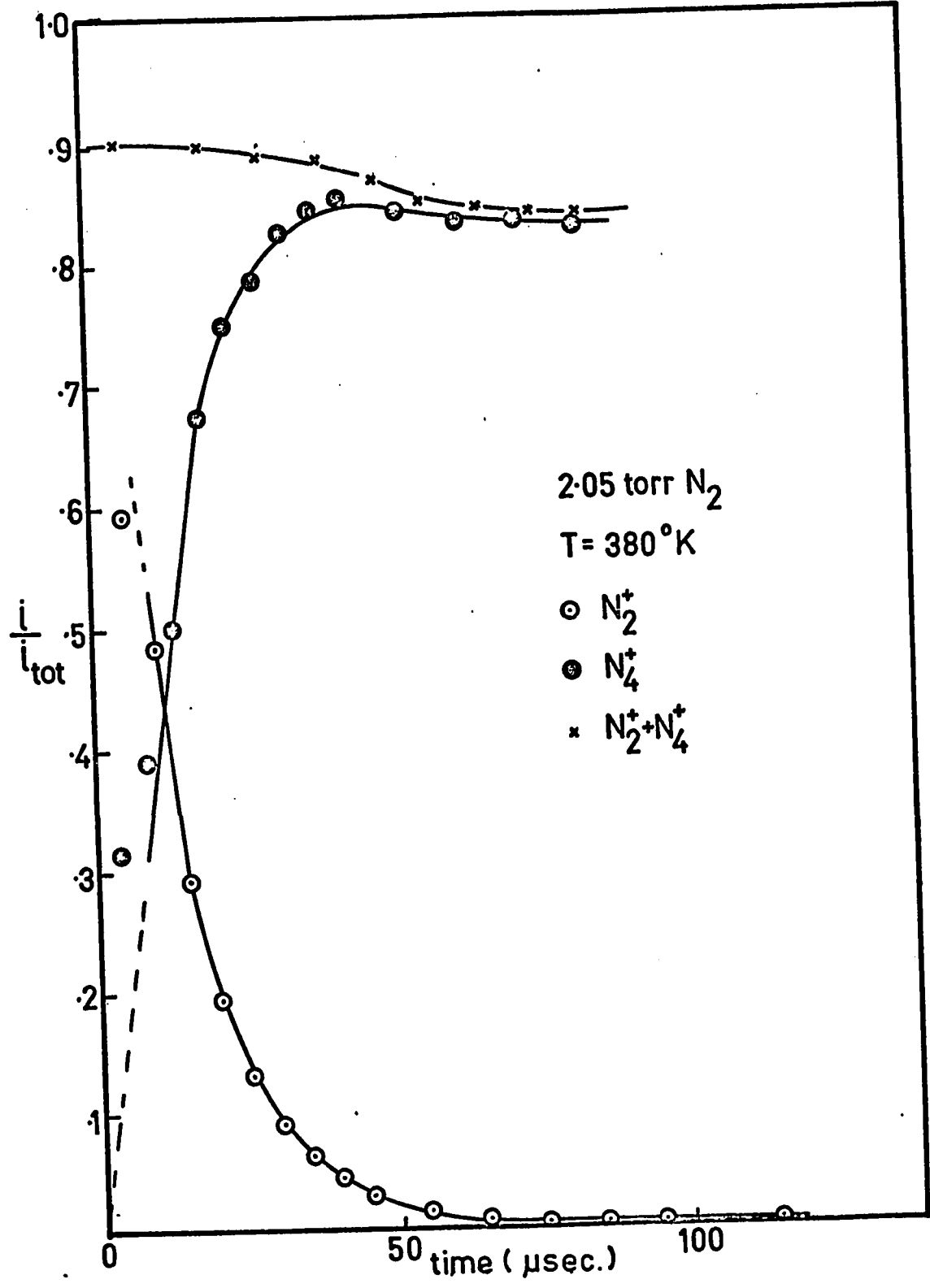


Figure 6:15 Normalized ion intensity curves of N<sup>+</sup> N<sub>2</sub><sup>+</sup> N<sub>3</sub><sup>+</sup> N<sub>4</sub><sup>+</sup> in nitrogen at 380°K, 2.05 torr.

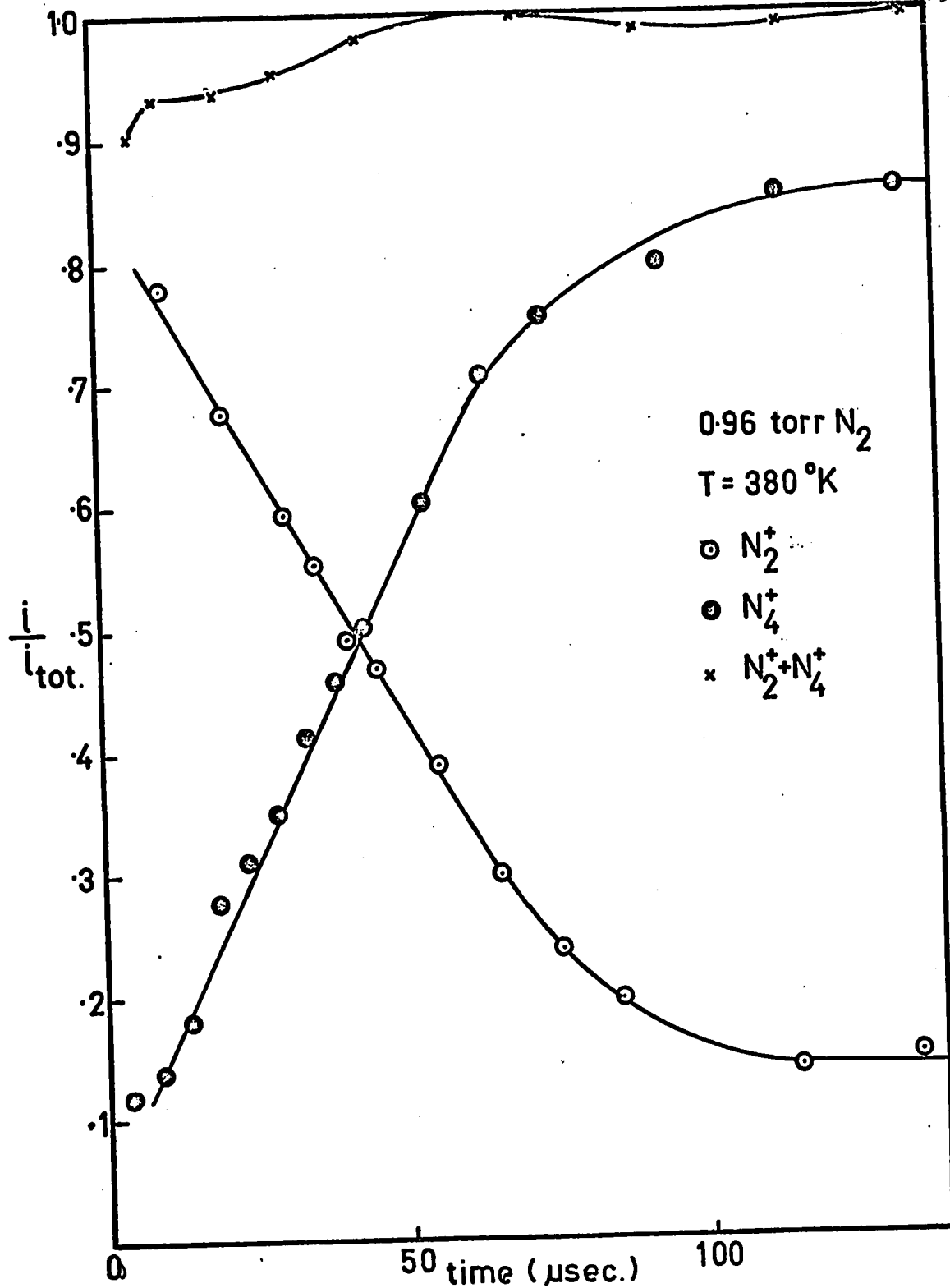


Figure 6:16 Normalized ion intensity curves of N<sup>+</sup> N<sub>2</sub><sup>+</sup> N<sub>3</sub><sup>+</sup> N<sub>4</sub><sup>+</sup> in nitrogen at 380°K, 0.96 torr.

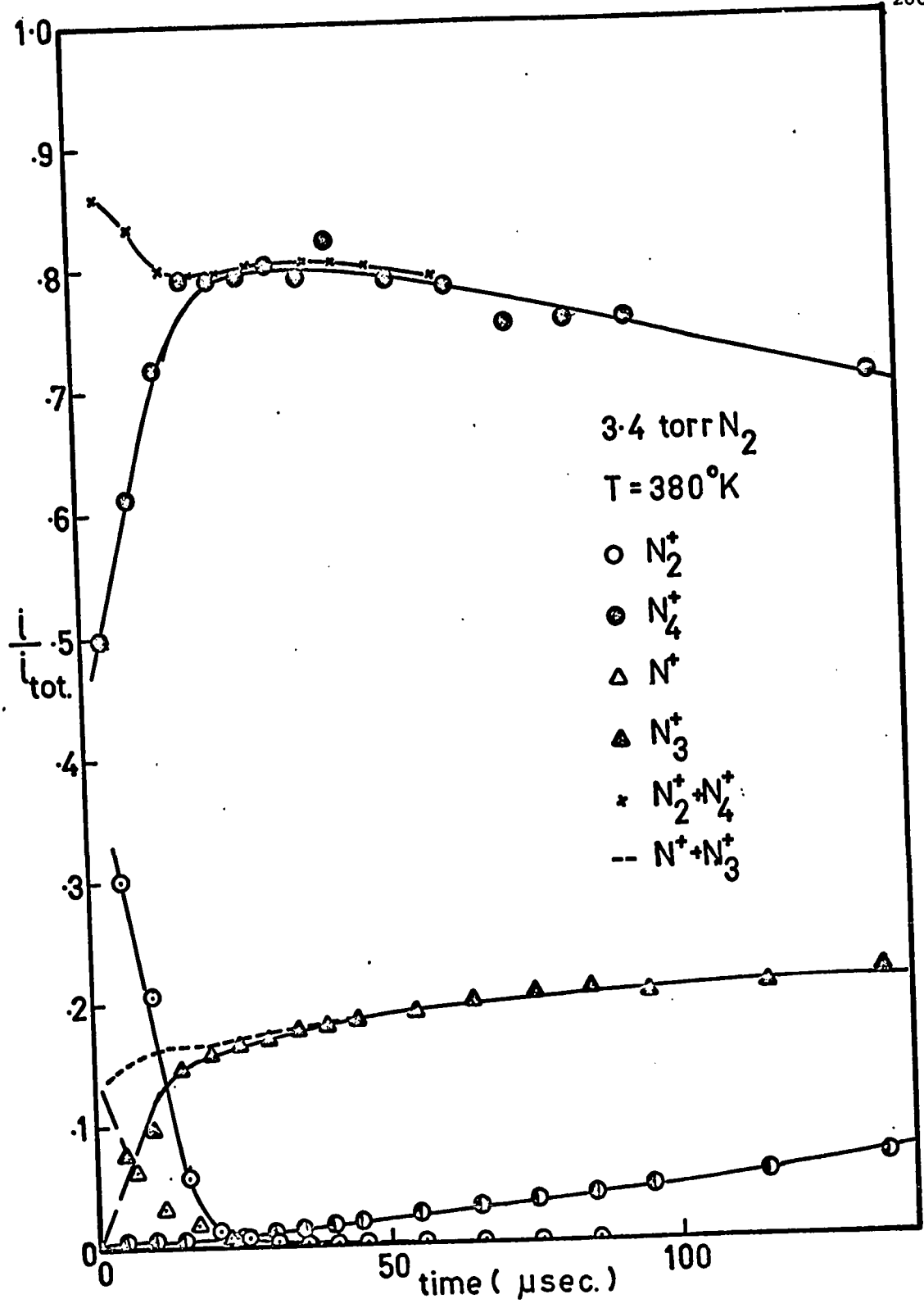


Figure 6:17 Normalized ion intensity curves of N<sup>+</sup> N<sub>2</sub><sup>+</sup> N<sub>3</sub><sup>+</sup> N<sub>4</sub><sup>+</sup> in nitrogen at 380°K, 3.40 torr.

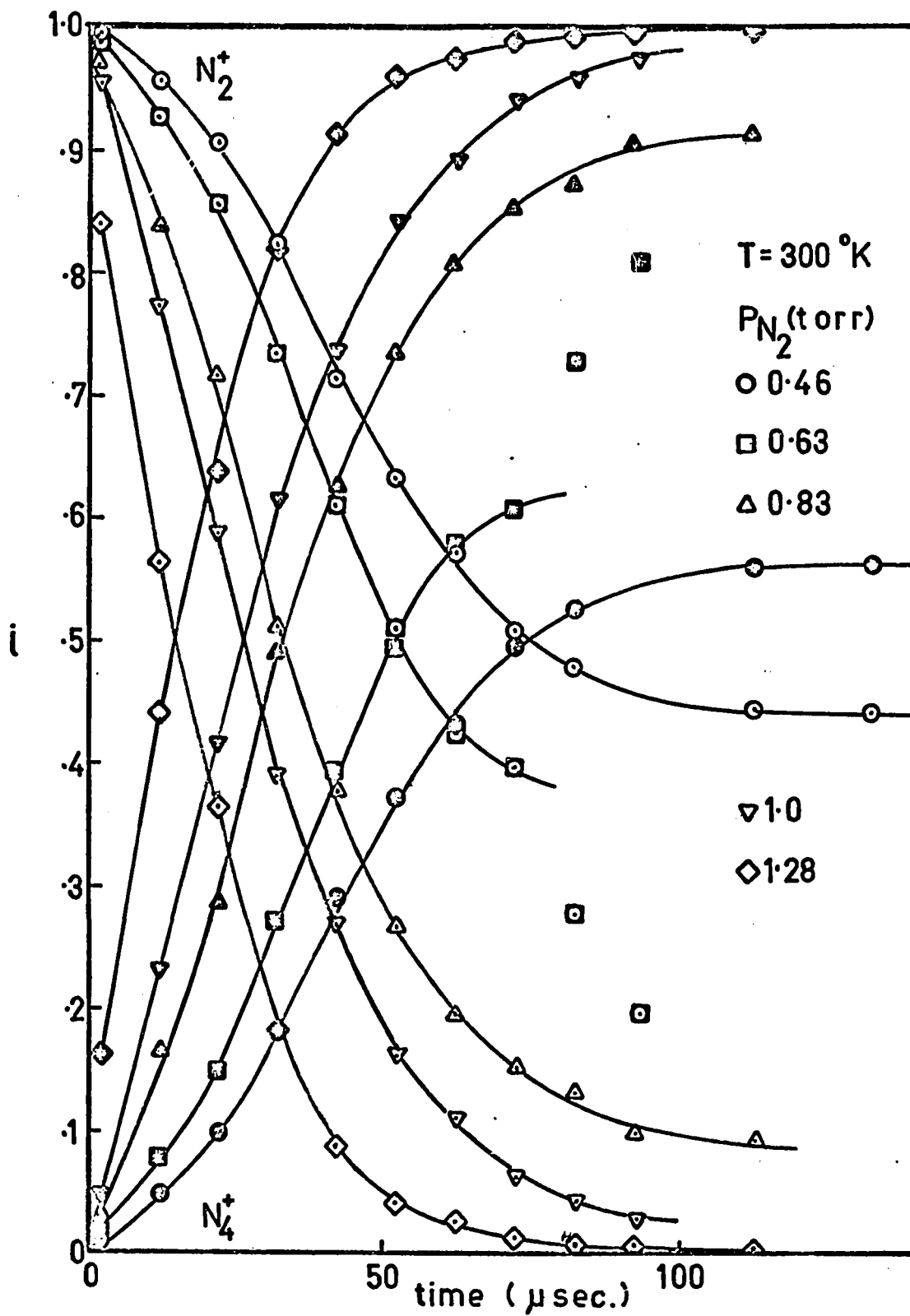


Figure 6:18 Normalized ion intensity curves of  $N_2^+$ ,  $N_4^+$  as fractions of  $i_{N_2^+} + i_{N_4^+}$ , nitrogen at  $300^\circ\text{K}$ , 0.38 to 1.0 torr.



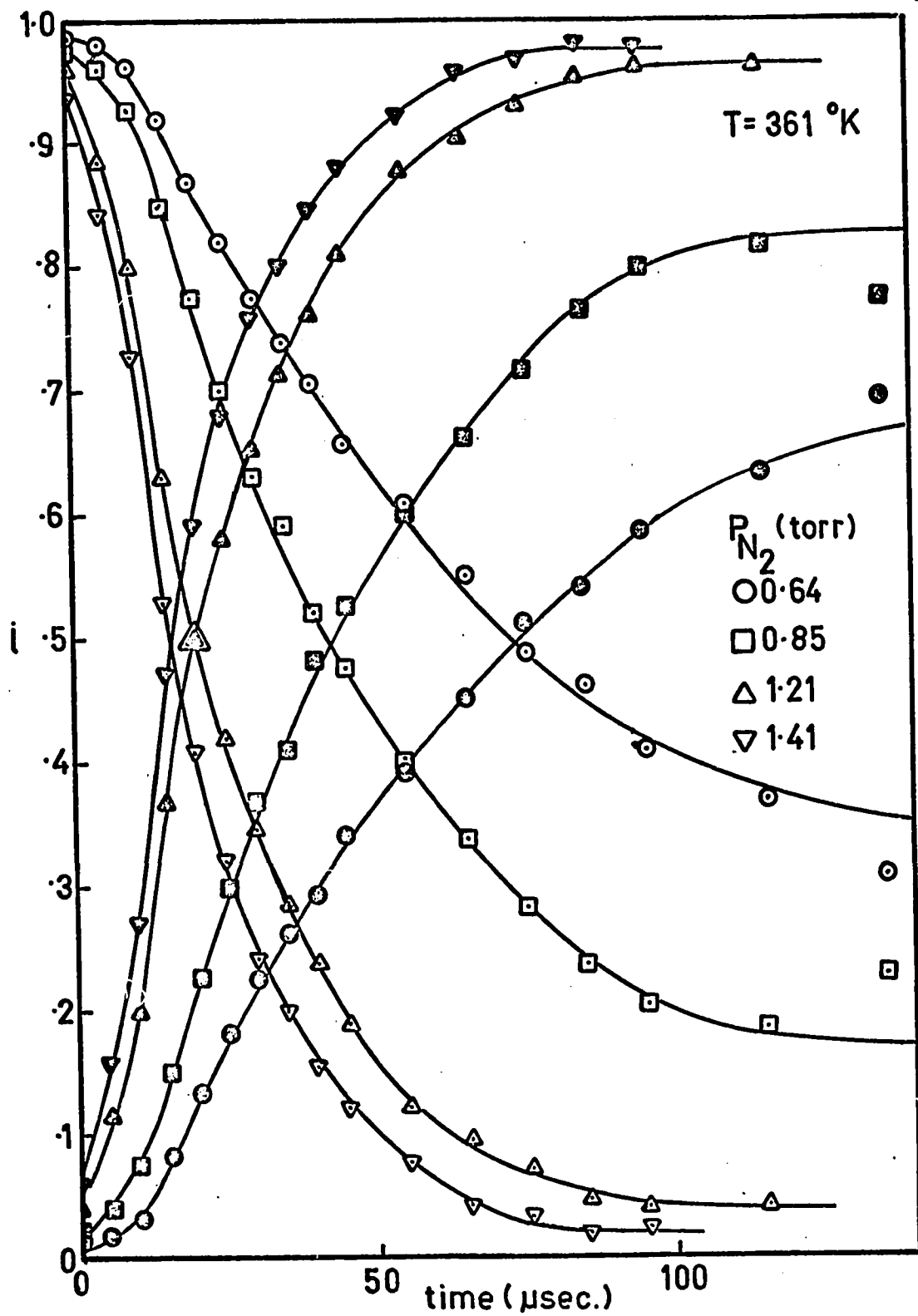


Figure 6:19 Normalized ion intensity curves of  $N_2^+$ ,  $N_4^+$  as fractions of  $i_{N_2^+} + i_{N_4^+}$ , nitrogen at 361°K, 0.64 to 1.41 torr.

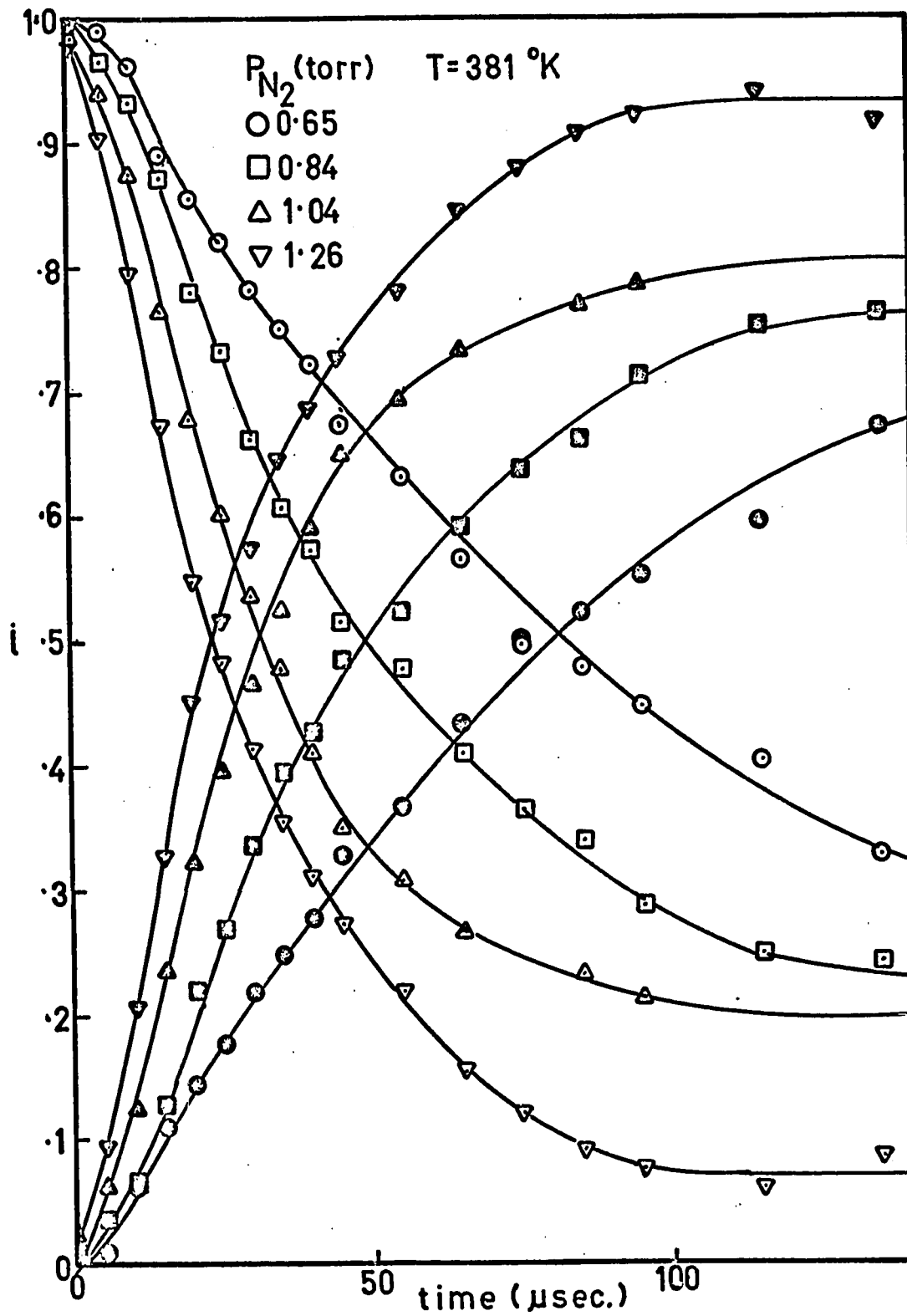


Figure 6:20 Normalized ion intensity curves of  $N_2^+$ ,  $N_4^+$  as fractions of  $i_{N_2^+} + i_{N_4^+}$ , nitrogen at  $381^\circ K$ , 0.65 to 1.26 torr.

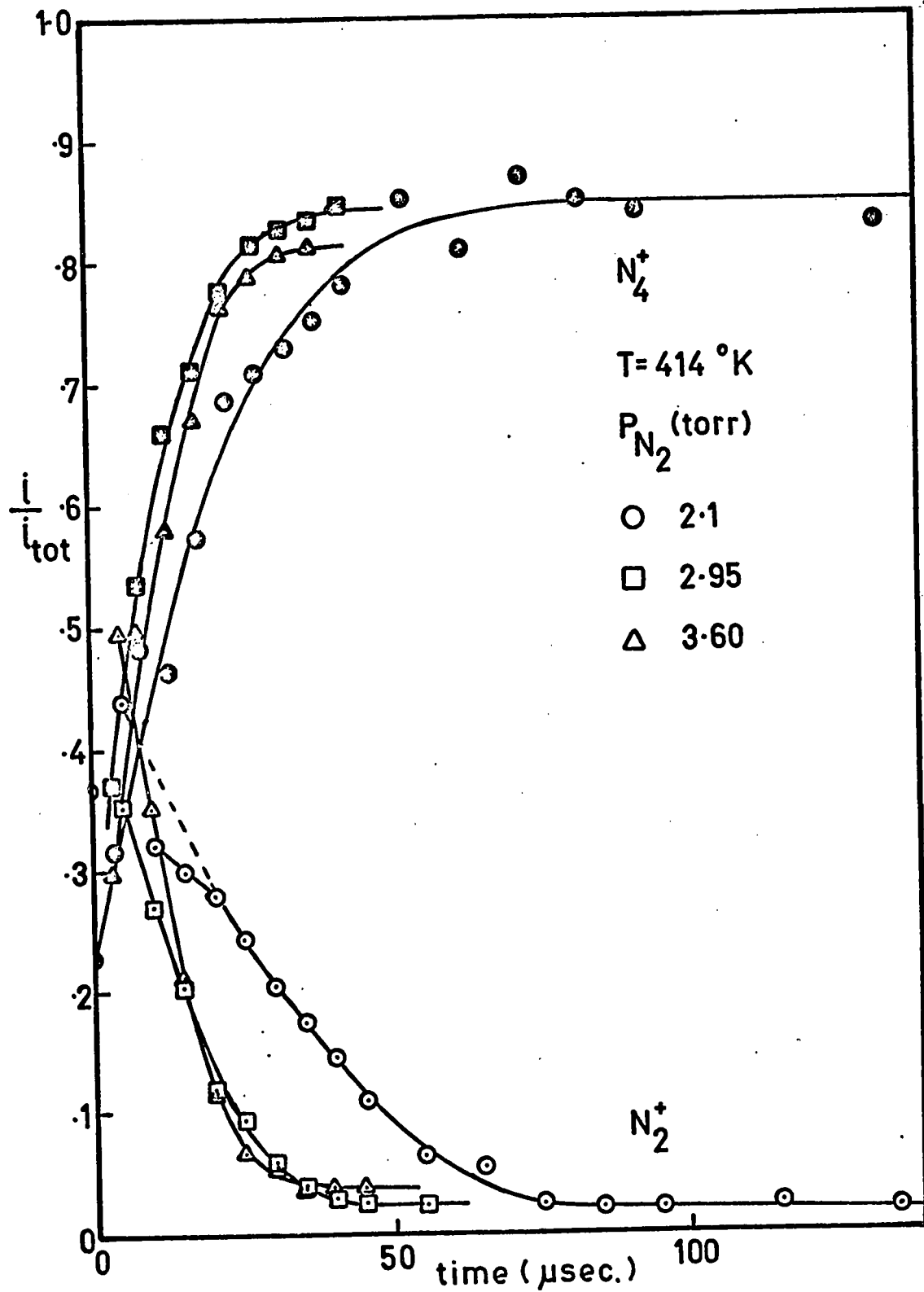


Figure 6:21 Normalized ion intensity curves of  $N_2^+$ ,  $N_4^+$  as fractions of Total Ionization, nitrogen at  $414^\circ K$ , 2.1 to 3.6 torr.

ion intensities were large the results were discarded. In figure (6:14) one can see that  $O_2^+$  ion appeared slowly with time. It is mainly responsible for the decrease of the normalized intensity of  $N_4^+$  at reaction times greater than 50 micro seconds. The oxygen concentration was very low, less than  $10^{-4}$  times that of nitrogen.

#### v Evaluation of the Rate Constants

The forward rate constant  $k_f$  of reaction (6:2a) was calculated from the maximum decrease of  $i_{N_2}^+$  from the normalized curves (both those which were expressed as fractions of  $(i_{N_2}^+ + i_{N_4}^+)$  and those as fractions of the total ionization). The equation used is similar to that used for oxygen (6:vii) = (6:xvii) where  $n=1$  for the second order reaction and  $n=2$  for

$$(6:xvii) \quad k_f = \frac{-2.303 \log (i_{N_2}^+ t_2 / i_{N_2}^+ t_1)}{(t_2 - t_1) [N_2]^n}$$

the third order reaction.

The order of the reaction was first determined from the data at 380 and 381°K, since at this temperature the data was measured over the widest pressure range. Figure (6:22) shows the values of  $k_f$  calculated for  $n=1$  and  $n=2$ . The values for the second order rate constants increased linearly with increasing pressure. The third order values were constant

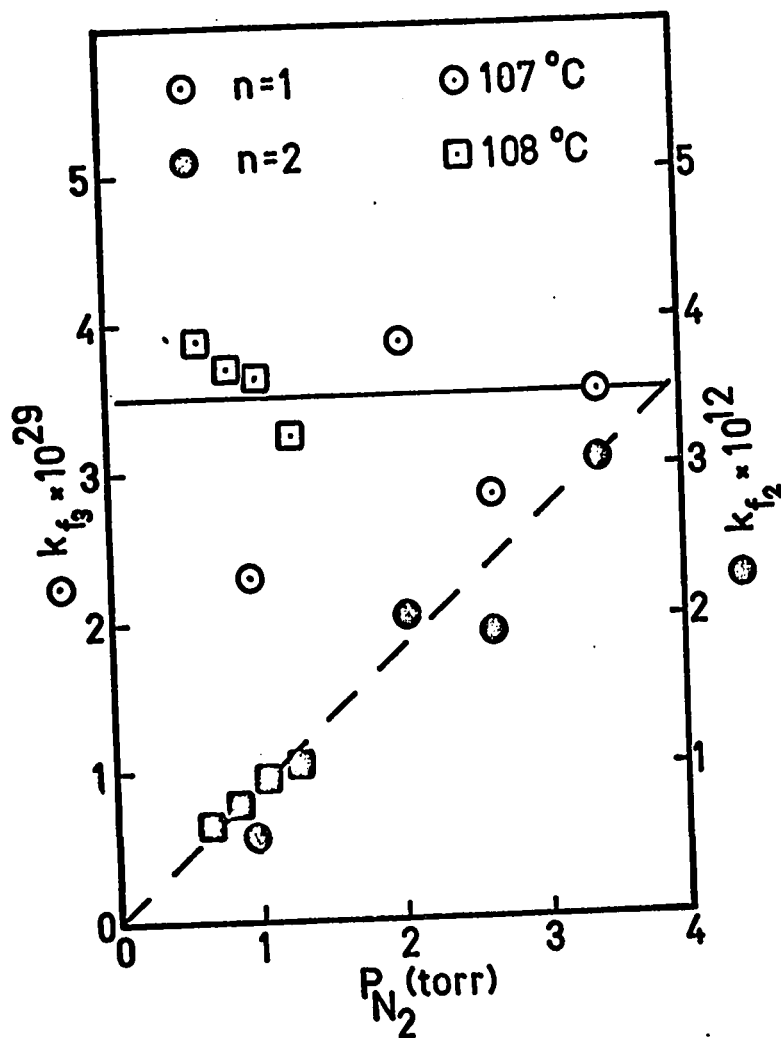
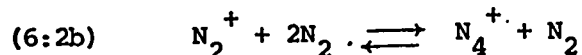


Figure 6:22 Third and second order rate constants  $k_f$ , for reaction (6:2), versus pressure. Results at 380 and 381°K.

within the experimental scatter and thus reaction (6:2a) is third order up to 3.5 torr of nitrogen and may be written as follows.



Third order rate constants were calculated for all other temperatures. An Arrhenius plot ( $\log k_f$  versus  $10^3/T$ ), figure (6:23), was prepared. The line is a least squares fit to the data it gives a value of  $k_f$  of  $8.3 \times 10^{-29} \text{ cc}^2/\text{molecule}^2 \text{ sec.}$  at 298°K and an apparent activation energy  $E_f = -2.3 \text{ kcal/mole.}$  These values are quite close to those of Warneck  $k_f = 8.5 \times 10^{-29}$  and of Knewstubb,  $k_f = 8.0 \times 10^{-29}$ ,  $E_f = -3.6 \text{ kcal/mole.}$

It can be seen from most of the figures that  $i_{\text{N}_2}^+$  decayed to very small values and that the effect of the reverse reaction was negligibly small. Thus the rate constants calculated by equation (6:xvii) should then be close to the true values. It was found that at low temperatures (300°K) the results at pressures less than 0.6 torr were unreliable. No ions were extracted at pressures less than 0.28 torr and consequently the results taken at pressures around 1 torr are the most reliable.

The technique of correcting for the reverse reaction was tried for a few of the results. A plot of  $\frac{2.303}{1+C} \log [i_{\text{N}_2}^+ (1+C) - C]$  versus  $t$ , (where  $C = i_{\text{N}_2}^+(\text{eq})/i_{\text{N}_4}^+(\text{eq})$ ), is shown in figure (6:24) for the data at 300°K from 0.63 to 1.28 torr. The corrected

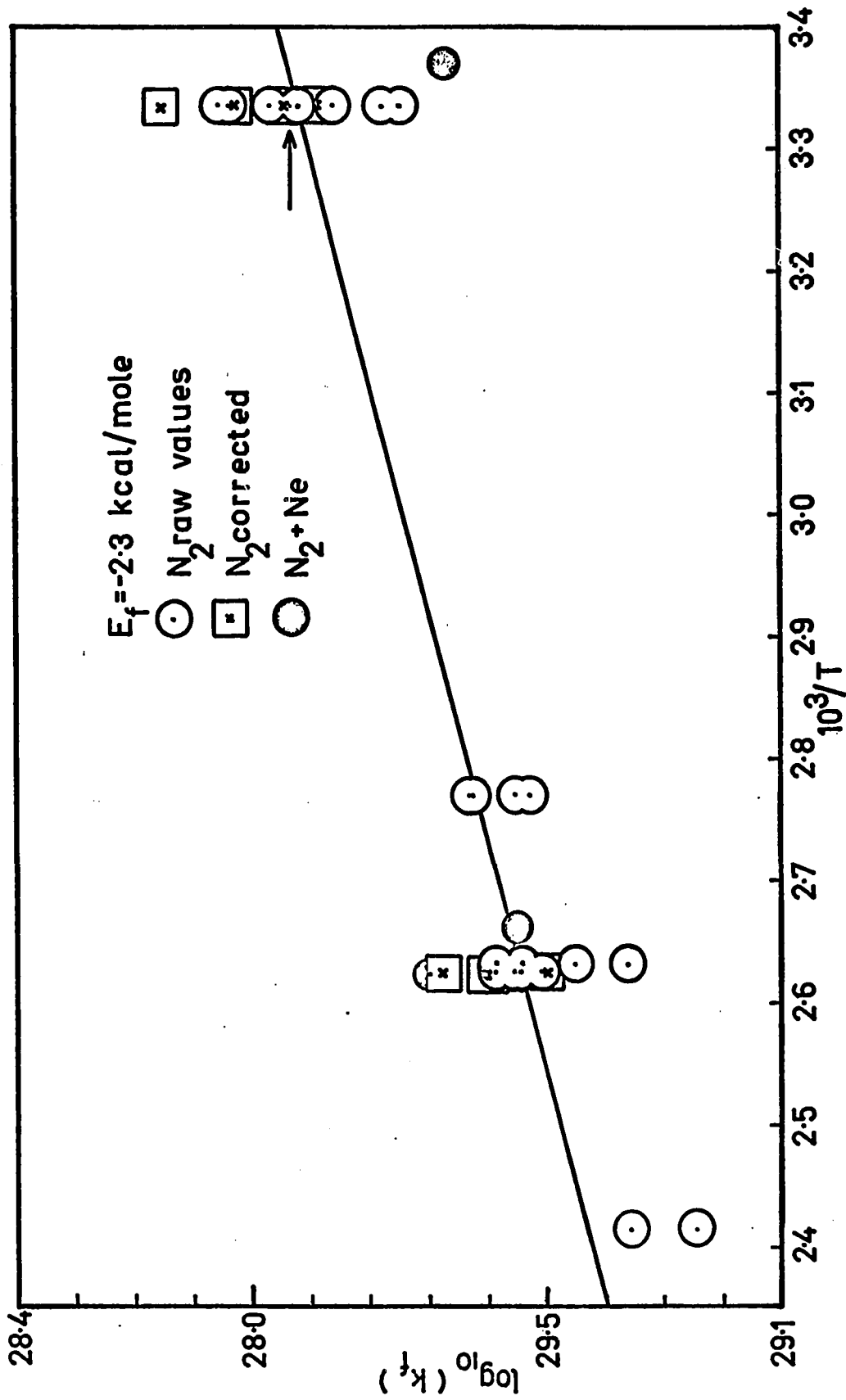


Figure 6:23 Arrhenius plot of  $k_f$  for reaction (6:2).

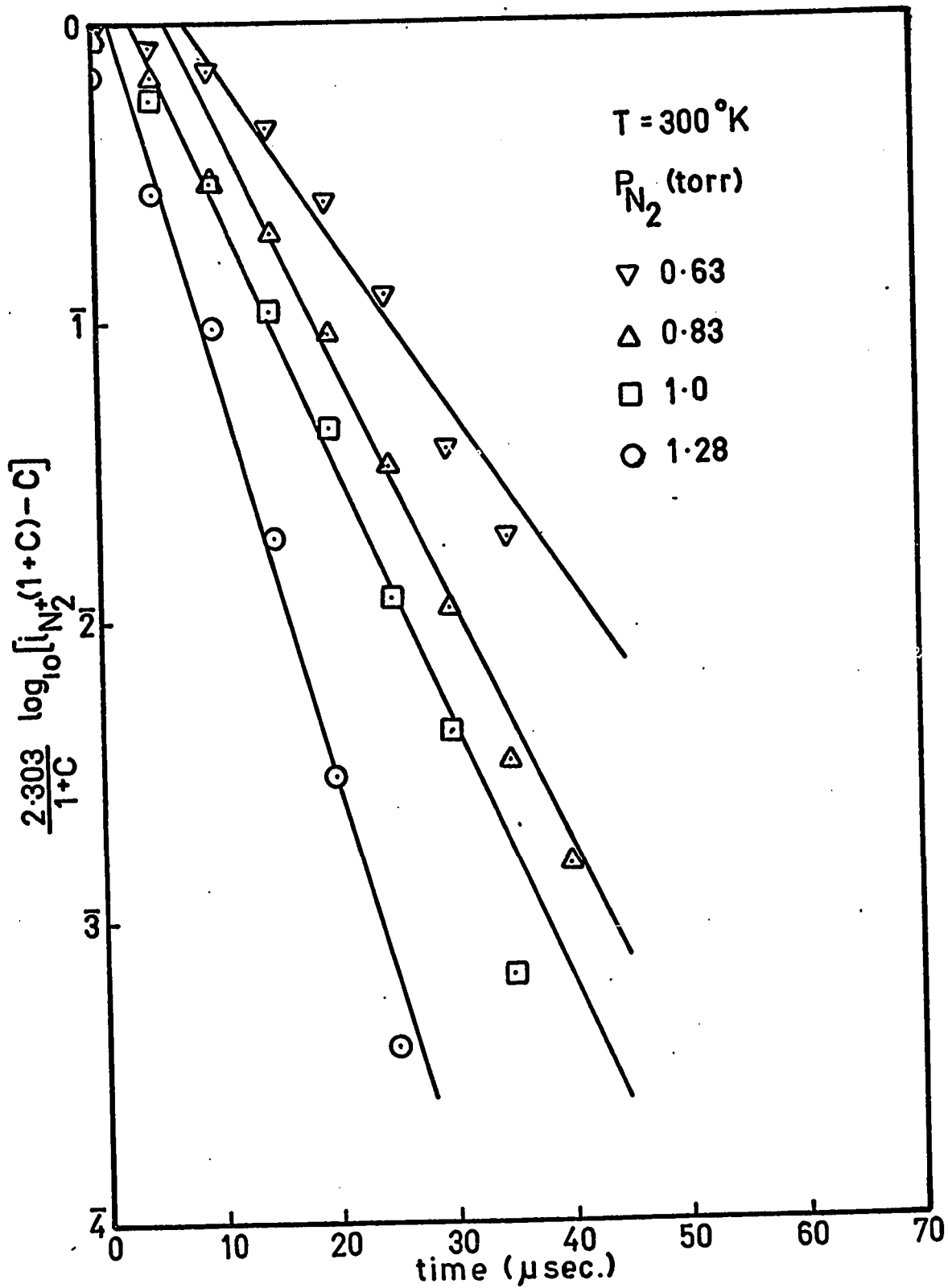


Figure 6:24 Plot from which "corrected" values of  $k_f$  were obtained at  $300^\circ\text{K}$ .



values for  $k_f$  are shown on figure (6:23) as squares. It can be seen that they gave essentially the same values for  $k_f$  at 298°K and do not change  $E_f$ . This type of plot for other data was unsuccessful as the ratio C was extremely small.

#### vi Evaluation of the Equilibrium Constant $K_p$

The measurements of  $K_p$ , from which a value of  $\Delta H$  might be determined, were unsuccessful. The values of  $K_p$  calculated from  $i_{N_2}^+$  and  $i_{N_4}^+$  at long reaction times from figures (6:14) to (6:21) were very dependent upon pressure and also not particularly reproducible. Under the low pressure conditions the total ion signal at reaction times greater than 100 micro seconds was small and this contributed to the lack of reproducibility. Attempts were made to obtain more sensitivity by setting the delay time  $t''$  to 100 micro seconds and the ion gate width  $\Delta t_1$  to 200 micro seconds. This method gave slightly better results. The  $K_p$  values calculated from the ion intensities at reaction times of 100 micro seconds were found to increase rapidly with pressure (figure 6:25). It appears that at low pressures the total ion signal decayed in a time (100 micro seconds) much shorter than that required for equilibrium to be established. Thus the small ion signals detected at low pressures would be those of ions not at equilibrium. Consequently one would expect the values of  $K_p$  to increase with pressure, since the

extent of reaction would increase. However at a certain point, when equilibrium would be established in less than 100 micro seconds the values of  $K_p$  would become constant. This behaviour was observed for the measurement of the oxygen reaction equilibrium constant (see figure 6:9). However it was not observed for the nitrogen reaction. This was probably due to the large value of  $K_p$ . If one takes Varney's extrapolated value of  $K_p$  of  $5 \times 10^5$  at  $300^\circ\text{K}$  one can calculate the ratio of  $i_{\text{N}_2}^+$  to  $i_{\text{N}_4}^+$  at a pressure of 1 torr from (6:xviii) as 0.00001 to .99999. Unfortunately

$$(6:xviii) \quad K_p = \frac{i_{\text{N}_4}^+}{i_{\text{N}_2}^+ P_{\text{N}_2}} = 10^5$$

the sensitivity of the mass spectrometer was not great enough to detect differences of this magnitude from the very small ion currents. The limit was perhaps 0.001 to 0.999 and thus the largest values of  $K_p$  measureable were  $10^3$ .

A calculation was carried out to see how the  $K_p$  calculated from ion intensities at 100 micro seconds would change with pressure, and at what pressure equilibrium would be established in less than 100 micro seconds. A theoretical  $K_p'$  was calculated by substituting the appropriate equations for  $i_{\text{N}_2}^+$  and  $i_{\text{N}_4}^+$  into (6:xviii). The resultant equation is (6:xix). The value for  $k_f$  was taken from the results figure (6:23)  $k_r$  was calculated from Varney's  $K_p$  ( $5 \times 10^5$  at  $300^\circ\text{K}$ ) and  $k_r$ . The value of  $K_p'$  was found

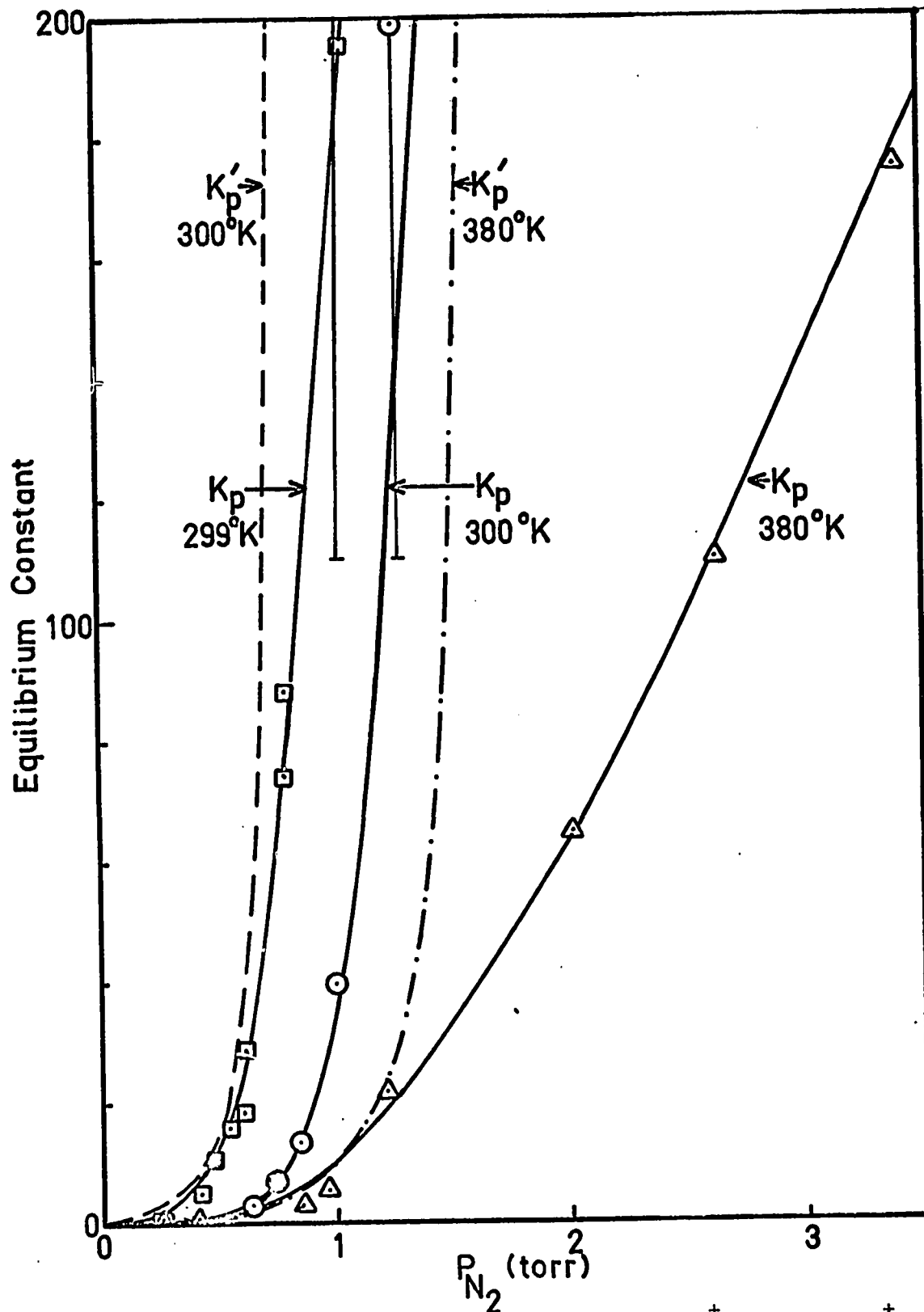


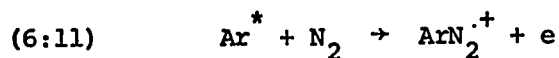
Figure 6:25 Variation of  $K_p$  of reaction (6:2)  $N_2^+ + N_2 \rightleftharpoons N_4^+$  versus pressure. Solid lines experimental. Dashed lines calculated from equation (6:xix).

$$(6:xix) \quad K_p' = \frac{k_f [N_2]^2 \left[ 1 - e^{-(k_r [N_2] + k_f [N_2]^2) t} \right]}{P_{N_2} \left[ k_r [N_2] + k_f [N_2]^2 e^{-(k_r [N_2] + k_f [N_2]^2) t} \right]}$$

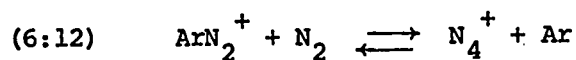
to increase rapidly up to pressures of 1.2 torr after which it remained constant at  $5 \times 10^5$ . Part of this curve is shown in figure (6:24). The calculation was repeated at 380°K with appropriate values of  $k_f$  and  $k_r$ . This is also shown. One can see that the theoretical values for  $K_p$  at any pressure are larger than the experimental values. This is most noticeable in the 380°K curves. One might assume that at the higher pressures, 3 to 4 torr, the reaction was close to equilibrium. That is, that the equilibrium constant at 380°K is larger than could be observed with the present instrument but perhaps smaller than the value obtained from an extrapolation of Varney's results (107).

An attempt was made to measure  $K_p$ , by having a low pressure of  $N_2$ , and a high temperature so that the ratio  $N_2^+ / N_4^+$  was within the range of the instrument detection (not less than 0.01), and yet have the total pressure high so that ions would be extracted efficiently by mass flow. Neon was added to increase the pressure. Neon was chosen since its ionization potential is greater than that of nitrogen ( $I_p Ne^+ = 21.56$  eV,  $I_p N_2^+ = 15.58$  eV). It was expected that  $N_2^+$  ions would be produced

by charge transfer and be essentially the only ions produced (as  $I_p N^+ = 24.3 \text{ eV} > I_p Ne^+$ ). Argon was not chosen even though  $Ar^+$  has an ionization potential slightly higher (15.8 eV) than  $N_2^+$ , as Knewstubb (109) had observed the ion  $ArN_2^+$  in mixtures of Argon and nitrogen at high pressures. Kaul and Fuchs (114) proposed this was formed by a Hornbeck-Molnar Process Reaction (6:11).



Munson *et al* (115) suggested that the following reaction (6:12) would also occur in  $N_2 - Ar$  mixtures.



It was felt that the presence of  $ArN_2^+$  would complicate the kinetics and hence neon was used.

Figures (6:26) and (6:27) show two typical runs of the  $N_2$ -Ne mixture. Apparently the  $Ne^+$  ion was unreactive towards  $N_2$  as one can see that its intensity changed only slightly. In retrospect, one could explain this by means of the Massey adiabatic hypothesis (80) (section 4:4); that the cross sections of charge exchange reactions are small for large differences in ionization energy (6 eV in this case). Figure (6:27) shows also that impurities such as  $O_2$  became the major ions at long reaction times, and thus obscured the results.

The new results for Kp showed no improvement. These are shown as filled-in points on figure (6:25). Thus it was impossible

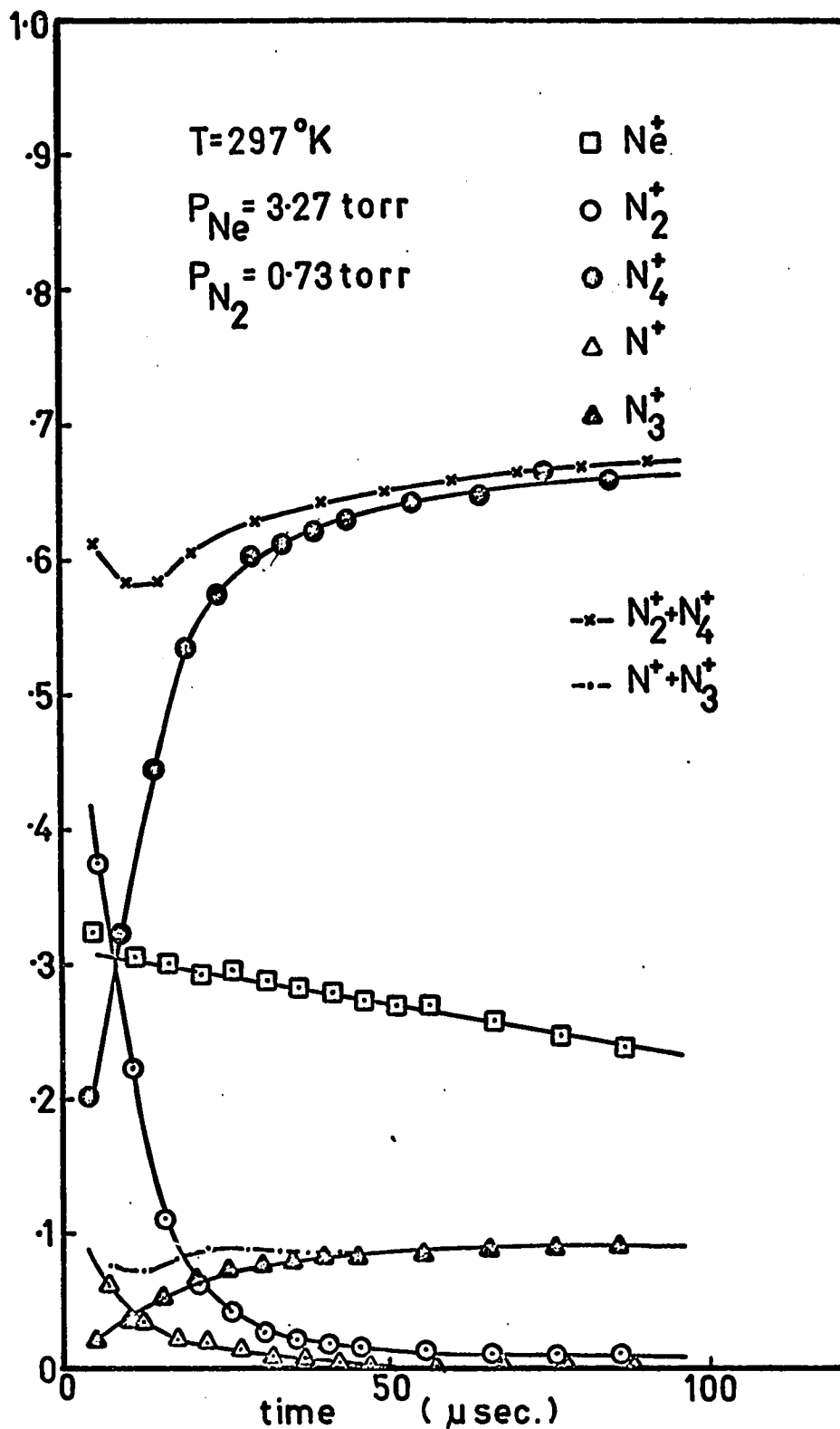


Figure 6:26 Normalized ion intensity curves for  $\text{N}_2$ -Ne mixture at  $297^\circ\text{K}$ , total pressure 4.0 torr, nitrogen 0.73 torr.

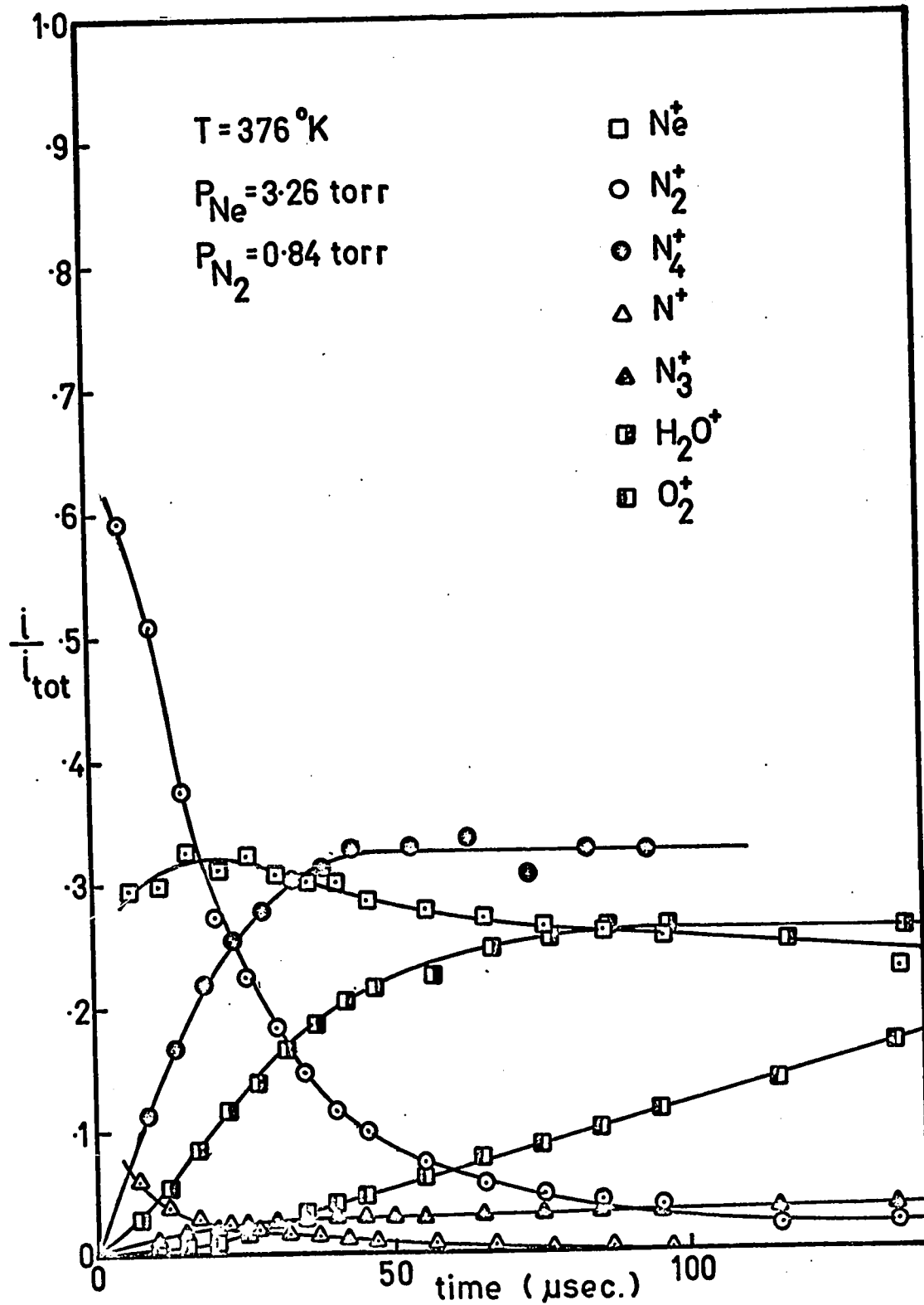
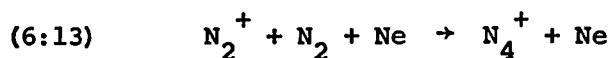


Figure 6:27 Normalized ion intensity curves for  $\text{N}_2$ -Ne mixture  
 at  $376^\circ\text{K}$ , total pressure 4.1 torr, nitrogen 0.84 torr.

to measure  $K_p$  under the pressure and temperature conditions available in this instrument. One concludes that the value for  $K_p$  must be almost as large as that calculated by Varney even though his ion temperature scale may be somewhat uncertain.

vii Further Evaluation of  $k_f$

The data of the  $N_2$ -Ne mixtures was used in an attempt to calculate rate constants for the forward reaction (6:13) in



which the third body was not  $N_2$ . The equation used was (6:xx).

$$(6:xx) \quad k_f = \frac{2.303 \log (i_{N_2^+}^{t_2} / i_{N_2^+}^{t_1})}{(t_2 - t_1) [N_2] [N_2 + Ne] \text{ where } [Ne] > [N_2]}$$

Three results are shown as solid points on figure (6:22). The results are of the same order of magnitude as those in pure nitrogen. The two points at  $10^3/T = 2.6$  were taken from runs in which the concentrations of impurity ions  $O_2^+$  and  $H_2O^+$  were large. Since the rate constant was based upon the decay of  $i_{N_2^+}$  the values are probably high since there would be a contribution from charge transfer from  $N_2^+$  to  $O_2$  and  $H_2O$ .

One might refer to the value  $5.9 \times 10^{-29} \text{ cc}^2/\text{molecule}^2 \text{ sec.}$  obtained at 297°K to propose that Ne is a less effective

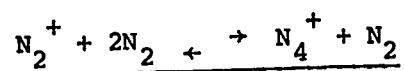


third body than is  $N_2$ . The value of  $1.9 \times 10^{-29}$  cc/molecule sec. measured by Fehsenfeld *et al* 280°K for the rate constant for reaction (6:7) in which He is the third body would tend to support this proposal.

A summary of the results is given in Table 6:3.

TABLE 6:3

Constants for the Attachment (6:2)



EXPERIMENTAL RESULTS

$$k_f = 8.3 \times 10^{-29} \text{ cc}^2/\text{molecule}^2 \text{ sec. at } 298^\circ\text{K}$$

$$= 3.0 \times 10^{-29} \text{ cc}^2/\text{molecule}^2 \text{ sec. at } 400^\circ\text{K}$$

$$E_f = -2.3 \text{ kcal/mole}$$

$$K_p \gg 10^2 \text{ (standard state 1 torr) at } 298^\circ\text{K}$$

$$> 10^2 \text{ (standard state 1 torr) at } 380^\circ\text{K}$$

PREVIOUS RESULTS

Warneck (101)

$$k_f = 8.5 \times 10^{-29} \text{ cc}^2/\text{molecule}^2 \text{ sec. at } 298^\circ\text{K}$$

Knewstubb (109)

$$k_f = 8.0 \times 10^{-29} \text{ cc}^2/\text{molecule}^2 \text{ sec. at } 298^\circ\text{K}$$

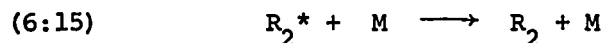
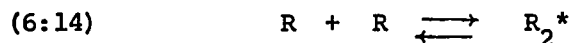
$$E_f \leq -3.6 \text{ kcal/mole.}$$

#### 6.4 Comparison of Oxygen and Nitrogen Reactions

##### i Theoretical Considerations of the Reaction Mechanism

##### The effect of Temperature and Bond Energy on $k_f$

The ion-molecule attachment reaction, which requires third body stabilization is very much like the recombination of two free radicals in the presence of a third body. The recombination has been discussed in terms of two mechanisms, the energy transfer mechanism and the radical-molecule complex mechanism (116). In both, the formation of an excited bimolecular complex occurs. In the energy transfer mechanism the complex is  $R_2^*$  formed from the two radicals and it is stabilized by collision with the third body  $M$ , as is shown in reactions (6:14) and (6:15). The radical-molecule complex mechanisms involves the formation of  $RM^*$  which reacts with a further radical to form  $R_2$  and  $M$ .

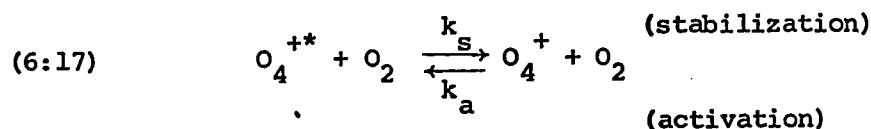
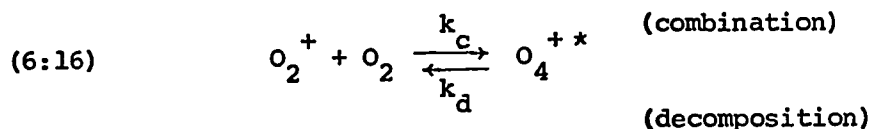


The two mechanisms were first proposed by E. Rabinowitch in 1937 (117) and have been investigated by many other workers (116,118).

When the third body is the same species as the reactant, the two major mechanisms become the same, and may be treated by the theory of the energy transfer mechanism.

A mechanism for the ionic attachment reaction may be

written as shown in the reaction sequence (6:16) and (6:17).



The sequence for oxygen is shown. The same reactions apply for nitrogen.

One may find equations for the rate constants by applying the steady state assumption that the concentration of  $\text{O}_4^{+*}$  is constant i.e.  $d[\text{O}_4^{+*}]/dt = 0$ . The concentration of  $\text{O}_4^{+*}$  is then given by equation (6:xxi).

$$(6:xxi) \quad [\text{O}_4^{+*}] = \frac{k_c [\text{O}_2^+] [\text{O}_2] + k_a [\text{O}_4^+] [\text{O}_2]}{k_d + k_s [\text{O}_2]}$$

The rate  $R_f$  of the forward reaction is given by the loss of  $\text{O}_4^{+*}$  to form  $\text{O}_4^+$ .

$$(6:xxii) \quad R_f = k_s [\text{O}_4^{+*}] [\text{O}_2]$$

$$(6:xxiii) \quad R_f = \frac{k_s k_c [\text{O}_2^+] [\text{O}_2]^2 + k_s k_a [\text{O}_4^+] [\text{O}_2]^2}{k_d + k_s [\text{O}_2]}$$

Similarly the rate  $R_r$  of the reverse reaction is the rate of decrease of  $\text{O}_4^{+*}$  to form  $\text{O}_2^+$ .

$$(6:xxiv) \quad R_r = k_d [O_4^{+*}]$$

$$(6:xxviii) \quad R_r = \frac{k_d k_c [O_2^+] [O_2] + k_d k_a [O_4^+] [O_2]}{k_d + k_s [O_2]}$$

When  $[O_4^+] = 0$ ,  $R_f$  is given by (6:xxvi) and when  $[O_2^+] = 0$ ,  $R_r$  is given by (6:xxvii).

$$(6:xxvi) \quad R_f = \frac{k_c k_s [O_2^+] [O_2]^2}{k_d + k_s [O_2]}$$

$$(6:xxvii) \quad R_r = \frac{k_a k_d [O_4^+] [O_2]}{k_d + k_s [O_2]}$$

Now if  $k_d \gg k_s [O_2]$ , the low pressure situation, the concentration of  $O_4^{+*}$  is controlled by  $k_c$  and  $k_d$ . The forward reaction is third order with rate given by (6:xxviii) and the reverse reaction is second order with rate given by (6:xxix).

$$(6:xxviii) \quad R_f = \frac{k_c k_s}{k_d} [O_2^+] [O_2]^2; \quad k_f = \frac{k_c k_s}{k_d}$$

$$(6:xxix) \quad R_r = k_a [O_4^+] [O_2]; \quad k_r = k_a$$

Conversely, if the concentration of  $O_4^{+*}$  is controlled by  $k_s$  and  $k_a$ , i.e.  $k_d \ll k_s [O_2]$ , the forward reaction is second order and the reverse reaction first order with rates given by (6:xxx) and (6:xxxi).

$$(6:xxx) \quad R_f = k_c [O_2^+] [O_2] ; \quad k_f = k_c$$

$$(6:xxxi) \quad R_f = \frac{k_a k_d}{k_s} [O_4^+] ; \quad k_r = \frac{k_a k_d}{k_s}$$

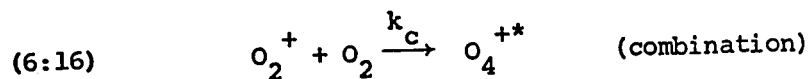
Under the conditions of pressure and temperature used in the present study, the reactions displayed third order kinetics and thus  $k_d \gg k_s [O_2]$ . The rate constants are given by (6:xxviii) and (6:xxix).

$$(6:xxviii) \quad k_f = \frac{k_c k_s}{k_d}$$

$$(6:xxix) \quad k_r = k_a$$

Since theories for the effect of temperature upon  $k_f$  and  $k_r$  have not previously been developed, it might be possible to get a qualitative prediction by taking simple equations for  $k_c$ ,  $k_s$ ,  $k_d$  and  $k_a$ .

The rate constant  $k_c$  is that of the combination process of reaction (6:16).

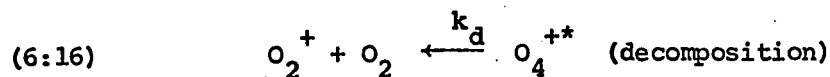


Since this involves the collision of an ion and a molecule to form an excited complex one might use the Gioumoussis-Stevenson equation (1:vi) to predict values of  $k_c$ .

$$(1:vi) \quad k_c = 2\pi e \sqrt{\frac{\alpha}{\mu}}$$

This equation does not predict any effect of temperature upon  $k_c$ .

The rate constant  $k_d$  for the decomposition of  $O_4^{+*}$  in reaction (6:16) is similar to that of a general unimolecular



reaction, and one might approximate it by application of the Rice-Ramsperger-Kassel model. The simplest R-R-K equation is given by (6:xxxii). The R-R-K model assumes that the molecule

$$(6:xxxii) \quad k_d = Z_d \left( \frac{E - E^*}{E} \right)^{r-1}$$

contains  $r$  coupled oscillators all of the same frequency. The probability that the total energy  $E$  may be transferred into one of the oscillators with a critical energy  $E^*$  is given by the term  $\left( \frac{E - E^*}{E} \right)^{r-1}$ . The factor  $Z_d$  is a proportionality constant related to the frequency. The critical energy  $E^*$  may be approximated to the bond energy  $D(O_2^+ - O_2)$  and the total energy, to the bond energy  $D$  plus some contribution from the thermal energies of the reactant species.  $E$  is given by (6:xxxiii).

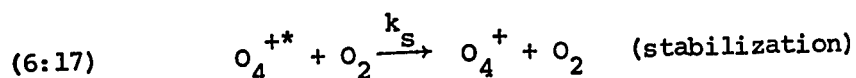
$$(6:xxxiii) \quad E = D + nRT$$

It is hard to assign a value to the thermal contribution  $nRT$ , but since the vibrational levels of oxygen and nitrogen molecules and ions have low populations at the temperatures used here (300 to 400°K) we might consider only the translational and rotational levels (i.e.  $nRT = \frac{3}{2} RT + \frac{3}{2} RT$ ). The R-R-K equation may be rewritten for  $k_d$  as (6:xxxiv).

$$(6:xxxiv) \quad k_d = Z_d \left( \frac{nRT}{D + nRT} \right)^{r-1}$$

Since  $D > nRT$ , we may neglect the thermal term in the denominator. Equation (6:xxxiv) indicates that  $k_d$  would increase with increasing temperature and decrease with increasing bond energy  $D$ . Increasing the number of oscillators  $r$  which could contribute energy would also decrease  $k_d$  since  $(nRT/D) < 1$ .

The rate constant  $k_s$  is for the stabilization step of (6:17).



Deactivation of  $O_4^{+*}$  will only take place if the kinetic energy of  $O_4^{+*}$  and  $O_2$  is less than a certain critical energy  $E_c$ . Husain and Pritchard (119) gave an equation (6:xxxv) for such a reaction. They used it for the recombination of iodine atoms. The energy  $E_c$

$$(6:xxxv) \quad k_s = pZ_s (1 - e^{-E_c/RT})$$

was small, less than 1 kcal/mole. One might apply a similar value for reaction (6:17).  $Z_s$  is the collision frequency and  $p$  the efficiency of each collision for removal of energy. The effect of an increase of temperature would be to decrease  $k_s$ . Since  $E_c$  is small, much less than the bond energy  $D$  one might not expect it to vary with  $D$ .

All these approximate equations may be combined so that  $k_f$  is defined by equation (6:xxxvi).

$$(6:xxxvi) \quad k_f = \frac{k_c p Z_s (1 - e^{-E_c/RT})}{Z_d \left( \frac{nRT}{D} \right)^{r-1}}$$

The effect of temperature change would be as follows. Since  $k_c$  is independent of temperature,  $k_s$  decreases and  $k_d$  increases,  $k_f$  must decrease with increasing temperature. This then agrees qualitatively with the observed data, as the Arrhenius plot gave an apparent negative activation energy for  $k_f$ .

One may compare the values for  $k_f$  of the oxygen reaction (6:1b) to that of the nitrogen reaction (6:2b) by comparing the bond energies of the complex ions  $O_4^+$  and  $N_4^+$ . ( $D(O_2^+-O_2) = 10$  kcal/mole  $D(N_2^+-N_2) \sim 14$  kcal/mole. As the bond energy  $D$  is increased, equation (6:xxxvi) predicts that  $k_f$  would increase, since  $k_d$  would decrease by a factor  $(D_{O_2}/D_{N_2})^{r-1}$ .

Equation (6:xxxvi.) may be used to qualitatively predict how the rate constant  $k_f$  would change as the third body was changed.  $k_c$  and  $k_d$  are independent of the third body.  $k_s$  would be affected by the collision efficiency factor  $p$  (equation 6:xxxv). One might expect that if the third body were an atom such as Ne or He, instead of a molecule, that  $p$  would be smaller. This qualitatively agrees with the findings for the nitrogen reaction. At 300°K  $k_f$  for reaction (6:2b) from the present results was about  $8.3 \times 10^{-29} \text{ cc}^2/\text{molecule}^2 \text{ sec}$ . When the

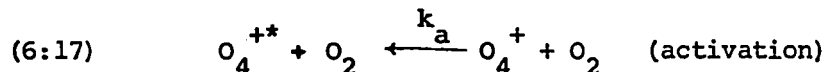


third body was neon (reaction 6:13)  $k_f$  at 297°K was about  $5.9 \times 10^{-29} \text{ cc}^2/\text{molecule}^2 \text{ sec}$ . Fehsenfeld *et al* measured a value for  $k_f$  of  $1.9 \times 10^{-29} \text{ cc}^2/\text{molecule}^2 \text{ sec}$ . at 280°K for the reaction with He as the third body. One might expect the efficiency to decrease with decreasing complexity and size  $\text{N}_2 > \text{Ne} > \text{He}$ .

Equations (6:xxxii) and (6:xxxv) may qualitatively show when the overall attachment reaction such as (6:1) or (6:2) displays third or second kinetic order. The case for third order was that  $k_d \gg k_s [\text{O}_2]$ . This would occur at low pressures, and at high temperatures for complex ions with a small bond energy. Conversely the second order kinetic situation  $k_d \gg k_s [\text{O}_2]$  would occur at high pressures and low temperatures and when the complex bond energy was large.

ii The Effect of Temperature and Bond Energy  
on  $k_x$  at Low Pressures

When the attachment reaction displays third order kinetics the rate constant  $k_x$  is given by  $k_a$ , the constant for the activation of  $\text{O}_4^+$  by collision. This activation is similar to the initial step



of a unimolecular decomposition reaction and the same equations may be used.

The most appropriate equation is the energy transfer equation developed independently by Hinshelwood and Lewis. It is discussed by Ritchie (120) and by Fowler and Guggenheim (121). It is derived from the simple collision theory. The simple collision theory equation (6:xxxvii) assumes that the molecules

$$(6:xxxvii) \quad k = pZe^{-E_0/RT}$$

are hard rigid spheres, and that upon collision (along the line of centres), translational energy is transformed into internal energy. The probability of gaining an energy greater than  $E_0$  is given by the Boltzmann factor  $e^{-E_0/RT}$ . For a complex molecule the approximation of rigid spheres is not satisfactory and the contribution of vibrational and rotational energy must be included. The bond which requires the energy  $E_0$  to break, gains this energy, not only by transformation of translational kinetic energy into internal energy, but also by transfer of energy from the vibrational and rotational modes. The probability of  $E_0$  being available is thus larger than that given by the Boltzmann factor. A term  $\frac{1}{s!} \left(\frac{E_0}{RT}\right)^s$  is added to account for the increase in probability. The integer  $s$  depends upon the number of square terms from which energy is acquired. This number is given by  $(2s+2)$ . The number of square terms for the degrees of freedom are, one term  $(\frac{1}{2}I\omega^2)$  for each rotational degree and two terms  $(\frac{1}{2}mv^2)$  kinetic

energy, and  $\frac{1}{2}kx^2$  potential energy) for each vibrational degree. Since the vibrational degrees of freedom will generally provide the largest number of square terms one might approximate  $s$  as the number of vibrations. The energy transfer equation for  $k_a$  is thus given by (6:xxxviii) in which  $Z$  is again the collision

$$(6:xxxviii) \quad k_a = \frac{Z}{s!} \left( \frac{E_0}{RT} \right)^s e^{-E_0/RT}$$

number and  $E_0$  the activation energy.

The energy transfer equation was used successfully by Palmer and Hornig (122) to describe the dissociation of  $Br_2$  into Br atoms in the presence of either bromine or argon under low pressure conditions. The log of the rate constant plotted versus  $1/T$  fitted over a range of  $10^{27}$ .

The value of  $k_r$  measured for the oxygen reaction may be used to determine  $s$ .  $Z$  is taken as the Gioumousis-Stevenson collision frequency which is of the order  $10^{-9}$  cc/molecule sec. If we use  $T=300^\circ K$ ,  $E_0 = 10$  kcals/mole and  $s = 4$ ,  $k_a$  is  $1.96 \times 10^{-13}$  cc/molecule sec. This corresponds very well with the present experimental value  $k_r = 2.44 \times 10^{-13}$  cc/molecule sec. At  $400^\circ K$   $k_a = 3.80 \times 10^{-12}$  cc/molecule sec. compared to the experimental  $k_r = 6.54 \times 10^{-12}$  cc/molecule sec.

If it is assumed that  $O_4^+$  and  $N_4^+$  have the same number of vibrations contributing energy and thus the same value for  $s$ ,  $k_a$  may be calculated for nitrogen. The bond dissociation

energy  $E$  may be taken as 14 kcal/mole as the value of 11.5 kcal/mole from Varney (107) had a large error, and the value of 13.8 from Asundi *et al* (103) should be a minimum value. At 300°K with  $s = 4$  equation (6:xxxviii) gives a value of  $k_a = 9.06 \times 10^{-15}$  cc/molecule sec. and at 400°K  $k_a = 9.8 \times 10^{-14}$  cc/molecule sec.

A value for  $s$  may be obtained from a method described by Porter (118). He first found an equation for  $k_f$  in the following manner.  $k_f$  may be defined by equation (6:xxxix) which is (6:xi)

$$(6:xxxix) \quad k_f = k_r K$$

rewritten.  $k_r$  is given by equation (6:xxxviii) for  $k_a$ . The equilibrium constant  $K$  is given by (6:x1). The energy required

$$(6:x1) \quad K = e^{(-\Delta H/RT)} \cdot e^{\Delta S/R}$$

by  $O_4^{++}$  (or  $N_4^{++}$ ) to dissociate  $E_0$  is the bond energy  $D(O_2^+ - O_2)$  which is  $-\Delta H$ .  $k_f$  is then given by (6:xli) as the activation

$$(6:xli) \quad k_f = \frac{Z}{s!} \left( \frac{E_0}{RT} \right)^s e^{\Delta S/R}$$

energy exponentials cancel. Porter assumed that the change of  $\Delta S$  with temperature was small so that the effect of  $e^{\Delta S/R}$  was small compared to  $(1/T)^s$ .  $Z$  and  $e^{\Delta S/R}$  are combined into a new constant  $C$ . Equation (6:xli) may then be rewritten.

$$(6:xli) \quad k_f = \frac{C}{s!} \left( \frac{E_0}{RT} \right)^s$$

Porter stated that an Arrhenius plot ( $\log k_f$  versus  $1/T$ ) of equation (6:xliv) gave an apparent negative activation energy with the form given by equation (6:xlvi).

$$(6:xlvi) \quad E_{app} = -sRT$$

The apparent negative activation energies obtained from the two Arrhenius plots, figures (6:13) and (6:22), were for oxygen  $E_f = -2.0$  kcals/mole and for nitrogen  $E_f = -2.3$  kcals/mole. If these values are substituted into (6:xlvi), with  $T = 300^\circ\text{K}$  the value of  $s$  for oxygen is 3.4 and for nitrogen 3.9. These values agree with the value of 4 used for the calculation of  $k_a$  by means of equation (6:xxxviii).

The number of vibrational modes of four centre ions are given by  $3N-5 = 7$  for a non-linear ion or  $3N-6 = 6$  for a linear ion.  $s$  should be less than either of these numbers as it is the effective number of vibrational modes contributing energy to the dissociation and not all will contribute with total efficiency.

The statement that equation (6:xlvi) gives values of  $k_f$  which plot versus  $1/T$  to give a negative activation energy was checked. At  $300^\circ\text{K}$ ,  $k_f = 2.9 \times 10^{-30} \text{ cc}^2/\text{molecule}^2 \text{ sec}$ . and  $E = -\Delta H = 10$  kcals/mole. If  $s = 3$ ,  $C = 3.76 \times 10^{-30}$ . At  $400^\circ\text{K}$  a new value of  $k_f$  was calculated  $1.22 \times 10^{-30} \text{ cc}^2/\text{molecule}^2 \text{ sec}$ . From an extrapolation of figure (6:13)  $k_f = 1.27 \times 10^{-30} \text{ cc}^2/\text{molecule}^2 \text{ sec}$ . The calculation was repeated for  $s = 4$ . The agreement

with the experimental results was not as good. This shows that  $s$  can be approximated from the value of the apparent negative activation energy.

iii Comparison of the Equilibrium Constants  $K_p$  for Oxygen and Nitrogen

Since the equilibrium constant for the nitrogen reaction (6:2) could not be measured experimentally, it would be instructive to evaluate a theoretical value by means of the energy transfer theory.  $k_a$  can be calculated from equation (6:xxxviii) and used with the experimental value for  $k_f$  so that  $K_p$  may be calculated.

Since the nitrogen reaction came closest to reaching equilibrium in the 380°K runs 400°K will be chosen for convenience of calculation. First the theoretical equilibrium constant for oxygen was calculated at 400°K with  $s = 4$  and  $E_o = 10$  kcals/mole and thus  $k_a = 3.80 \times 10^{-12}$  cc/molecule sec. The experimental values were  $k_r = 6.54 \times 10^{-12}$  cc/molecule sec. and  $k_f = 1.27 \times 10^{-30}$  cc<sup>2</sup>/molecule sec. Thus the theoretical value for  $K_p$  is given by (6:xliv) from (6:xiii).

$$(6:xliv) \quad K_p = \frac{k_f}{k_a} T \times 1.034 \times 10^{-19}$$

$K_p$  (theoretical) =  $8.0 \times 10^{-3}$  compared to  $K_p$  (experimental) =  $4.7 \times 10^{-3}$  and the difference is less than a factor of two.

This procedure may be repeated for nitrogen where  $T = 400^\circ\text{K}$   $s = 4$  and  $E = 14$  kcals/mole.  $k_a = 9.8 \times 10^{-15}$  cc/molecule sec.

If we use the experimental value  $k_f = 3.0 \times 10^{-29} \text{ cc}^2/\text{molecule sec.}$  the theoretical value of  $K_p = 7.4 \times 10^1$ . The significance of this value is seen by comparing  $K_{p_{N_2}}$  to  $K_{p_{O_2}}$ . The ratio  $K_{p_{N_2}}/K_{p_{O_2}}$  at 400°K is:

$$\frac{K_{p_{N_2}}}{K_{p_{O_2}}} = 9 \times 10^3 \quad (\text{Theoretical})$$

If we take the experimental value of  $K_{p_{N_2}}$  at 400°K to be  $> 10^2$ , and if the experimental  $K_{p_{O_2}} = 4.7 \times 10^{-3}$  the ratio is then:

$$\frac{K_{p_{N_2}}}{K_{p_{O_2}}} > 2 \times 10^4 \quad (\text{Experimental})$$

The ratio may also be obtained by an extrapolation of Varney's (107) results.

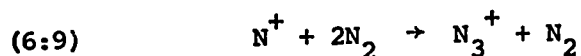
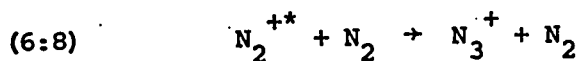
$$\frac{K_{p_{N_2}}}{K_{p_{O_2}}} > 7 \times 10^5 \quad (\text{Varney})$$

Since the predicted value of  $K_{p_{N_2}}$  using the experimental  $k_f$  and the theoretical  $k_a$  calculated from the bond energy by means of the energy transfer theory equation (7:vii) is smaller than either of the experimental values (even though they may be only approximate), the greater stability of  $N_4^+$  compared to  $O_4^+$  must be due not only to a larger bond energy but also to a more favourable entropy.

## 6:5 The Attachment $N^+ + N_2 \rightarrow N_3^+$

### i Previous Work

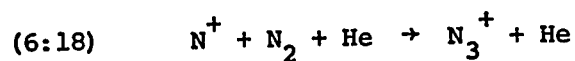
It was stated in section (6:3:iii) that  $N_3^+$  is produced by two reactions (6:8) and (6:9). The first is important at low pressures and the second at high pressures. The formation of  $N_3^+$  was studied at pressures up to 0.2 torr by Saporoschenko(110).



who observed that the reaction was second order and that the appearance potential for  $N_3^+$  was 22.1 eV which corresponded to the excited state  $N_2^+ \cdot ({}^4\Sigma_u^-)$ . Thus  $N_3^+$  was formed by reaction (6:8). This mechanism was supported by observations of Cermak and Herman(123), Keller *et al* (102) and by Munson *et al* (115).

Dreeskamp(124) observed  $N_3^+$  at higher pressures (0.8 torr) and ascribed its source to reaction (6:9). This was also reported by Luhr(125). Knewstubb and Tickner(126) studied glow discharges in nitrogen at a pressure of 0.4 torr. They also concluded that  $N_3^+$  resulted from the third order reaction (6:9). McKnight *et al* (104) recently studied the mobilities of nitrogen ions in  $N_2$  at pressures up to 0.9 torr and observed that  $N^+$  and  $N_3^+$  had very similar mobilities. They calculated a rate constant for the third body reaction (6:9) of  $3 \times 10^{-29} \text{ cc}^2/\text{molecule}^2 \text{ sec.}$  for conditions of low drift velocity. More recently Fehsenfeld *et al* (113) reported reaction (6:18) in which the third body is helium.

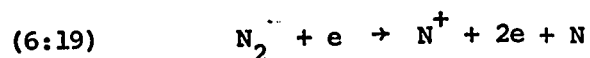




### ii Purpose of This Study

The reaction conditions in the present experiment were similar to those used earlier by Dreeskamp, Luhr and Knewstubb and Tickner, who showed that  $\text{N}_3^+$  was formed from  $\text{N}^+$  by the third order reaction (6:9). It was shown earlier (section 6:3:iv) that the ions  $\text{N}^+$  and  $\text{N}_3^+$  reacted independently of  $\text{N}_2^+$  and  $\text{N}_4^+$ .

$\text{N}^+$  is formed from  $\text{N}_2$  by reaction (6:19) with an appearance



potential of 24.2 eV. The intensity of  $\text{N}^+$  could be decreased by reaction with  $\text{N}_2$  to form  $\text{N}_3^+$ , or by charge exchange reactions with impurities. The rate of appearance of impurity ions was too slow to account for the rapid rate of disappearance of  $\text{N}^+$ . The rate of formation of  $\text{N}_3^+$  agreed quite well and thus it appeared that  $\text{N}^+$  reacted only to form  $\text{N}_3^+$ . The rate constant for the formation of  $\text{N}_3^+$  was measured so that it could be compared to that of  $\text{N}_4^+$  (reaction 6:1b).

### iii Results

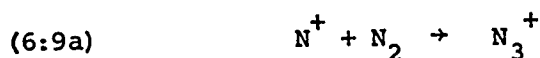
The time dependence of the ion intensities of  $\text{N}^+$  and  $\text{N}_3^+$  had been measured with those of  $\text{N}_2^+$  and  $\text{N}_4^+$ . The intensities of  $\text{N}^+$  and  $\text{N}_3^+$  were normalized in two ways. Some were plotted as fractions of the total ionization. The plots for pure

nitrogen at pressures from 0.96 to 3.60 torr at 380°K are shown in figures (6:14) to (6:17). Two plots for mixtures of nitrogen and neon at total pressures of 4.1 torr are shown in figures (6:26) and (6:27). The temperatures were 297°K and 376°K respectively. One can see that in these figures the sum ( $i_{N^+} + i_{N_3^+}$ ) remained reasonably constant. For some runs only  $N^+$  and  $N_3^+$  intensities were measured. They were normalized as fractions of ( $i_{N^+} + i_{N_3^+}$ ). These plots are shown in figures (6:28) to (6:30).

For most of the data the rate constant for the forward reaction was calculated from the decay of  $i_{N^+}$  by means of equation (6:xlv) where  $n=1$  for a second order reaction and

$$(6:xlv) \quad k_f = \frac{2.303 \log_{10} (i_{N^+} / i_{N^+})}{(t_2 - t_1) [N_2]^n}$$

$n=2$  for a third order reaction. For the data obtained from the  $N_2$ -Ne mixtures (figures 6:26 and 6:27) the increase of  $i_{N_3^+}$  was used as the decrease of  $i_{N^+}$  was rather unreliable. The rate constants are shown in table (6:4). Plots of  $k_{f(n=2)}$  and  $k_{f(n=3)}$  (second and third order constants) are shown in figure (6:31). The plot indicates that the reaction is second order since the second order values are constant with pressure, and the third order values form a hyperbolic curve. The overall reaction should then be written as second order as (6:9a).



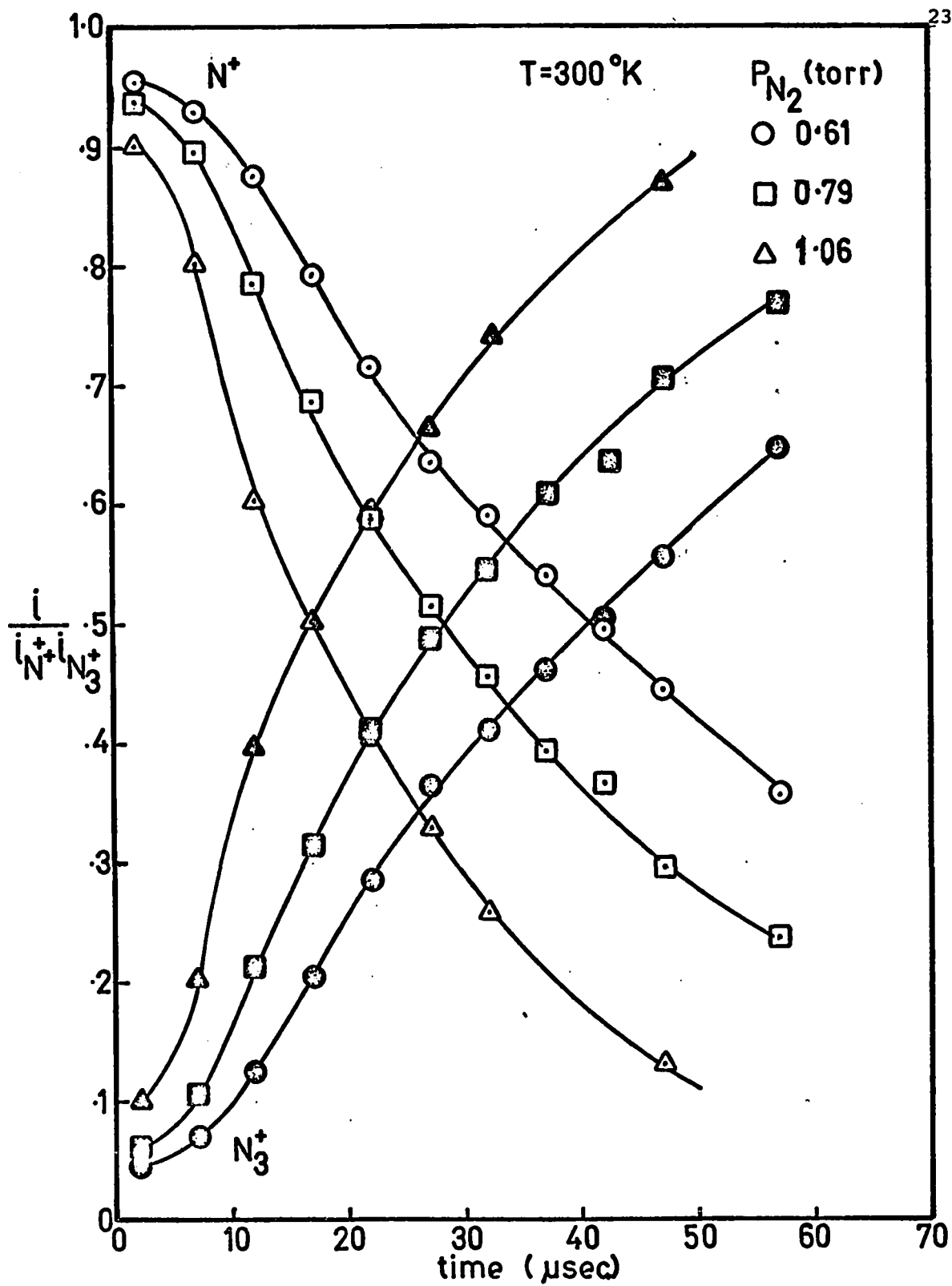


Figure 6:28 Normalized ion intensity curves of  $N^+$ ,  $N_3^+$  as fractions of  $i_{N^+} + i_{N_3^+}$ , nitrogen at  $300^\circ\text{K}$ , 0.61 to 1.06 torr.

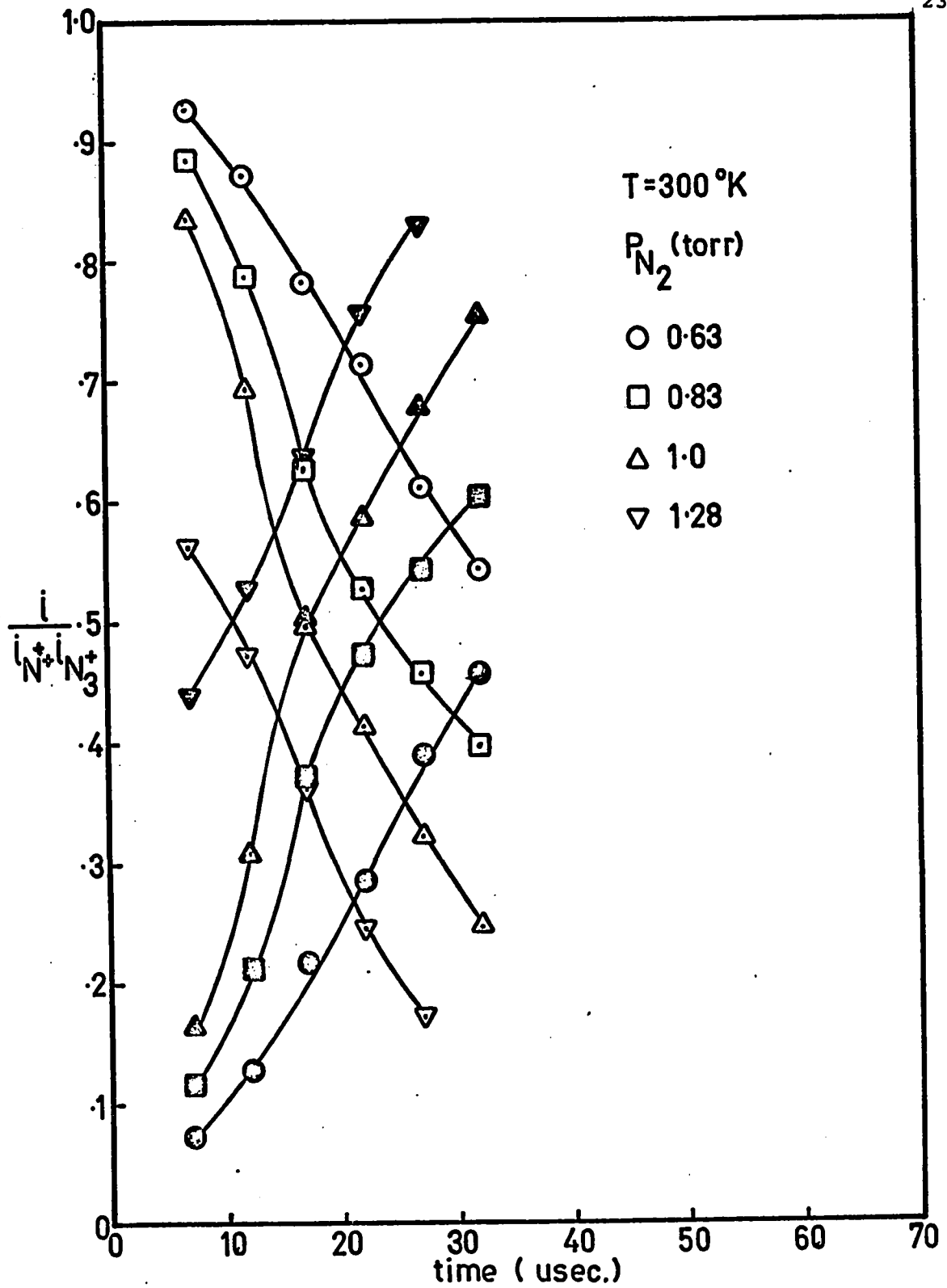


Figure 6:29 Normalized ion intensity curves of  $N^+$ ,  $N_3^+$  as fractions of  $i_{N^+} + i_{N_3^+}$ , nitrogen at  $300^\circ K$ , 0.63 to 1.28 torr.

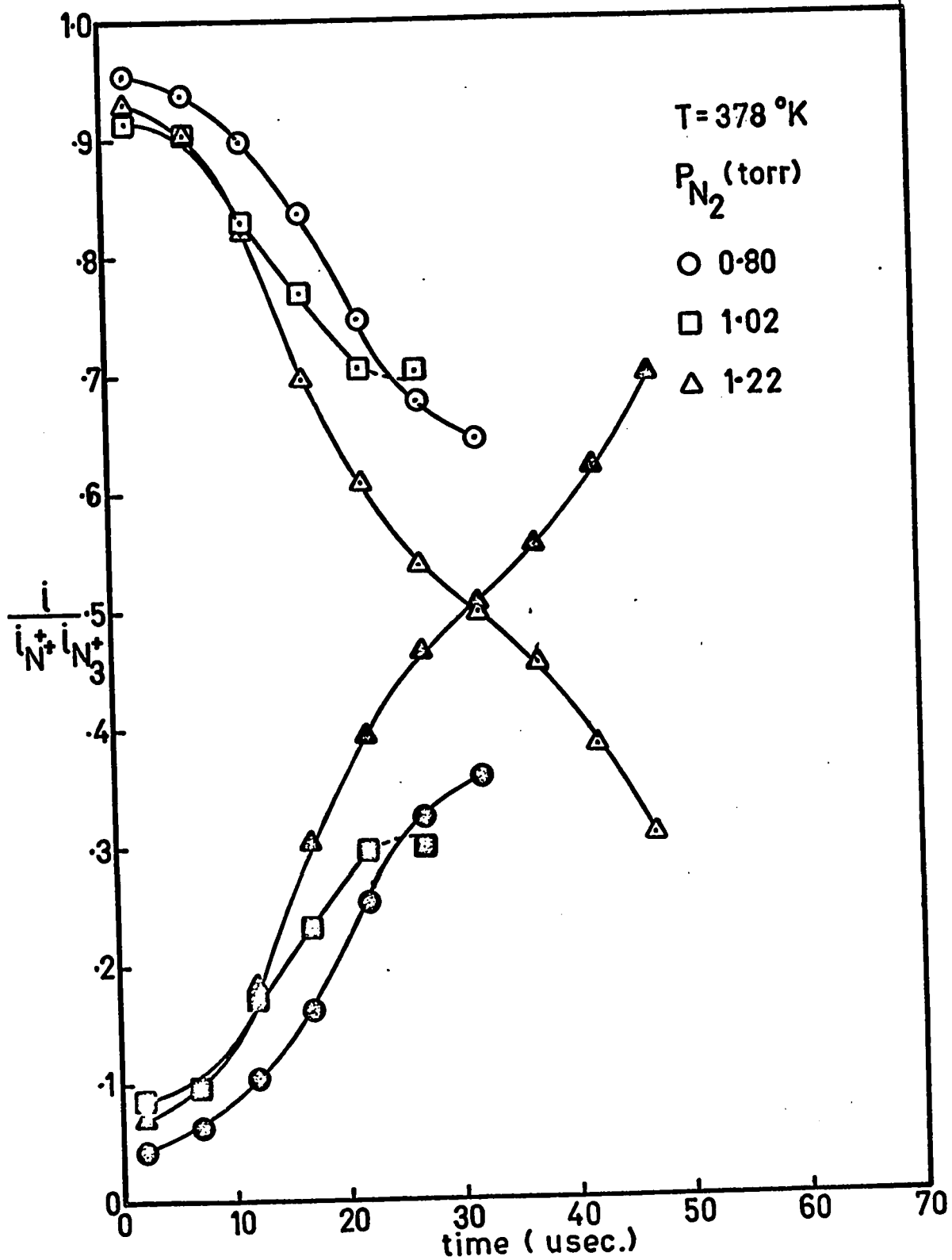
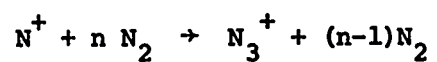


Figure 6:30 Normalized ion intensity curves of  $\text{N}^+$ ,  $\text{N}_3^+$  as fractions of  $i_{\text{N}^+} + i_{\text{N}_3^+}$ , nitrogen at  $378^\circ\text{K}$ , 0.80 to 1.22 torr.

The second order rate constant appears to be temperature independent. The reactions did not appear to reach any equilibrium in the short time that they could be observed (0 to 60 micro seconds).

TABLE 6:4

## Rate Constants for the Reaction



Temperature	N <sub>2</sub> Pressure (torr)	2nd order k cc/molecule secx10 <sup>12</sup> n=1	3rd order k cc <sup>2</sup> /molecule <sup>2</sup> secx10 <sup>29</sup> n=2	
300°K	0.63	1.79	8.84	
	0.83	1.71	6.38	from $\frac{i_N^+}{i_N^+ + i_{N_3}^+}$
	1.0	2.06	6.39	
	1.28	1.86	4.51	
300°K	0.61	1.24	6.33	
	0.79	1.21	4.77	from $\frac{i_N^+}{i_N^+ + i_{N_3}^+}$
	1.06	1.43	4.19	
378°K	0.80	1.12	5.49	
	1.02	0.68	2.63	from $\frac{i_N^+}{i_N^+ + i_{N_3}^+}$
	1.22	1.06	3.70	
380°K	2.05	2.10	4.04	from $\frac{i_N^+}{i_{\text{total}}}$
	2.65	1.41	2.09	
	3.4	1.64	1.89	

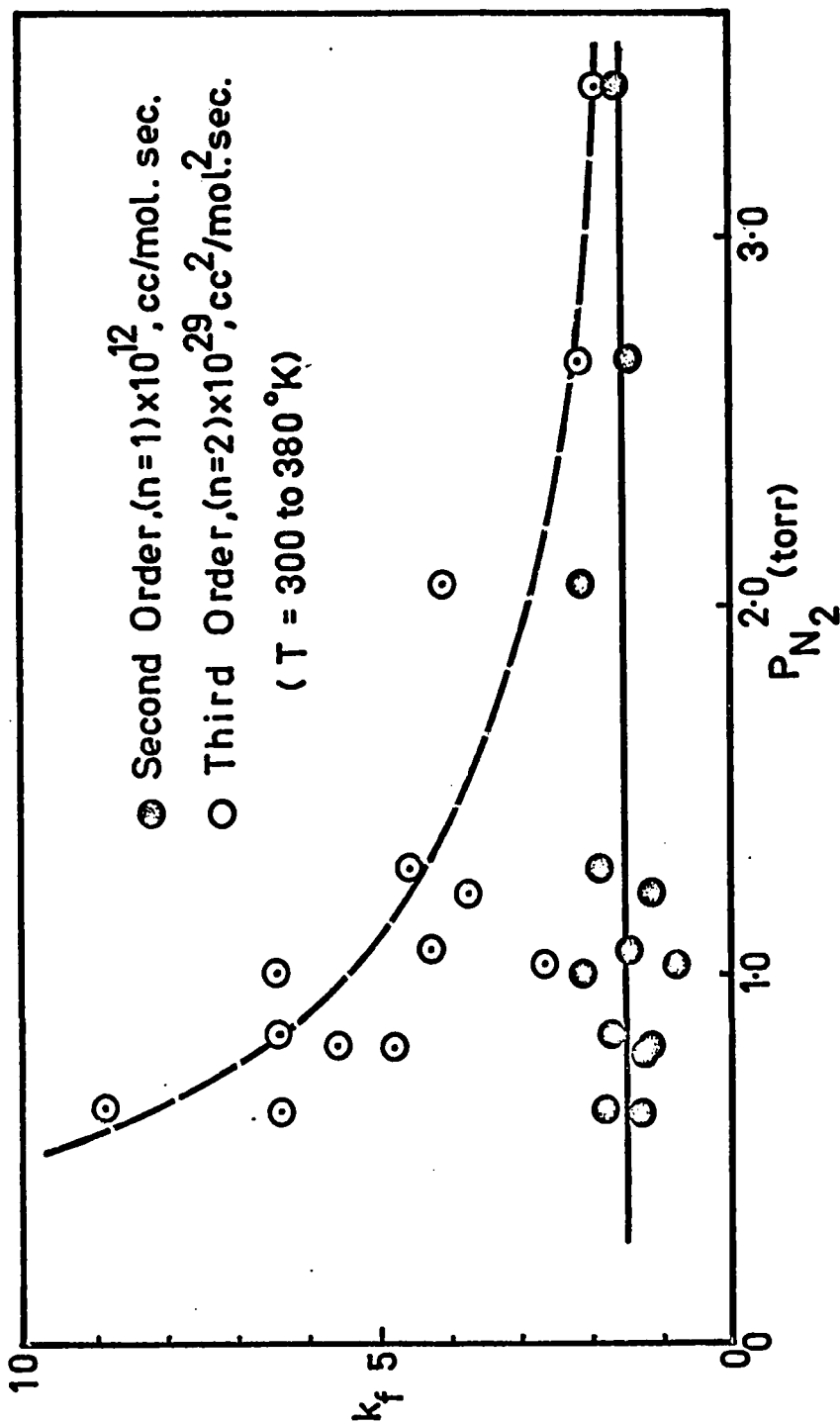
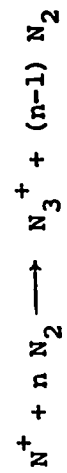


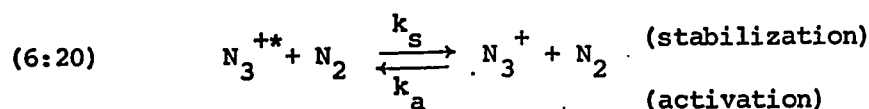
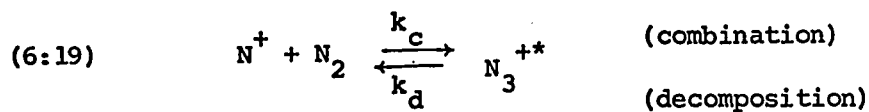
Figure 6:31 Change of third and second order rate constants for the reaction



with pressure. Values from Table 6:4.

iv Discussion of the Results

A mechanism for the attachment of  $N_2$  to  $N^+$  may be written exactly like that for attachment of  $N_2$  to  $N_2^+$ .



The same conditions for order apply here. The overall forward reaction was second order when  $k_d \ll k_s [N_2]$ .

The experimental rate constants are given by (6:xxx) and (6:xxxii).

$$(6:xxx) \quad k_f = k_c$$

$$(6:xxxii) \quad k_r = \frac{k_a k_d}{k_s}$$

$k_d$  and  $k_s$  were defined earlier by (6:xxiv) and (6:xxv).

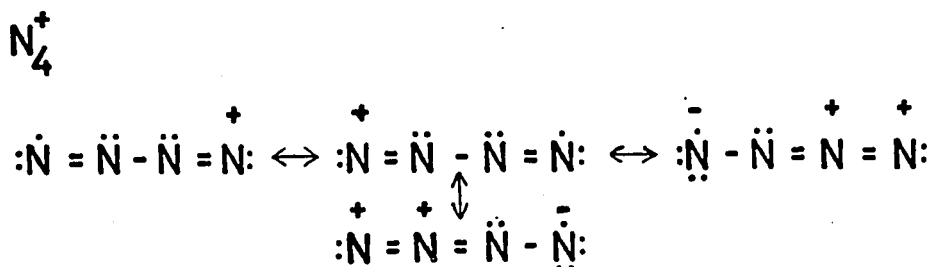
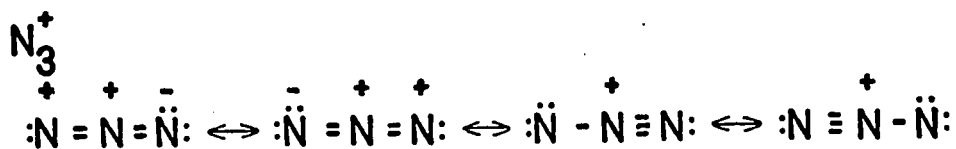
$$(6:xxiv) \quad k_d = Z_d \left( \frac{nRT}{D+nRT} \right)^{r-1}$$

$$(6:xxv) \quad k_s = pZ_s (1 - e^{-E_c/RT})$$

The conditions that  $k_d \ll k_s [N_2]$  are that the pressure be high, the temperature be low and the bond energy of the complex be high. The pressure and temperature under which the reactions



(6:2) and (6:9) were observed in the present study were identical. The bond energies and the number of vibrations are different. The bond energy  $D(N_2^+-N_2)$  was determined from appearance potential results of Asundi *et al* (103) to be greater than 0.6 eV (13.8 kcal/mole). These workers also measured the appearance potential of  $N^+$  (from reaction 6:19) to be  $24.2 \pm 1$  eV and that of  $N_3^+$  (from reaction 6:8) to be  $21.1 \pm 1$  eV. The difference between these ( $3.1 \pm 2$  eV) is the minimum energy for the bond  $N^+-N_2$ . Thus  $D(N^+-N_2) \sim 71$  kcal/mole. Since the bond energy of the complex  $N_3^+$  is five times larger than that of  $N_4^+$  one would expect that  $k_d$  for  $N_3^+$  would be much smaller than  $k_d$  for  $N_4^+$  and this is probably the reason that the reaction (6:9) appeared to be second order in the present experiment. The greater bond energy of  $N_3^+$  is probably due to its structure.  $N_3^+$  has an even number of electrons in the valence shell whereas  $N_4^+$  has an odd number. Simple Lewis structures for  $N_3^+$  and  $N_4^+$  are shown below.



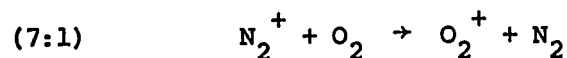
The lack of temperature dependence for  $k_f$  (second order) agrees with the theory presented earlier as  $k_f = k_c$ , and  $k_c$  was shown to be the Gioumouisis-Stevenson constant which is temperature independent.

The value of McKnight *et al* (104) of  $3 \times 10^{-29}$  cc<sup>2</sup>/molecule<sup>2</sup> sec. measured at 300°K and at 0.9 torr N<sub>2</sub> can be converted into a second order constant with the value of  $0.87 \times 10^{-12}$  cc/molecule sec. This is very close to the average of the present results,  $1.5 \times 10^{-12}$  cc/molecule sec. McKnight *et al* suggested that a reverse reaction took place under drift field conditions at high ion energies. This was not observed. One would not expect it to be, as the reverse reaction would be smaller than that for N<sub>4</sub><sup>+</sup> which also could not be observed.

## 7 SUGGESTIONS FOR FURTHER RESEARCH

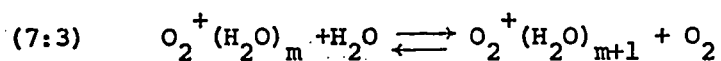
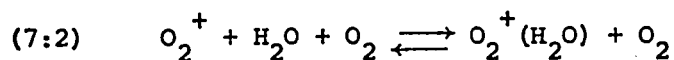
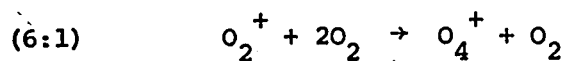
### 7:1 Introduction

The most abundant molecule in the Earth's atmosphere after  $N_2$  and  $O_2$  is  $H_2O$  which is present in trace quantities. Attachment reactions between these molecules and their ions are expected to occur in the D region of the ionosphere where the pressure is high. One of the major ions in the D-region is  $O_2^+$  which is produced by ultraviolet and x-ray radiation, and by charge exchange from  $N_2^+$  (127) by reaction (7:1).



### 7:2 Attachment Reactions in $O_2$ - $H_2O$ Mixtures

The first suggestion would be to study reactions in oxygen containing traces of  $H_2O$ . While performing the experiments described in chapter 6 the presence of two masses corresponding to the hydrates  $O_2^+(H_2O)$  and  $O_2^+(H_2O)_2$  were observed when a trace of water, about  $1 \times 10^{-3}$  torr per torr  $O_2$  was present. One could therefore propose the following series of reactions:



One would expect the reactions to require third body stabilization, and since one would expect the water to be in only trace concentrations  $O_2$  would be the third body.

This instrument could be used to measure the rate constants for the forward (and reverse) reactions, to establish the time required for equilibrium, and to measure the equilibrium constant  $K_p$ . From temperature studies the activation energy  $E_f$  of the forward reaction and the enthalpy  $\Delta H$  could be determined. It would be interesting to see if the reactions had small negative activation energies of 1 to 2 kcal/mole as did the attachment reactions of oxygen and nitrogen (reactions 6:1 and 6:2), and to see if there was any trend in  $E_f$  as the cluster size increased.

The bond energies ( $-\Delta H$ ) of other clusters  $H^+(H_2O)_n$ ,  $K^+(H_2O)_n$ , and  $NH_4^+(H_2O)_n$ , have been previously measured (31). The bond energies of hydrates of other ions  $Li^+$ ,  $Na^+$ ,  $Rb^+$ ,  $Cs^+$ , are presently being measured (128). It would be interesting to see how the stability of the oxygen hydrates  $O_2^+(H_2O)_n$  compared with these hydrates of atomic ions. The bonding of the hydrates with atomic centres has been explained as attraction of dipoles to a spherically symmetrical charge, and the stability of the ions found to change systematically with the charge radius (31). The molecular ion  $O_2^+$  would not have a spherical charge centre. One might be able to modify the

theory discussed by Searles (31) to fit this situation. Finally hydrates of  $O_2^-$  have been observed (129). A comparison of the positive versus the negative ions could be made.

### 7:3 Preliminary Investigation of $O_2$ - $H_2O$ Mixtures

The investigation of the attachment of  $H_2O$  and  $O_2^+$  was undertaken by Dr. Good and myself while this thesis was being written. Since it was not part of the thesis project, only a brief description will be given.

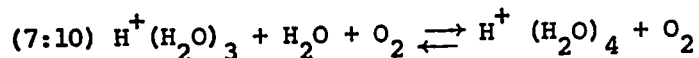
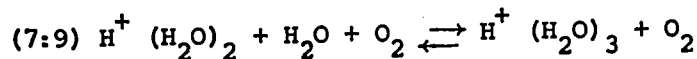
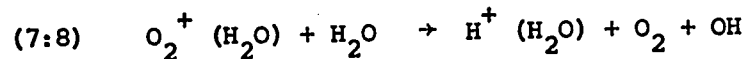
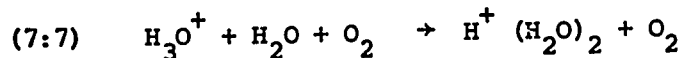
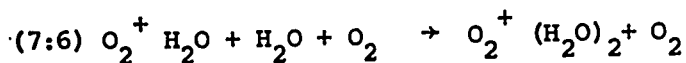
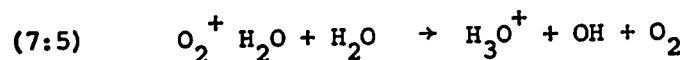
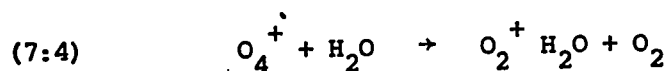
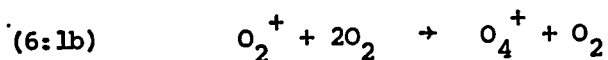
#### i Experimental

A flow system was set up whereby oxygen was admitted through the variable leak into the manifold. The gas passed through the ion source, and then through a capillary into a mechanical vacuum pump. At the atmospheric side of the pump the gas passed into a flow meter. Water was admitted to the oxygen between the variable leak and the manifold, through a small capillary set into the gas flow line. The total pressure of oxygen and water was read off the M.C.T. manometer. The ratio of oxygen to water was calculated from the weight of water added to the oxygen, from the total pressure and from the oxygen flow rate.

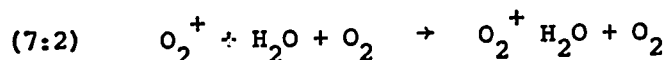
#### ii Results

Many more ions than expected were observed. Besides  $O_2^+$ ,  $O_4^+$ ,  $O_2^+(H_2O)$  and  $O_2^+(H_2O)_2$ , the water ions  $H_2O^+$ ,  $H_3O^+$ ,  $H^+(H_2O)_2$ ,

$\text{H}^+(\text{H}_2\text{O})_3$  etc. were observed. Figure (7:1) shows the data for a mixture of  $3 \times 10^{-3}$  torr  $\text{H}_2\text{O}$  in 2.2 torr  $\text{O}_2$  at 308°K. A kinetic system much more complex than proposed earlier was suggested by the data, this is shown below.



It appeared that under the present conditions the reaction (7:2) had too slow a rate to compete with the formation of  $\text{O}_4^+$  by



reaction (6:1b). The concentration of  $\text{O}_2$  was about 100 times that of  $\text{H}_2\text{O}$ . Thus the rate constant for (7:2) must be smaller than  $3 \times 10^{-28}$  cc<sup>2</sup>/molecule<sup>2</sup> sec. as  $k_f$  for (6:1b) was measured as  $3 \times 10^{-30}$  cc<sup>2</sup>/molecule<sup>2</sup> sec.

Another observation was the transformation of  $\text{O}_2^+(\text{H}_2\text{O})$

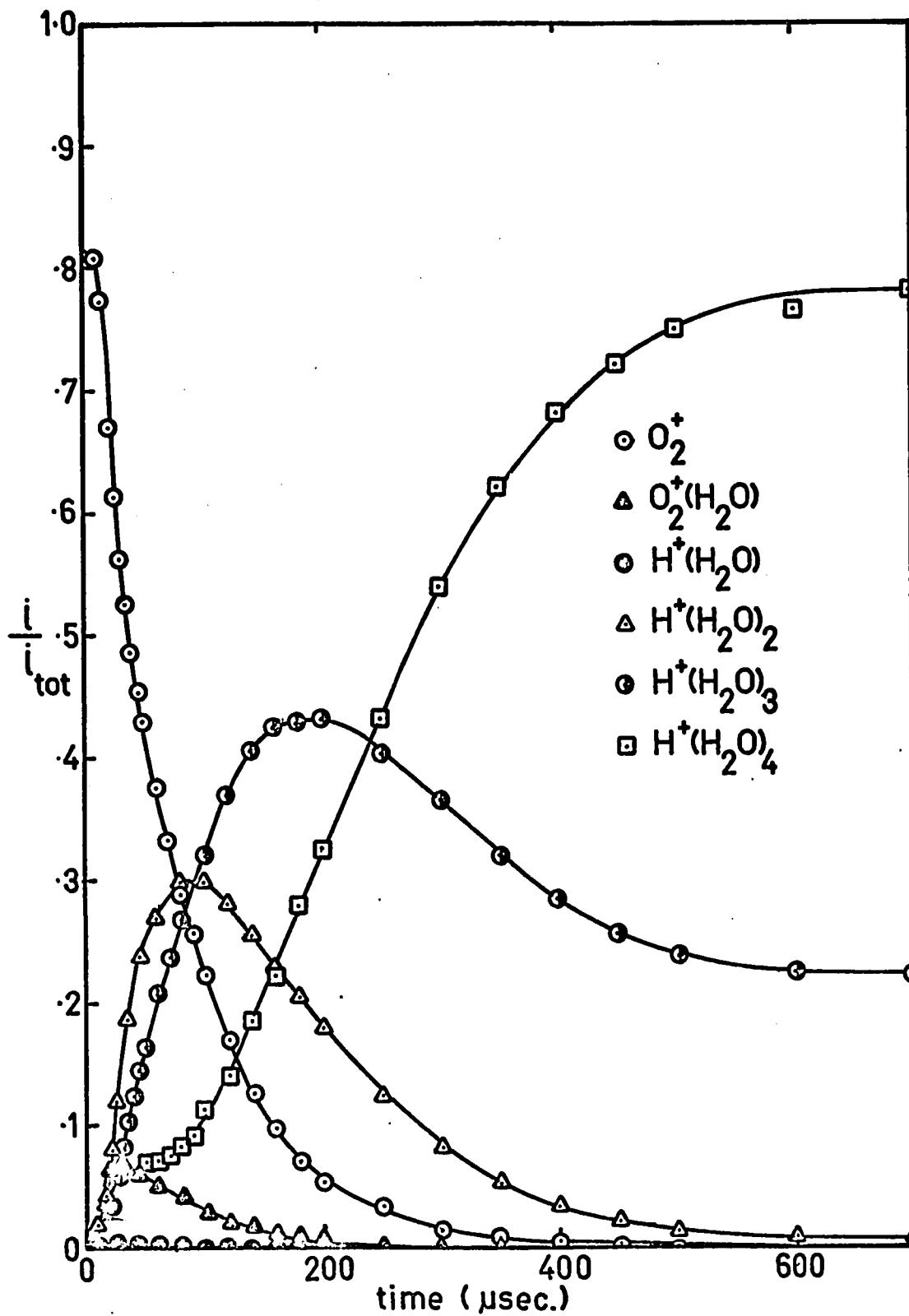


Figure 7:1 Normalized ion intensities for  $O_2-H_2O$  mixture at  $308^\circ K$ ,  $2.28 \text{ torr } O_2$ ,  $3.82 \times 10^{-3} \text{ torr } H_2O$ .

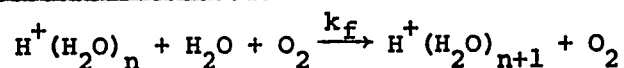
into  $\text{H}_3\text{O}^+$ . It appears that the hydrated protons are much more stable than the hydrated  $\text{O}_2^+$  ions. One would expect the electrophilic nature of  $\text{H}^+$  to be much larger than that of  $\text{O}_2^+$ . This may explain the reason for the transformation.

The formation of  $\text{H}^+(\text{H}_2\text{O})$  via reactions (7:5) and (7:7) which display second order kinetics appeared to be much larger than via reactions (7:6) and (7:8) which would display third order kinetics. Shahin(130) also observed the transformation but ascribed its formation to reactions (7:6) and (7:8). However the pressure in his apparatus was very high (30 torr), about 10 times that in the present apparatus and thus the third order mechanism might be expected to predominate.

The rate constants for the successive water hydration reactions were measured. They are shown in Table 7:1.

TABLE 7:1

Rate Constants for the Forward Reactions for Hydration Reactions



Reaction	n	$k_f$	$\text{cc}^2/\text{molecule}^2 \text{ sec.}$
7:7	1	$1.5 \times 10^{-26}$	
7:9	2	$2.4 \times 10^{-27}$	
7:10	3	$1.6 \times 10^{-27}$	



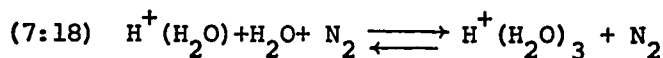
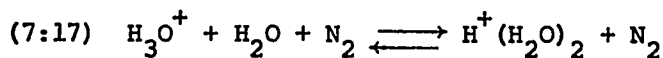
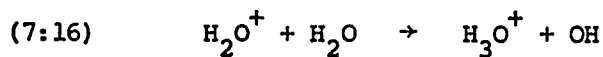
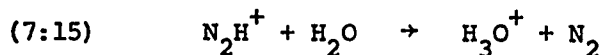
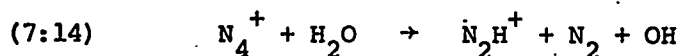
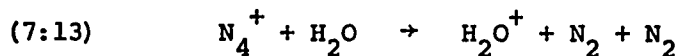
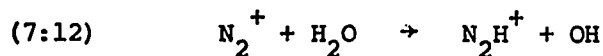
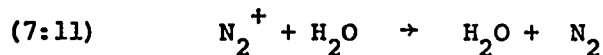
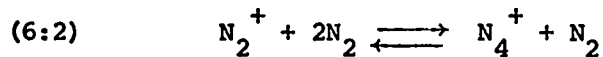
A previous value for the rate constant  $k_f$  for the hydration of  $H_3O^+$  (reaction 7:7) but with  $N_2$  as the third body has been previously reported as  $7 \times 10^{-28} \text{ cc}^2/\text{molecule}^2 \text{ sec.}$  (131). No details of the experimental conditions were given but one would expect that the presence of  $N_2$  instead of  $O_2$  as the third body would not affect the rate constant.

Since the reaction has so far been studied at only one temperature the parameters discussed earlier  $E_f$ ,  $E_r$ ,  $\Delta H$ , and  $K_p$  have yet to be measured.

#### 7:4 Attachment Reactions in $N_2$ - $H_2O$ Mixtures

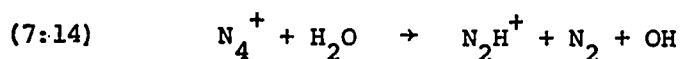
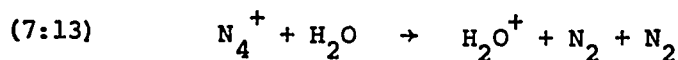
A second set of reactions would involve reactions in  $N_2$  containing traces of  $H_2O$ . One would not expect hydrates of the form  $N_2^+(H_2O)_n$  to be observed however, as the ionization potential of  $N_2^+$  15.58 eV is much larger than that of  $H_2O$  (12.61) and if one expects such a hydrate to have a recombination energy less than 12.61 to remain stable, 3 eV excitation energy would have to be removed by collision with third bodies. Rather one would expect charge exchange to occur to give  $H_2O^+$ . This system has been studied somewhat previously. Shahin has observed the ions from a corona flow of  $N_2$ - $H_2O$  mixtures and measured some reaction cross sections (132). He proposed a reaction sequence which is shown below. We also observed ions  $H_2O^+$ ,  $H_3O^+$ ,  $N_2H^+$  and  $H^+(H_2O)_2$  as well as  $N^+$ ,  $N_2^+$ ,  $N_3^+$  and  $N_4^+$  when traces of

H<sub>2</sub>O were present in the N<sub>2</sub>.



Shahin (132) measured the cross sections for reactions (6:2 and 7:11,12,15) but did not calculate rate constants.

Further studies on this system are warranted. Accurate values for the rate constants instead of cross sections (obtained by Shahin by making many approximations) might be obtained by means of the pulsed mass spectrometer in spite of the apparent complexity of the reaction system. Neither rate constant nor cross section have been measured for the reactions involving N<sub>4</sub><sup>+</sup>.



The irradiation of  $N_2-H_2O$  mixtures might be more useful than irradiation of  $O_2-H_2O$  mixtures, to study the kinetics of the hydrates of water as no other hydrates e.g.  $O_2^+(H_2O)_n$  are formed. The discrepancy between the rate constant measured in the present instrument for reaction (7:7) and that reported for (7:17) might be resolved. The forward reaction, combined with the  $K_p$  previously obtained by Searles (31) and Kebarle (133) would give the rate constants for decomposition of the hydrates. It would be interesting to establish the order of the forward reactions in the presence of  $N_2$ . Searles (31) stated that one might expect that, as the cluster size increased, the reactions would not need stabilization since the increased number of vibrational and rotational degrees of freedom could absorb the excess energy due to bond formation and therefore would go from third order to second order.

The prediction of the equations for  $k_f$  from Section (6:4:ii) is not the same. The third order rate, occurs when  $k_d \gg k_s [O]$ .  $k_d$  and  $k_s$  are given by (6:xxxiv) and (6:xxxv).

$$(6:xxxiv) \quad k_d = Z_d \left( \frac{nRT}{D+nRT} \right)^{r-1} \quad r = \text{number of vibrational modes}$$

$$(6:xxxv) \quad k_s = pZ_s (1 - e^{-E_c/RT})$$

As the cluster size increases, the bond energy decreases, which would increase  $k_d$  and thus decrease  $k_f$ . However the effective number of vibrational modes  $r$  increase also and since  $nRT/(D+nRT) < 1$

this would decrease  $k_d$  and increase  $k_f$ . The addition of one  $H_2O$  molecule to the hydrate increases the total number of vibrational modes. If  $r$  is always proportional to this number  $(3N-6)$  a change in  $N$  would have a greater effect than changes in  $D$  and thus  $k_d$  would decrease. The measured rate constants  $k_f$  for further reaction of the water hydrates  $H^+(H_2O)_n$  in  $O_2$  decrease which indicates that changes in  $D$  have larger effects than changes in  $r$  through addition of more  $H_2O$  clusters. Thus the fraction of the effective number of vibrational modes contributing to the decomposition of the excited state, out of the total number of vibrational modes decreases. Thus the third body requirement would increase. This is in contradiction with Searles statement. Further measurements of the  $N_2-H_2O$  system might clarify this. The ideal situation would be to find a pressure-temperature region in which the addition of the first  $H_2O$  molecule to  $H_3O^+$  were second order and then test whether the addition of further  $H_2O$  molecules to the cluster were second or third order.

The measurement of these reaction rates and their temperature dependencies would be useful to help explain the processes occurring in the D region of the ionosphere.

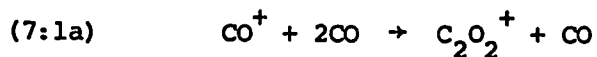
7:5 Further Work on the Attachment  $N_2^+ + N_2 \rightarrow N_4^+$

Improved values for  $K_p$  and  $\Delta H$  and thus the bond energy  $D(N_2^+-N_2)$  should be obtained by studying the attachment reaction (6:2)

at temperatures from 500 to 600°K. These could also be used to correlate Varney's ion temperature (107) with the thermal temperature. The ion source of the present instrument would have to be modified so that it could operate at such high temperatures as the present limit is 450°K.

7:6 The Attachment Reaction  $\text{CO}^+ + \text{CO} \rightleftharpoons \text{C}_2\text{O}_2^+$

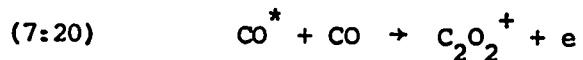
The attachment of CO to  $\text{CO}^+$  has been observed by Saporoschenko (134). Since  $\text{CO}^+$  has a bond length and vibrational frequency intermediate to those of  $\text{O}_2^+$  and  $\text{N}_2^+$  (135) one might by the study of the formation of  $\text{C}_2\text{O}_2^+$  be able to correlate all three attachment complexes. Recently Conway (136) has studied the complex  $\text{N}_2\text{O}_2^+$  which one might expect to have a similar structure to  $\text{C}_2\text{O}_2^+$ . The formation of  $\text{C}_2\text{O}_2^+$  in CO would probably be third order (reaction 7:1a).



Saporoschenko estimated the bond energy  $D(\text{CO}^+-\text{CO})$  to be  $\sim 0.81$  eV.

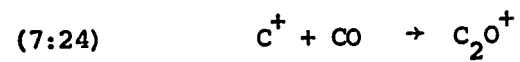
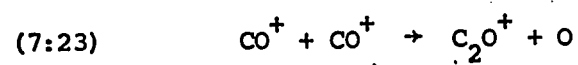
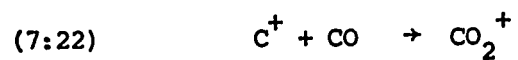
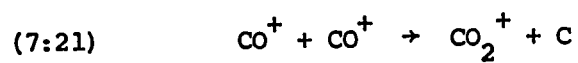
It can also be estimated from the appearance potential of  $\text{C}_2\text{O}_2^+$  produced by the Hornbeck-Molnar reaction (7:20) ( $12.8 \pm 0.3$  eV).

The ionization potential of  $\text{CO}^+$  is 14.00 eV. Thus the bond



energy should be about  $1.2 \pm 0.3$  eV. Since this value is large, a van't Hoff plot of  $\log K_p$  versus  $10^3/T$  would have a large slope. It might be necessary to operate at high temperatures.

Rudolph and Lind (137) and Munson *et al* (115) postulated that the following reactions produced the observed ions  $\text{CO}_2^+$  and  $\text{C}_2\text{O}^+$ .



The presence of these reactions would complicate the observation of the kinetics of reaction (7:1a).

BIBLIOGRAPHY

1. J.J. Thomson, *Phil. Mag.*, 24, 241 (1912).
2. A.J. Dempster, *Phil. Mag.*, 31, 438 (1916).
3. H.D. Smyth, *Phys. Rev.*, 25, 452 (1925).
4. T.P. Hogness and E.G. Lunn, *Phys. Rev.*, 26, 44 (1925).
5. V.L. Talroze and A.K. Lyubinoва, *Doklady Akad. Nauk. SSSR*, 86, 909 (1952) per *Chemical Abstracts*, 47, 2590 (1953).
6. D.P. Stevenson and D.O. Schissler, *J. Chem. Phys.*, 23, 1353 (1955).
7. D.O. Schissler and D.P. Stevenson, *J. Chem. Phys.*, 24, 926 (1956).
8. D.P. Stevenson and D.O. Schissler, *J. Chem. Phys.*, 29, 282 (1958).
9. R.P. Pottie, R. Barker and W.H. Hammil, *Rad. Res.*, 10, 664 (1959) and earlier papers.
10. F.H. Field, J.L. Franklin and F.W. Lampe, *J. Amer. Chem. Soc.*, 78, 5697 (1956); 78, 2419 (1956).
11. F.H. Field, J.L. Franklin and F.W. Lampe, *J. Amer. Chem. Soc.*, 79, 2665 (1957).
12. G. Gioumousis and D.P. Stevenson, *J. Chem. Phys.*, 29, 294 (1958).
13. D.P. Stevenson, Mass Spectrometry, C.A. McDowell Ed., McGraw Hill, New York, 1963, p. 589.
14. V.L. Talroze and E.L. Frankevitch, *J. Amer. Chem. Soc.*, 80, 2345 (1958).

15. D.P. Stevenson and D.O. Schissler, The Chemical and Biological Actions of Radiations, M. Haissinsky Ed., Academic Press, London, 1961, p. 247.
16. V.L. Talroze and E.L. Frankevitch, *Russ. J. Phys. Chem.*, 34, 1275 (1960).
17. V.L. Talroze, *Pure. Appl. Chem.*, 5, 455 (1962).
18. C.W. Hand and H. von Weysenhoff, *Can. J. Chem.*, 42, 195 (1964).
19. K.R. Ryan and J.H. Futrell, *J. Chem. Phys.*, 42, 824 (1965); 43, 3009 (1965).
20. T.W. Shannon, F. Meyer and A.G. Harrison, *Can. J. Chem.*, 43, 159 (1965).
21. A.G. Harrison, A. Ivko and T.W. Shannon, *Can. J. Chem.*, 44, 1351 (1966).
22. F.W. Lampe, F.L. Franklin and F.H. Field, Progress in Reaction Kinetics, Vol. 1, G. Porter Ed., Pergamon Press, New York, 1961, p. 68.
23. C.D. Wagner, P.A. Wadsworth and D.P. Stevenson, *J. Chem. Phys.*, 28, 517 (1958).
24. F.H. Field, J.L. Franklin and F.W. Lampe, *J. Amer. Chem. Soc.*, 79, 2419 (1957).
25. D.R. Bates, Atomic and Molecular Processes, Academic Press, New York, 1962, pp. 601, 708.
26. E. Lindholm, I. Szabo and P. Wilmenius, *Arkiv Fysik*, 25, 417 (1963).



27. H. von Koch, *Arkiv Fysik*, 28, 529 (1965).
28. G.R. Freeman, *Radiation Chemistry*, University of Alberta, Edmonton, 1966, p. 193.
29. F.H. Field and F.W. Lampe, *J. Amer. Chem. Soc.*, 80, 5583, (1958).
30. F.H. Field and F.W. Lampe, *J. Amer. Chem. Soc.*, 81, 3238 (1959).
31. S.K. Searles, Thesis, University of Alberta, 1968, Ch. 4.
32. F.H. Field, *J. Amer. Chem. Soc.*, 83, 1523 (1961).
33. F.H. Field, J.L. Franklin and M.S.B. Munson, *J. Amer. Chem. Soc.*, 85, 3575 (1963).
34. F.H. Field and M.S.B. Munson, *J. Amer. Chem. Soc.*, 87, 3289 (1965).
35. M.S.B. Munson and F.H. Field, *J. Amer. Chem. Soc.*, 87, 3294 (1965).
36. C.E. Melton and P.S. Rudolph, *J. Chem. Phys.*, 32, 1128 (1960).
37. P.S. Rudolph and C.E. Melton, *J. Phys. Chem.*, 63, 916 (1959).
38. C.E. Melton and P.S. Rudolph, *J. Chem. Phys.*, 33, 647 (1960); 33, 1594 (1960).
39. S. Wexler, A. Lifshitz and A. Quattrochi, *Advances in Chemistry*, Series No. 58, American Chemical Society, Washington, D.C., 1966, p. 193.

40. P. Kebarle and E.W. Godbole, *J. Chem. Phys.*, 39, 1131 (1963).
41. P. Kebarle and A.M. Hogg, *J. Chem. Phys.*, 42, 668 (1965).
42. P. Kebarle, R.M. Haynes and S. Searles, Advances in Chemistry, Series No. 58, American Chemical Society, Washington, D.C. 1966, p. 210.
43. P. Kebarle and A.M. Hogg, *J. Chem. Phys.*, 42, 798 (1965).
44. P. Kebarle, R.M. Haynes and S.K. Searles, *J. Chem. Phys.*, 47, 1684 (1967).
45. W.L. Fite, J.A. Rutherford, W.R. Snow and V.A.J. van Lint, *Disc. Faraday Soc.*, 33, 264 (1962).
46. J. Sayers, and D. Smith, *Disc. Faraday Soc.*, 37, 167 (1964).
47. F.C. Fehsenfeld, A.L. Schmeltekopf and E.E. Ferguson, *J. Chem. Phys.*, 44, 4087 (1966).
48. A.L. Schmeltekopf, F.C. Fehsenfeld, G.I. Gilman and E.E. Ferguson, *Planet.Space Sci.*, 15, 401 (1967).
49. W.L. Fite, Symposium on Laboratory Measurements of Aeronomic Interest, International Association of Geomagnetism and Aeronomy, Toronto (1968), p. 59.
50. Advances in Chemistry, Series No. 72, American Chemical Society, Washington, D.C., 1968.
51. Advances in Mass Spectrometry, Volume 4, Institute of Petroleum, Elsevier, New York, 1968.
52. P. Ausloos and S.G. Lias, The Chemical and Biological Actions of Radiations, M. Haissinsky Ed., Volume 11, Academic Press, New York, 1967.

53. S. Dushman, Scientific Foundations of Vacuum Technique, John Wiley and Sons, Inc., New York, 1949.
54. A. Guthrie, Vacuum Technology, John Wiley and Sons, Inc., New York, 1963.
55. O. Klemperer, Electron Physics, The Physics of the Free Electron, Butterworths Scientific Publications, London, 1959, p. 11.
56. W. Paul and H. Steinwedel, Z. Naturforsch., 8A, 448 (1953).
57. W. Paul, H.P. Reinhard and U. von Zahn, Z. Physik, 152, 143 (1958).
58. W. Paul and M. Raether, Z. Physik, 140, 262 (1955).
59. U. von Zahn, S. Gebauer and W. Paul, 10th Annual Meeting of the ASTM Committee E-14 on Mass Spectrometry, New Orleans, La., June 1962, p. 232.
60. W.M. Brubaker and J. Tuul, Rev. Sci. Instr., 35, 1007 (1964).
61. C. Brunée, L. Delgmann and K. Kronenberger, 11th Annual Meeting of the ASTM Committee E-14 on Mass Spectrometry, San Francisco, California, May 1963.
62. B.L. Schram, Ionization of Noble and Molecular Gases by High Energy Electrons, Thesis, Amsterdam, 1966.
63. P. Kebarle, E.W. Godbole, J. Chem. Phys., 36, 302 (1962).
64. J.H. Beynon, Mass Spectrometry and its Application to Organic Chemistry, Elsevier, New York, 1960, p. 214.
65. H.E. Stanton, W.A. Chupka and M.G. Ingrham, Rev. Sci. Instr., 27, 109 (1956).

66. W.H. Kasner and M.A. Biondi, *Phys. Rev.*, 137, A 317 (1965).
67. L.B. Loeb, Basic Processes of Gaseous Electronics, Univ. of California Press, Berkeley, 1961.
68. E.W. McDaniel, Collision Phenomena in Ionized Gases, John Wiley & Sons, Inc., New York, 1964.
69. A. Galli, A. Giardini-Guidoni and G.G. Volpi, *J. Chem. Phys.*, 39, 518 (1963).
70. K. Birkinshaw, A.J. Masson, D. Hyatt, L. Matus, I. Opauszky and M.J. Henchman, Advances in Mass Spectrometry, Volume 4, Institute of Petroleum, London, 1968, p. 379.
71. J.L. Franklin, Y. Wada, P. Natalis and P.M. Hierl, *J. Phys. Chem.*, 70, 2353 (1966).
72. K.R. Ryan, J.H. Futrell and C.D. Miller, *Rev. Sci. Instr.*, 37, 107 (1966).
73. A.G. Harrison, J.J. Myer and J.C.J. Thynne, Advances in Chemistry, Series No. 58, American Chemical Society, Washington, D.C., 1966, p. 164.
74. W.J. Moore, Physical Chemistry, 3rd edition, Prentice Hall, New Jersey, 1962, p. 263.
75. P. Kebarle and R.M. Haynes, *J. Chem. Phys.*, 45, 3899 (1965).
76. E. Lindholm, Advances in Chemistry, Series No. 58, American Chemical Society, Washington, D.C., 1966, p. 1.
77. V. Cermak and Z. Herman, *Nucleonics*, 19, 106 (1961).
78. F.H. Field and J.L. Franklin, *J. Amer. Chem. Soc.*, 83, 4509 (1961)

79. N.M. Rodiguin and E.M. Rodiguina, Consecutive Chemical Reactions, Translated by R.F. Schneider, Van Nostrand, New Jersey, N.Y., 1964.
80. H.S.W. Massey and E.H.S. Burhop, Electronic and Ionic Impact Phenomena, Oxford, Clarendon Press, 1952, p. 441
81. A.D. Baker, C. Baker, C.R. Brundle and D.W. Turner, J. Mass Spectrometry and Ion Physics, 1, 285 (1968).
82. S. Wexler and R. Marshall, J. Amer. Chem. Soc., 86, 781 (1964).
83. T.O. Tiernan and J.H. Futrell, J. Phys. Chem., 72, 3080 (1968).
84. C.D. Wagner, J. Phys. Chem., 66, 1158 (1962).
85. P. Kebarle and R.M. Haynes, J. Chem. Phys., 47, 1676 (1967).
86. I. Szabo, Arkiv Fysik, 31, 287 (1966).
87. G.V. Karachevtsev, M.I. Markin and V.L. Talroze, Kinetika i Kataliz, 5, 377 (1964).
88. G.G. Meissels, Advances in Chemistry, Series No. 58, American Chemical Society, Washington, D.C., 1966, p. 243.
89. G.G. Meissels, J. Chem. Phys., 42, 3237 (1965).
90. F.W. Lampe, Radiation Research, 10, 691 (1959).
91. R. Gorden Jr. and P. Ausloos, J. Chem. Phys., 47, 1799 (1967).
92. R.N. Varney, Phys. Rev., 89, 708 (1953).

93. H.J. Saunders, Chemistry and the Atmosphere, Chemical and Engineering News, Washington, D.C., 1967.
94. M.A. Biondi, Symposium on Laboratory Measurements of Aeronomic Interest, International Association of Geomagnetism and Aeronomy, Toronto, 1968, p. 1.
95. G. Brederlow, *Ann. Physik*, 5, 414 (1960).
96. P.F. Knewstubb and A.W. Tickner, *J. Chem. Phys.*, 38, 1031 (1963).
97. J.H. Yang and D.C. Conway, *J. Chem. Phys.*, 40, 1729 (1964).
98. D.C. Conway and J.H. Yang, *J. Chem. Phys.*, 43, 2900 (1965).
99. R.K. Curran, *J. Chem. Phys.*, 38, 2974 (1963).
100. R.E. Winters, J.H. Collins, W.L. Courchene, *J. Chem. Phys.*, 45, 1930 (1966).
101. P. Warneck, *J. Chem. Phys.*, 46, 502 (1967).
102. G.E. Keller, D.W. Martin, E.W. McDaniel, *Phys. Rev.*, 140, A 1535 (1965).
103. R.K. Asundi, G.I. Schultz and P.J. Chantry, *J. Chem. Phys.*, 47, 1584 (1967).
104. L.G. McKnight, K.B. McAfee and D.P. Sipler, *Phys. Rev.*, 164, 62 (1967).
105. R.N. Varney, *Phys. Rev.*, 88, 362 (1952).
106. F.R. Kovar, E.C. Beatty and R.N. Varney, *Phys. Rev.*, 107, 1490 (1957).
107. R.N. Varney, *J. Chem. Phys.*, 31, 1314 (1959).

108. R.N. Varney, *J. Chem. Phys.*, 33, 1709 (1960).
109. P.F. Knewstubb, *Advances in Mass Spectrometry*, Volume 4, Institute of Petroleum, Elsevier, New York, 1968.
110. M. Saporoschenko, *Phys. Rev.*, 111, 1550 (1958).
111. R.K. Curran, *J. Chem. Phys.*, 38, 2974 (1963).
112. R.N. Varney, *J. Geophys. Res.*, 72, 5578 (1967).
113. F.C. Fehsenfeld, D.B. Dunkin, D.K. Bohme and E.E. Ferguson, Communication at 16th Annual Conference on Mass Spectrometry and Allied Topics, ASTM Committee E-14, Pittsburgh, May 1968.
114. W. Kaul and R. Fuchs, *Z. Naturforsch.*, 159, 326 (1960).
115. M.S.B. Munson, F.H. Field and J.L. Franklin, *J. Chem. Phys.*, 37, 1790 (1962).
116. H.S. Johnston, *Gas Phase Reaction Rate Theory*, Ronald Press, New York, 1966, p. 258.
117. E. Rabinowitch, *Trans. Faraday Soc.*, 33, 283 (1937).
118. G. Porter, *Disc. Faraday Soc.*, 33, 198 (1962).
119. D. Husain and H.O. Pritchard, *J. Chem. Phys.*, 30, 1101 (1959).
120. M. Ritchie, *Chemical Kinetics in Homogenous Systems*, Oliver and Boyd, Edinburgh, 1966.
121. R.H. Fowler and E.A. Guggenheim, *Statistical Thermodynamics*, Cambridge University Press, London, 1939, p. 497.
122. H.B. Palmer and D.F. Hornig, *J. Chem. Phys.*, 26, 98 (1957).
123. V. Cermak and Z. Herman, *Collection Czech. Chem. Commun.*, 27, 1493 (1962).

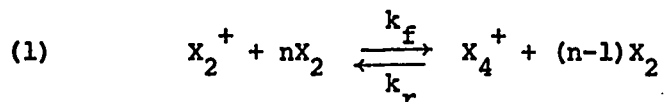
125. O. Luhr, *Phys. Rev.*, 44, 459 (1933).
126. P.F. Knewstubb and A.W. Tickner, *J. Chem. Phys.*, 37, 2941 (1962).
127. F.C. Fehsenfeld, A.L. Schmeltekopf and E.E. Ferguson, *Planet. Space Sci.*, 13, 219 (1965).
128. P. Kebarle and I. Dzidic, private communication.
129. P. Kebarle and M.R. Arshadi, private communication.
130. M.M. Shahin, 153rd National Meeting, American Chemical Society Division of Fuel Chemistry, Miami, Florida, 1967, Volume 11, No. 2, Part 1, p. 138.
131. A.P. Mitra, *J. Atmosph. Terr. Phys.*, 30, 1065 (1968).
132. M.M. Shahin, Advances in Chemistry, Series No. 58, American Chemical Society, Washington, D.C., 1966.
133. P. Kebarle, S.K. Searles, A. Zolla, J. Scarborough and M. Arshadi, *J. Amer. Chem. Soc.*, 89, 6393 (1967).
134. M. Saporoschenko, *J. Chem. Phys.*, 49, 768 (1968).
135. H. Shin, Advances in Chemistry, Series No. 58, American Chemical Society, Washington, D.C., 1966, p. 44.
136. G.S. Janik and D.C. Conway, *J. Phys. Chem.*, 71, 823 (1967).
137. P.S. Rudolph and S.C. Lind, *J. Chem. Phys.*, 33, 705 (1960).
138. F.H. Field and J.L. Franklin, Electron Impact Phenomena, Academic Press Inc., New York, 1957.
139. R.E. Huffman and D.H. Katayama, *J. Chem. Phys.*, 45, 138 (1966).



## APPENDIX I

Equation for theCorrect Value for the Forward Rate Constant for a Reversible Reaction

Consider the reversible reaction (1) where  $n=1$  or  $2$ , for



a second order or third order reaction. If we assume that the ion concentration is proportional to the measured fractional intensity we may write the change in intensity ( $i$ ):

$$(i) \quad \frac{d i_{X_2}^+}{dt} = -k_f i_{X_2}^+ [X_2]^n + k_r i_{X_4}^+ [X_2]^{n-1}$$

at equilibrium  $\frac{d i_{X_2}^+}{dt} = 0$ .  $k_f$  and  $k_r$  are related to the equilibrium constant, and  $i_{X_2}^+$  to the ion concentrations at equilibrium.

$$(ii) \quad k = \frac{k_f}{k_r} = \frac{i_{X_4}^+ \text{ eq}}{i_{X_2}^+ \text{ eq} [X_2]}$$

Thus

$$(iii) \quad k_r = k_f [X_2] C \text{ where } C = \frac{i_{X_2}^+ \text{ (eq)}}{i_{X_4}^+ \text{ (eq)}}$$

Since the two intensities  $i_{X_2}^+$  and  $i_{X_4}^+$  are fractions of the total ion intensity we have (iv)

$$(iv) \quad i_{X_4}^+ = 1 - i_{X_2}^+$$

we may substitute (iii) and (iv) into (i).

$$(v) \quad \frac{di_{X_2}^+}{dt} = -k_f [O_2]^n [i_{X_2}^+ (1+C) - C]$$

This may be rearranged and integrated from 0 to t. Let  $i_{X_2}^+ = x$  for convenience.

$$(vi) \quad \int_{x_0}^x \frac{dx}{x(1+C)-C} = \int_0^t -k_f [X_2]^n dt$$

$$(vii) \quad \frac{\ln [x (1+C) - C]}{1+C} \Bigg|_{x_0}^x = -k_f [X_2]^n (t-t_0)$$

at  $t = 0$ ,  $x_0 = 1$  and at  $t = t$ ,  $x = i_{X_2}^+$ . The final equation is then written:

$$(viii) \quad -k_f = \frac{2.303 \log_{10} [i_{X_2}^+ (1+C) - C]}{(1+C)}$$

APPENDIX II  
Ionization Potentials

Ion	Source	Ionization Potential	Reference
$\text{He}^+$	$\text{He} + e$	24.58	15
$\text{He}_2^+$	$\text{He}^* + \text{He}$	23.18 Ap.	138
$\text{Ne}^+$	$\text{Ne} + e$	21.56	15
$\text{Ne}_2^+$	$\text{Ne}^* + \text{Ne}$	20.86 Ap.	138
$\text{Ar}^+ \begin{matrix} 2P_{3/2} \\ 2P_{1/2} \end{matrix}$	$\text{Ar} + e$	15.76	15
	$\text{Ar} + e$	15.97	15
$\text{Ar}_2^+$	$\text{Ar}^* + \text{Ar}$	14.71 Ap.	139
$\text{Kr}^+ \begin{matrix} 2P_{3/2} \\ 2P_{1/2} \end{matrix}$	$\text{Kr} + e$	14.00	15
	$\text{Kr} + e$	14.67	15
$\text{Kr}_2^+$	$\text{Kr}^* + \text{Kr}$	13.00 Ap.	139
$\text{Xe}^+ \begin{matrix} 2P_{3/2} \\ 2P_{1/2} \end{matrix}$	$\text{Xe} + e$	12.13	15
	$\text{Xe} + e$	13.44	15
$\text{Xe}_2^+$	$\text{Xe}^* + \text{Xe}$	11.16 Ap.	139
$\text{N}^+$	$\text{N} + e$	14.54	138
$\text{N}^+$	$\text{N}_2 + e$	24.2	103

APPENDIX II (Cont'd)

Ion	Source	Ionization Potential	Reference
$N_2^+ 2\Sigma_g$	$N_2 + e$	15.58	103
$N_2^+ 4\Sigma_u$	$N_2 + e$	21.1	103
$N_3^+$	$N_2^+ + N_2$	21.1 Ap.	
$N_4^+$	$N_2^* + N_2$	15.0 Ap.	103
$O^+$	$O_2 + e$	18.9	138
$O_2^+ 2\Pi_g$	$O_2 + e$	12.07	100
$O_2^+ 4\Pi_u$	$O_2 + e$	16.2	100
$H_2O^+$	$H_2O + e$	12.61	138
$CH_4^+$	$CH_4 + e$	13.12	138
$CH_3^+$	$CH_4 + e$	14.39 Ap.	138
	$CH_3 + e$	9.95	138
$CH_2^+$	$CH_4 + e$	15.6 Ap.	
$C_2H_4^+$	$C_2H_4 + e$	10.51	138
$C_2H_3^+$	$C_2H_4 + e$	13.93 Ap.	138
$C_2H_2^+$	$C_2H_4 + e$	13.5 Ap.	138

N.B. Ap. = appearance potential.